Hansen Solubility Parameters as a Predictive Tool for the Development of Oral Polymeric Nanoparticle Delivery Systems

---

A thesis submitted in partial fulfilment of the requirement for the degree of Doctor of Philosophy

September 2022

Akunnaya Ezekwem

Research Department of Pharmaceutical and Biological Chemistry

UCL School of Pharmacy

Declaration

I, Akunnaya Ezekwem confirm that the work presented in this thesis is my own. Where information has been derived from other sources, I confirm that this has been indicated in the thesis.'

Akunnaya Ezekwem

4th September 2022

Abstract

Oral drug delivery proves to be the ideal means of drug administration however it is associated with challenges such as drug dissolution and drug permeability, particularly in BCS class IV drugs. These contribute to a reduction in drug bioavailability which accounts for 40% of failures in the developmental stages of oral drug formulations. As a result, drug delivery systems have been designed to alleviate these obstacles and improve oral delivery of various drugs.

An example of such drug delivery systems is the use of N-palmitoyl-N-monomethyl-N,N-dimethyl-N,N,N-trimethyl-6-O-glycolchitosan (GCPQ) as nanocarriers. An amphiphilic polymer which has the ability to self-assemble into micelles in solution which are then able to traverse the mucosal layer – a common limitation in oral drug delivery. GCPQ comprises of a range of functional groups which could be chemically modified to achieve required properties. Investigation of various modifications using polymer chemistry allows for a better understanding of the independent effects and relative importance of each individual modification on the process of drug delivery.

However, the empirical approach to optimisation of drug delivery systems can be time consuming and resource intensive, potentially also contributing to an increase in time to market. Theoretic predictions have been utilised as a means to evade these challenges. An example of these approaches is the Hansen Solubility Parameters (HSP) predictive tool. HSP was employed using two class IV drugs (curcumin and caspofungin), and their interactions with GCPQ constituents was analysed to guide experimental design. This showed unfavourable predictions despite evidence to support encapsulation capability of GCPQ.

Encapsulation experiments carried out with varying degrees of palmitoylation (DP) and quaternisation (DQ) showed data contrary to HSP predictions with EE of curcumin and caspofungin reaching 90% and 96% respectively. A thin film method was used and formulations characterised, with their accelerated stability in aqueous solution studied under two storage conditions for one week.

Upon oral administration *in vivo*, GCPQ-CFG 5mg/kg enhanced bioavailability to a comparable degree as caspofungin acetate, the soluble formulation of caspofungin, with plasma C_{max} values of 242±361ng/mL at a T_{max} of two hours. Biodistribution analysis showed trace amounts of caspofungin were also found in liver and heart tissues up to 12 hours post dosing at 20 ng/kg and 60ng/kg respectively. An oral CFG formulation has been prepared with the ability to increase oral bioavailability of drug systemically.

Impact Statement

The oral route of delivery is the ideal route of administration due to its flexibility in dosing, cost effectiveness and safety for a wide range of medications. However, physicochemical properties such as poor solubility, poor permeability and degradation in gut present challenges in oral formulation of drug compounds, particularly BCS class II, III and IV drugs. The ability to successfully achieve efficient systemic delivery of oral drug formulation is therefore dependent on a thorough understanding of the effects of a drug compound's physicochemical properties and their resulting biological effect. To facilitate drug delivery through the oral route, chemical modifications are sometimes employed. An example of this is seen in caspofungin acetate, where salt formation is employed. Despite the solubility challenge of caspofungin being resolved, oral bioavailability still proves to be a challenge hence, caspofungin acetate is still administered through intravenous injection. Various delivery systems have been employed to circumvent the challenge of oral bioavailability in preclinical studies and some clinical studies. While these showed promising results, there were limitations associated with approach, some of which resulted in failed clinical trials. This project aims to provide base knowledge for the prediction of designing efficient oral delivery systems for class IV drug molecules.

One of such delivery systems is the use of polymeric nanoparticles. We used -N-palmitoyl-N-monomethyl-N,N-dimethyl-N,N,N-trimethyl-6-O-glycolchitosan (GCPQ), a mucoadhesive, biocompatible, self-assembly nanoparticle in the formulation of hydrophobic drugs caspofungin and curcumin. This was done in attempt to increase oral bioavailability of caspofungin as it has been shown to have a similar effect on amphotericin B, another BCS class IV drug. Data from these studies showed a correlation between degree of structural modification of GCPQ and encapsulation ability of GCPQ-Drug formulation. This information can be useful to pharmaceutical industries and drug delivery researchers as it can help in predicting optimal polymer properties for future GCPQ formulations.

In vivo experiments using GCPQ-CFG showed comparable pharmacokinetics and biodistribution data to caspofungin acetate. Thus, this formulation improved obstacle of solubility for caspofungin and may be developed further to improve permeability

parameters in order to serve as an alternative to invasive intravenous injection. Caspofungin is currently only administered by the intravenous route which is associated with high costs, risk of infection due to invasive methods and higher risk of toxicities. Successful oral formulation of caspofungin will potentially have an impact in the clinical management of patients using caspofungin and perhaps other similar chemotherapeutic agents.

Acknowledgement

My PhD journey would not have been possible without the mentorship and guidance of my supervisors, Professor Andreas Schätzlein and Professor Ijeoma Uchegbu. Your moral support and scientific knowledge were especially crucial to my research and in developing my self-confidence.

I would also like to thank Dr Rui Lopez for helping me get started on my project and for providing invaluable advice, contributing to the progression of my work. I am extremely grateful to my GCPQrew colleagues in Lab 326 and 105 past and present: Dr Liisa Niitsoo, Savvas Dimiou, Ryan Mellor, Dr Asya Petkova, Dr Gang Li, Dr Uchechukwu Odunze, Dr Ilona Kubajewska, Corinna Schosser, Omar Mokrane, Andy Wan, and Dr Abdurahman Halwanii. I would like to especially thank Dr Moutaz Badr for not letting me lose the LCMS vs Akunna battle and Dr Alex Vaideanu for being a supportive and integral part of my *in vivo* experiments.

Finally, a special thank you to my family and friends for surviving my multiple mood swings while still choosing to support my journey.

List of Figures

List of Tables

List of Abbreviations

1H-NMR	Proton NMR
δ _	Chemical shifts
ACN	Acetonitrile
ANOVA	Analysis of variance
AUC	Area under the curve
Caco-2 +	Colon adenocarcinoma cell line
CFG	Caspofungin
CMC	Critical micelle concentration
Da	Dalton
dGC	degraded GC
DP	Degree of palmitoylation
DQ	Degree of quaternisation
dRI	Differential refractive index
DL	Drug loading
DLS	Dynamic light scattering
DMSO	Dimethyl sulfoxide
dRI	Differential refractive index
DVLO	Derjaguin, Verwey, Landau and Overbeek
EE	Encapsulation efficiency
ESI	Electrospray ionisation

FDA	Food and drug administration
FA	Formic acid
GC	Glycol Chitosan
GCPQ	N-palmitoyl-N-monomethyl-N, N-dimethyl-N, N, N-trimethyl-6-O-glycol-chitosan
GPC-MALLS	Gel Permeation Chromatography with Multi-Angle Laser Light Scattering
HCL	Hydrochloric acid
HPLC	High performance liquid chromatography
ICH	International Conference on Harmonisation
IS	Internal standard
IV	Intravenous
kDa	Kilo Daltons
LCMS	Liquid chromatography–mass spectrometry
LLOQ	Lower limit of quantification
LOD	limit of detection
LOQ	Limit of quantification
Mn	Number averaged molecular weight
MRM	Multiple reaction monitoring
Mw	Weight averaged molecular weight
MWCO	Molecular weight cut off
NaOH	Sodium hydroxide

NMP	N-methyl-2-pyrrolidone
NMR	Nuclear magnetic resonance
PBS	Phosphate buffer saline
PDI	Polydispersity index
PEG	Polyethene glycol
pGC	palmitoylated GC
P-gp	Permeability glycoprotein
PK	Pharmacokinetics
PLGA	Poly(lactic-co-glycolic acid)
PNS	Palmitic acid N-hydroxysuccinimide ester
PTFE	Polytetrafluoroethylene
PVA	Poly vinyl alcohol
QELS	Quasielastic light scattering
QPR	Ratio of quaternary ammonium to palmitoyl groups
RI	Refractive index
RP-HPLC	Reversed phase HPLC
SD	Standard deviation
SE	Standard error
SNP	Solubilising nanoparticle technology
Stks	Working stocks solutions

TEA	Triethylamine
TEM	Transmission electron microscopy
UK	United Kingdom
USA	United States of America
UV	Ultraviolet
WS	Working standards

1 Polymeric Nanoparticles as Oral Drug Delivery Systems

1.1 Introduction

Since the discovery of drug-receptor interactions in 1996, there has been a large focus on the production of novel drug compounds which interact with specific receptors to bring about desired changes in receptor activity (Lefkowitz, 2004). This approach is now used to define the efficacy of a drug compound as its ability to drive a significant biological response (Galandrin et al., 2007) in relation to ligand-receptor interaction. However, factors preceding ligand-receptor interactions are in fact equally important in determining efficacy and specificity and include the concentration of drug present at the site of disease and residual time before the drug is subjected to degradation. Drug delivery methods are therefore used to influence both these factors in order to optimise drug exposure at the site of disease and circumvent challenges created as a result of challenging physicochemical properties of a drug compound.

The specific delivery methods employed will depend on the route of administration. Examples of such delivery methods include parenterally e.g. by intravenous or subcutaneous injection, or, preferably through non-invasive methods. Non-invasive methods typically involve transdermal delivery which can be via the skin (Zhou et al., 2015) or various mucosal surfaces in the body. Alternative mucosal surface delivery intranasal or sublingual administration (Narang and Sharma, 2011), inhalation (Serralheiro et al., 2015), or via the gastrointestinal mucosa with the help of rectally administered suppositories (Jannin et al., 2014) and, most importantly, oral administration as capsule, table, or suspension/solution (Cyriac and James, 2014). In essence, the method of delivery for any drug compound has a significant effect on its efficacy (Bhagwat and Vaidhya, 2013).

Oral drug delivery is considered the ideal route of drug administration as it is patient friendly and allows for flexibility in dosing (Verma et al., 2010; Bromberg, 2008). Compared to parenteral delivery, there is a reduced risk of disease transmission as invasive techniques are not utilised (Kuper, 2008). Also, less expenses are incurred, and costs are reduced as no extra equipment such as needles, nurses and syringes are needed (M. Jensen and A. Paladino, 1997; Kuper, 2008).

However, a large proportion of therapeutic compounds such as peptides and polar molecules have physical chemical properties which result in poor solubility, poor absorption, and susceptibility to degradation in the gut (Goldberg and Gomez-Orellana, 2003). Hence, limiting their oral bioavailability in the body (Serrano et al., 2015a). In addition to that, there is an increased requirement for more specific interactions between drug and receptors. These may be achieved by chemical conjugation or physical complexation, leading to larger, more hydrophobic drug molecules (Al-Hilal et al., 2013) As a result, many potential therapeutic compounds are unsuccessful in early clinical drug developmental stages, contributing to the unmet clinical demand for therapeutic agents in areas such as antifungal infections and cancer (Peterson et al., 2007; Roemer and Krysan, 2014). There is therefore an urgent demand for the development of solutions to improve oral bioavailability of such therapeutic compounds, providing the opportunity for them to be used as medicines. One such approach is employing drug delivery systems to overcome the physical chemical limitations imposed by the drug; conceptually the interaction of drug and body are replaced by those of the drug with the carrier on the one hand, and those of the carrier with the body on the other hand. Drug delivery is an interdisciplinary approach that combines polymer science, bioconjugate chemistry, molecular biology and pharmaceutics (Bhagwat and Vaidhya, 2013). One method of improving oral bioavailability of therapeutic agents is through the use of drug carriers. These may be lipid, micellar or nanoparticle-based systems.

The potential use of nanoparticles-based drug delivery systems has gained much focus in recent times (Uchegbu and Siew, 2013) with particular emphasis on the use of polymeric nanoparticles. (Chaturvedi *et al.*, 2013). Extensive research has shown these particles have favourable properties such as biodegradability, high encapsulation efficiency, the ability to traverse the mucosal layer, biocompatibility and specificity for targeting tumour cells (Beloqui et al., 2016). In addition to that, some polymeric nanoparticles are highly modifiable and hence relatively easy to achieve desirable physicochemical properties, encapsulation efficiency and drug release profile (Plapied et al., 2011).

The use of polymeric nanoparticles as drug delivery systems will be further discussed with a focus on its application in enhancing oral drug delivery of hydrophobic drug compounds.

1.2 Challenges of Oral Drug Delivery

Biological barriers play a crucial role in the protection of the human body and segregating individual organs, so they are best suited to their functions (Kiptoo, Calcango and Siahaan, 2016). These act as a protection against damage by pathogens like bacteria and viruses and also pathogenic substances for example, toxins (Kiptoo et al., 2016)

The largest biological barrier is the skin which protects the human body from its environment. The blood brain barrier is a more specific barrier which utilises selective permeation in protecting the brain from unwanted molecules present in the blood stream. The intestinal mucosal layer works in a similar way by acting as a filter which prevents pathogens and toxins from infiltrating the blood stream (Kiptoo et al., 2016). Although, these barriers exist as a means of protection from pathogens, they also create a barricade for successful drug delivery of oral drug compounds.

A concise understanding of structure as well as interactions between biological barriers like the mucosal layer and compounds which traverse these barriers is essential in the design of drugs intended to possess permeability properties. To traverse the mucosal layer, a drug compound must first dissolve in aqueous solution as the content of the gut is of course mostly aqueous. Dissolved drug is then required to partition through the cell membrane and into the cytoplasm. Following that, drug is expected to cross the basolateral cell membranes to allow access into the body's systemic circulation. Simultaneously, the drug compound must be able to evade biochemical barriers such as metabolising enzymes which target and degrade foreign substances (Kiptoo et al., 2016). To enhance absorption characteristics of drug compounds, all these factors must be taken into consideration during the process of drug design (Kiptoo et al., 2016).

1.2.1 Physiological Barriers

Gastrointestinal tract (GIT) anatomy

The digestive tract which extends from the mouth to the anus is lined by an epithelium associated with accessory organs and glands which aid in the digestive process. The GIT is divided into four layers namely, the mucosa, submucosa, muscularis and serosa. The mucosa is the innermost layer, which is made up of loose connecting tissue called lamina propria as well as an outer smooth muscle layer called muscularis mucosae. The primary function of these epithelial cells is absorption and may be specialised, depending on their location in the GIT. An example of this is seen in the mucosa of the intestine where modifications such as villi, pilcae increase surface area for absorption and other modifications such as crypts and goblet cells secrete mucus.

Molecules absorbed through the mucosa enter the blood vessels of the submucosa. This is a thick and highly vascular layer. Beyond the submucosa is the muscularis, a thick layer of muscles containing an inner layer of circular smooth muscle and an outer layer of longitudinal smooth muscle. The myenteric plexus is also located within the muscularis and is responsible for peristaltic movement within the GIT. The serosa is an avascular connective tissue layer which provides support and protection to the GIT. As the GIT progresses from the mouth to the anus, it may be divided into 7 different sections based on functionality of each region. These regions and associated functions are; the mouth for ingestion, the pharynx for mastication of ingested food, the oesophagus for propulsion of ingested food into the canal, the stomach for secretion of enzymes and digestive juices, the small intestine, the large intestine for absorption and the anus for elimination of waste (van de Graff, 1986).

Digestion of starch begins in the mouth and is aided by the production of amylase. The pharynx and oesophagus then present a pathway for the transfer of food to the stomach. Within the stomach, ingested food is churned and masticated while enzymes are released to convert food into chyme. It is in the stomach that protein digestion begins with the help of hydrochloric acid and pepsin enzyme. Here, mostly water, weak acids, alcohol and basic drugs such as warfarin are absorbed. The stomach then moves chyme into the small intestine, where majority of digestion and absorption of nutrients, water and electrolytes occur. The small intestine is divided into three sections known as the duodenum, jejunum and ileum, all lined with tiny projections

called the villi. Surface area for absorption, particularly in the jejunum and ileum of the small intestine is increased with the help of the villi. Epithelial cells lining the villi release protease and carbohydrase which aid in the final stage of digestion of proteins and carbohydrates. The large intestine is the final site for absorption of electrolytes, water and vitamins such as vitamin K and B12. It also propels faeces towards the anus for elimination (Tate et al., 2003)

The Mucus Layer

Prior to its arrival at the epithelial cell surface, drug compounds are required to traverse the mucous membrane lining the gastrointestinal tract (Fricker and Drewe, 1996). This is a moist surface which lines various body cavities. One of such examples is the gastrointestinal and respiratory tract (Boddupalli et al., 2010). Its structure consists of one or more epithelial cells overlaying a layer of loose connective tissues known as the lamina propria. Within the stomach, bronchi, small and large intestines, there is a single epithelial layer. However, the vagina, cornea and oesophagus have multiple layers of stratified epithelial layers. In both instances, epithelial layer is constantly being protected by a layer of mucus secreted by specialised glands such as goblet cells or salivary glands (Boddupalli et al., 2010).

The luminal side of the gastrointestinal tract is overlaid by a layer of aqueous mucin secreted by the goblet cells within the mucosa. This structure comprises of glycoproteins known as mucin which contributes towards the structure and function of the mucus layer (Fricker and Drewe, 1996). Mucin is believed to offer protection to epithelial cells by at least three different mechanisms; Firstly, by creating a gel viscous enough to serve as a physical barrier to the underlining epithelia. Secondly, mucin can facilitate specific interactions by binding to proteins, infectious agents, and luminal molecules. Lastly, mucin disposes of molecules which are cross linked with it, by transforming from an immobile viscous gel to mobile, and soluble glycoproteins which flows along the length of the epithelial membrane carrying entrapped harmful molecules into the stomach for degradation. Here, entrapped molecules are destroyed by enzymatic activity with a turnover of approximately 12-24 hours (Fricker et al., 1992; Forstner et al., 1984). To overcome the mucus barrier, a drug molecule is required to traverse approximately 100-500 μm of the mucus layer (with an exclusion size of 600-800 Da which allows it to act as a molecular filter, before crossing the epithelial cells layer underneath (Fricker and Drewe, 1996).

An advantage of mucin's networks is that it allows for selective permeability. This means that it is able to control to some degree what permeates its viscous layer by influencing diffusional properties of molecules via steric obstruction or adhesive interactions such as ionic interactions, hydrophobic interactions, hydrogen bonds, and size exclusion based on its mesh sizes (Authimoolam and Dziubla, 2016). So, it remains a physical barrier which needs to be overcome due to its effect on drug permeability and therapeutic availability (Authimoolam and Dziubla, 2016). Multiple efforts are now being made following recent advancements in nanomedicine to minimize nanoparticle interactions which hinder permeation of the mucin barrier (Coaker, 2014).

Underneath the mucus layer are epithelial cells joined together by tight junctions which form an added barrier against systemic delivery of oral drugs (Laksitorini et al., 2014). These are composed of enterocytes, goblet cells, paneth cells and endocrine cells. The villi are lined with this same epithelial layer to increase surface area of absorption of digested food in the small intestine into the systemic circulation (Kiptoo et al., 2016).

Transporters and Efflux Pumps

Transporters are located along the membrane of the intestinal layer and aid in the transport of molecules such as peptides, which would otherwise not be able to traverse the membrane. As this often occurs against a concentration gradient, the transport is said to be energy dependant (Liu and Liu, 2013) and is usually paired with the co transport of a second molecule. The transport of molecules such as peptides, amino acids, nucleotides and other nutrients is facilitated through this mechanism. Examples of these transporters are oligopeptide transporter (PepT1) which is of scientific interest as it plays a role in the uptake of peptide-like drugs (Terada et al., 2004).

In contrast to that, efflux pumps also exist along the length of the intestinal layer. An example of such transporters is the P-glycoprotein (Pgp) (Wagner et al., 2001; Tournier et al., 2011). Its main function is to inhibit membrane partitioning of peptides and small molecules by returning drug into the lumen where they are subjected to enzymatic metabolism (Kiptoo, Calcango and Siahaan, 2016). With reference to drug molecules, tertiary and hydrophobic aromatic amines present on the molecule serve as characteristic recognition sites for the efflux pump (Kiptoo et al., 2016). As the duodenum transitions into the ileum, the concentration of Pgp increases (Martinez et

al., 2002) hence intensifying the rate of efflux of drug, making it another barrier to overcome.

1.2.2 Biochemical Barriers

Bile

The gallbladder stores bile, a mixture of inorganic and organic molecules, mostly comprising bile salts (BS). BS (Figure 1-1) are amphipathic biosurfactants which means they possess both hydrophobic and hydrophilic moieties, made up of a rigid steroid nucleus with a linked aliphatic side chain (Maclerzanka et al., 2011). Bile not only functions as an excretory secretion by breaking down fat through the process of emulsion (shown in Figure 1-1), bilirubin and other waste products but, it also acts as a digestive secretion by promoting lipid absorption through micelle formation in the proximal small intestine (Hofmann and Eckmann, 2006). Bile acids are not solubilised alongside lipids but instead, transported into the distal small intestine where an active transport system in the epithelial cells of the terminal ileum is used to ensure its efficient absorption. This allows for bile to be recovered, recycled and recirculated multiple times during ingestion of food (Hofmann, 1989). Following the active transport of bile salts into the epithelium, bile salts are involved in extensive enterohepatic circulation, resulting in recycling of conjugated bile salts. This way, large amounts of bile salts are maintained for digestion (Hofmann, 1989) The transport system of bile salts has since been explored in the design of delivery systems to improve intestinal absorption while also maintaining therapeutic concentrations in systemic circulation (Sievänen, 2007; Fricker et al., 1992).

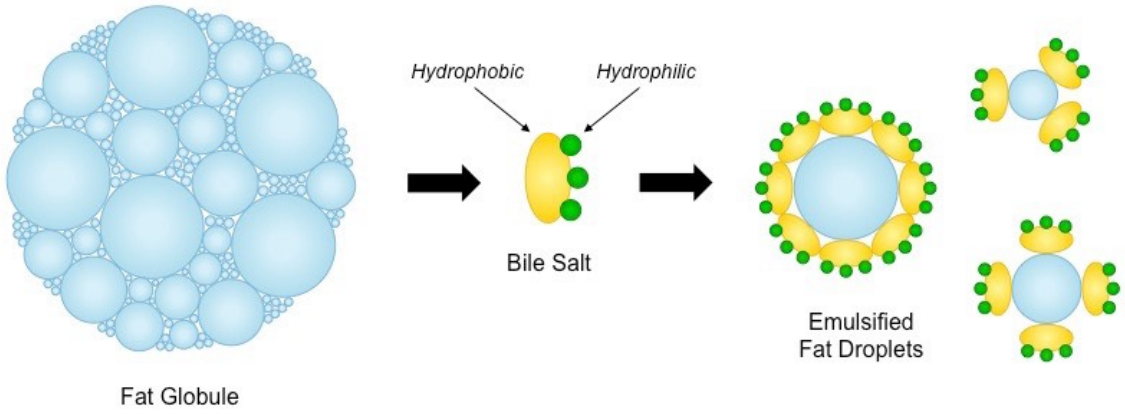

Figure 1-1: Schematic diagram of emulsification of fat using bile salt (Cornell, 2016)

Digestive Enzymes

Following oral administration, drug compounds are faced with acidic secretions within the lumen of the stomach known as gastric juice. This secretion has pH ranging from 2-5 and contains proteolytic pepsin and hydrochloric acid, which subjects drug compound to chemical degradation (Fricker and Drewe, 1996). A second metabolic barrier exists within the upper small intestine where, luminal enzymes known collectively as pancreatic proteases are secreted into the duodenum. These consist of chymotrypsin, trypsin, carboxypeptidase A and B and elastase, and degrade 30-40% of small peptides and large proteins within 10 minutes of contact (Fricker and Drewe, 1996). Optimum activity of proteolytic juices is at a pH of 8 which is the pH of the small intestine, maintained by the constant release of sodium bicarbonate from the pancreas (Fricker and Drewe, 1996).

A further enzymatic barrier is the presence of peptidases on the brush boarder of enterocytes. The activity of peptidases on the brush boarder increases along the length of the upper duodenum and into the lower ileum. These enzymes are responsible for the degradation of smaller peptides usually ranging from dipeptides, selected for by cytosolic peptidases to tetrapeptides, selected for by brush border peptidases (Fricker & Drewe, 1996).

Enzyme activity is therefore a crucial factor to consider when developing drug delivery systems particularly where the drug is a substrate of a digestive enzyme. Strategies such as structural modification of peptides can be utilised to evade enzymatic activity on drug molecules. This may involve molecular conjugation, as observed in PEGylation of proteins (Veronese and Pasut, 2005), co-administration of drug compound with peptide inhibitors (Lee et al., 1991), protecting the C-terminal carboxyl and N-terminal amino groups on proteins (Gupta et al., 2011) and encapsulation within nanoparticles (van der Lubben et al., 2001). Alternatively, drug delivery systems can be made to target the colon as enzymatic activity decreases along the intestine and reaches a negligible activity in the colon, where drug permeation is good (Lipka et al., 1996). The drug therefore would bypass the enzymatic degradation through this route; however, the microbial populations of the large intestine provide their own bioactive milieu.

1.2.3 Physicochemical Properties of Drug Compound

In addition to the properties of the gastrointestinal tract, the physicochemical properties of the drug molecules can also pose challenges for oral bioavailability. Lipinski attempted to describe the ideal drug properties required to achieve good solubility and absorption using his rule-of-five theory (Kirkpatrick, 2003). This states that drug compounds are more likely to have high solubility and absorption rates when log P is less than 5, molecular mass is less than 500 Daltons and there are less than 5 hydrogen bond donors (determined by the sum of OHs and NHs within the compound) but, more than ten hydrogen bond acceptors (determined by the sum of oxygens and nitrogens within the compound) (Lipinski et al., 2001). These factors mostly influence physicochemical properties such as drug dissolution rate, enzymatic degradation and drug solubility which in turn determines the bioavailability of drug compound in the body. While a certain degree of hydrophilicity is required to allow drug solubilisation in the *in vivo* aqueous environment, it is also necessary for drugs that they possess a degree of hydrophobicity to traverse the lipid layers e.g., of cell membranes (Waring, 2010).

Thus, the water solubility of a drug compound is one of two crucial limiting factors that affects its rate of absorption *in vivo*. The other being the rate of drug permeation across membranes. Hence, the solubility of a drug compound in aqueous environments is often an indication of its dissolution rate so, drugs which have low solubility will also tend to have slower dissolution rates. This in turn reduces the rate of absorption (Khadka et al., 2014). Both solubility and permeability have been used as predictive tools for oral absorption of drug molecules in the Biopharmaceutics Classification System (BCS) (Wu and Benet, 2005).

The BCS (Figure 1-2) was introduced in 1995 as an experimental system aimed to investigate drug permeability and solubility under prescribed concentrations of orally administered drugs (Wu and Benet, 2005). It utilised transport models and human drug permeability data to investigate the importance of solubility and permeability on oral drug absorption by estimating *in vivo* absorption rates (Amidon et al., 1995). Since the BCS discovery, drugs have been classified into one of four biopharmaceutical classes based on both parameters (Figure 1-2).

The four groups as defined by the Biopharmaceutical Classification System (BCS) are as follows (Amidon et al., 1995):

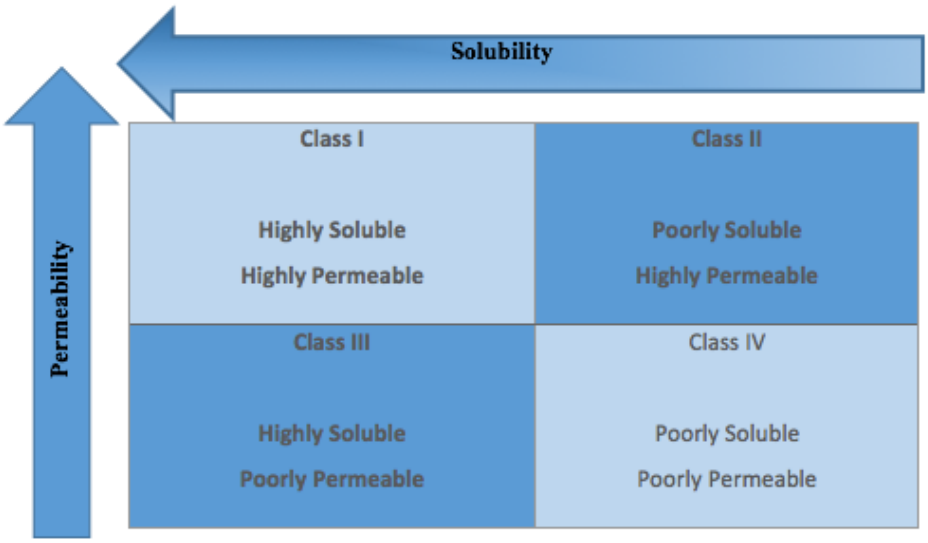

Figure 1-2: Biopharmaceutics Classification as defined by Amidon et al (Amidon et al., 1995)

Class I – High Solubility/High Permeability: These types of drugs are efficiently absorbed although, they may have low systemic availability as they are subjected to first pass metabolism. Drug dissolution is therefore a rate limiting step for drugs in this category (Amidon et al., 1995). In the event of rapid dissolution, gastric emptying presents itself as the new rate limiting step because absorption is more efficient in the small intestines due to the large surface area. Hence, a quicker gastric emptying rate would result in faster absorption (Heading et al., 1973). Consulting drug dissolution profiles of drugs in this class is therefore essential in optimising drug bioavailability (Amidon et al., 1995).

Class II – Low Solubility/High Permeability: Just like in Class I drugs, a dissolution profile is essential as here, the dissolution is considered the main rate limiting step while high absorption rates mean that drug molecules are rapidly taken up once in solution (Amidon et al., 1995).

Class III – High Solubility/Low Permeability: The rate limiting step for drugs in this category is gastrointestinal permeability. While an accurate definition of a dissolution profile may be helpful, there are additional factors which contribute to the optimisation of drugs in this class. For example, rate and extent of drug absorption is dependent on varying environments present in the luminal content, gastrointestinal transit, and membrane permeability (Amidon et al., 1995).

Class IV – Low Solubility/Low Permeability: This class of drugs all share significant problems which hinder effective oral delivery. Amidon predicted drugs classed under this group will depend on individual limitations used for permeability and solubility classifications in the future (Amidon et al., 1995).

For drug compounds which are weak acids or weak bases with different ionisation constants (Ka), solubility will be dependent on the pH of the surrounding solvent and the pKa of the drug compound. Weak basic drugs have increased solubility as the pH decreases while weak acids increase in solubility as pH increases. This means that weak acid drugs such as aspirin will be less ionised in gastric pH and hence, absorption is at an optimum in the stomach, while weak bases like ephedrine will experience the exact opposite in gastric environments (Mitra and Kesisoglou, 2013).

Where less favourable properties make dissolution challenging, particle size reduction is a strategy which has been employed for years in attempt to improve the dissolution of drug compounds (Khadka et al., 2014). This is because decreasing particle size increases the surface area of the molecule, therefore increasing surface area to volume ratio and resulting in more rapid solvation. Particle sizes ranging 3-5 μm have been shown to enhance dissolution rates therefore, micronization efforts are sometimes employed to achieve smaller particle sizes (Hörter and Dressman, 2001). Alternative methods such as high-pressure homogenisation, cryogenic spray process and more recently, nanoparticle encapsulation have since been employed to achieve a reduction in particle size of drug compounds.

Overall, with knowledge from the BCS, drug design scientists can manipulate NCE structures and physicochemical properties to attain lead compounds with more desirable therapeutic effects (Chavda et al., 2010). In another instance, the classification using the BSC enables more targeted drug development phase to increase both bioavailability and permeability of drug depending on their classification.

1.3 Strategies to Overcome Oral Drug Delivery Challenges

Development of oral formulations requires a thorough understanding of limitations associated with this route of delivery. A major contributor to these limitations is drug solubility, which contributes to low oral bioavailability of hydrophobic drug compounds (Boyd et al., 2019). A range of solutions to overcome this limitation have been developed and utilised in oral drug development stages. Some of these solutions will be discussed below.

1.3.1 Crystal Engineering

Crystal engineering involves the utilisation of noncovalent interactions between molecular or ionic components for the rational design of solid-state structures, in this case drug delivery systems (Subramanian and Zaworotko, 1995). Applications of crystal engineering can be seen in the formation of metastable polymorphs. Effects of crystalline modification was first defined in the late 1960's where metastable polymorphs were shown to greatly improve absorption *in vivo* (Aguiar et al., 1967). Improvement of absorption may then be exploited to enhance absorption and bioavailability of poorly soluble drugs. One main advantage of crystal engineering is only minimal amounts of polymer and surfactants are required for formulation stabilisation. This way, high drug loading and high energy systems are achieved, which are both beneficial in drug dissolution (Blagden et al., 2007; Varshosaz et al., 2018). Challenges affected with crystal engineering is in drug-polymer miscibility and excipients compatibility for the chosen drug. Often times, storage may prove difficult due to physical instability of crystal formed (Blagden et al., 2007; Varshosaz et al., 2018).

1.3.2 Chemical Modification

Within the chemical modification approach, drugs may be subjected to formation of prodrug or simple salt formation. Prodrugs are compounds which are biologically

inactive but, may be transformed into active compounds by chemical or enzymatic reactions (Ettmayer et al., 2004; Rautio et al., 2008). The use of prodrug approaches presents a range of pharmaceutic benefits such as; increased chemical and metabolic stability, improved aqueous solubility, improved lipophilicity, enhanced transporter-mediated absorption (Müller, 2009). All of which can improve on the drug's ability to achieve site-specific delivery. This approach has been utilised in Fosamprenavir, the phosphate prodrug of HIV protease inhibitor, amprenavir (Vierling and Greiner, 2003). Here, solubility of Fosamprenavir is increased by 10-fold, resulting in higher bioavailability (Vierling and Greiner, 2003). Despite realised benefits of prodrug formation, the high probability of degradation and poor chemical stability contribute to the limitations associated with prodrug screening and development (Sanches and Ferreira, 2019).

Salt formation is an alternative strategy within chemical modification of drugs and is used to enhance absorption of weak acidic and basic drugs (Serajuddin, 2007). It is based on the principles that the salts of a weak acidic and basic drug have higher solubility than the pure forms. Hence, the pH may be adjusted in order to increase the apparent intrinsic solubility of a drug (Serajuddin, 2007). Salt formation benefits from its ability to increase solubility, often by an order of three magnitude (Elder et al., 2013) and dissolution rates without extensive chemical modification of drug molecule. In addition to that, salt formation has an easy synthesis process and low cost of raw materials (Paulekuhn et al., 2007) however, it is not without drawbacks. A major drawback of this method is the requirement of ionizable groups in drug molecule (Boyd et al., 2019). This means that methods are limited to weak acid and weak basic drugs so, unsuitable for neutral drug compounds. Finally, the trial-and-error process involved in determining the optimal salt form of drug candidate (Boyd et al., 2019).

1.3.3 Amorphization

Ideal amorphous solid dispersions are defined as a glass solution containing poorly soluble drug within an amorphous carrier, representing a single-phase amorphous system (van den Mooter, 2012). This solid dispersion provides increased stability and protection of drug. during formulation process. Both solubility and dissolution rates are enhanced in this process compared to with traditional crystal modification.

Amorphization techniques can be grouped into three main categories; 1) mechanical energy input methods involving different types of mills and wet granulation (Descamps and Willart, 2016), 2) solvent methods involving anti-solvent techniques, lyophilisation and spray drying(Singh and van den Mooter, 2016) and 3) melt methods involving hot-melt extrusion (Sarode et al., 2013; Vasconcelos et al., 2016). Each method presents benefits and limitations (Vasconcelos et al., 2016).

The major disadvantage of amorphous solid dispersions is their thermodynamic instability although, stabilisation may be achieved using hydrophilic polymers (Ubbink, 2016). These polymers form molecular dispersion within the drug hence, limiting mobility of drug molecule and eventual crystal growth as well as nucleation (Liu et al., 2015). Resulting formulation leads to supersaturation in GI fluid, creating a higher concentration gradient and increased dynamic force for drug transport across cell membrane. This approach is commonly used for BCS class II drugs which have dissolution rate-limited absorption (Serajuddin, 2018). An application of amorphization technique was used in a study involving celecoxib, a BCS class II drug formulated with polyvinylpyrrolidone. Here, amorphous formulation dramatically increased drug dissolution rate compared to the crystalline drug (Knopp et al., 2018) following oral administration in rats.

1.3.4 Drug Carrier Systems

Lipid Based Formulations

Lipid-based formulations are non-immunogenic, biocompatible formulations which can stimulate the secretion of phospholipids, bile salts and cholesterol. Therefore, forming vesicles and micelles that in turn facilitate drug absorption *in vivo* (Pouton, 2000). BCS class II and IV greatly benefit from this method of formulation due to their poor aqueous solubility. Lipid based formulations may be classed into subgroups based on their individual composition, chemical characteristics and size. Some examples of these subgroups are lipid nanoparticles, liposomes, niosomes and nano emulsions (Hauss, 2007). Lipid-based carriers may deliver small hydrophobic molecules through a range of mechanisms. One of such mechanisms is through the enhancement of dissolution rate and solubility in the GI tract. This occurs as a result of lipid digestion in the

stomach, leading to emulsification of drug prior to duodenum emptying. The pancreatic enzyme, lipase is then secreted alongside co-lipase in order to facilitate metabolism of glycerides to diglycerides, monoglycerides and fatty acids. It is the presence of these fatty acids in the intestine that stimulates biliary secretion from the gall bladder therefore, leading to lipid digestion yield being assembled into a colloidal structure. Colloidal structures are therefore able to increase solubilisation in the intestine as well as contribute to enhanced absorption (Hauss, 2007; Savla et al., 2017). Overall, lipid-based formulation maintains high drug concentration gradient, facilitating diffusion of drug across aqueous layer and eventually, the mucosal membrane (Hauss, 2007; Lee, 2020). Lipid-based systems are also able to protect poorly soluble drugs from enzymatic degradation.

Lipid-based carriers such as liposomes have been observed to be absorbed whole through the lymphatic system by pinocytosis (Lee, 2020). Oral drugs like cyclosporin benefit from this process as lymphatic transport of liposomal formulation occurs through the mesenteric lymph, therefore avoiding hepatic first pass metabolism(O'Driscoll, 2002). Further evidence on liposomal transport shows lipid-based formulations can inhibit the P-gp efflux transporter (Sachs-Barrable et al., 2007), presenting a huge benefit to BCS class IV drugs which are major substrates of the P-gp pump, e.g. paclitaxel (Wang et al., 2014).

Although lipid-based drug carriers present a potential solution to BCS class II and IV oral drug delivery, achieving and maintaining ideal characteristics such as particle size, drug release kinetics and drug loading is difficult (Phan et al., 2014). The problem of low drug loading is observed particularly in brick dust molecules e.g. itraconazole, which is has low aqueous and lipid solubility. One way of overcoming this challenge is by adapting the hydrophobic ionic liquids concept, where drug is dissolved in nicotine acid-based ionic liquids before being reformulated in lipid-based formulations (Williams et al., 2014). Another major drawback of this method of drug delivery is poor physical and chemical instability, resulting in short shelf life (Alqahtani et al., 2021).

Micelles

Drug solubility may be enhanced by encapsulating poorly soluble drug compound in surface-active agents called copolymers. These copolymers assemble into micelles when the concentration of surfactant is above their critical micellar concentration (CMC) (Bromberg, 2008). Amphiphilic copolymers consist of a hydrophobic moiety

which forms the core of the micelle and a hydrophilic moiety which forms the external shell of the micelle. Through hydrogen bonding, the water molecules are able to interact with the hydrophilic copolymer heads, forming a lattice structure around the molecule. It is this lattice structure that establishes the micelle shape (Hwang et al., 2020). Micelles are often used to solubilise lipophilic drugs through encapsulation (Gaucher et al., 2005). An example of this is in the micellar formulation of fenofibrate, a hypercholesterolemia drug. Here, pH sensitive micellar formulation was used to improve oral bioavailability by 15% compared to its coarse suspension (Sant et al., 2005). In instances where micelle formation is unable to occur instantly, methods are employed to encourage micelle formation process. These include thin film method, change in ionic strength or pH of the solution and direct dissolution (Simões et al., 2015).

Drawbacks of micellar drug carriers are poor *in vivo* stability below critical micelle concentration and low drug loading (Zhang et al., 2017; Keskin and Tezcaner, 2018).

Nanoparticles

Nanoparticles are particles that range between 10 – 1000 nm in size (Mohanraj and Chen, 2006). When employed as delivery systems, nanocarriers are solid, colloidal particles and are usually synthesised from materials such as polymers (Cho et al., 2008; Biswas et al., 2014). These nanoparticles delivery systems have been developed to overcome some of the recurring challenges for oral administration. Typically, nanoparticles for oral drug delivery can be dispersed as colloids in aqueous media while creating an internal hydrophobic environment in which hydrophobic drugs can be encapsulated at high concentrations. An added benefit of nanoparticle carriers is their ability to carry a range of agents for diagnosis and therapy and release them in a controlled manner; these include peptides, nucleic acids and proteins.

Examples of nanoparticles being utilised in pharmaceutical formulations are magnetic nanoparticles, lipid-based nanoparticles (solid lipid NPs) and polymeric nanoparticles (Cho et al., 2008). The use of polymeric nanoparticles will be explained below.

Polymeric Nanoparticles

Polymeric nanoparticles are nanoparticles synthesised from either natural or synthetic polymers (Hillaireau and Couvreur, 2009). Natural polymers commonly used in oral drug delivery are dextran, chitosan and alginate while common synthetic based

polymers include polyactide-coglycolide (PLGA), polylactide (PLA)and polycaprolactone (PCL) (Ritika and Aggarwal, 2012). These nanoparticles are synthesised using various approaches based on the cargo being carried and the intended application. Pharmaceutical, biochemical, electrical, optical or magnetic characteristics of the particle are other parameters to consider during the synthesis process (Kothamasu et al., 2012).

Polymeric nanoparticles work by reducing drug particle size to the nanometre range, hence creating a larger surface area which in turn enhances both drug dissolution rate and drug solubility (Mei et al., 2013). An example of this is in silica-based resveratrol nano formulation. Here, drug particle was reduced to 90 nm, resulting in enhanced solubility, permeability and anti-inflammatory activity of encapsulated resveratrol (Juère et al., 2017).

Polymeric nano capsules

Polymeric nanoparticles may be defined as polymeric nano capsules (Jäger et al., 2007) when they possess a core-shell structure where drugs can be encapsulated and a polymer membrane surrounding the core (Mohanraj and Chen, 2006). The characteristics of encapsulated drug may vary depending on the composition of nano capsule core-shell. This means that a nano capsule with a hydrophobic core is more likely to encapsulate hydrophobic drug compounds and a nano capsule with a hydrophilic core-shell is more efficient at encapsulating hydrophilic drug compounds.

Methods employed in the synthesis of nano capsules include but are not limited to polymer coating, emulsion-diffusion, double emulsification techniques and nanoprecipitation (Mora-Huertas et al., 2010). Final method being employed determines the characteristics of final nano capsule and the type of drug compound which can be encapsulated (Mora-Huertas et al., 2010). Methodology will therefore depend on intended use of nano capsule.

The most common method of nano capsule formation is nanoprecipitation, where polymer and drug are initially dissolved in an organic, water miscible solvent. Organic solvent is then precipitated in water, forming oily colloidal systems with drug entrapped within oil core and surrounded by polymer bilayer (Radhika and Sivakumar, 2011). Stabilisers are often added to formulations to reduce the surface tension of the water, promoting miscibility (Nagavarma et al., 2012). Organic polymers such as

polycraprolactone (PCL) and poly (lactide) (PLA) are typically formulated using this method (Pohlmann et al., 2008; de Assis et al., 2008).

These polymeric nano capsules have been extensively studied for enhanced oral drug delivery and have been shown to increase bioavailability of drugs. In one study, oral polymeric nano capsule formulations were created for the controlled release of cyclosporin. Here, poly-dl-lactide (PDLLA) was used in this approach and a significant increase in drug availability was observed in nano capsule formulation compared to con-encapsulated formulation (Park et al., 2013). Another study showed lychnopholide encapsulated in PEG-PLA nano capsules and PCL nano capsules attained significantly higher cure rates in trypanosoma cruzi infected rats compared to non-capsulated lychnopholide (de Mello et al., 2016). Alternative benefits include reduction of unpleasant side effects. This occurs because drugs can be encapsulated at a reduced dose as nano capsules are able to protect from degradation *in vivo* (Radhika and Sivakumar, 2011).

Physicochemical Properties of Nanoparticles and Effect on Biological Properties

Size

Formulation of sub-micron sized particles is of particular interest in drug delivery nanotechnologies as it has been observed to increase drug absorption with decreasing size (Desai et al., 1996). One study supporting this theory investigated mucin permeability of carboxylate-modified latex particles of increasing diameter. There was a negative correlation between increasing particle diameter and permeability (Norris and Sinko, 1997). Another study on the influence of particle size on the uptake of FITC-MSNs by HeLa cells showed that uptake of nanoparticle is particle-size-dependent, with the optimum uptake rate achieved at 50nm (Lu et al., 2009). Another example is observed in polystyrene latex studies, where particle sizes ranging from 50-100nm were transported at a faster rate than larger particle sizes. With particles greater than 1μm found entrapped within Peyer's patches (Jani et al., 1990).

Surface Charge

In addition to nanoparticle size, the surface charge of particles has been shown to influence degree of interaction with mucin and epithelial cells. Mucin comprises a carbohydrate side chain, rich in negatively charged sialic acid and sulphates which form electrostatic interactions with positively charged particles (Bruschi and de Freitas,

2005). Studies have shown that cationic polymers with high valence have stronger binding interactions to porcine gastric mucus (Crowther and Marriott, 2011), establishing a proportional relationship between degree of binding and charge density of the polymer (Park & Robinson, 1984). It is these same electrostatic interactions that is suggested to be the main source of mucoadhesive properties in chitosan-based nanoparticles (Sogias et al., 2008).

The cell membrane consists mostly of a negative charge and so, is expected to only favour positively charged particles through electrostatic interactions. This, however, is not the case as negatively charged particles are also internalised but, at a slower rate than positively charged particles (Cho et al., 2009). It has been hypothesised that the process of cell internalisation of negatively nanoparticles is due to nonspecific binding and clustering of particles at cationic sites on the plasma membrane. These sites are relatively scarce and so, contribute to the slow cellular uptake (Verma et al., 2010). Cationic particles on the other hand, bind readily to anionic groups on the cell membrane through electrostatic interactions, resulting in internalisation. Charge density of a particle not only influences method and rate of cell internalisation, but also the eventual fate of nanoparticles. Example cases of effect of charge density can be seen in research carried out by Chung et al. It was demonstrated that actin and clathrin dependent endocytic mechanism was observed in silica nanoparticles at lower charge density. Although both mechanisms were bypassed with an increase in charge density of nanoparticles (Chung et al., 2007).

Potential benefits of Polymeric Nanoparticle Systems for oral delivery in the GIT

Polymeric nanoparticle systems allow for the optimisation of drug delivery mechanisms as it is able to encapsulate and therefore, allow the oral delivery of poorly soluble drug compounds. Also, nanoparticles may be modified to have higher affinity for specific regions in the GI tract hence, integrates an aspect of specificity through targeting. Due to their ability to traverse the mucosal membrane through transcytosis, nanoparticles can transport encapsulated drug compounds across biological membranes therefore, overcoming the mucin barrier (Farokhzad and Langer, 2009). This is particularly beneficial to BCS class III and IV drugs.

Micelle Stability in GI Tract

Within the GI tract, polymeric nanoparticles encounter physicochemical conditions. These include biological fluids which aim to destabilize particles before they interact with the membrane. Degradation of polymeric micelles is possible in the presence of enzymes, bile salts and extreme pH levels, conditions identical to that of the GI tract (Plapied et al., 2011). Stability would then depend on the composition of the nanocarrier. If nanoparticles are synthesised with insoluble polymers, they would not be subjected to rapid degradation or release of encapsulated drug (Singh and Lillard, 2009).

Amphiphilic polymers can self-assemble above their critical micellar concentration (CMC) into micelles (Plapied et al., 2011). Their hydrophobic moiety forms the core of the micelles and creates a site for encapsulation of hydrophobic drug molecules. Thus, drugs that are encapsulated in a nanocage are effectively protected from premature enzymatic degradation (Bhagwat and Vaidhya, 2013) also, solubility of poorly soluble drugs is increased (Gaucher et al., 2010). Ideally for oral delivery systems, polymeric micelles must self-assemble in aqueous solution, enhance drug solubility, remain stable in the GI tract, be biocompatible and non-toxic as well as relatively easy to synthesise in large scale (Plapied et al., 2011).

Mucoadhesion

Drugs which encounter the mucosal layer are usually efficiently eliminated by mucus clearance mechanisms hence, polymeric nanoparticle systems can be used to adhere to the mucosal layer and eventually traverse it (Tang et al., 2009). Mucoadhesion is driven by a combination of strong hydrogen bonding, Van Der Waals interactions, hydrophobic and electrostatic interactions (Lai et al., 2009) so, it is expected that surface charge of nanoparticle plays an important role in uptake.

To increase interactions between nanoparticle and the mucosal layer located on the intestinal membrane, surface modification is considered. For example, PEG could be grafted on to the surface of a nanoparticle to increase its hydrophilic nature or chitosan may be used to increase bioadhesive properties. It is also possible to graft ligands such as glycoproteins antibodies and peptides to the surface of nanoparticles to increase specificity of the nanoparticle (des Rieux et al., 2006). Overall, nanoparticles are widely modifiable.

Polymeric nanoparticles, particularly micelles can undergo modulation of their physicochemical properties such as hydrophobicity and surface charge which directly influences their extent of drug loading, drug release profile and biological behaviours. The ability to extensively modulate these particles makes them suitable systems for oral drug delivery (Galindo-Rodriguez et al., 2005). Nanoparticles are generally more stable in the GI tract compared to colloidal nanocarriers such as liposomes. They can enhance drug absorption by protecting drug from unfavourable conditions in the GI tract, elongating residual time in the gut by mucoadhesive mechanisms, endocytose particles and/or permeate the membrane. This is possible due to physicochemical parameters such as particle size, polymer nature and hydrophobicity of particle (des Rieux et al., 2006).

1.4 Uptake of Nanoparticles

The uptake of nanoparticles by epithelial cells occurs either via the paracellular route or transcellular route (Conner and Schmid, 2003). Both pathways are outlined in Figure 1-3.

1.4.1 Transcellular Transport

Transcytosis is an energy dependent strategy employed by cells to regulate the transport of macromolecules across the membrane (Odds et al., 2003). Factors such as cell type, type of cargo being transported and mechanism involved all influence the transcytosis process (Gao et al., 2008). At the intestinal epithelium, the process of transcytosis begins with clathrin-mediated endocytosis performed by both enterocytes and M cells of Peyer patches (Florence and Hussain, 2001; Lavelle et al., 2000).

Internalisation of extracellular molecules within the cell occurs through a process called endocytosis. Endocytosis can occur via different pathways such as macropinocytosis, caveolea-mediated phagocytosis, clathrin-mediated endocytosis and clathrin-/caveolae-independent endocytosis (Conner and Schmid, 2003). In respect to transport of orally administered drugs, much focus is placed on clathrin dependent endocytosis as it involves the uptake of nutrients across the GI tract

(Conner and Schmid, 2003). Typically, chitosan particles and its derivatives utilise this same endocytosis pathway (Sahay et al., 2010).

1.4.2 Paracellular Transport

Paracellular transport, illustrated as pathway (3) in Figure 1-3 is used to describe the transport of electrolytes and ions through pores present in the intracellular junctions. Unlike transcellular transport, this movement occurs down a concentration gradient, making it a passive process. However, absorption through the paracellular route is limited as only 1% of the mucosal surface area is utilised. Also, tight junctions between epithelial cells further restrict movement of molecules due to the limited pore size of tight junctions present in humans. These are 0.8 nm in the jejunum and 0.3 nm in the ileum and colon (Powell, 1981). Hence, transport of particles such as polymeric micelles which are usually above 1nm is limited via this route (Deli, 2009; Anderson and van Itallie, 2009).

Hydrophilic proteins are an exception as they able to traverse the membrane via the paracellular route but usually below potent concentrations (Drewe et al., 1993). More research is needed to discover ways of optimising paracellular transport so it can be utilised in the absorption of drugs administered orally. Currently, the use of surfactants and water-soluble polymers (chitosan), thiolated polymers and chelating agents have been employed as strategies to improve transport (des Rieux et al., 2006). These strategies often involve modulation of tight junctions through chelation or depletion of Ca^{2+}, therefore activating protein kinase C (PKC). Activation of PKC causes the internalisation of cadherin family proteins and triggers a cellular signalling cascade which results in the disassembly of cellular junction components such as Zonnula Occludens-1 (ZO-1) (Salamat-Miller and Johnston, 2005). Studies have reported evidence supporting chitosan's ability to open tight junctions. An example is in research carried out by Vllasaliu et al, were changes in the distribution of the tight junction protein, ZO-1 suggested chitosan nanoparticle's ability to open cellular tight junctions (Vllasaliu et al., 2010).

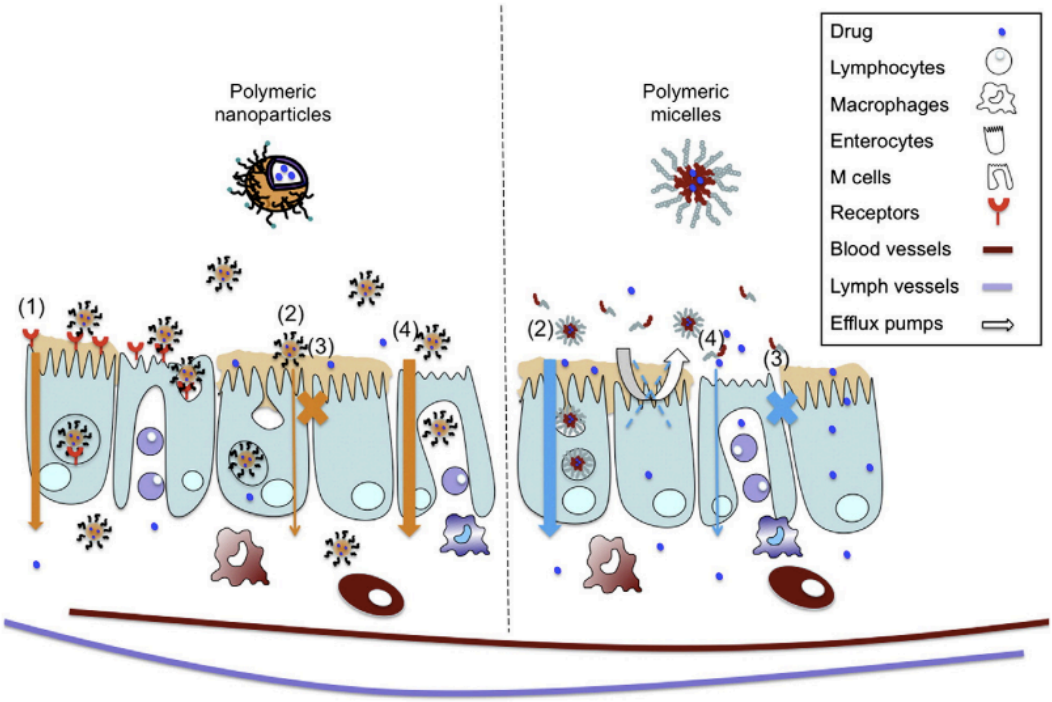

Figure 1-3: Schematic representation polymeric nanoparticles and micelles following oral administration. (1) receptor mediated endocytosis (2) transcellular transport (3) paracellular transport (4) M cell mediated transport. Size of arrows represents contributions of each kind of transport (Plapied et al., 2011)

1.5 Chitosan and chitosan-derivative based nanoparticles

Chitin $(C_8H_{13}O_5N)_n$ is a natural polysaccharide and the second most abundant polymer on earth after cellulose (Synowiecki and Al-Khateeb, 2003; Sato et al., 1998). It may be sourced from various organisms such as arthropods (crustaceans, arachnids and insects), and molluscs (endoskeleton and beaks of cephalopods). Microorganisms such as fungi and yeast are also able to produce chitin in their cell walls and diatoms produce chitin in their spines (Sharp, 2013; Jothi and Nachiyar, 2012; Merzendorfer, 2006). However, the most important source of chitin is from crustacean (crabs and shrimps) shells due to them being produced as waste in the seafood processing industry (Kaur and Dhillon, 2015).

It is composed of 2-acetamide-2-deoxyD-glucopyranose (N-acetyl-D-glucosamine, GlcNAc) units linked by β(1-4) linkage (Figure 1-4) and has good biodegradability and biocompatibility (Sato et al., 1998; Ramírez Arrebato et al., 2010; Cheba, 2011). However, it is highly hydrophobic, making it insoluble in under aqueous conditions and in most organic solvents (Dutta et al., 2004). Solubility profile is thought to be as a result of strong intramolecular hydrogen bonds which contributes to the rigidity of chitin (Wilson and Omokanwaye, 2013). Hence, it is often synthesised into chitosan to improve its physicochemical properties.

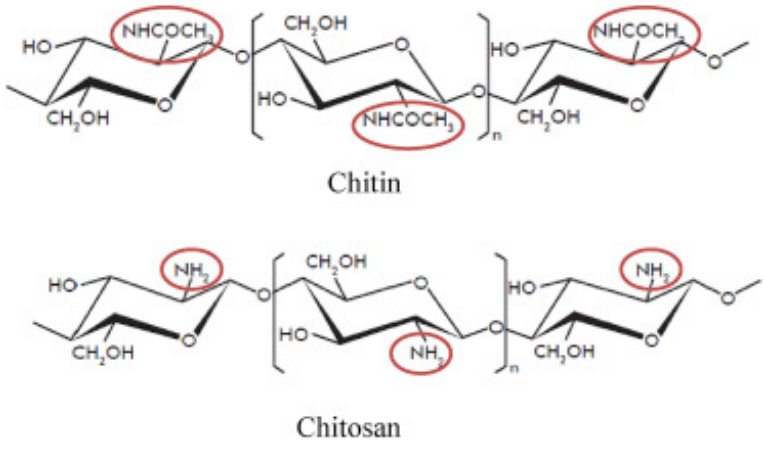

Figure 1-4: Structure of chitin and chitosan (Hamed, Özogul and Regenstein, 2016)

Chitosan, an N-deacetylated derivative of chitin Figure 1-4 is composed of 2-amino-2-deoxy-D-glucopyranose (D-glucosamine, GlcN) units (Sato et al., 1998; Domard and Domard, 2001). The deacetylation of chitin is able to give rise to a primary amine group in chitosan which can be protonated in solution (Haugstad et al., 2015). N-Acetyl groups have been shown to mediate hydrophobic interactions while amine and hydroxyl groups encourage hydrogen bonding, electrostatic interactions and hydrophobic interactions (Haugstad et al., 2015; Schatz et al., 2003).

According to Jayakumar, chitosan possesses advantageous physicochemical and biological properties (Jayakumar et al., 2007). These include its ability to encourage healing of wounds, its low toxicity, its ability to form complexes with nucleic acids and the fact that only a select few enzymes can degrade chitosan (Kean and Thanou, 2010). Enzymes known to degrade chitosan are chitonase, lysozyme and human chitotriosidase (Kean and Thanou, 2010). Chitosan is also considered to be polycationic, biocompatible, and biodegradable (Yuan et al., 2011; Teng, 2011; Zhang et al., 2010; Anaya et al., 2013). Chitosan is thought to enhance oral absorption of drugs by combining its mucoadhesive properties with its ability to widen tight junctions *in vivo* hence, facilitating transport of encapsulated drug through paracellular route (Lehr et al., 1992; Illum, Lisbeth; Farraj, Nidal F.; Davis, 1994). Its cationic moieties are proposed to be important for interaction with mucin as mucin possesses an overall negative charge (Haugstad et al., 2015). It is the possibility of chitosan to interact with mucin along with its multiple advantageous properties mentioned above which have led to the use of chitosan as an absorption enhancer in the pharmaceutical industry.

Although chitosan possesses multiple beneficial properties, (Suh and Matthew, 2000; Kumari et al., 2010; Dodane and Vilivalam, 1998), a major drawback is chitosan's ability to swell in solution. This makes it unsuitable for drug release as it encourages the fast release of encapsulated drug compound, therefore, limiting its use in sustained or slow-release formulations (Prabaharan, 2008; Thanou et al., 2001). In addition to that, chitosan has poor solubility in neutral and alkaline pH hence (Thanou, Verhoef and Junginger, 2001), providing limitations in its therapeutic potential at physiological pH values. Because of this, chitosan has been subjected to multiple chemical modifications, usually involving the substitution or grafting at the free amine (-NH2) group of chitosan. These have resulted in variants of chitosan with improved mechanical strength, stimuli sensitivity, controlled swelling and hence, slow drug

release as well as improved solubility at a wider range of pH (Mourya and Inamdar, 2008). All of which have broadened the utility of chitosan in drug formulations.

Polysoaps are soluble polymers which consist of pendant amphiphilic groups and have been investigated from as far back as 1995 due to their ability to solubilise hydrophobic molecules (Laschewsky and Zerbe, 1991). These polysoaps can assemble into micelles (Cochin et al., 1995) while still retaining their solubilisation capacity upon dilution (Laschewsky and Zerbe, 1991). It is these polymeric micelles that are applied in the pharmaceutical industry to improve efficacy of drugs (Kazunori et al., 1993). Previously, polysoaps have been synthesised from N-lauryl 6-carboxymethyl chitosan (Miwa et al, 1998), alkylated poly(L-lysine citramide) (Gautier, Boustta and Vert, 1999) and N-acyl 6 sulphated chitosan (Yoshioka et al., 1995). Although, more recently, quaternary ammonium palmitoyl glycol chitosan (GCPQ), a new type of chitosan based polysoap has displayed interesting solubilisation activity (Uchegbu et al., 2001).

1.5.1 Quaternary Ammonium Glycol Chitosan

An example of modifications being made to the chitosan backbone is in the synthesis of N-palmitoyl- N-monomethyl- N,N-dimethyl- N,N,N-trimethyl-6-O-glycolchitosan (GCPQ). This is a polymer synthesised from glycol chitosan by the introduction of positively charged quaternary ammonium groups and palmitoyl groups in order to incorporate both positive and negative moieties (Figure 1-5). Its amphiphilic properties allow GCPQ to spontaneously form stable micellar nanoparticles with critical micellar concentrations (CMCs) in the μM range in aqueous environments (Qu et al., 2006a). These values are considerably smaller than previously used nano-carrier particles with CMC values in the mM range and hence, makes these ideal candidates for drug delivery applications (Siew et al., 2011). Within these micellar nanoparticles, drugs can be encapsulated (Uchegbu et al., 2001). As a highly stable nano-system, there is a lesser chance for drug carriers to disaggregate upon interaction with biological fluids *in vivo*. This means that nano-carriers would be able to get their encapsulated drug to the site of action efficiently (Siew et al., 2011). This is important in the delivery of hydrophobic drug compounds and preclinical studies have shown GCPQ being used to enhance the oral delivery of hydrophobic drugs and peptides. (Lalatsa et al., 2012a;

Siew et al., 2011; Serrano et al., 2015a; Odunze, 2018). GQPQ is also thought to protect drug from enzymatic degradation (Guggi and Bernkop-Schnürch, 2003; Zhang et al., 2016).

Initially, it was believed that GCPQ was unable to augment oral drug delivery via the paracellular transport (Lalatsa et al., 2012a; Siew et al., 2011). The Caco-2 monolayer which has been used to investigate cellular uptake of nanoparticles at the GI tract membrane was used to show that GCPQ had no effect on the integrity of tights junctions (Siew et al., 2011). However, GCPQ polymer particles investigated had a DP% of 16% and DQ% of about 8%. In contrast to that, more recent results from Odunze's work showed that GCPQ polymers with a DP% of about 20% and DQ% of about 22% open tight junctions and hence encourage transport of encapsulated bulk (Odunze, 2018). It is then possible that transport via the paracellular pathway can occur depending on the degree of modification of GCPQ polymers. Also, mucoadhesive properties allow for micellar nanoparticles to adhere and penetrate the mucus layer hence, elongating the contact time between drug molecule and absorptive cells located on the intestine, therefore facilitating transcytosis of hydrophobic drugs (Siew et al., 2011).

An added advantage is GCPQ's ability to increase the solubility and dissolution rate of hydrophobic drugs which poses as a solution to BCS Class II and IV drugs and therefore increase bioavailability of drugs. This was investigated in GCPQ-based formulations of amphotericin B. Results showed an enhancement in the oral bioavailability of amphotericin B from 1.5% to 24.7%. Translocation of drug to tissues in organs such as the liver, brain and lungs were also increased compared to other lipid based oral formulations of amphotericin B (Serrano et al., 2015a). Its ability to increase oral bioavailability of hydrophobic drug compounds makes GCPQ an interesting polymeric nanoparticle to study as a possible oral drug delivery system.

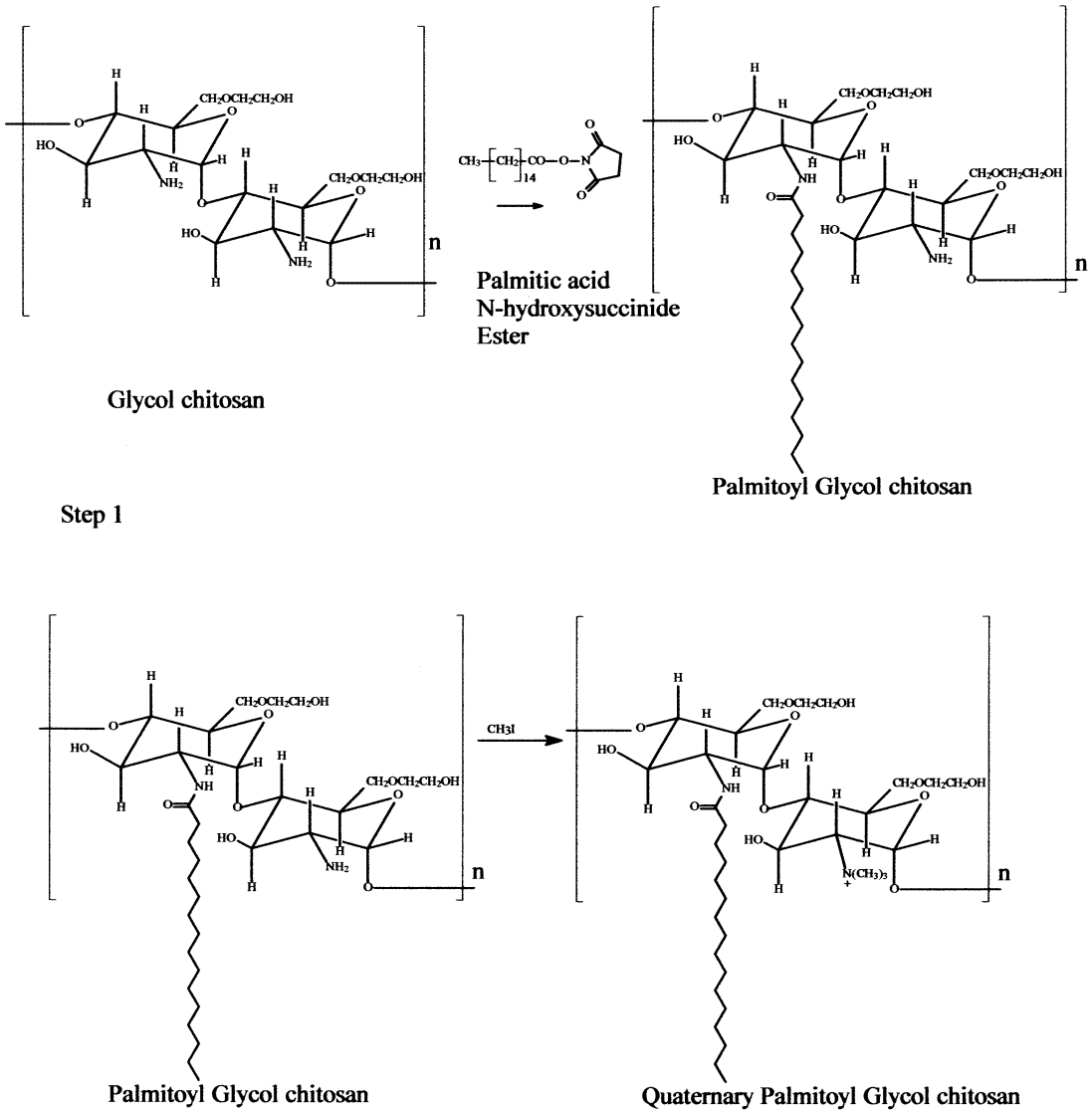

Figure 1-5: Steps involved in the synthesis of quaternary ammonium palmitoyl glycol chitosan (Uchegbu et al., 2001)

GCPQ formulations of Class IV Drugs

Oral GCPQ formulations with Amphotericin B, a BCS class IV drug proved to be useful in increasing oral bioavailability (Serrano et al., 2015a). However, the oral GCPQ formulations of paclitaxel, another BCS class IV drug appeared to have no effect on bioavailability (Odunze, 2018). It was of interest to further investigate the effect of GCPQ on oral bioavailability of two other class IV drugs – curcumin and caspofungin.

Curcumin

With 70-80% of the world's population relying on herbal medicine as a major source of pharmaceutical agents (Ahmad, Aqil and Owais, 2006), it is important to exploit these sources and develop them further. An example of such phytomedicine is curcumin, also known as diferuloylmethane. This is a yellow polyphenolic compound extracted from turmeric (*Curcuma longa*) which has pharmacological properties such as antioxidant, anti-inflammatory, anti-angiogenic and anti-proliferative activity (Shishodia, Sethi and Aggarwal, 2005). It has been shown experimentally to be potent as an anti-inflammatory agent (Hanai and Sugimoto, 2009; Chan et al., 1998), an antitumor agent (Hatcher et al., 2008; Arbiser et al., 1998; Jiang et al., 1996) and cardiovascular diseases (Morimoto et al., 2008; Gusterson et al., 2003) to name a few, making curcumin a potential treatment for a varied number of diseases.

Curcumin is purchased as a mixture of three main curcumoids – Curcumin, Demethoxycurcumin (DMC) and Bisdemethoxycurcumin (BDMC). The curcumin used here was 98% pure curcumin. It is practically insoluble in water (3.13 mg/L). It has very low bioavailability and high metabolism in the GI tract. It is then essential to improve the oral bioavailability of curcumin by applying formulation strategies such as encapsulation strategies. These have been investigated using liposomes (Thangapazham et al., 2008; Li, Braiteh and Kurzrock, 2005) and encapsulation in micelles (Wang, Ma and Tu, 2015; Thong et al., 2014; Duan et al., 2016; Ha et al., 2012; Mohanty et al., 2010; Song et al., 2011).

Caspofungin

In the US, *Candida* infections are the fourth leading cause of bloodstream infections in paediatric patients, hospitalized patients and cancer patients (Raymond and Aujard, 2000; Wisplinghoff et al., 2004). Mortality rates in paediatric patients is up to 20 % and 47 % in intensive care unit patients (Wisplinghoff et al., 2003, 2004). This means candida makes huge contribution to the mortality rate of immunosuppressed patients.

Caspofungin belongs to a class of antifungals called echinocandins. These are cyclic lipopeptide molecules which function by inhibiting the enzyme activity of B-1,3-D-glucan synthase, the enzyme responsible for cell wall synthesis in fungi. Echinocandins are therefore fungicidal, as fungal cell are prone to osmotic lysis due

to weakness in their cell wall configuration. They are also fungistatic because cell growth is now limited due to limited cell wall synthesis (Wiederhold and Lewis, 2003; Odds et al., 2003). The fungal species targeted include candida spp and aspergillus spp. Its salt formulation, caspofungin acetate has a solubility of 28mg/mL in water and so, is freely soluble in aqueous solution. It is also soluble methanol and slightly soluble in ethanol.

Although, data on caspofungin absorption when administered orally is inconsistent and so, intravenous (IV) administration is still being employed for this drug (Kofla and Ruhnke, 2011). The IV formulation is typically reconstitution of a given mass of lyophilised caspofungin powder in 10mL of an aqueous solution containing excipients like lactose, citric acid, and sodium hydroxide. Clinically, an initial loading dose of 70 mg is administered through IV followed by a subsequent dose of 50mg once a day in adults. The total of dose is roughly 1 mg/kg/day (Blyth et al., 2007).

Due to their large molecular weight of 1093.3 g/mol, this class of drugs are poorly bioavailable. Oral bioavailability after administering 50 mg/kg in rats was less than 0.2 % making oral administration an inefficient route of administration (European Medicines Agency, 2005). The acetate salt is classified under the BCS Class III drugs however, pure caspofungin was found to be poorly soluble in water, methanol and ethanol at 0.2 µg/mL hence, making is a BCS Class IV drug instead. Functional group modifications such as ionisation may be considered however, ionisable groups like amide groups present are mostly buried within the core of the molecule so, access proves difficult. This makes it difficult to improve solubility by adjusting the pH.

Furthermore, drugs classified under the echinocandins group are not major substrates of Pgp proteins and neither are they metabolised by CYT P50 (Chen, Slavin and Sorrell, 2011) hence, the major problem is their size and solubility which can potentially be solved with the use of nano encapsulations.

1.6 Aims and Objectives

Oral drug delivery of hydrophobic drug compounds such as caspofungin and curcumin is unable to maintain blood plasma levels sufficient to bring about therapeutic effects. This is due to physicochemical properties that they possess. Drug delivery systems may be employed to improve drug bioavailability of oral drug delivery. One of such delivery systems is GCPQ, which has been shown to increase oral bioavailability of hydrophobic drugs (Serrano et al., 2015a).

Investigative experimental methods are often employed when selecting the best polymer properties to encourage polymer-drug interactions. Although, this can be time consuming and intensive, contributing to an increase in time to market. One way of evading such time-consuming process is by utilising theoretic analytical methods in the form of computational models to inform experimental design. An example of such computational models is the Hansen Solubility Parameters (HSP) Model (Abbott et al., 2008). This has been applied in pharmaceutical dosage form design, solvent selection in artwork conservation materials, and more recently, solubility parameters have been improved on to allow applications in predicting permeation rates, chemical resistance, compatibility of polymers and characterization of surfaces of fibres or pigments (Abbott et al., 2008; Fardi et al., 2014; Hancock, York and Rowe, 1997).

HSP makes predictions based on polymer and drug chemical structures, and thermodynamics theory (Abbott et al., 2008; Hansen, 1967) to give insight as to whether an interaction is thermodynamically favourable or not. Therefore, understanding and interpretation of HSP data can be crucial in identifying key factors affecting polymer-drug interaction. Predictions on GCPQ constituents and drug compounds were simulated to inform GCPQ modulation efforts to increase encapsulation and potentially, oral bioavailability. The hypothesis that HSP based predictions will correlate with experimental data will be investigated using encapsulation studies. To test predictions, this project will vary the degree of palmitoylation (hydrophobic moiety) and quaternisation (hydrophilic moiety) for GCPQ polymer, each time investigating effects on drug encapsulation efficiency and comparing experimental data to HSP predictions.

Physicochemical properties of polymers employed as delivery systems have great impact in their ability to enhance drug adsorption. These properties include molecular weight, charge, size and pKa, all of which impact the stability of polymer-drug formulations on the shelf and in physiological environments. These are therefore critical to their clinical applications. Size and charge of nanoparticles impact their colloidal stability in aqueous solution as well as their cellular uptake methods (Norris and Sinko, 1997; Sogias et al., 2008). Colloidal stability is an important factor to consider in nano drug delivery systems and has been described using forces influencing aggregation and disaggregation. These forces include Van Der Waal's force, Electrostatic forces, Hydrophobic interactions, hydration forces (Hwang et al., 2020) Derjaguin, Verwey, Landau and Overbeek (DLVO) theory of colloidal stability (Behrens et al., 1998). It is therefore hypothesized that degree of modulation of GCPQ polymers will influence physicochemical properties of resulting formulations. This hypothesis will be tested by varying proportions of DP % and DQ % of polymer and determining effects on encapsulation efficiency, micelle morphology, colloidal stability, size and charge measurements.

As size and charge values of polymers and polymer-drug formulations influence rate of cellular uptake *in vivo*, effects of GCPQ modification on permeability can be investigated by measuring drug biodistribution after oral administration. Hypothesis is that optimum GCPQ-Drug formulation with ideal size and charge data will have positive effect on drug permeability *in vivo*. In this study, the effect of structural modifications on drug encapsulation and eventual permeative capacity will be examined in comparison to free drug.

In summary, this project is aimed at understanding the relationship between solubility parameters and chemical structure of GCPQ constituents and hydrophobic drug compounds. It will then investigate the accuracy of solubility parameters predictions in determining GCPQ-Drug interactions using experimental encapsulation methods. Finally, resulting formulations will be tested *in vivo* for bioavailability and permeability compared to free drug.

2 Prediction of GCPQ nanoparticle drug loading using Hansen Solubility Parameters

2.1. Introduction

2.1.1 Nanoparticles and Poorly Soluble drugs

Polymeric micelles are examples of colloidal systems which can be employed to improve bioavailability of poorly soluble drugs through the oral route (Bromberg, 2008; Gaucher et al., 2010; Luo et al., 2016; Plapied et al., 2011).One example of a poorly soluble drug is curcumin, the bioactive component in *Curcuma longa* and a BCS class IV drug. This drug compound has been shown to have a wide range of pharmacological and biological effects such as anti-inflammatory, anti-tumour, anti-virus, and anti-oxidation activities (López-Lázaro, 2008). Another example is caspofungin, also a BCS class IV drug and an antifungal derivative of pneumocandin B_o and the first echinocandin to be approved (Balkovec et al., 2014a). Caspofungin has been shown to have fungicidal and fungistatic activity against invasive *Candida spp* and *Aspergillus spp* species (Kurtz et al., 1994; Ernst et al., 1999). In both instances, low water solubility and poor permeative ability resulting in efficacy through the oral route is attributed to the chemical structure of active drug compound. This prevents the realisation of the clinical benefits of both drugs through oral dosing (López-Lázaro, 2008; Letscher-bru and Herbrecht, 2003a).

Polymeric micelles have been proposed as a delivery system for the oral administration of curcumin and caspofungin. This is because they are able to solubilise hydrophobic drugs, which provides a pathway to increase rate of drug dissolution and subsequently, expected systemic bioavailability (Yu & Huang, 2012).

Investigative experimental methods are often employed when selecting the best combination of drug carrier materials to empirically determine conditions for optimal drug loading.

In the case of the GCPQ polymeric micelles, the specific polymer properties to encourage polymer-drug interactions would be considered important design parameters. However, the empirical approach to optimisation can be time consuming and resource intensive, potentially also contributing to an increase in time to market.

One way of accelerating this process is by using theoretic methods in the form of computational models to inform experimental design. An example of such computational models is the Hansen Solubility Parameter (HSP) Model (Abbott et al., 2008).

2.1.2 HSP as a Predictive Tool

The HSP model was developed by Hansen during his PhD research (Hansen, 1967). Over the years, HSP applications have ranged from pharmaceutical dosage form design (Hancock, York and Rowe, 1997), to solvent selection in artwork conservation materials (Fardi et al., 2014) and understanding plant surface-agrochemical interactions (Khayet and Fernández, 2012). More recently, solubility parameters have been improved upon to also allow applications in predicting permeation rates, chemical resistance, compatibility of polymers and characterization of surfaces of fibres or pigments (Abbott et al., 2008). The underlying concept for this theory is based on the idea that "like dissolves like" and allows the evaluation of affinity and therefore miscibility between substances, extending for example, to the dispersibility of particles (Fujiwara, Imai and Yamamoto, 2019) and solubility of compounds in different solvents (Hansen and Smith, 2004). Predictions are based on solubility parameters as defined by Hansen and correlate with the physical properties of the compound or solvent (Abbott et al., 2008).

2.1.3 Hildebrand Solubility Parameter

The concept of solubility was first conceptualised and developed by Scratchard and further extended by Hildebrand and Scott (Hildebrand, 1951). Solubility parameters have since proven valuable in correlating polymer solution phenomena and chemical resistance (Auras, Harte and Selke, 2006).

Here solubility was described as total solubility parameter, δ_t and defined as the square root of the cohesive energy density (CED), which is the energy required to move a molecule from liquid to vapour phase (Hildebrand, 1951):

Equation 1

$$\partial_t = (CED)^{\frac{1}{2}} = (\frac{\Delta E^v}{V})^{\frac{1}{2}}$$

Equation 2

$$\Delta Ev = \Delta Hv - RT$$

According to Equation 1, δ_t is expressed as the square root of the vaporisation energy for the pure solvent, ΔE_v divided by the molar volume of the involved liquid, V (Hildebrand, 1951). The vaporisation energy (or vaporisation enthalpy) for the liquid can be calculated using Equation 2, where ΔH_v is the heat of vaporisation for the liquid, R is the universal gas constant, and T is the absolute temperature. There is a directly proportional relationship between E_v and volume of involved liquid. SI unit for δ_t is $MPa^{1/2}$.

Both equations operate based on the basic principle of solubility parameters which is "like dissolves like" hence, liquids with similar solubility parameters are believed to be miscible (Hildebrand, 1951). The same principles are applied to polymers where polymers are expected to dissolve in solvents with similar solubility parameters. Hence, solubility parameters can be utilised in predicting the affinity of a polymer and solvent.

2.1.4 Hansen Solubility Parameters Defined

As with most predictive models, the Hildebrand solubility parameter present limitations. The original approach could only be applied in regular solutions (Hildebrand, 1962) as it did not factor in other intermolecular interactions such as polar and hydrogen bonding. Hence, research was undertaken to improve on these

limitations (Barton, 1983). One such efforts was by Blanks and Prausnitz, who segmented solubility parameters into nonpolar and polar groups (Blanks and Prausnitz, 1964) which greatly influenced Hansen's early work (Abbott et al., 2008). Hansen proposed dividing the single Hildebrand solubility parameter into three solubility parameters namely nonpolar, polar, and hydrogen-bonding parameters, now referred to as the Hansen solubility parameters (HSP) (Hansen and Smith, 2004; Abbott et al., 2008). These are defined as:

- Dispersive or nonpolar interaction (δ_d, atomic) – These are general van der Waals forces derived from atomic interactions. All molecules experience this type of attractive forces due to the powerful attraction between the atoms that make up the molecule (Abbott et al., 2008).
- Polar interactions (δ_p, molecular) – These are electrical interactions caused by permanent dipole moments due to unequal sharing of electrons between atoms within a molecule. They are important in most molecules, except some hydrocarbons and chemicals which contain only carbon and fluorine (Abbott et al., 2008).
- Hydrogen bonding interactions (δ_h, molecular) – These are sometimes considered to be polar forces although, sometimes called the electron exchange parameter (Abbott et al., 2008).

The HSP model utilises a combination of dispersive, polar and hydrogen bonding to predict thermodynamic interactions. This is sufficient as the influence of ionic bonding parameters is limited to reactions in aqueous environments (Abbott et al., 2008). The HSP concept considered the fact that all physical bonds are broken during evaporation and hence improved on the limitations presented in Hildebrand solubility parameter. For example, according to the Hildebrand solubility parameter, ethylene carbonate and methanol are identical (29 $MPA^{1/2}$) hence expected to dissolve; however, their solvencies are different (Auras et al., 2010). This can be explained by the HSP parameters of both solvents. Ethylene carbonate δ_d, δ_p and δ_h are 18 MPA ½, 21.7 $MPa^{1/2}$ and 5.1 $MPa^{1/2}$, respectively, while methanol δ_d, δ_p and δ_h are 15.1 MPa1/2, 12.3 $MPa^{1/2}$ and 22.3 $MPa^{1/2}$, respectively (Auras et al., 2010). It is apparent that the HSP for both solvents are not the same and that the refined definition of interaction forces better predicts experimental miscibility data.

2.1.5 Quantitative description of HSP Interactions

According to HSP, the total cohesion energy, E^v (J) is the sum of three individual energies (dispersion interactions ΔE^v_d (J/mol), dipole interactions ΔE^v_p (J/mol) and hydrogen bonding interactions ΔE^v_h (J/mol)), as expressed in

Equation 3 (Hansen and Smith, 2004; Abbott et al., 2008).

Equation 3

$$\Delta E^v = \Delta E^v_d + \Delta E^v_p + \Delta E^v_h$$

Equation 4

$$\delta^2_t = \delta^2_d + \delta^2_p + \delta^2_h$$

Equation 4 shows the relationship between HSP and Hildebrand solubility parameters where δ_d [$(MPa)^{1/2}$], δ_p [$(MPa)^{1/2}$] and δ_h[$(MPa)^{1/2}$] represent the dispersive force factor, dipole interaction force factor and hydrogen bonding force factor of the HSP.

Both, theoretical and experimental methods can be used to estimate HSP of a given material. In instances where experimental data for a given material is unavailable, group contributions are used as a first estimate of the solubility behaviour of the material. Although, it is recommended to confirm HSP for polymers determined by group contributions with experimentally determined HSP data (Abbott et al., 2008).

2.1.6 Experimental Method

Experimental data is based on observing interactions between the studied material and well-known solvents. The observations made include clarity of solution, degree of swelling by visual observation, surface attack, etc. Solvents which have similar or close HSP to the studied material will dissolve the material. If any visual change is observed, it is assumed that interactions between solvents and studied material is inconsequential (Abbott et al., 2008). Solvents are then considered to be ‘good’ or

'bad' based on the interactions involved. "Good" solvents have strong interaction with the studied material, meaning they have more similar HSP to the material than the "bad" solvents do. Experimental data is converted to a score scale then processed to determine HSP parameters. Further calculations are carried out to determine the three HSP parameters as well as the radius value, R_o, of the sphere of interaction for materials.

Radius of Interaction, R_o

The sphere defined by the radius of interaction represents the solubility sphere of a given material, with the centre of the sphere showing the optimum HSP for good solvency. The radius of the sphere, R_o represents the maximum distance allowed to define a good interaction between the solvent and material or between two materials. The solvency of two materials reduces the further way they are from the centre of their spheres hence, reducing probability of interaction. To determine if a material resides within the sphere of high affinity of another material, the distance, R_a between these two materials can be calculated using Equation 5, where δ_d, δ_p and δ_h represent dispersion, polar and hydrogen bonding (Abbott et al., 2008).

Equation 5

$$Ra = \sqrt[2]{4\left[(\delta_{d2} - \delta_{d1})^2 + \left(\delta_{p2} - \delta_{p1}\right)^2 + (\delta_{h2} - \delta_{h1})^2\right]}$$

Equation 6

$$RED = \frac{Ra}{Ro}$$

Relative Energy Difference (RED) is calculated from the ratios between R_a and R_o as shown in Equation 6. The RED value gives information on whether both compounds of interest are located within each other's sphere of affinity. A perfect solvent will have a RED value of 0 as its distance from the centre of the sphere is 0. Alternatively, a solvent located just on the surface of the sphere has a RED value of 1 and a value above 1.0 means reaction is unfavourable (Díaz de los Ríos and Hernández Ramos,

2020; Abbott et al., 2008). Red values are quick ways of getting insight on whether a reaction is likely to occur or not.

2.1.7 Group Contribution Calculations

Measuring HSP through experimental method is time consuming hence, only a limited number of compounds have experimentally predetermined HSP values. As a result, predicted values are often used for defining HSP based on the molecular structure of compounds. However, experimental data suggests that accurate predictions of solubility parameter components is very challenging (van Krevelen, te Nijenhuis and van Krevelen, 2009), making these predictions only rough estimates of HSP when experimental data is unavailable.

Krevelen's research published data with the basic assumption expressed in

Equation 3 and Equation 4 for predicting near accurate HSP values. He proposed to utilise a set of group contribution values of cohesive energy, E and molar attraction constant F, based on the concept of additive group contributions. Hence, the structure of a given material can be compartmented into smaller groups, which possess individual F and E values obtained from the published group contribution tables. This means that HSP of a material can be estimated by either the Hoftyzer-Van Krevelen or Hoy method (van Krevelen and te Nijenhuis, 2009).

Krevelen's research was supported by two core ideas; firstly, while there are thousands of chemical compounds of interests in science, the structural and functional groups within these compounds are much more limited. Finally, the assumption that a compound's physical property is determined by the sum of contributions made by each individual structural and functional group. Functional groups therefore provide the basis of a method for estimating and corelating compound properties (van Krevelen and te Nijenhuis, 2009). It is important to note that these group contribution techniques are estimates as the contribution of a functional group can be different, depending on its surrounding environment, presenting a major limitation (van Krevelen and te Nijenhuis, 2009). When this limitation presents itself, it is sometimes possible to apply rules for corrections to be made. Each correction made requires consideration of additional parameters and eventually, the advantage of the group contribution method

is completely lost. It is therefore ideal for the number of distinct functional groups to remain relatively small so group contribution method can be employed.

In this chapter, HSP values for GCPQ nanocarrier and a range of hydrophobic drug compounds were predicted using HSPiP software. This was done to investigate and predict the possibility of reaction between GCPQ polymer and specific hydrophobic drug compounds based on thermodynamic principles.

2.2 Materials and Methods

To determine the HSP of compounds analysed, the Hansen Solubility Parameters in Practice 5th Edition 5.0.05 software was used and theoretical group contribution method was employed. This was done in three main steps; Firstly determining the SMILES of the compound, secondly determining the HSP parameters of the compound and finally, determining RED values and Hansen sphere of the compounds.

2.2.1 Determine SMILES of compounds

The HSPiP software was first opened, and a blank table created to display compounds needed to be analysed. In this instance, compounds were GCPQ constituents – Glycol chitosan, chitosan and palmitic acid subunits as well as drug compounds paclitaxel, amphotericin B, curcumin, caspofungin and caspofungin acetate. The simplified molecular input line entry system (SMILES) was determined for each compound. This is a simplified description of the structure of a chemical compound which enables the HSPiP software to convert back into a 3D model and allow for HSP parameters to be calculated. SMILES for each compound was determined using the PubChem website.

2.2.2 Determine HSP parameters of compounds

The DIY function was opened on the HSPiP software and the SMILES determined from PubChem was copied and pasted in the appropriate location. Following this, the calculate function was used and HSPiP was allowed to calculate HSP values for the selected SMILES. After a few minutes, HSPiP was able to determine chemical properties such as $\log K_{OW}$, melting point, boiling point, etc as well as HSP parameters such as M_{vol} δ_D and δ_H and δ_P. HSP parameters were copied from DIY function and pasted in blank table created in 2.2.1. Figure 2-1 shows steps taken to determine HSP parameters. Data gotten from DIY function is displayed in Table 2-1Table 2-2 and HSP parameter values were used to calculate HSP distances displayed in Table 2-4.

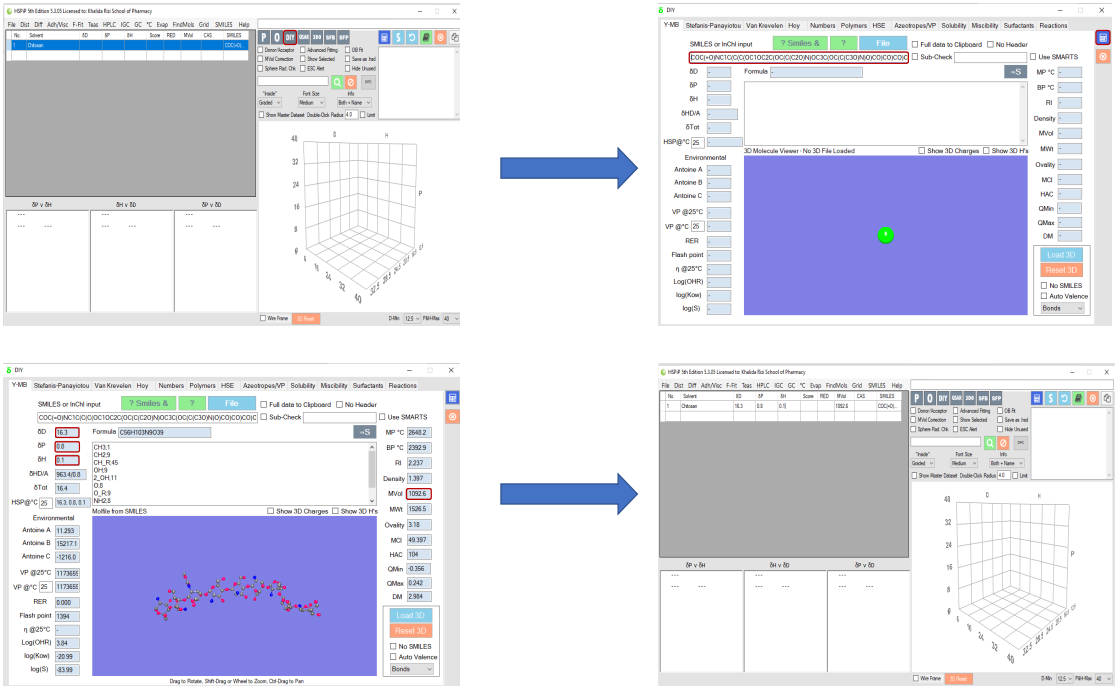

Figure 2-1: Steps followed in determining HSP parameter on HSPiP software.

2.2.3 Determine RED values and Hansen spheres of compounds

Steps described in 2.2.1 and 2.2.2 were repeated for all the compounds to be analysed. RED values of a specific drug compound in relation to the GCPQ constituents was then determined by the HSPiP software. This was done by double clicking the drug compound of interest in the table. RED values were then automatically calculated by the HSPiP software based on HSP parameters previously determined from chemical structures. In addition to RED values, Hansen plots were also plotted for the drug compound of interest. The process was repeated for each drug compound of interest and data displayed in Table 2-3 and Figure 2-3 to Figure 2-6.

2.3 Results

Hansen solubility data was determined using Hansen Solubility Parameters in Practice (HSPiP) software, version 5.3.05. The results show HSP parameter predictions for GCPQ polymer constituents and a range of hydrophobic, BCS Class IV drug compounds. These predictions include solubility parameters, RED values, HSP distance values and finally, HSP sphere illustrations. Predictions were based on chemical structure of all compounds investigated and on thermodynamic principles. When combined, HSP data is said to give insight to whether a reaction is likely to occur or not.

GCPQ Polymer Constituent	**δ_D[a]**	**δ_P[b]**	**δ_H[c]**	**Mvol[d]**	**Solubility Parameter**
Chitosan	16.3	0.80	0.10	1092.6	16.3
Glycol Chitosan	17.3	8.4	6.4	568.9	27.0
Palmitoyl Group	17.6	9.50	18.1	375.7	27.0

Table 2-1: Hansen Solubility Parameter values and molecular volume of polymer used. Where a – dispersion component, b – polar component, c – hydrogen bonding component and d – molecular volume

HSP parameters and molar volume of GCPQ polymer components and drug compounds were determined using HSPiP and data shown Table 2-1. GCPQ polymer was broken down into its three main components: the chitosan polysaccharide $[C_6H_{11}NO_4]_n$, glycol chitosan derivative $[C_8H_{15}NO_5]_n$ and palmitoyl chain $[CH_3(CH_2)_{14}CO]_n$. Within the polymer, the highest molar volume (M_{vol}) is observed in the glycol chitosan backbone at 1092.6 $MPa^{1/2}$, followed by glycol chitosan at 568.9 $MPa^{1/2}$, while the palmitic chain has the lowest Mvol 375.7 $MPa^{1/2}$.Their chemical

structures reflect these values as chitosan has 104 heavy atoms, followed by glycol chitosan which has 44 heavy atoms and finally, palmitoyl group with 28 heavy atoms.

δ_D for all three components were of similar magnitude with glycol chitosan and palmitic chain having the most similar dispersive forces at 17.3 and 17.6 respectively. This is a measure of Van Der Waals forces, which are the forces of attraction within the molecules present in individual monomers. Dispersion force values were expected to follow a similar trend as observed in molecular volume as Van Dar Waals forces increase with increased polymer volume. Data is therefore not consistent to chemical structure of all three compounds.

δ_P values, a measure of polarity are similar for both glycol chitosan and palmitoyl monomers at 8.4 and 9.5 respectively. Data appears to be inconsistent as palmitoyl group consists mostly of -CH bonds and a -CO bond which contributes slightly to the polarity of the molecule. Therefore, its polar bonding value being greater than glycol chitosan appears inaccurate as glycol chitosan contains amino, acetamino and hydroxy groups. The same can be said about δ_P and δ_H values for chitosan because its molecular structure is similar to that of glycol chitosan so, δ_P and δ_H values should be similar but, instead are close to zero.

δ_H represents hydrogen bonding forces within the compounds. We observe significantly low hydrogen bonding in chitosan which is surprising. Chitosan possesses 76 Hbond acceptors and donors, giving it the highest potential for hydrogen bonding yet δ_H predictions are close to zero. Palmitoyl group is expected to have the lowest δ_H value due to it having the least Hbond donors and acceptors (9 total). What is observed however, varies. Palmitoyl group has more than twice the δ_H (18.1) than glycol chitosan at 6.4.

Drug	δ_D[a]	δ_P[b]	δ_H[c]	Mvol[d]	Solubility Parameter
AmphotericinB	18.8	0.1	0.1	869.3	18.8
Paclitaxel	20.0	8.1	3.7	668	21.9
Curcumin	20.1	8.10	11.3	295.4	24.4
Caspofungin	20.5	28.1	12.5	941	37.0
Caspofungin Acetate	20.6	27.1	13.0	1024.3	36.4

Table 2-2: Hansen Solubility Parameter values and molecular volume of drugs used. Where a – dispersion component, b – polar component, c – hydrogen bonding component and d – molecular volume

Table 2-2, shows the HSP of four BCS class IV; Amphotericin B [$C_{47}H_{73}NO_{17}$], Paclitaxel [$C_{47}H_{51}NO_{14}$], Curcumin [$C_{12}H_{20}O_6$] and Caspofungin. Caspofungin [$C_{52}H_{88}N_{10}O_{15}$] and Caspofungin acetate [$C_{56}H_{96}N_{10}O_{19}$], were analysed as two separate compound to understand if HSP characteristics for the acetate salt form were significantly different. The highest molar volume (Mvol) is observed in the caspofungin acetate salt, followed by caspofungin. This is expected as caspofungin is a large lipopeptide with 77 heavy atoms. The difference in Mvol of caspofungin and its acetate base is due to the addition of two acetic acid molecules, each with a Mvol of 41.5, therefore contributing to the final Mvol of caspofungin acetate. Caspofungin and its acetate base formulation have similar HSP values which is as expected. As this has been established, only caspofungin will be referenced moving forward.

Curcumin has the lowest Mvol as this is the smallest drug compound with 27 heavy atoms in its molecule. This is almost three times less than half the number of heavy atoms present in the paclitaxel which has the second smallest Mvol at 668. Mvol for drug compounds correlates directly to their chemical structures.

δ_D for all drug compounds were of similar magnitude with caspofungin having the largest dispersive force value of 20.5. This is attributed to its large lipopeptide structure. Dispersive forces data is expected to follow a similar trend to Mvol data although, that is not the case. Amphotericin B which has a larger molecule, with more dipole moments than curcumin is seen to have a smaller dispersion force value than curcumin (20.1 vs 18.8). The same can be said about curcumin and paclitaxel as well as amphotericin B and paclitaxel. This poses a possible limitation in HSP predictions.

Large differences are observed in δ_P values for drugs. This is a measure of polarity and should increase as drug compounds become more polar. Caspofungin has the highest δ_P value at 28.1, consistent with its chemical structure which consists mostly of multiple polar groups such as primary and secondary amines and hydroxyl groups. Both curcumin and paclitaxel have high density of polar functional groups. Curcumin possesses two phenol, ether and ketone groups, all contributing to polarity of the compound. While paclitaxel contains more polar groups than curcumin, it is also a larger molecule hence, similarities in δ_P of both compounds can be attributed to their polarity as a measure of total size. Amphotericin B is shown to have almost no polar bonding value which is inconsistent with its chemical structure.

δ_H represents hydrogen bonding forces within the compounds. Again, amphotericin B data is inconsistent with its chemical structure. Caspofungin is shown to have the highest δ_H value at 12.5, consistent with its structure as it has 34 total hydrogen bond donors and acceptors within the molecule. The second highest value is observed in curcumin which is inconsistent as curcumin has less hydrogen bond donors and acceptors than paclitaxel (14 vs 18) but a δ_H value more than 3 times that of paclitaxel.

HSP predictions show certain discrepancies in solubility parameters of some compounds measured. This may be one of the limitations which predictions present as incorrect data will influence further HSP predictions. On the other hand, it is possible that some HSP predictions such as δ_H may have been adjusted based on thermodynamics theory. For example, while amphotericin B may have 30 H-bond acceptors and donors, hydrogen bonding between molecules may not be thermodynamically favoured based on other factors such as structural configuration of functional groups in space. This could then explain differences in expected and predicted HSP values.

GCPQ Component	Amphotericin B	Paclitaxel	Curcumin	Caspofungin	Caspofungin Acetate
Chitosan	1.26	2.75	3.84	7.78	7.63
Glycol Chitosan	2.71	1.51	1.86	5.40	5.23
Palmitoyl Group	5.11	3.81	2.14	5.07	4.82

Table 2-3: Relative Energy Differences (RED) values expressed for the drug compounds when compared to GCPQ polymer components.

The Relative Energy Difference (RED) can be described as the ratio of the distance between the HSP values of the drug compounds and GCPQ polymer components to the radius of the Hansen sphere. These RED values for the drug compounds and GCPQ constituents were calculated using the HSPiP software and results are shown in Table 2-3. The distance between the centre of HSP sphere and the radius is 1 hence, ideal RED values are below 1. A perfect solution with high affinity will have a RED value of 0. Overall, there is no standard RED values for polymer-drug interactions so RED data is often interpreted based on individual set limits.

RED values for GCPQ components and some BCS class IV drugs were determined to give insight into what specific components within GCPQ that drug molecules have affinity for. This can then be used to modulate GCPQ parameters to increase polymer-drug interaction and increase encapsulation efficiency. There is no obvious trend in RED values of BCS class IV drugs and GCPQ constituents in Table 2-3.

All drugs have RED values above 1, implying low affinity for GCPQ constituents and unfavourable interaction predictions. Amphotericin B has the lowest RED value overall with chitosan at 1.26, predicting the strongest interactions with chitosan polysaccharide. This presents chitosan-based polymers as ideal nanocarriers for Amphotericin B. Glycol chitosan is the second closest constituent to amphotericin B, followed by the palmitoyl chain. Data implies very little affinity for palmitoyl chain which

may be something to consider during GCPQ-Amphotericin B formulation. With paclitaxel and chitosan, RED values are almost three times the ideal value, and twice that of amphotericin B, implying lower affinity for chitosan polysaccharide. Glycol chitosan has the smallest RED value for paclitaxel and similar to amphotericin B, the palmitoyl chain has the largest RED value. Again, suggesting the least affinity for palmitoyl groups within the polymer.

Curcumin is shown to have its highest affinity for glycol chitosan, at 1.86, followed by the palmitoyl chain at 2.14. This may mean that GCPQ parameter modulations such as overall degree of modification and specific degree of palmitoylations will have a greater impact on curcumin encapsulation. Caspofungin is seen to have generally unfavourable RED values for all GCPQ constituents as it has the largest RED values on average. These predictions suggest encapsulation of caspofungin is thermodynamically unfavourable.

GCPQ Component	Amphotericin B	Paclitaxel	Curcumin	Caspofungin	Caspofungin Acetate
Chitosan	5.04	11.0	15.4	31.1	30.5
Glycol chitosan	10.7	5.52	7.01	21.4	20.7
Palmitoyl group	20.4	15.2	8.6	20.3	19.3

Table 2-4: Hansen Solubility Parameter (HSP) distance between the HSP of GCPQ polymer components and different drug compounds $MPa^{1/2}$.

Table 2-4 shows the difference between HSP values of GCPQ components and drug compounds, also known as HSP distances. Chemically similar components are expected to have the same HSP values. Hence, the sum of the difference of all three HSP values for these components should equal zero. This means that materials with fairly similar HSP values will have a difference value close to zero while a perfect solvent is one that has a net difference of 0 $MPa^{1/2.}$

Similar to RED values, there is no standard HSP distance for polymer-drug interactions. Also, no clear trend is observed in HSP distances between drugs and GCPQ constituents. One observation is that HSP distances support RED data, where Drug-GCPQ constituent with the lowest RED value also has the lowest HSP data. This is expected as both parameters define distance between two compounds, in this case, drug and polymer constituent.

While shorter HSP values are preferred, it is not possible to make estimates on whether interaction is predicted to occur without experimental data to confirm this. Therefore, drug-distance comparisons can only be relative to other drug-distances being analysed. For example, HSP distances of curcumin and paclitaxel are 8.6 and 15.2 respectively. This simply means that Curcumin is predicted to have more affinity for the palmitoyl groups than Paclitaxel due to shorter HSP distance. However, there is no clear indication that an HSP distance of 8.6, in the case of curcumin and palmitoyl group results in actual interactions experimentally or not. And so, a distance of 8.6 is only good relative to a distance of 15.2.

Hansen Sphere plots for the different drug compounds are shown in Figure 2-3 to Figure 2-5. The sphere represents the reactivity bubble surrounding a specific compound. Hence, if a drug compound is within the sphere of one of the GCPQ constituents, then a reaction between both drug and subunit is predicted to occur. Additionally, the closer the polymer subunit is to the centre of the sphere, the stronger the interaction. 2D plots comparing dispersion and polar bonding components were also considered as these contribute the most to thermodynamic interactions.

Figure 2-3 shows the solubility parameters for all GCPQ components lie outside of the Hansen sphere generated for paclitaxel suggesting low affinity between GCPQ and Paclitaxel. A similar trend is observed in Figure 2-2 to Figure 2-5, indicating reactions between each drug compound and GCPQ component is thermodynamically unfavourable. Figure 2-6 focusses on the palmitoyl group within the GCPQ polymer. Here we observe the chitosan sphere within that of the palmitic chain, suggesting high affinity. All drugs lie outside the sphere of reactivity for the palmitoyl group, although to varying extents; with caspofungin and caspofungin acetate furthest away and amphotericin B relatively close to the sphere.

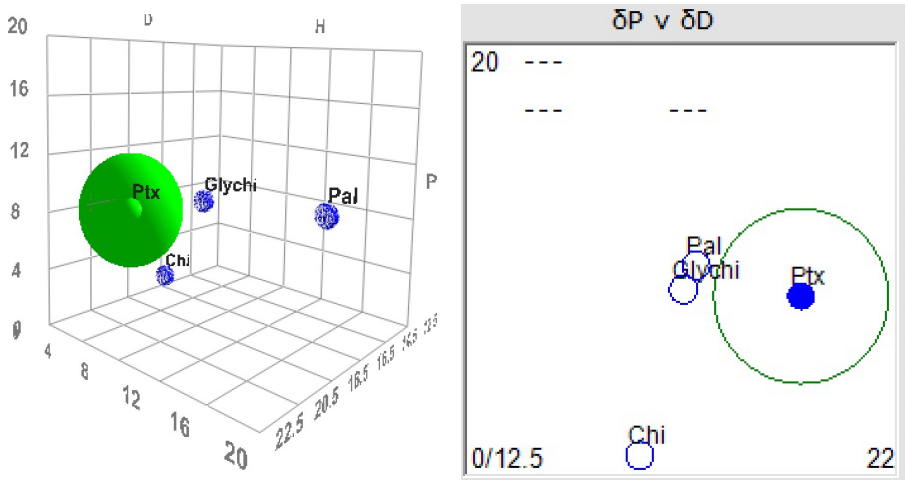

Figure 2-3: Schematic of the Hansen Solubility sphere for Paclitaxel. Left: Each axis is a component of Hansen Solubility Parameters, δD, δH, or δP. These represent the dispersive or van der Waals forces, hydrogen bonding and polar bonding respectively. The green sphere represents the area of reactivity for paclitaxel while the blue spheres represent the area of reactivity for individual GCPQ components namely; Chitosan, glycol chitosan and palmitoyl group. Radius of the sphere is 4MPa½. Right: 2D image of Hansen Solubility sphere for Paclitaxel (Green) and individual GCPQ components (Blue) comparing van der Waals forces against Polar bonding for each component.

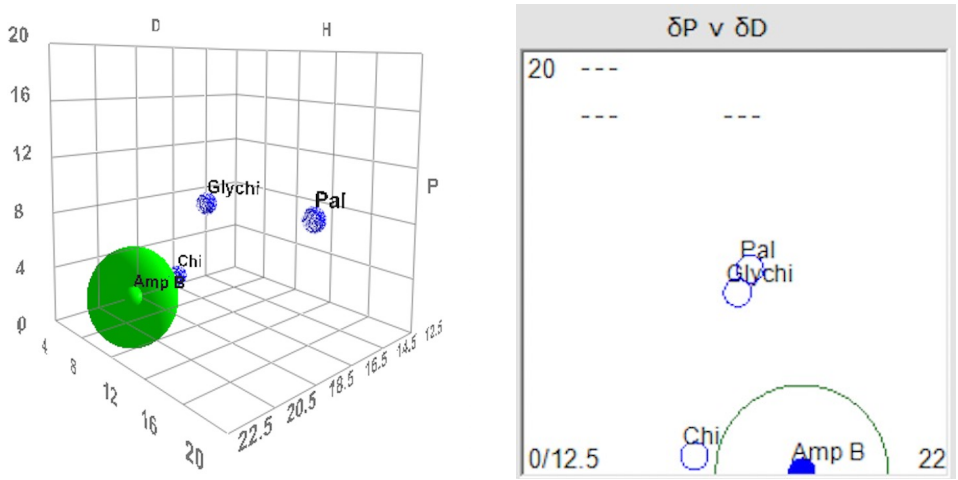

Figure 2-2: Schematic of the Hansen Solubility sphere for Amphotericin B. Left: Each axis is a component of Hansen Solubility Parameters, δD, δH, or δP. These represent the dispersive or van der Waals forces, hydrogen bonding and polar bonding respectively. The green sphere represents the area of reactivity for Amphotericin B while the blue spheres represent the area of reactivity for individual GCPQ components namely; chitosan, glycol chitosan and palmitoyl group. Radius of the sphere is 4MPa½. Right: 2D image of Hansen Solubility sphere for Amphotericin B (Green) and individual GCPQ components (Blue) comparing van der Waals forces against Polar bonding for each component.

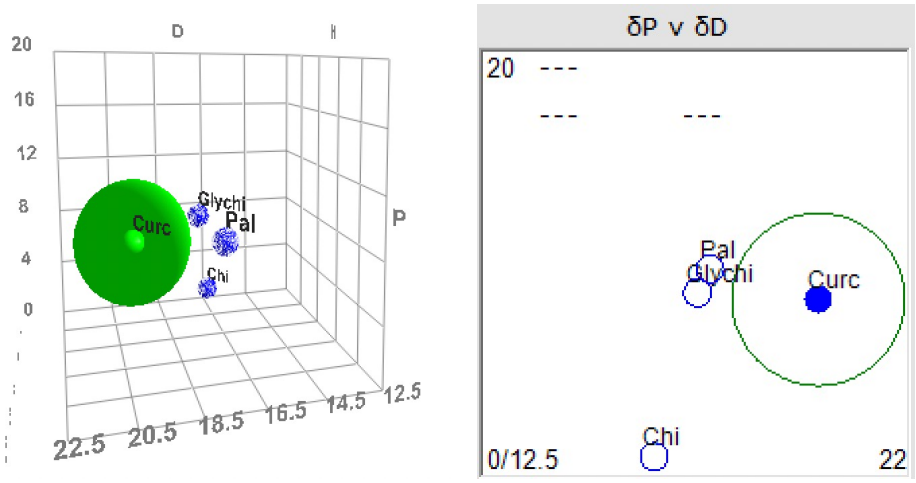

Figure 2-4: Schematic of the Hansen Solubility sphere for Curcumin. Left: Each axis is a component of Hansen Solubility Parameters, δD, δH, or δP. These represent the dispersive or van der Waals forces, hydrogen bonding and polar bonding respectively. The green sphere represents the area of reactivity for Curcumin while the blue spheres represent the area of reactivity for individual GCPQ components namely; chitosan, glycol chitosan and palmitoyl group. Radius of the sphere is 4MPa ½. Right: 2D image of Hansen Solubility sphere for Curcumin (Green) and individual GCPQ components (Blue) comparing van der Waals forces against Polar bonding for each component.

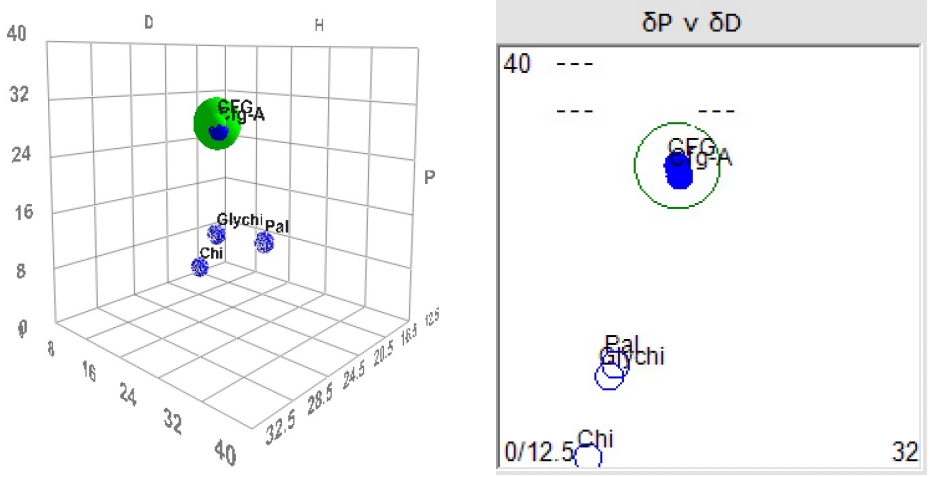

Figure 2-5: Schematic of the Hansen Solubility sphere for Caspofungin (CFG). Left: Each axis is a component of Hansen Solubility Parameters, δD, δH, or δP. These represent the dispersive or van der Waals forces, hydrogen bonding and polar bonding respectively. The green sphere represents the area of reactivity for Caspofungin while the blue spheres represent the area of reactivity for individual GCPQ components namely; chitosan, glycol chitosan and palmitoyl group. Radius of the sphere is 4MPa ½. Right: 2D image of Hansen Solubility sphere for Caspofungin (Green) and individual GCPQ components (Blue) comparing van der Waals forces against Polar bonding for each component.

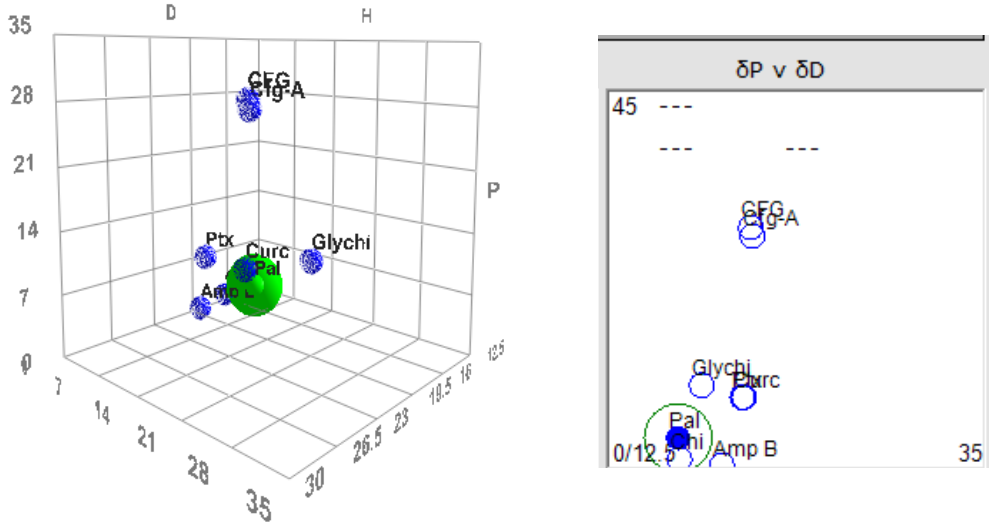

Figure 2-6: Schematic of the Hansen Solubility sphere for the GCPQ palmitoyl group. Left: Each axis is a component of Hansen Solubility Parameters, δD, δH, or δP. These represent the dispersive or van der Waals forces, hydrogen bonding and polar bonding respectively. The green sphere represents the area of reactivity for the GCPQ palmitoyl group while the blue spheres represent the area of reactivity for individual GCPQ components namely; chitosan, glycol chitosan and palmitoyl group, Also the different drug compounds namely; amphotericin B, paclitaxel, curcumin, caspofungin and caspofungin acetate. Radius of the sphere is 4MPa ½. Right: 2D image of Hansen Solubility sphere for GCPQ palmitoyl group (Green) and individual GCPQ components and drug compounds (Blue) comparing van der Waals forces against Polar bonding for each component.

2.4 Discussion

GCPQ is a proposed oral nano carrier system for reasons mentioned in Chapter 1. The nanoparticles are based on a chitin derived polymer, comprised of a glycol chitosan backbone, pendant palmitoyl side chain and quaternary ammonium groups (Chooi et al., 2014).

The oral bioavailability of a drug is influenced by multiple factors such as drug permeability, dissolution rate, aqueous solubility, first pass metabolism and susceptibility to efflux systems (Savjani et al., 2012). With the most frequent cause being poor solubility and permeability. Thus, making solubility one of the most important parameters in achieving desired concentration of drug in systemic circulation and subsequently, pharmaceutical response (Vemula Varun Raj et al., 2010).

As GCPQ has the ability to encapsulate and solubilise hydrophobic drug compounds (Siew et al., 2011; Lalatsa et al., 2012b, 2012a; Serrano et al., 2015b), it is crucial to determine ideal GCPQ modifications for optimum encapsulation efficiencies. This can be done experimentally however, due to the complexities involved in drug-polymer interactions, experimental design addressing all variables involved in each individual interaction may be time consuming. One way of bypassing the long experimental process is by employing computational models such as HSP.

2.4.1 HSP group contributions to predict favourable interactions between subunits and drugs

HSP has been employed to predict favourable interactions between therapeutic agents and delivery vehicle in the pharmaceutical industry (Fujiwara et al., 2019; Hancock et al., 1997; Weng, 2016; Xavier-Junior et al., 2016). Simulations are run to make predictions based on molecular structures and thermodynamics theory (Abbott et al., 2008; Hansen, 1967). Interpretation of HSP data can therefore be used to identify key factors affecting polymer-drug interaction.

In this model, GCPQ was separated into three constituents: Chitosan, as this is the polysaccharide which glycol chitosan is derived from; Glycol chitosan, which is the backbone on which quaternary ammonium salts and palmitoyl groups are added to;

and Palmitoyl group which is the hydrophobic moiety of the polymer (Chooi et al., 2014). Quaternary ammonium salts were excluded for two reasons; Firstly, this is a less easily controlled parameter of the polymer and secondly, experimental design was based on the theory that hydrophobic drug compounds will interact more strongly with the hydrophobic moiety of the GCPQ polymer, which is the palmitoyl chain. Parameters considered were Solubility Parameter, HSP parameters and RED to give a wholistic view on thermodynamic predictions (Table 2-1 to Table 2-4)

2.4.2 Solubility Parameter

The molecular size of compounds analysed are expressed in terms of molar volume Table 2-1. A further description of compound properties consider other parameters such as size, shape, HSP values and solubility parameters. The solubility parameter is a measure of how much the compound adheres to itself during vaporisation (Equation 4). Based on the theory of "like dissolves like", solubility parameter values of nanocarrier constituents should match with that of the drug compound. This is to enhance strong interactions between both compounds. Interaction between drug molecule and polymer subunit is predicted to be a maximum when the difference between solubility parameter of subunit and drug is zero.

All GCPQ constituents selected in this study have a range of solubility parameters 16.3 – 27.0 $MPa^{1/2}$ and the drug compounds, which by definition, are hydrophobic, have solubility parameters ranging from 24.4 for curcumin to 36.4 $MPa^{1/2}$ for caspofungin acetate. Glycol chitosan and palmitoyl groups have the same solubility parameter value (27 $MPa^{1/2}$), resulting in a difference of zero. Hence, there is maximum, strong interactions between both constituents within the GCPQ polymer. The third strongest interactions predicted is observed between curcumin and both glycol chitosan and palmitoyl group monomers. Here there is a difference of 2.6 $MPa^{1/2}$. Due to strong interactions between curcumin and palmitoyl groups, it may be possible to increase encapsulation capacity of GCPQ polymer by increasing number of palmitoyl groups on the GCPQ polymer. Glycol chitosan and palmitoyl groups have a solubility difference of 5.1 $MPa^{1/2}$ with paclitaxel. As this is larger than that of

curcumin, it is proposed that curcumin has higher affinity for GCPQ polymer hence, encapsulation should be less difficult in GCPQ-curcumin formulations.

Paclitaxel has similar solubility parameter difference with the chitosan polysaccharide at 6 $MPa^{1/2}$, suggesting similar degree of affinity to all investigated constituents of GCPQ polymer. Amphotericin B solubility differences with chitosann is much smaller than that of paclitaxel at 2.5 $MPa^{1/2}$. Suggesting strong affinity for chitosan polysaccharide. Caspofungin is seen to have a difference of 10 $MPa^{1/2}$, 10 $MPa^{1/2}$ and 20.7 $MPa^{1/2}$ with glycol chitosan, palmitoyl group and chitosan predicting weak interactions with GCPQ constituents compared to other class IV drugs. so it is unlikely that encapsulation efforts will be successful. However, further insights from individual Hansen Solubility Parameters and RED values found in Table 2-1 to Table 2-3 are needed to make more accurate predictions.

The order of interaction for GCPQ constituents based on solubility parameters is Curcumin > Paclitaxel > Amphotericin B > Caspofungin Acetate > Caspofungin. This may be used to inform experimental design as data predicts the effect of increasing palmitoyl groups length on affinity of drug compounds to polymer, which in turn influences encapsulation efficiency. Experimental data will be required to confirm predictions.

2.4.3 Hansen Solubility Parameters and RED Values

Hansen Solubility Parameter values in Table 2-1 and Table 2-2 reiterate solubility parameters. It is possible to compare similarities between individual HSP values for example, curcumin has the most similar HSP to palmitoyl group and so is predicted to have the highest affinity compared to other drug compounds analysed. This also correlates with solubility predictions mentioned above however, a more accurate approach is comparing HSP distances which considers all HSP parameters. These HSP distance comparisons will be discussed in the next section.

RED values of curcumin, caspofungin and caspofungin acetate were determined using HSPiP software and data was presented in Table 2-3. Amphotericin B and paclitaxel RED values were also determined for comparison, as these are hydrophobic drug compounds previously encapsulated in GCPQ. In general, RED values below 1

indicate high affinity (Abbott et al., 2008). Results show that paclitaxel and amphotericin B would have RED values of 5.11 and 3.81 respectively, suggesting a lack of 'miscibility' or affinity to GCPQ components. However, experimental data demonstrate that both drugs can be encapsulated in GCPQ at concentrations of 2.0 mg/mL for paclitaxel and oral bioavailability of 24% for amphotericin B (Serrano et al., 2015b; Odunze et al., 2019).

This suggests a discrepancy between the forces at play when encapsulation with GCPQ polymers is considered compared to HSP model predicted behaviour and a potential need to adjust ideal RED value based on composition of compounds being analysed. Perhaps, general rules for simple compounds do not apply in complex polymers – or alternatively mixing in bulk and within systems in which drug and nanoparticles are dispersed in aqueous bulk medium. RED limit for this analysis has been adjusted to fit amphotericin B and paclitaxel limits.

Focus was placed on palmitic chain RED values as this is an easily modifiable parameter of GCPQ polymer. The new adjusted range for palmitic chain was between 3.81 and 5.11 as these correlates to amphotericin B and paclitaxel RED values. Other investigated drug compounds; curcumin, caspofungin and caspofungin acetate have RED value within this range, at 2.14, 4.82 and 5.07 respectively so, predictions favour encapsulation. Overall, predictions based on RED data supports HSP and solubility parameter data.

2.4.4 HSP Distance

A perfect thermodynamically favourable interaction will have a net difference of 0 $MPa^{1/2}$ however, Table 2-4 shows large HSP distances ranging from 8.60 to 20.4 $MPa^{1/2}$. This data suggests that the GCPQ components and drug compounds are significantly different and based on the concept that like dissolves like, there is no favourable interaction between drug compounds and GCPQ polymer.

Here, there is a focus on affinity to GCPQ constituents based on HSP differences between GCPQ constituents and drug compounds. Palmitoyl group is a focus point for comparison as this parameter is easily modulated to encourage drug encapsulation. The order of drug affinity to palmitoyl group is Curcumin > Paclitaxel >

Caspofungin Acetate > Caspofungin and Amphotericin B. This generally follows the sequence predicted by solubility parameter with the exception of amphotericin B moving from third strongest interaction to the weakest interaction.

As both paclitaxel and amphotericin B have been previously encapsulated in GCPQ to form stable oral formulations, assumptions on ideal HSP distances can now be reassessed. Stronger interactions between compounds which have shorter HSP differences has been proposed (Abbott et al., 2008). While this is wildly accepted, there is no maximum HSP distance which prevents polymer and drug interactions in the literature. These values may be proven experimentally for a set group of polymers however, values will not apply to all polymer constituents due to variability in chemical structures. For this reason, ideal HSP distances can be set using previous experimental data as a guide. In this case, while a shorter distance is encouraged, HSP distances up to 20.4 $MPa^{1/2}$, corresponding to amphotericin B and palmitoyl group HSP distance can be defined as an acceptable range for palmitoyl-drug interactions. This presents the opportunity for caspofungin to be encapsulated within the GCPQ polymer as its HSP difference (20.3 $MPa^{1/2}$) is within the new limit.

2.4.5 Hansen Spheres

Figure 2-3Figure 2-5 show a visual representation of reactivity sphere of GCPQ constituents and drug compounds (Curcumin, Caspofungin, Caspofungin Acetate, Paclitaxel and Amphotericin B) as well as HSP distances. Drugs of particular interest were curcumin and caspofungin however, paclitaxel and amphotericin B spheres were also plotted for comparison as these are both hydrophobic drug compounds that have previously been formulated with GCPQ polymers. There is no clear trend between the distance of sphere of drugs investigated and that of GCPQ constituents. 2D plots focussed on δ_D and δ_P bonding components of compounds as these have the largest contributions towards thermodynamic interactions (Abbott et al., 2008).

Paclitaxel Hansen plot showed all GCPQ constituents were located outside the sphere. This reflects the RED values above 1 in Table 2-3 and suggests interactions between paclitaxel and GCPQ polymer is theoretically unfavourable. In addition to that, glycol chitosan and chitosan Hansen spheres are located closest to that of

paclitaxel while the palmitoyl group sphere is further away, also supporting RED value data. When comparing 2D data of δ_D and δ_P interactions however, there is a slight difference. Here, the Hansen sphere of glycol chitosan and palmitoyl group are located close to the circumference of paclitaxel's sphere. While Hansen spheres do not overlap, this suggests a more favourable interaction between paclitaxel and palmitoyl groups and glycol chitosan backbone which could possibly be further encouraged under different conditions. Research of paclitaxel formulations in the literature showed high loading efficiency (up to 96.8%) of paclitaxel in alternative glycol chitosan based nanocarrier (Koo et al., 2013; Liang et al., 2018; Kim et al., 2006), supporting the sphere predictions. Further experimental research with varied reaction conditions such as temperature, pressure, external energy in the form of sonication, etc may be altered and effect on paclitaxel-GlyChi interaction studied.

As GCPQ palmitoyl group and paclitaxel have been predicted to have less favourable interactions, the question of effect of degree of palmitoylation (DP %) and degree of quaternisation (DQ %) on paclitaxel encapsulation arises. Theoretic data suggests increase in DP will result in less interaction between polymer and paclitaxel hence, less encapsulation efficiency can be assumed. This goes against the notion that "like dissolves like". In this instance, "like" represents hydrophobic molecules. Analysis of GCPQ-Paclitaxel formulations showed increasing degree of palmitoylation of polymer from 20% to 37% resulted in a slight increase in encapsulation efficiency from 96.63±5.27 % to 99.81±3.12 % (Odunze, 2018). It is also important to note that in formulations where DP% is similar at 19 % and 20 % but DQ is almost doubled from 12 % to 22 %, encapsulation efficiency also increased from 57 % to 97 % (Odunze, 2018). This suggests that addition of another moiety, in this case, quaternary ammonium salts can alter reactivity profile of a polymer and hence, its ability to encapsulate otherwise unsuitable drugs.

Similar to paclitaxel, the Hansen plot of amphotericin B shows all GCPQ constituents lie outside the sphere of reactivity (Figure 2-2) also reflecting high RED values in Table 2-3. 3D plots show chitosan polysaccharide sphere is in closer proximity to that of amphotericin B, followed by the glycol chitosan sphere and then the palmitic chain sphere, both a noticeable distance away. This suggests two things: Firstly, a high affinity for chitosan polysaccharide and secondly, palmitoyl groups and glycol chitosan have similar impact on amphotericin B - GCPQ interactions. To address the first

assumption, comparison of amphotericin B and other chitosan based nanocarriers showed encapsulation efficiency values up to 95%, supporting HSP sphere data (Mehrizi et al., 2018; Parvez et al., 2020; Sohail et al., 2021; Vásquez Marcano et al., 2018).

The second assumption allows the assumption that increasing the molar volume of palmitoyl sidechains within the GCPQ polymer will result in higher amphotericin B encapsulation efficiencies. Experimental data shows GCPQ encapsulated amphotericin B formulations have been created and have encapsulation efficiency of 90% and oral bioavailability of 24 %, on par with amphotericin B cochleates formulations (Serrano et al., 2015b). Polymer used had a DP % and DQ % of 17 %, giving it equal degrees of hydrophobicity and hydrophilicity. Data showed DP % values over 25 % failed to form nanosized complexes and resulted in aggregates (Serrano et al., 2015b). The Hansen plot only accounts for one unit of palmitoyl groups so, it is possible that increasing the molar percentage of palmitoyl groups causes interaction to be more favourable until eventually, reactivity spheres of both amphotericin B and palmitoyl group overlap. Although, this increase can be assumed to have a limit of 17 %.

Curcumin Hansen plot mirrors that of paclitaxel where all the GCPQ constituents lie outside its sphere of reactivity. When comparing the δ_D v δ_P 2D plot, it is observed that the Hansen sphere of glycol chitosan and palmitoyl group are near that of curcumin, while that of chitosan polysaccharide is a significant distance away. This mirrors HSP distance values in Table 2-4. Where palmitoyl group and glycol chitosan have the similar distances of 8.6 $MPa^{1/2}$ and 7.0 $MPa^{1/2}$ from the centre of the curcumin sphere, and chitosan has almost twice the distance at 15.4 $MPa^{1/2}$.

Curcumin formulations in the literature showed above average loading efficiency (up to 69 %) of curcumin in alternative glycol chitosan based nanocarrier (Arya et al., 2018; Mollaei et al., 2016). Due to similarities in Hansen sphere plot, it can be assumed that curcumin will have similar encapsulation efficiencies with GCPQ polymers as paclitaxel has. Perhaps a similar technique to what was employed in paclitaxel formulations can be used to encapsulate curcumin. This would mean that %DP between 20 % and 37 % are proposed to be optimum polymer parameters. However, experimental research will be required to validate this assumption.

When looking at the Caspofungin Hansen 3D and 2D plot, it is important to note that the image has been zoomed out by a factor of two, compared to Curcumin, Amphotericin B and Paclitaxel. Therefore, distances between GCPQ parameters and Caspofungin are twice as large in caspofungin plot, reflecting HSP distance values in Table 2-4. What this suggests is there is extremely low binding affinity between Caspofungin and GCPQ constituents hence, reaction is thermodynamically unfavourable. Caspofungin is therefore not a good drug candidate for GCPQ encapsulation. Currently, it only clinically exists as its diacetate base (Letscher-bru and Herbrecht, 2003a), possibly due to unfavourable properties as predicted by HSP. As there are presently no caspofungin-glycol chitosan formulations in the literature, no comparisons between Glycol chitosan-based formulations can be made. Finally, caspofungin sphere data varies largely from paclitaxel and amphotericin B, two other class IV drugs and so, there is no clear trend to help guide experimental method for formulation or GCPQ modifications to encourage interaction.

2.5 Conclusion

In conclusion, this study does not support the notion that HSP data can be independently employed as a prediction tool in drug-polymer interactions. Data shows GCPQ constituents (chitin, glycol chitosan and palmitoyl group) interact with drug compounds to varying extents. Strength of interaction depends on the molecular size, molecular structure, and shape of the drug compound as these influence Hansen solubility parameters namely; δ_d, δ_p, δ_h and Mvol. The literature suggest Hansen solubility parameter values and distance from the centre of a compound's reactivity sphere can give insight into drug-polymer interactions however, ideal conditions for thermodynamic interactions aren't clearly defined. One example of this is in RED values; where stable polymer-drug formulations with RED values up to 5.11 have been created with high encapsulation efficiencies. Such ideal conditions may therefore be prone to change based on compounds being analysed. It appears there is no clear trend to be observed with hydrophobic, BCS class IV drug compounds and GCPQ as Amphotericin B and Paclitaxel have varied HSP values. Finally, 2D Hansen spheres show more favourable interaction between the palmitoyl chain and most drug compounds hence, particular interest in degree of palmitoylation of GCPQ polymers should be considered in encapsulation studies. Overall, the use of experimental data is encouraged due to limitations currently present in HSP predictions.

3 Polymer Synthesis and Characterisation

3.1 Introduction

Outlined in this chapter are the methods employed in the synthesis of N-palmitoyl-N-monomethyl-N,N- dimethyl-N,N,N-trimethyl-6-O-glycolchitosan, or quarternary ammonium palmitoyl glycol chitosan (GCPQ), described in 1.5.1 (Uchegbu et al., 2014). Characterisation techniques used include proton nuclear magnetic resonance (NMR) to determine the degree of palmitoylation and quaternisation, gel permeation chromatography combined with multi-angle laser light scattering (GPC-MALLS) to determine molecular weight and dynamic light scattering (DLS) to determine particle size and zeta potential. The aim of this chapter was to synthesis GCPQ polymers which will be used to for encapsulation efficiency experiments in Chapter 4. Experimental data will then be compared to theoretical HSP data.

3.2 GCPQ Polymer Synthesis

3.2.1 Materials

Most of the reagents and chemicals were obtained from both, Sigma Aldrich Chemical Company and Fischer Scientifics UK Ltd, unless stated otherwise:

Reagents: Glycol Chitosan (WAKO GmbH, Batch LEJ7169), Palmitic acid N-hydroxysuccinimide ester (Carbosynth), Sodium hydroxide, Sodium Chloride, Sodium Iodide, Hydrochloric acid, Glacial acetic acid, Methyl iodide, Triethylamine, Methyl tertiary-butyl ether (Acros Organics), N-methyl-2- pyrrolidone (Acros Organics);

Materials: Amberlite IRA-410 Resin PES Filters 0.22 μm, PTE Filters 0.45 μm, Visking seamless cellulose dialysis tubing (3.5 kDa) (Medicell International Ltd., London, UK);

Solvents: Millipore double deionized water (<18Ω), Deionized water, Diethyl ether, Dimethyl Sulphoxide (Acros Organics), Deuterated Methanol, Methanol HPLC gradient, Acetone, Absolute ethanol;

Equipment: GPC-MALLS equipped with: Dawn Heleos II MALLS detector (120 mW solid-state laser operating at λ = 658 nm), Optilab rEX interferometric refractometer (flow cell: 7.4 uL, λ = 658 nm), quasielastic light scattering (QELS) detectors (Wyatt Technology Corporation, Santa Barbara, CA, USA), and Agilent 1200 auto sampler (Agilent Technologies, UK). Zetasizer Nano S90 (Malvern, UK), Biotwin NMR (Bruker Avance, UK) 400MHz NMR spectrometer, Water bath, Magnetic stirrer, Magnetic stirrer bar, Oil bath, Hot plate.

3.2.2 Method

GCPQ was synthesised using an acid degradation step followed by a palmitoylation and a quaternisation reaction. Synthesis and characterisation of GCPQ polymer were adapted from protocols set up in the lab (Uchegbu et al., 2001; Siew et al., 2011; Lalatsa et al., 2012b) as shown in Figure 3-2. The order of synthesis is outlined below:

Glycol Chitosan (GC) degradation (dGC)

GC [Molecular weight (MW) ~ 120 kDA, 10 g] was suspended in HCL (4 M, 332 mL) in a 500 mL conical flask and left to dissolve while being magnetically stirred for 5 minutes at RT. The resulting solution was then left to shake in a water bath at 50 ˚C for 6 hours, 12 hours and 24 hours to produce polymer with target molecular weights of about 20 kDa, 12 kDa and 8 kDa. Relationship between molecular weight of dGC and degradation time is shown in Figure 3-1. Once the degradation step was complete, dGC was precipitated using 80mL of acetone. The crude product was then triturated three times against 20 mL of acetone. Purified dGC was collected by vacuum filtration using a sintered glass filter porosity 3 (16-40 µm pore size) and left to dry in vacuo for at least 24 hours. The yield of the process was 24 % for 6 hours dGC, 95 % and 43 % for 24 hours dGC.

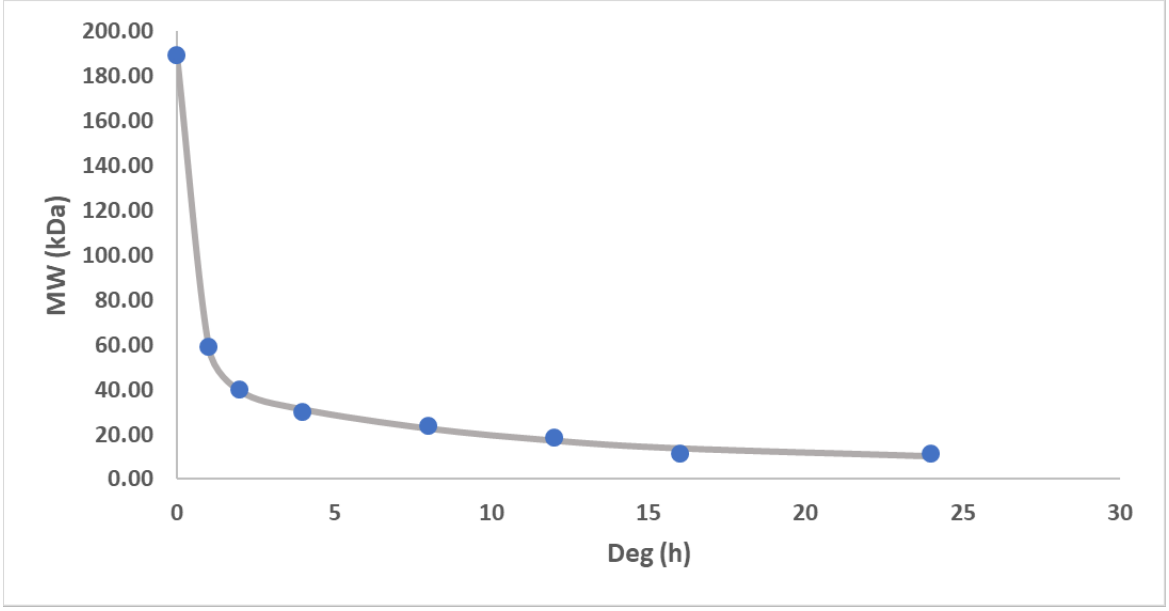

Figure 3-1: Graph showing relationship between degradation time of GC and final molecular weight of dGC.

Palmitoylation of dGC

One gram of dGC was dissolved in 30.88 mL of 3.7 % TEA in DMSO and magnetically stirred at room temperature in a round bottom flask. Upon complete dissolution of dGC in DMSO, a required mass of palmitic acid N-hydroxysuccinimide (PNS) was added and left to magnetically stir for 16 hours, protected from light. The mass of PNS used was calculated using molar equivalents, depending on the degree of palmitoylation required. To achieve a 10 % degree of palmitoylation, 0.182 g of PNS was added to the round bottom flask and the reaction was left to stir magnetically overnight in a fume cupboard while being shielded from light. After 16 hours, the reaction was precipitated using a 150 mL solution of acetone/MTBE (1:2) and left to precipitate overnight. The supernatant was removed from settled precipitate and product was washed with 150 mL of acetone and left to filter out under pressure. Then washed three times with 25 mL of acetone and MTBE to remove NHS and palmitic acid, also under pressure filtration. The solid *N*-palmitoyl glycol chitosan (pGC) was collected and left to dry in vacuo for at least 24 hours.

The above process was repeated using varying amounts of PNS to achieve a range of DP % on the pGC product. The yield of pGC synthesized is shown in Table 3-1.

Quaternisation of Palmitoyl Glycol Chitosan

One gram of pGC was dispersed in 58.08 mL of N-methyl-2-pyrrolidone (NMP) and left to magnetically stir overnight in a fume hood. Once dissolved, 16.59 mL of NaOH (8.137 mg/mL in NMP) and 8.3 mL of NaI (18.554 ng/mL in NMP) were added to the solution, purging with nitrogen gas and stirring for 15 minutes in between each addition. Following that, an appropriate amount of methyl iodide (MeI) was injected into the solution and left to stir magnetically in hot oil for 3 hours at 36^{o}C to achieve desired degree of quaternisation. The mass of MeI used was calculated using molar equivalents, depending on the degree of quaternisation required. To achieve a 20 % degree of palmitoylation, 1.5 mL of MeI per gram of pGC was added to the reaction. At the end of the quaternisation process, the product was precipitated by adding 250 mL of 0.1 M of NaOH and 5 M NaCL and left to settle overnight. The supernatant of precipitation was removed by vacuum and crude product washed twice with 83 mL of 0.1 M NaOH. The resulting GCPQ was resuspended by slow addition of 32 % HCL (1%v/v) under magnetic stirring until a pH of 3 was achieved. Dialysis was carried out using 3.5 kDa dialysis tubes. These were placed in a 5L beaker and left to dialyse against 5 L of distilled water with magnetic stirring. Each hour, the water within the bucket was replaced until the value shown when measured with a conductance meter was below 10 µs. This took a total of 10 changes.

To remove any free iodide in dialysate, 3 g of Amberlite IRA 410 ion exchange resins were dispersed in solution, stirred for 15 minutes. After 15 minutes, 200 mg of sodium nitrate was dissolved in 1 mL of a 2.5 % acetic acid solution. A small volume of GCPQ-amberlite solution was added to a clean vial along with 2 drops of chloroform before adding 10 drops of solubilised sodium nitrate was also added to the vial. A clear chloroform layer confirmed the absence of iodide in the dialysate. Once confirmed, Amberlite resin was removed using filter paper and the solution was subjected to snap freezing and freeze-drying.

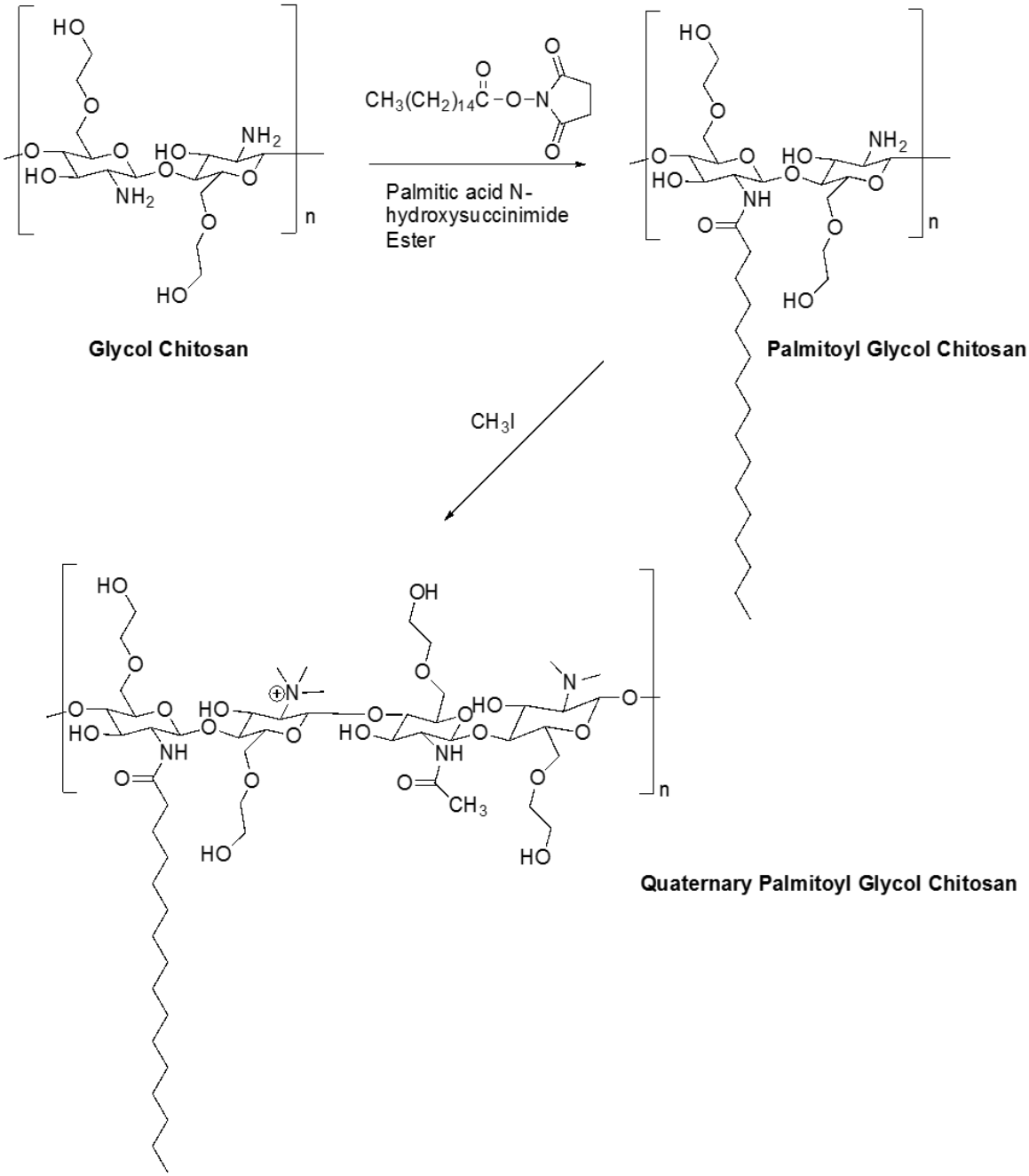

Figure 3-2: Scheme showing the steps in the synthesis of GCPQ

3.3 GCPQ characterisation

3.3.1 ^{1}H-NMR

Proton Nuclear Magnetic Resonance is a widely used technique in the characterisation or organic compounds. It can aid in identifying unique structures within a compound

based on their carbon-hydrogen framework. Thus, it has been employed in the characterisation of the degrees of palmitoylation and quaternisation of the GCPQ polymers synthesized.

NMR operates on the principle that; the nucleus of the sample being analysed can absorb energy when exposed to radiofrequency radiation at the appropriate frequency within a magnetic field. Ideal frequency of radiation required for energy absorption is determined by the chemical environment and type of the nucleus (James, 1998). When this occurs in the presence of an external magnetic field, the nucleus resonates between high and low energy states due to aligning (parallel) and misaligning (antiparallel) with the magnetic field. The strength of the magnetic field determines the difference in energy between the high and low energy states. While in its low energy state, a nucleus can flip into its high energy state by absorbing energy equal to the difference between both states. This energy flip results in a peak on the NMR spectrum. In proton NMR, the position of the peaks on the spectrum is termed its chemical shift, δ and is determined by the electrons orbiting the nuclei. The position of the electron in relation to the nuclei varies due to the shielding and de-shielding effects resulting from electrons withdrawing and donating groups to adjacent nuclei (James, 1998). NMR can combine information on chemical shifts, coupling and integration to determine the structure of a given sample.

In this instance, pGC had ^{1}H-NMR (CD_3OD, D_2O, CD_3COOD, 4:2:0.5) δ: 0.86 (3H, CH_3CH_2), 1.2-1.4 (24H, $CH_3(CH_2)_{12}$), 1.6 (2H, CH_2CH_2CO), 2.13 (3H, CH_3CO), 2.14 (2H, CH_2CO), 3.15 (1H, CH – C2 sugar monomer), 3.5 - 4.5 (9H, $HOCH_2CH_2$ and H-3, H-4, H-5, H-6 CH –sugar monomer). And GCPQ had ^{1}H-NMR (CD_3OD, DCl, 99.99:0.001) δ: 0.86 (3H, CH_3CH_2), 1.2-1.4 (24H, $CH_3(CH_2)_{12}$), 1.6 (2H, CH_2CH_2CO), 2.13 (3H, CH_3CO), 2.14 (2H, CH_2CO), 2.8 - 3.2 (9H, CH_3NH and $(CH_3)_2N$, 3.15 (1H, CH – C2 sugar monomer), 3.4 (9H, $(CH_3)_3N+$), 3.5 - 4.5 (9H, $HOCH_2CH_2$ and H-3, H-4, H-5, H-6 CH –sugar monomer).

Samples were prepared according to protocols set up in the lab SOP 251. 10 mg of GCPQ was dissolved in 700 µL of Methanol-D4. The solution was placed into NMR glass tubes for ^{1}HNMR analysis. The degree of palmitoylation was calculated using Equation 7 which compares the ratio of palmitoyl methyl protons (0.89 ppm) to sugar protons (3.5-4.5 ppm) and the degree of quaternisation was calculated using

Equation 8 which compares the ratio of quaternary ammonium (3.45 ppm) to sugar protons.

Equation 7:

$$\%\ \text{Palmitoylation} = \frac{\text{ratio of palmitoyl protons (0.89ppm)}}{\text{ratio of sugar protons (3.5 - 4.5ppm)}} \times 100$$

Equation 8:

$$\%\ \text{Quaternisation} = \frac{\text{ratio of quaternary ammonium (3.45ppm)}}{\text{ratio of sugar protons (3.5 - 4.5ppm)}} \times 100$$

The ratio of quaternary ammonium to palmitoyl groups (QPR) was determined using the equation below.

Equation 9:

$$QPR = \frac{Mole\ \%\ quaternisation}{Mole\ \%\ palmitoylation}$$

3.3.2 Gel permeation chromatography – Multi Angle Laser Light Scattering (GPC-MALLS)

The molecular weight of GCPQ was determined using GPC MALLS, a technique which couples gel permeation chromatography (GPC) with multi-angle laser light scattering (MALLS) in order to characterise a particles' molecular weight, size distribution and branching (Podzimek, 1994).

GPC was first employed in 1964 and is an example of a size exclusion chromatography technique (Moore, 1964). In this technique, a column packed with beads which vary in pore sizes makes up the stationary phase while the mobile phase is the solvent in which the samples are dissolved in. The sample is dissolved in the mobile phase before being introduced to the system via the column at a steady rate

(Skoog et al., 2007). In the separation process, molecules with higher molecular weights move faster through the column as they do not fit into the pores in the beads. Hence, higher molecular weight molecules elute first and lower molecular weight molecules elute last (Lecchi and Abramson, 1999). Although, this is based on two assumptions; firstly, that there are no interactions between molecules and surface of the bead, and secondly, polymers fully extended. Interactions between polymer and surface beads (e.g., for hydrophobic or charge polymers) will skew results. Results will also be skewed in instances where polymer experiences swelling, resulting in a change in radius. With GCPQ, this challenge presents for high DP % formulas, resulting in aggregation.

Molecular weight is then determined using a calibration standard in order to establish the relationship between molecular weight and elution volume. However, this fractionationation based on hydrodynamic volume method is only applicable for narrowly distributed, excluding branched polymers. These branched polymers have been reported to have smaller sizes compared to linear polymers of the same molecular weight (Mukerjee and Vishwanatha, 2009; Grcev et al., 2004). With branched polymers, a simultaneous measurement of light scattering intensity and concentration is required to measure molecular weight (Mukerjee and Vishwanatha, 2009; Grcev et al., 2004). For this reason, there is a multi-angle laser light scattering (MALLS) detector attached to the GPC. This light scattering signal is proportional to the product of the concentration of the solution, c, and the weight average molecular weight, Mw. Meaning polymers with very low MW require a high concentration for detectable light scattering (LS) signals. An accurate dn/dc (refractive index increment of the polymer) is also required to interpret light scattering data (Mukerjee and Vishwanatha, 2009; Grcev et al., 2004). Dn/dc is determined by injecting a series of dilutions of the polymer solution directly into a refractive index detector. A higher dn/dc value reflects a greater increase in refractive index of the polymer solution at any given concentration.

Method

GCPQ polymer molecular weights were determined using Wyatt gel permeation chromatography-multi angle laser light scattering instrument (GPC-MALLS) equipped with: Dawn Heleos II MALLS detector (120 mW solid-state laser operating at λ = 658

nm), Optilab rEX interferometric refractometer (flow cell: 7.4 uL, λ = 658 nm), quasielastic light scattering (QELS) detectors (Wyatt Technology Corporation, Santa Barbara, CA, USA. The mobile phase was a 0.3 M anhydrous sodium acetate buffer, 0.2 M glacial acetic acid, pH = 4.5 for GC and a mixture of acetate buffer and methanol at 35:65 v/v for GCPQ. PEG standard was also measured to validate results gotten

For dn/dc measurements, series dilutions were made of polymer dissolved in buffer (0.1, 0.2, 0.3, 0.4, 0.5, 0.6 mg/mL). Samples were filtered using a 0.2 µm, PES, Millipore Millex-HA filter and 100 µL of filtered solution was injected using an Agilent 1200 series auto sampler (Agilent Instruments, Stockport, U.K.) on to a POLYSEPGFC-P guard column (35 Å~ 7.8 mm, Phenomenex, Macclesfield, U.K.) attached to a POLYSEP-GFC-P 4000 column (300 Å~ 7.8 mm, exclusion limit for PEG = 200 kDa, Phenomenex) at a loading concentration of 5 mg mL^{-1}. Measurements were carried out in triplicates and at room temperature. Flow rate of mobile phase was 0.7 mL min^{-1} (Agilent 1200 series isocratic pump attached to an Agilent 1200 series degasser). The data were processed using ASTRA for Windows version 5.3.4.14 software (Wyatt Technology Corporation) (Lalatsa et al., 2012a).

3.3.3 Dynamic Light Scattering (DLS) – Size and Zeta Potential Measurements

3.3.3.1 Size Measurement

Dynamic Light Scattering (DLS), also known as Photon Correlation Spectroscopy or Quesi-Elastic Light Scattering is a technique used to study the diffusion behaviour of particles in solution. In this technique, particles in solution are subjected to a beam of monochromatic light which leads to light scattering at multiple angles. Fluctuations in light scattering intensity is due to Brownian motion of the particles which is dependent on the particles' shape and size. Therefore, the intensity of the scattered light can be analysed as a time-averaged intensity, giving information on the hydrodynamic radius of particles in solution (Hoo et al., 2008).

Stokes-Einstein's equation:

$$d(H) = \frac{kT}{3\pi\eta D}$$

Describes the relationship between hydrodynamic radius and the diffusion coefficient of particles in solution. Where d(H) is the hydrodynamic radius (m), D is the translational diffusion coefficient (m^2/s), k is the Boltzmann's constant (J/K), T is the absolute temperature (K) and η is the viscosity of the solvent (kg/ms^{-1}).

As the hydrodynamic radius is the diameter of a sphere with the same translational diffusion coefficient as the particles being measured in solution, the Z-average measurements are therefore a cumulative average of particle diameter. Polydispersity index (PDI) is the square of the normalised standard deviation of the size distribution (Nobbmann et al., 2007).

Method

Particle size was measured using dynamic light scattering (DLS) on a fixed scattering angle Zetasizer nano-S system (Malvern Instruments Ltd., Malvern, UK). Samples were vortexed and then a minimum volume of 70 µL was placed in a 200 µL quartz cuvette at 25 ^oC. Light scattering was detected at 173^o and obtained in automatic mode. Total calibration time was 120 seconds and measurement duration took a total of 150 seconds. Data was analysed on DTS (Version 4.2) software.

3.3.3.2 Zeta Potential Measurement

Zeta potential (ζ) analysis measures the surface charge of nanoparticles in solution. Based on the electrokinetic phenomena (EKP), the electric state of nanoparticles in solution is determined by the spatial distribution of surrounding ions, often referred to as the electrical double layer (EDL). The zeta potential is therefore the electric potential of a particle at a position away from the particle's surface, somewhere within the diffuse layer (Xu, 2008).

The zeta potential is an important parameter as it is an indicator for colloidal stability of nanoparticles in suspension (Delgado et al., 2007) with the limits of stability being more positive than +30 mV and more negative than -30 mV (Instruments, 2000). The stability of colloidal systems has been described according to the Derjaguin, Verwey, Landau and Overbeek (DLVO) theory which considers the van der Waals forces of attraction and repulsion of particles within the colloidal system (Behrens et al., 1998). It is the balance of these forces which predicts the likelihood of a stable system or flocculation/coagulation (Instruments, 2000; Behrens, Borkovec and Schurtenberger, 1998). pH, conductivity and concentration of formulation are all factors which affect the zeta potential of a solution (Instruments, 2000; Clogston and Patri, 2011).

In order to determine the zeta potential of a solution, an electric field is applied across the sample. This causes charged particles in solution to be attracted towards the electrode of opposite charge. Zeta potential is hence the electrophoretic mobility of the particles as defined in the Henry equation (Clogston J.D. and Patri A.K., 2011).

$$U_E = 2\varepsilon z f(\kappa a)/3\eta$$

Where U_E = is the electrophoretic mobility, ε is the dielectric constant, $f(\kappa a)$ is the Henry function, η is the absolute zero-shear viscosity of the medium, and κa is a measure of the ratio of the particle radius to the Debye length.

Method

Zeta potential measurements were carried out using the same machine. A minimum of 700µL of solution to be analysed was loaded into folded capillary tubes also known as zeta cells. These are polycarbonate cells with two gold plated electrodes supplied by Malvern, UK (DTS1060C). Zeta Potential measurements were also run at 25 °C and 40 V.

3.4 Results and Discussion

Glycol and Palmitoyl Glycol Chitosan Characterisation

Degradation Time (Hours)	Polymer	Yield (%)	MW (kDa)	Mn (kDa)	PDI (Mw/Mn)	Mole % Palmitoyl
6	GC01	43	16.8	12.4	1.36	Not applicable
	PGC10	87	N.D.	N.D.	N.D.	10
	PGC22	97	N.D.	N.D.	N.D.	22
12	GC02	95	15.8	15.6	1.01	Not applicable
	PGC10	63	N.D.	N.D.	N.D.	10
	PGC25	93	N.D.	N.D.	N.D.	25
	PGC30	88	N.D.	N.D.	N.D.	30
	PGC45	78	N.D.	N.D.	N.D.	45
24	GC03	54	12.3	9.1	1.35	Not applicable
	PGC10	56	N.D.	N.D.	N.D.	10
	PGC22	92	N.D.	N.D.	N.D.	24

Table 3-1: Glycol chitosan and palmitoyl glycol chitosan characterisation

Table 3-1 shows the synthesised degraded GC (dGC) and palmitoylated GC (pGC) and their percentage yield as well as molecular weight measurements for dGC. The yield was calculated by comparing the final mass of the product as a percentage of the initial mass using Equation 10 and Equation 11 below:

Equation 10:

$$\%\, Yield\ \ of\ dGC = 100 \times \frac{final\ mass\ of\ dried\ dGC}{mass\ of\ undegraded\ GC}$$

Equation 11:

$$\%\, Yield\ \ of\ pGC = 100 \times \frac{final\ mass\ of\ dried\ pGC}{mass\ of\ dGC}$$

The reaction yield for dGC ranges from 43 % to 95 % while the yield range for pGC synthesis is from 56 % to 97 %. The molecular weights of dGC were determined using GPC-MALLS (shown in Figure 3-8) based on Equation 12. The polydispersity index (PDI) of the polymers was calculated as a ratio of their average molecular weight (Mw) to the number average molecular weight (Mn) (Equation 13).

Equation 12:

$$MW = 8.92 + 52.02 * e^{-1.56*DEG} + 33.29 * e^{-0.18*DEG}$$

Equation 13:

$$PDI = \frac{Mw}{Mn}$$

GCPQ Characterisation

Polymer	Yield (%)	MW (kDa)	Mn (kDa)	Mole % Palmitoyl group	Mole % Quaternary ammonium group
GC12P24Q9	37	39.2	22.4	24	9
GC12P11Q12	77	N.D.	N.D.	11	12
GC16P10Q25	74	N.D.	N.D.	10	25
GC16P8Q7	53	7.1	14.6	8	7
GC16P24Q11	81	17.1	13.6	24	11
GC16P25Q19	88	17.6	15,5	25	19
GC16P25Q25	72	20.3	22.4	25	25
GC16P25Q35	N.D.	N.D.	N.D.	25	35
GC16P30Q40	33	29.1	19.7	30	40
GC16P45Q54	45	33.9	20.1	45	50
GC12P10Q11	N.D.	N.D.	N.D.	10	11
GC12P22Q16	N.D.	N.D.	N.D.	22	16

Table 3-2: GCPQ polymer characterisation defined as GCxPnQm where 'x' is the molecular weight of polymer, 'n' is the mole percentage of palmitoyl group substitutions and 'm' is the mole percentage. of quaternary ammonium group substitutions.

Table 3-2 shows the reaction yield of GCPQ polymers, calculated by comparing the final mass of GCPQ polymers produced with the initial mass of pGC as a percentage (Equation 14), their respective molecular weight, as well as their degree of palmitoyl and quaternary ammonium group substitutions of synthesised.

Equation 14:

$$\%\, Yield\ \ of\ GCPQ = 100\ \times \frac{final\ mass\ of\ \ dried\ GCPQ}{mass\ of\ pGC}$$

Similar to dGC, calculated PDI was less than 1.7 for all GCPQ polymers, indicative of a narrow weight distribution for synthesised GCPQ polymers. Mole % of both palmitoyl (DP) and quaternary ammonium (DQ) group substitutions were determined using Equation 7 and

Equation 8 respectively. DP for GCPQ polymers ranged from 9% to 45% and DQ from 7 % to 54 %.

NMR spectrums below also reflect some of these parameters. In each spectrum, peak at 0.89 ppm represents palmitoyl protons, the peak at 3.45 ppm represents quaternary ammonium protons while the peak at 3.45 - 4.5 ppm represents sugar protons. Values in red represent the area under the curve.

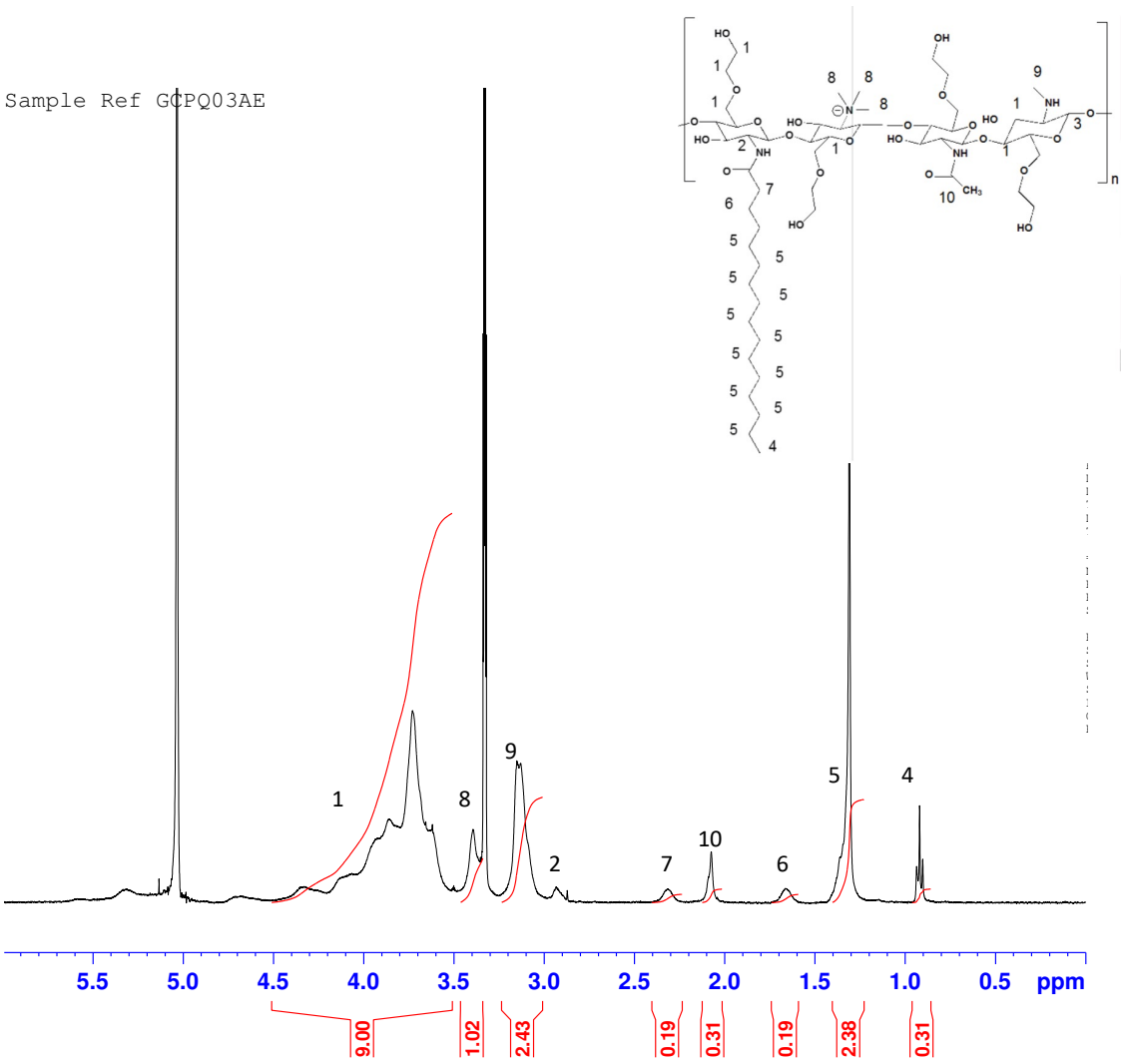

Figure 3-3: Proton NMR of GCxP10Q11. Degree of palmitoylation and quaternisation were 10.3 and 11.3 % respectively. Both calculated using Equation 10 and Equation 11

^{1}H-NMR (CD_3OD, DCl, 99.99:0.001) δ: 0.86 (3H, C**H**$_3$CH$_2$), 1.2-1.4 (24H, CH$_3$(C**H**$_2$)$_{12}$), 1.6 (2H, C**H**$_2$CH$_2$CO), 2.13 (3H, C**H**$_3$CO), 2.14 (2H, C**H**$_2$CO), 2.8 - 3.2 (9H, C**H**$_3$NH and (C**H**$_3$)$_2$N, 3.15 (1H, CH – C2 sugar monomer), 3.4 (9H, (C**H**$_3$)$_3$N+), 3.5 - 4.5 (9H, HOC**H**$_2$C**H**$_2$ and H-3, H-4, H-5, H-6 CH –sugar monomer).

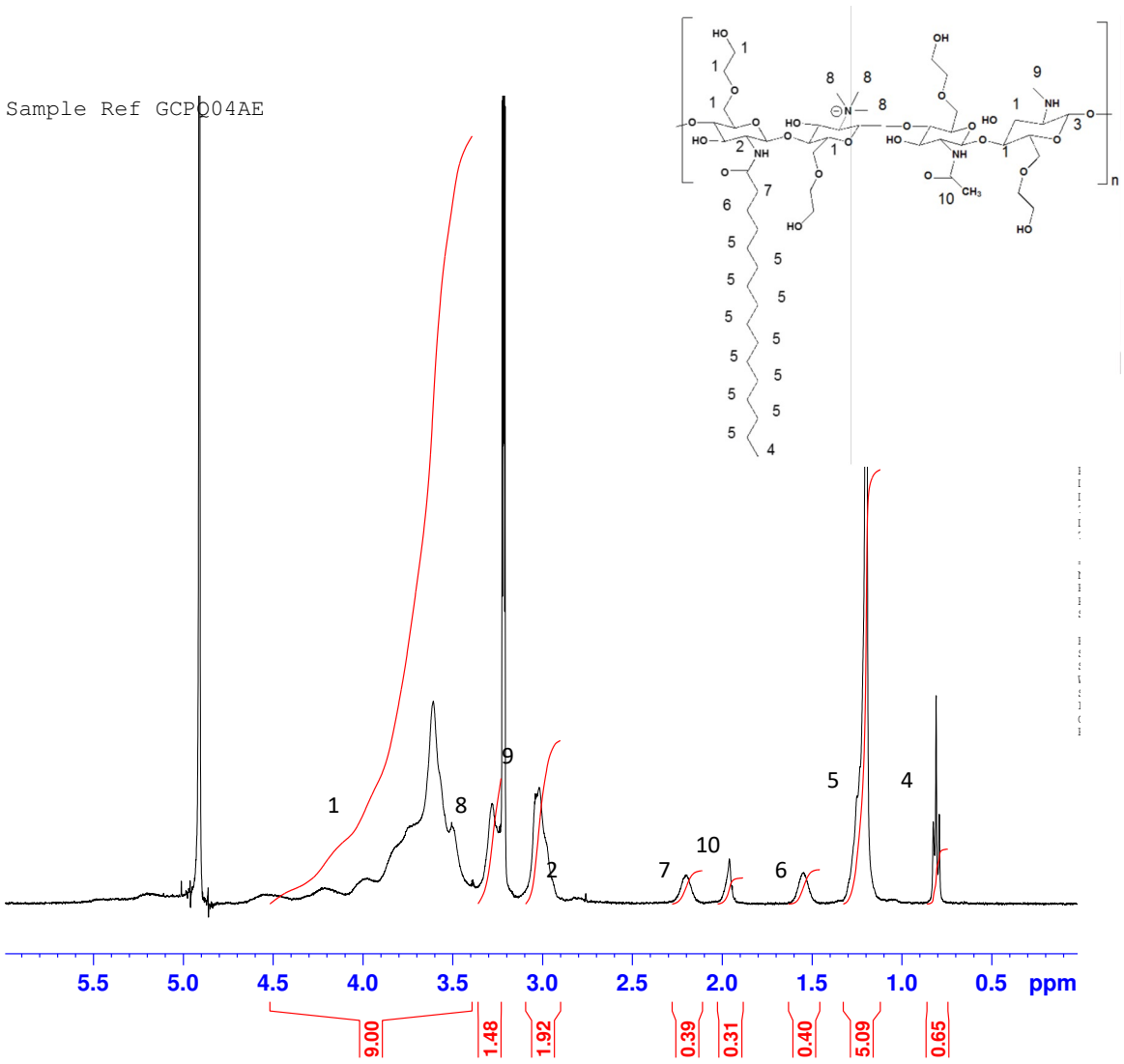

Figure 3-4: Proton NMR of GCxP22Q16. Degree of palmitoylation and quaternisation were 21.6 and 16.4 % respectively. Both calculated using Equation 10 and Equation 11.

^{1}H-NMR (CD_3OD, DCl, 99.99:0.001) δ: 0.86 (3H, C**H**$_3$CH$_2$), 1.2-1.4 (24H, CH$_3$(C**H**$_2$)$_{12}$), 1.6 (2H, C**H**$_2$CH$_2$CO), 2.13 (3H, C**H**$_3$CO), 2.14 (2H, C**H**$_2$CO), 2.8 - 3.2 (9H, C**H**$_3$NH and (C**H**$_3$)$_2$N, 3.15 (1H, CH – C2 sugar monomer), 3.4 (9H, (C**H**$_3$)$_3$N+), 3.5 - 4.5 (9H, HOC**H**$_2$C**H**$_2$ and H-3, H-4, H-5, H-6 CH –sugar monomer).

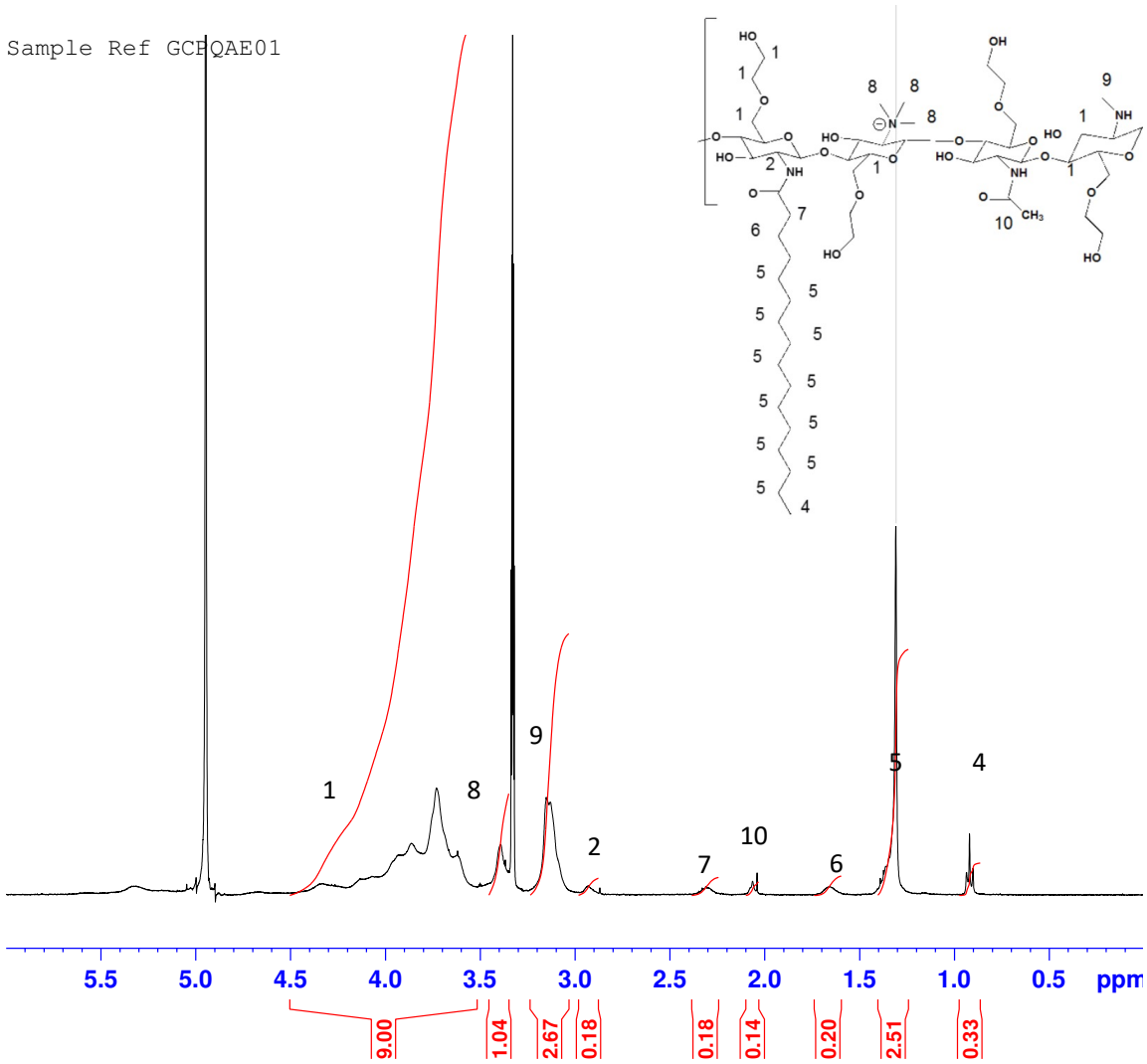

Figure 3-5: Proton NMR of GCxP11Q12. Degree of palmitoylation and quaternisation were 11 and 11.5 % respectively. Both calculated using Equation 10 and Equation 11.

^{1}H-NMR (CD_3OD, DCl, 99.99:0.001) δ: 0.86 (3H, C**H**$_3$CH$_2$), 1.2-1.4 (24H, CH$_3$(C**H**$_2$)$_{12}$), 1.6 (2H, C**H**$_2$CH$_2$CO), 2.13 (3H, C**H**$_3$CO), 2.14 (2H, C**H**$_2$CO), 2.8 - 3.2 (9H, C**H**$_3$NH and (C**H**$_3$)$_2$N, 3.15 (1H, CH – C2 sugar monomer), 3.4 (9H, (C**H**$_3$)$_3$N+), 3.5 - 4.5 (9H, HOC**H**$_2$C**H**$_2$ and H-3, H-4, H-5, H-6 CH –sugar monomer).

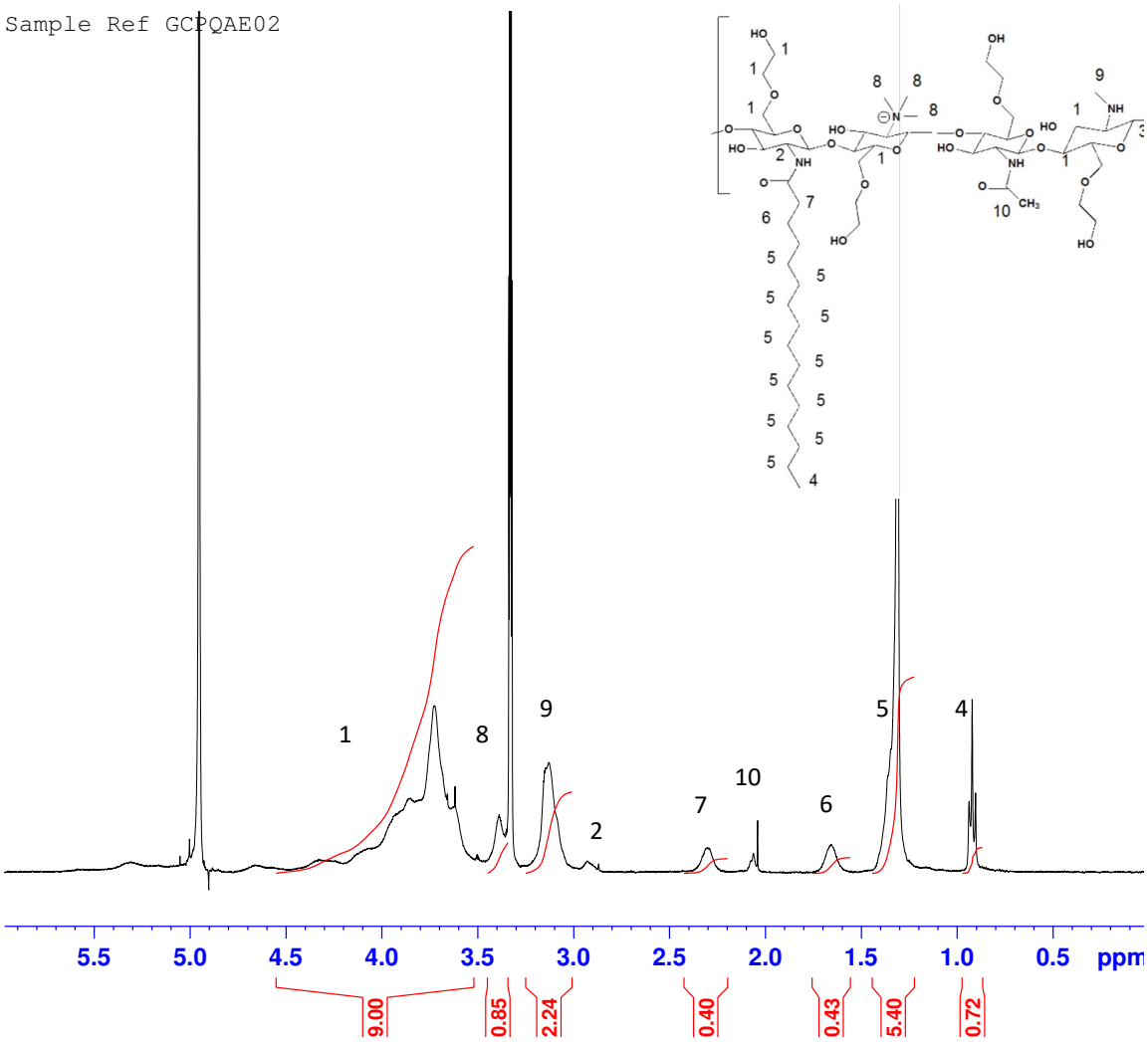

Figure 3-6: Proton NMR of GCxP24Q9. Degree of palmitoylation and quaternisation were 24 and 9.4 % respectively. Both calculated using Equation 10 and Equation 11.

^{1}H-NMR (CD_3OD, DCl, 99.99:0.001) δ: 0.86 (3H, C**H**$_3$CH$_2$), 1.2-1.4 (24H, CH$_3$(C**H**$_2$)$_{12}$), 1.6 (2H, C**H**$_2$CH$_2$CO), 2.13 (3H, C**H**$_3$CO), 2.14 (2H, C**H**$_2$CO), 2.8 - 3.2 (9H, C**H**$_3$NH and (C**H**$_3$)$_2$N, 3.15 (1H, CH – C2 sugar monomer), 3.4 (9H, (C**H**$_3$)$_3$N+), 3.5 - 4.5 (9H, HOC**H**$_2$C**H**$_2$ and H-3, H-4, H-5, H-6 CH –sugar monomer).

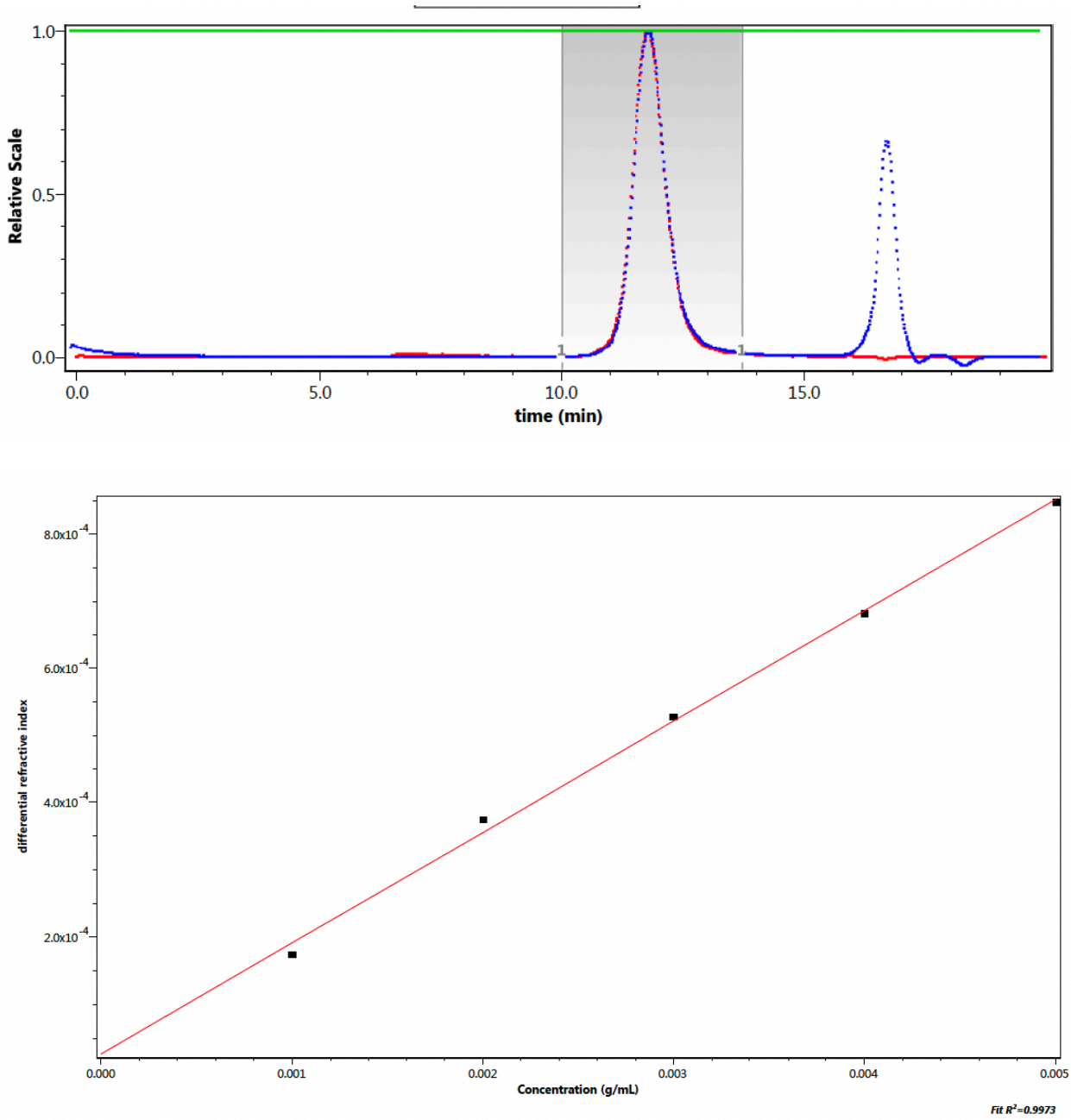

Figure 3-7: GPC chromatogram showing (Top): dGC03; Mw: 12.3e+3Da; Mw/Mn: 9.10(6%); (Bottom): dn/dc 0.1444±3.5197. Red line: Light scattering. Blue line: Refractive index

Figure 3-7 shows GPC MALLS with an elution time of 12 minutes for dGC03, corresponding to 12.3 kDa with a polydispersity of 1.35. The dn/dc for GCPQ polymer was 0.1444±3.5197 mL/g. The refractive index shows two peaks at about 16-17 minutes which is assumed to be ghost peaks as a result of salts present in the mobile phase. Alternatively, these may be aggregates of dGC being formed. Measured

molecular weight is consistent with expected molecular weight as degradation time was hours which correlates with 12 kDa of dGC.

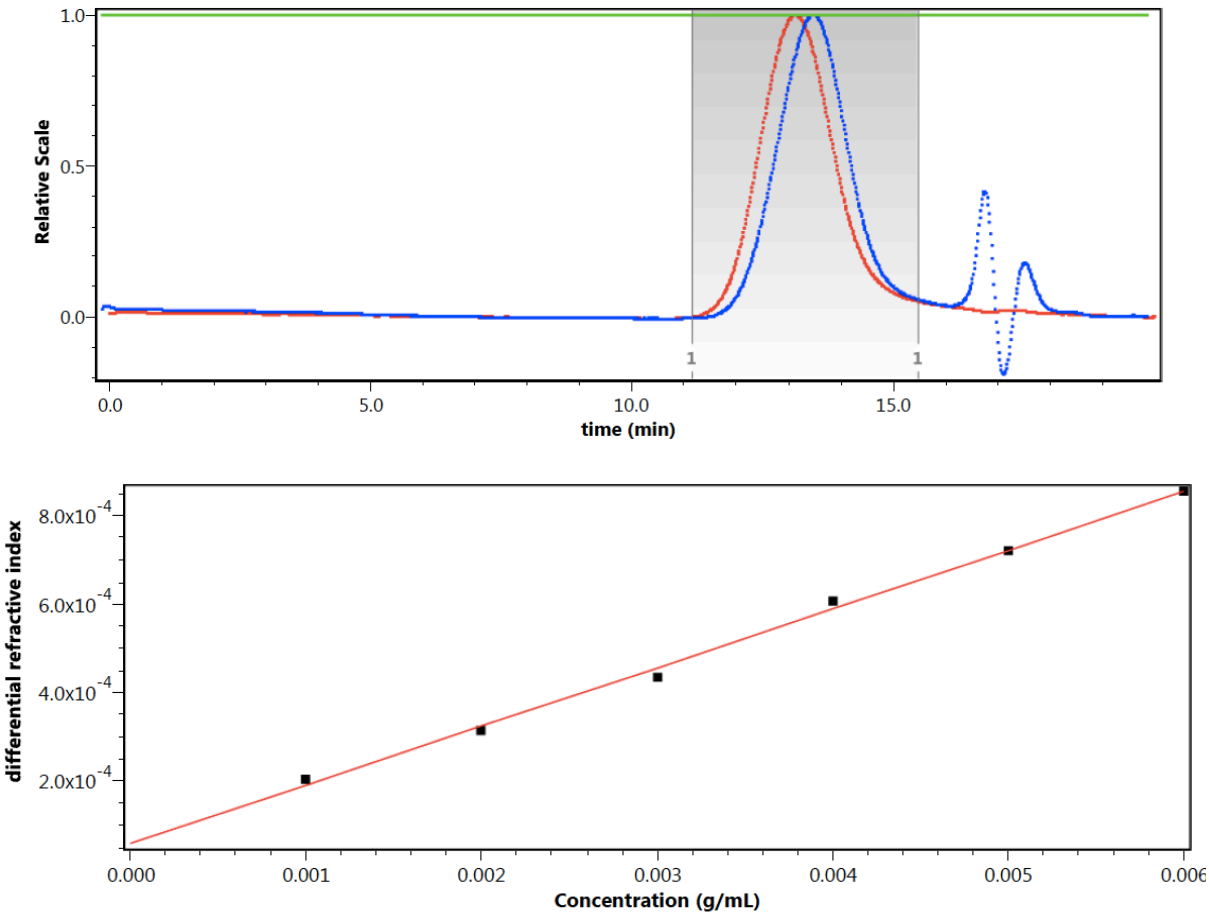

Figure 3-8: GPC Chromatogram showing (top) GCP25Q19 MW; 17.6e+3Da; Mw/Mn: 1.14 (5%); (Bottom); dn/dc 0.1325 ± 0.0029mL/g. Red line represents light scattering and blue line represents refractive index.

Figure 3-8 shows GPC MALLS with an elution time of 12 minutes for GCP25Q19 corresponding to 17.6 kDa with a polydispersity of 1.14. The dn/dc for GCPQ polymer was 0.1325±0.0029 mL/g. The refractive index shows two peaks at about 16-17 minutes which is assumed to be ghost peaks as a result of salts present in the mobile phase. Alternatively, these may be aggregates of GCPQ being formed as a result of relatively high degree of palmitoylation. Measured molecular weight is consistent with expected molecular weight as degradation time was hours which correlates with 15 kDa of GC. Extra weight is attributed to added palmitoyl and quaternary ammonium functional groups.

POLYMER	Z-Average ±SD (d.nm)	PDI±SD	Zeta Potential ±SD (ζ)	QPR
GCP8Q7	454.6±12.5	0.44±0.06	31.9±2.58	0.88
GCP11Q12	100±0.74	0.90±0.17	35.9±2.35	1.09
GCP10Q25	570.1±71.8	0.75±0.71	28.8±2.51	2.27
GCP24Q9	1136±20.5	0.91±0.08	40.67±1.20	0.38
GCP24Q11	334.3±19.6	0.93±0.09	35.3±0.62	0.45
GCP25Q19	187.9±0.03	0.40±0.07	37.8±3.32	0.76
GCP25Q25	284.5±41.5	0.41±0.05	32.6±2.01	1
GCP25Q35	103.5±4.46	0.37±0.06	43.5±2.88	1.4
GCP30Q40	329.7±0.05	0.41±0.05	34.1±1.42	1.33
GCP45Q50	587.3±0.07	0.44±0.07	51.1±1.70	1.11

Table 3-3: Size and Zeta Potential values of GCPQ nanoparticles synthesised

Table 3-3 shows synthesised GCPQ polymers and their physiochemical properties. Polymers with very low DP % and DQ % values (≤10 %) were observed to have the largest z-average values (above 400 nm). With GCP24Q9 having size values in the micrometre range, this was supported by the opacity of the sample in the cuvette. The same is observed for polymers with very high DP % and DQ % values. Smaller particle sizes are observed where DP % (≥24 %) remains the same and DQ % increases, with the exception of GCP25Q25. This also correlates with an increase in zeta potential and QPR. Polymers with DP% below and above 24-25 % show no obvious trends in effects of degree of modification on the size distribution and zeta potential. PDI values for some polymers are considered to be high (>0.5), suggesting broad distribution of particles and so, a more accurate method to determine particle size would have been with TEM images. Some distribution graphs of some polymers are shown in Figure 3-9 to Figure 3-11.

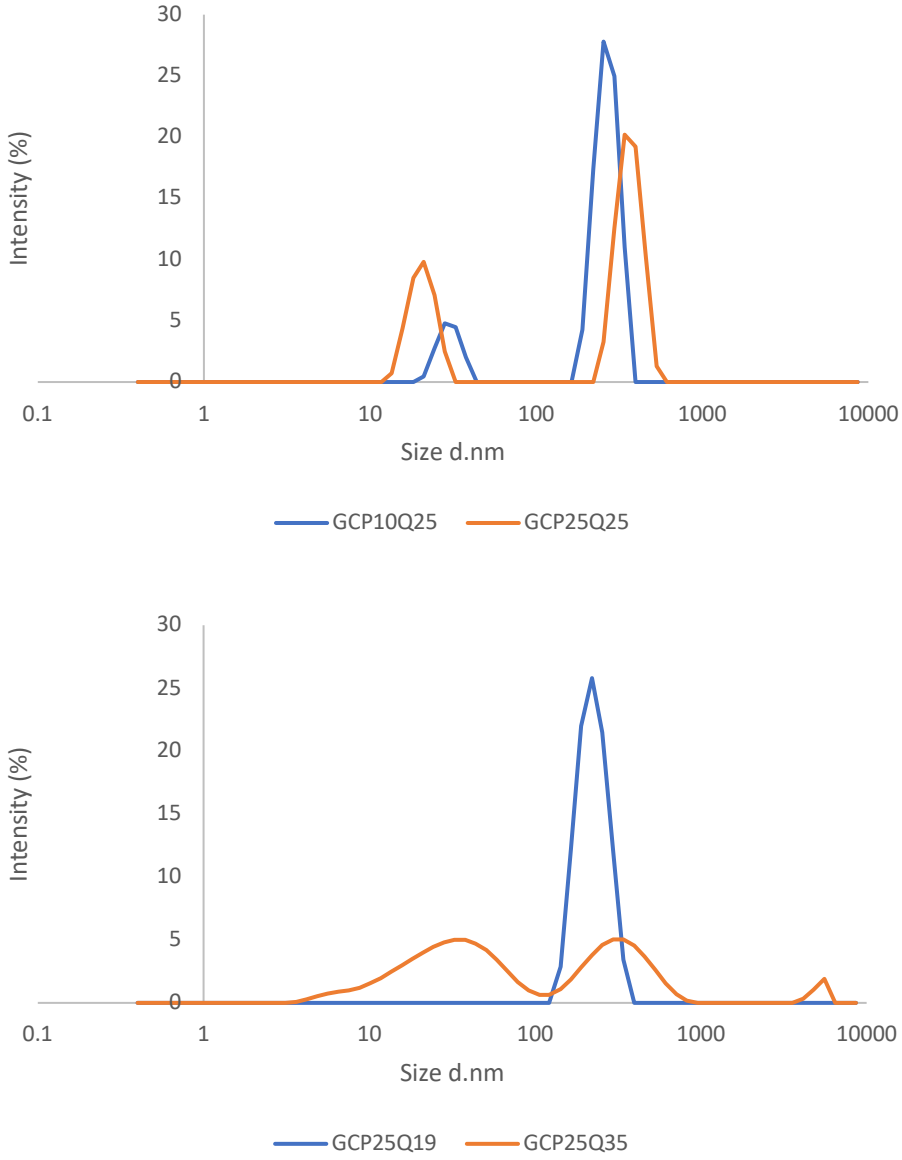

Figure 3-9: Size distribution of GCPQ polymers with varied degrees of hydrophobicity. (Top) GCP10Q25 and GCP25Q25 with QPR of 2.27 and 1.0 respectively. The more hydrophobic polymer, GCP25Q25 has a lower mean size distribution. (Bottom) More hydrophilic polymers GCP25Q19 and GCP25Q35 with QPR of 0.76 and 1.40 respectively. The more hydrophilic polymer, GCP25Q35 has a lower mean size value however, a broader size distribution than the more hydrophobic polymer, GCP25Q25.

Figure 3-9 compares the size distribution of four different polymers with varying degrees of palmitoylation and quaternisation. Analysis was split into two groups; effect of hydrophobicity on particle size by comparing GCP10Q25 and GCP25Q25 and effect of hydrophilicity on particle size by comparing GCP25Q19 and GCP25Q35. In the first

instance, two peaks were observed in both GCP10Q25 and GCP25Q25 suggesting two populations present. As GCPQ nanoparticles form micelles in aqueous solution, this could mean that each peak represents one of the two thermodynamically stable GCPQ micelles. However, this isn't observed in a more hydrophilic polymer, GCP25Q19. As both GCP25Q25 and GCP25Q19 have the same degree of palmitoylation but varying degrees of quaternisation, it is possible that suggests that degree of quarterisation may have a greater influence on particle size distribution. The second observation made was an increase in average size in the more hydrophobic polymer (GCP25Q25). When comparing more hydrophilic polymers, a monomodal nanoparticle population, represented by a single peak in GCP25Q19 is observed while GCP25Q35 shows a broader distribution of nanoparticle size. This is similar to what is observed between GCP25Q25 and GCP25Q19, where and increase in degree of quarterisation results in two micelle populations being formed. The third peak is in the micrometre range and is assumed aggregates.

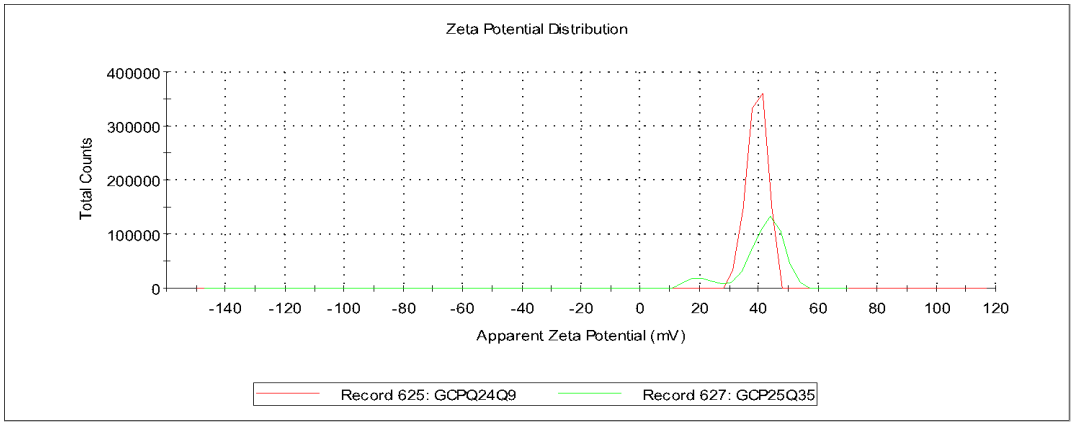

Figure 3-10: DLS measurements comparing zeta potential of a more hydrophilic GCPQ polymer, GCP25Q35; QPR: 1.4, Zeta potential 43.5±2.88 mV and a more hydrophobic polymer, GCP24Q9; QPR: 0.38, Zeta potential: 40.6±1.20 mV. Where difference in hydrophobicity is observed in DQ %.

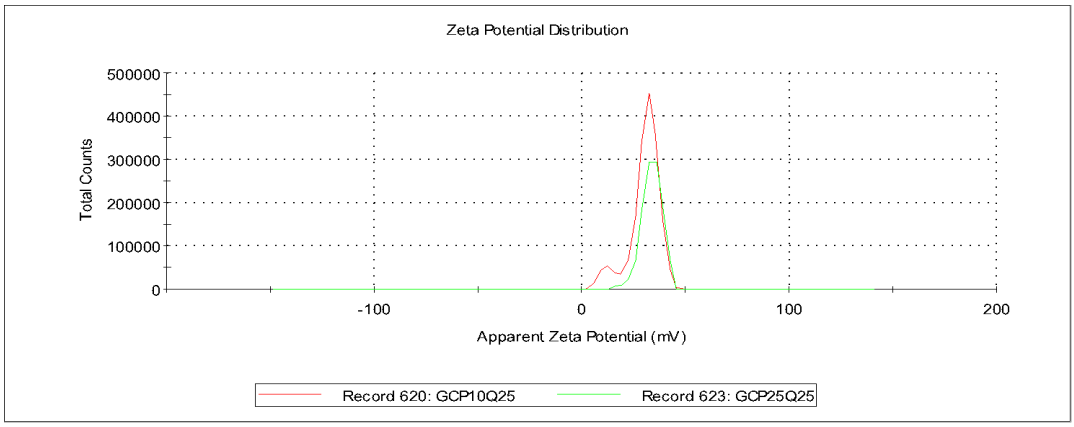

Figure 3-11: DLS measurements comparing zeta potential of a less hydrophobic GCPQ polymer, GCP10Q25; QPR: 2.27, Zeta potential 28.8±2.51 mV and a more hydrophobic polymer, GCP25Q25; QPR: 1, Zeta potential: 43.5±2.88 mV. Where difference in hydrophobicity is observed in DP %.

Figure 3-10 and Figure 3-11 shows Zeta potential values of four different polymers with varying degrees of palmitoylation and quaternisation. Analysis was split into two groups; effect of hydrophilicity on zeta potential by comparing GCP24Q9 and GCP25Q35 and the effect of hydrophobicity on Zeta potential by comparing GCP10Q25 and GCP25Q25. In the first instance, a larger zeta potential value is observed in the more hydrophilic polymer (GCP25Q35). This is attributed to the increase in positively charged quaternary ammonium groups present in this polymer.

3.5 Conclusion

GCPQ polymers with varied degrees of structural modifications with regards to molecular weight, degree of palmitoylation and degree of quaternisation. were synthesised and characterised. The physiochemical properties such as molecular weight, particle size, and zeta potential were measured and compared to investigate the effect of modification on polymer characteristics. The ratio of DP % and DQ % (QPR) had no significant effect on the average size of zeta potential of polymers. Zeta potential of GCPQ range from 29 mV to 51 mV. Table 3-3 shows no trend in particle size based on DP %. However, smaller particle sizes are observed where DP % (≥24 %) remains the same and DQ % increases. This also correlates with an increase in zeta potential. These polymers will be used for further encapsulation and *in vivo* studies to compare experimental encapsulation data of GCPQ-drug and HSP predictions as well as determine effect of physiochemical properties on encapsulation efficiency and biodistribution in rodent models.

4 Drug Encapsulation Studies

4.1 Introduction

Physiochemical properties of drugs create limitations to the approach which may be employed to enhance delivery. The Biopharmaceutical Classification System (BCS) gives groups drug compounds into one of four classes based on these physiochemical properties. The four classes are as follows: Class I – high solubility and high permeability drugs, Class II – low solubility and high permeability drugs, Class III – high solubility and low permeability drugs and finally, Class IV – low solubility and low permeability drugs (Yu et al., 2002). Drug delivery strategies which enhance solubility and permeability are aimed at drug compounds in Class II, III and IV. It is the physicochemical properties of these drug candidates that determine the type of delivery approach employed when conventional medicinal chemistry is unable to overcome solubility and/or permeability limitations. In these instances, drug formulation strategies are used to achieve required solubility and permeability rates. For example, chemical modifications such as prodrug formation and salt formation may be used to improve solubility of lipophilic drug compounds (Alqahtani et al., 2021).

Nanomedicines also provide an opportunity to circumvent limitations presented by drug physicochemical properties. For example, nanoparticles may be used to increase the solubility of hydrophobic drugs, addressing poor solubility in Class II and IV drugs. They are also able to encourage transcytosis drugs across intestinal membranes therefore, addressing the issue of poor permeability in Class III and IV drugs (Plapied et al., 2011). A range of different polymeric materials may be used and modulated to influence the extent of drug loading, drug release profile and biological behaviours and physiochemical properties such as hydrophobicity and surface charge of the resulting nanoparticle (Plapied et al., 2011). For this reason, there has been an increasing number of studies investigating the application of polymeric nanoparticles as oral drug delivery systems. Other possible benefits of polymeric nanoparticles include small particle size, biodegradability, mucoadhesive properties and are biocompatible with cells and tissues (Panyam and Labhasetwar, 2003).

Chitosan based nanoparticles have been studied in some detail previously, establishing its ability to enhance drug solubility and hence be utilised as a drug delivery system (Serrano et al., 2015b). One of such chitosan-based nanoparticles is GCPQ, an amphiphilic polymer which has been shown to facilitate dissolution of hydrophobic drugs by encapsulating them in polymeric micelles (Chen et al., 2013). Previous studies have shown that GCPQ micelles adhere to and traverse the mucus layer (Siew et al., 2011). In addition to that, GCPQ has been shown to increase oral bioavailability of amphotericin B (Serrano et al., 2015b). *In vivo* experiments investigating the oral uptake of Cyclosporine A and Griseofulvin, both BCS class II drugs using chitosan derivative, GCPQ as nanocarriers showed higher drug absorption compared to administering the drug alone (Siew et al., 2011). This data suggests that the modifications to the chitosan backbone, i.e., quaternisation and palmitoylation, increase absorption and eventual bioavailability of drugs encapsulated within the polymeric GCPQ nanoparticle.

In order, to build up a more detailed mechanistic understanding of the role of different modifications to drug encapsulation for different types of drug molecules, the encapsulation of caspofungin and curcumin, BCS class IV drugs, respectively, were carried out using GCPQ polymers with varied degrees of modification. This was done to validate the predictions gotten from HSPiP simulations, explained in Chapter 2. The effects of GCPQ modifications such as DP % and DQ % on shape, size and encapsulation efficiency were then investigated in order to optimise encapsulation efficiency and stability profiles for the oral delivery of these drugs.

4.2 Model drugs:

4.2.1 Curcumin

Curcumin (Figure 4-1) is the bioactive ingredient of Curcuma longa (turmeric) and has shown therapeutic effect in a range of diseases (Keihanian et al., 2018; Oppenheimer, 1937). Some of these therapeutic effects include anti-inflammatory (Aggarwal and Harikumar, 2009), anti-carcinogenic (Inano, 1999), anti-microbial (Negi et al., 1999), neuro and cardio protective (Keihanian et al., 2018; Aggarwal and Harikumar, 2009) and more recently, antiviral effects against SARS-CoV-2 comparative to hydroxychloroquine (Maurya et al., 2020; Pawar et al., 2021).

Curcumin has poor bioavailability, with low to undetectable concentrations in blood and tissues. Possibly due to its poor absorption, rapid metabolism, chemical instability and rapid clearance *in vivo* (Anand et al., 2007; Toden and Goel, 2017). Physicochemical properties of curcumin (Table 4-1) give insight on why curcumin is unlikely to succeed as an oral formulation.

4.2.2 Caspofungin

Caspofungin (Figure 4-1) belongs to a class of antifungals called echinocandins. These are cyclic lipopeptide molecules which function by inhibiting the enzyme activity of B-1,3-D-glucan synthase, the enzyme responsible for cell wall synthesis in fungi. B-1,3-D-glucan synthase is a heteromeric enzyme complex bound to the cell membrane. It comprises a catalytic membrane subunit known as Fks p, which binds to intracellular UDP-glucose and regulatory subunit, Rho1 p before binding to intracellular GTP (Letscher-bru and Herbrecht, 2003b). This complex polymerises UDP-glucan to glucan which is exported extracellularly and incorporated into the fungal cell wall. Caspofungin binds noncompetitively to the catalytic Fks p subunit, blocking it and preventing glucan synthesis (Letscher-bru and Herbrecht, 2003b). Echinocandins are therefore fungicidal, as fungal cell are prone to osmotic lysis due to weakness in their cell wall configuration. They are also fungistatic because cell growth is now limited due to limited cell wall synthesis (Wiederhold and Lewis, 2003; Odds et al., 2003). The

fungal species targeted include candida spp and aspergillus spp. Its salt formulation, caspofungin acetate has a solubility of 28 mg/mL in water and so, is freely soluble in aqueous solution. It is also soluble methanol and slightly soluble in ethanol.

The current formulation of caspofungin is its acetate base. Absorption data of orally administered caspofungin acetate is inconsistent and so, intravenous (IV) administration is still being employed for this drug (Kofla and Ruhnke, 2011). The IV formulation is typically reconstitution of a given mass of lyophilised caspofungin powder in 10 mL of an aqueous solution containing excipients like lactose, citric acid, and sodium hydroxide. Clinically, an initial loading dose of 70 mg is administered through IV followed by a subsequent dose of 50 mg once a day in adults. The total of dose is roughly 1 mg/kg/day (Blyth et al., 2007).

Physicochemical properties of caspofungin (Table 4-1) give insight on why caspofungin is unlikely to succeed as an oral formulation. These include poor water solubility (28 mg/L), high molecular weight (1093.3 g/mol). Functional group modifications such as ionisation may be considered however, ionisable groups like amide groups present are mostly buried within the core of the molecule so, access proves difficult. This makes it difficult to improve solubility by adjusting the pH.

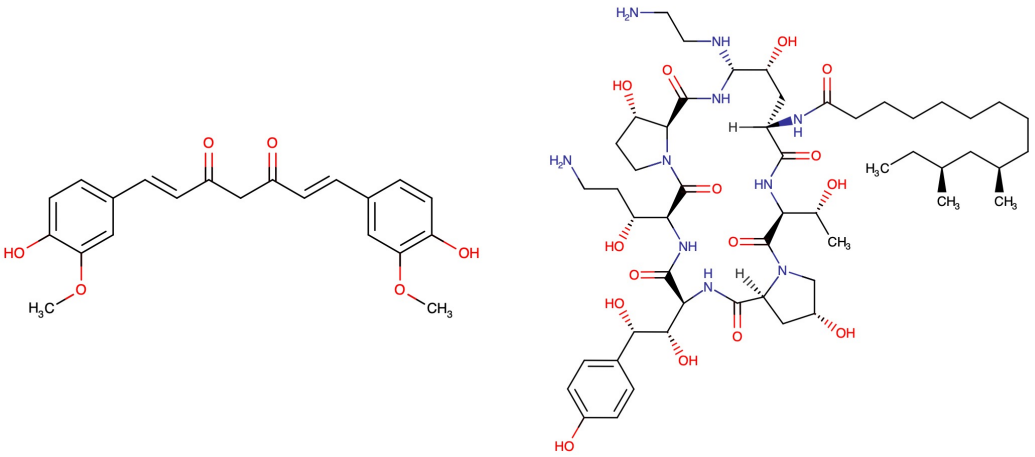

Figure 4-1: Chemical structures of curcumin and caspofungin.

Property	**Curcumin**	**Caspofungin**
Appearance	Orange-yellow crystalline powder	White to off-white powder
Molecular formular	$C_{21}H_{20}O_6$	$C_{52}H_{88}N_{10}O_{15}$
Molecular weight	368.4 g/mol	1093.3 g/mol
Water solubility	3.13 mg/L	28 mg/L
Log P	3.29	N.D

Table 4-1: Physicochemical properties of curcumin and caspofungin

4.3 Encapsulation Studies

4.3.1 Materials

Majority of the reagents and chemicals were obtained from both Sigma Aldrich Chemical Company and Fischer Scientifics UK Ltd unless stated otherwise:

Reagents and Solvents: Curcumin (Sigma-Aldrich, UK), Caspofungin Acetate (Glentham Life Sciences, UK), Deionized water, Methanol HPLC Gradient, Acetone, Phosphoric Acid.

Equipment: MSE soniprep 150 sonicator (MSE UK Ltd), Zetasizer Nano S90, (Malvern, UK), HPLC (Agilent, UK), Vortex, RV 10 Rotary Evaporator (IKA, UK), Savant SPD131DDA vacuum evaporator (Thermo Scientific), Centrifuge, Biotwin NMR (Bruker Avance 400), Agilent 1220 infinity chromatographic system, Agilent Technologies 1200 series chromatographic system fitted with a vacuum degasser, quaternary pump, standard and preparative auto-sampler, column compartment with a thermostat and a UV detector, onyx monolithic CS18 column (100 x 4.6 mm; particle size, 5µm) (Phenomenex, UK).

4.3.2 Methods

4.3.2.1 Encapsulation of Curcumin

A thin-film formation method was used to encapsulate curcumin with GCPQ. This method was adapted from previous research involving the encapsulation of curcumin (Sahu et al., 2011; Suresh and Srinivasan, 2007). Encapsulation efficiency and drug loading achieved with this method were then calculated based on previously reported methods (Kakde et al., 2016; Sahu et al., 2011). Below is an outline of the steps involved in the formulation.

Curcumin powder (Sigma Aldrich, UK) was weighed into a glass vial wrapped in tin foil to protect from light degradation. Curcumin was then dissolved in a known volume of HPLC grade methanol to achieve required concentration which was a 1 mg/mL stock

solution. 20 mg of GCPQ polymer was weighed out in a glass vial and dissolved in 4 mL of methanol (HPLC grade) to make a 5 mg/mL solution. 0.5 mL of this GCPQ solution was transferred into a 1.5 mL Eppendorf and 0.5 mL of curcumin solution was also added to obtain a ratio of 5:1 of GCPQ to curcumin.

The mixture was vortexed for one minute after which the Eppendorf tubes were subjected to different evaporation methods. One set of formulations were placed in an RV 10 Rotary Evaporator (IKA, UK) for 2 minutes at 41 ^{o}C and 135 rpm. The other set of formulations were placed in a Savant SPD131DDA vacuum evaporator (Thermo Scientific) at 45 °C under vacuum until a dry, thin film was formed. This took a total of 2 hours to achieve.

The thin film was then rehydrated by adding 1 mL of deionized water and the mixture was vortexed until a clear amber coloured solution was formed, indicating complete dissolution. Following this step, formulations were then subjected to different processes;

1) Rehydration.
2) Rehydration followed by sonication using MSE Soniprep 150 sonicator (MSE UKLtd) at 5 microns amplitude for 3 minutes in an ice bath.
3) Rehydration followed by lyophilisation using ALPHA 1-4 LDplus freeze dryer (CHRIST, UK) and then sonication using MSE soniprep 150 sonicator (MSE UK, Ltd) at 5 amplitude microns for 3 minutes in an ice bath.

The resulting formulations were then centrifuged at 3000 g for ten minutes to collect any precipitate of un-encapsulated curcumin. The supernatant was removed and transferred into a new Eppendorf tube before being analysed for drug content, particle size and zeta potential.

4.3.2.2 Characterisation of Curcumin Formulation

4.3.2.2.1 High-performance Liquid Chromatography Analysis of Curcumin

An HPLC gradient method was developed for curcumin using an Agilent 1220 infinity chromatography system, fitted with a quaternary pump, vacuum degasser, auto sampler, column compartment, thermostat and an ultraviolet detector (Agilent Technologies, UK). A gradient method was developed using a mobile phase consisting of phosphoric acid (0.1 %) and acetonitrile alongside a reverse phase onyx monolithic CS18 column (100 x 4.6 mm; particle size, 5µm) (Phenomenex, UK). The column temperature was maintained at 35 ^{o}C and absorption monitored at a wavelength of 430 nm. The flow rate was 1.2 mL/min was maintained, and the total run time was 12 minutes. Retention time of curcumin was at 4.77 minutes.

For curcumin quantification, 100 µL of prepared GCPQ-Curcumin formulation was diluted in 200 µL methanol, vortexed and transferred to HPLC vial for injection. Ten µL of the sample was injected and curcumin concentration was determined from standard curve.

The standard curve was prepared as followed: curcumin solution was prepared at a concentration of 2 mg/mL in methanol. Curcumin working solutions were then prepared by serially diluting curcumin stock solution to obtain working solutions ranging from 0.065 - 1 mg/mL.

A standard curve was created using curcumin concentrations ranging from 4 to 250 µg/mL in methanol ($y = 57430x – 84.218$, $R^2 = 0.9992$) (n = 3).

Time (min)	0.1% H_3PO_4 in H_2O Solvent A (%)	Acetonitrile Solvent B (%)
0.00	80	20
4.0	20	80
8.0	20	80
12.00	80	20

Table 4-2: HPLC gradient conditions for curcumin.

4.3.2.2.2 Particle Size and Zeta Potential Measurements

Particle size and size distribution of the formulations created were analysed using Dynamic light scattering measurements taken from the fixed scattering angle Zetasizer Nano-S system (Malvern Instruments Ltd, Malvern, UK).

The size distribution analysis was performed using detected at an angle of 173 ^{o} at 25 ^{o}C and collected in automatic mode. An aliquot of 100 µL was placed in a disposable cuvette and loaded into zetasizer without diluting. Particle size was reported as an intensity distribution which is the relationship between light scattering intensity and the particle hydrodynamic diameter (Stetefeld et al., 2016). Particle mean size of the individual peaks were determined and recorded as a mean ± standard deviation from three measurements.

Zeta potential is the electrokinetic potential of a colloidal system and measures the surface charge of particles in each solution(Gumustas et al., 2017). Zeta potential was measured using the electrophoretic light scattering technique. An aliquot of 700 µL was placed into a folded capillary cell (zeta cells, polycarbonate cell with gold-plated electrodes; Malvern Instruments DTS1060C) and measured at 25 ^{o}C, 40 V. Triplicates measurements were made and results presented as mean ± SD.

Transmission Electron Microscopy (TEM) images were taken using the Philips/FEI CM120 Bio Twin (Orego, USA). Samples were imaged by a technician and prepared by drying a drop of each GCPQ formulation on a copper TEM grid (300 mesh-formvar/carbon coated) and stained with a drop of uranyl acetate (1 % w/v). Dried samples were then imaged under the microscope and used for further analysis.

4.3.2.2.3 Stability Study of GCPQ-Curcumin Formulations

The stability of GCPQ-Curcumin formulations was determined by measuring their physicochemical properties over one week. Formulations were stored under refrigerated conditions at 5 ± 3 ^{o}C and measurements were done in triplicates.

Aliquots of 1 mL were taken from the formulation immediately after preparation and every 24 hours over 7 days of storage. The samples were analysed to investigate

changes in encapsulated drug concentration, zeta potential, particle size and visible colour changes.

Two-way ANOVA statistical analysis was performed to determine significance of data.

4.3.2.3 Encapsulation of Caspofungin

4.3.2.3.1 Caspofungin Extraction

Salt formation is a formulation technique which increases intrinsic solubility of hydrophobic drugs (Alqahtani et al., 2021). This was employed in the current marketed caspofungin formulation (CANCIDAS). Caspofungin was obtained as an acetate salt with high water solubility. To favour encapsulation within GCPQ micelles, caspofungin was extracted to obtain the free hydrophobic base.

Caspofungin was first extracted from its base salt formulation, caspofungin acetate (Glentham Life Sciences, UK). This was achieved by creating a 25 mg/mL solution of caspofungin acetate in phosphate-buffered saline (PBS) with its pH adjusted to 3.5 using 1.0 M hydrochloric acid (HCL). The pH of the resulting solution was then adjusted to pH 10 using 1.0 M sodium hydroxide (NaOH). The resulting solution was centrifuged at 4500 g for a total of 30 minutes to force precipitate down to the bottom of the Eppendorf. A wash step was introduced every 10 minutes where supernatant was collected using a 1 mL syringe with a 0.8 mm guage needle and replaced using 200 μL of water. This was then vortexed and process repeated three times. This was to dissolve and remove the sodium chloride (NaCl) salts formed during pH adjustment step. Each wash step was analysed using HPLC to ensure no caspofungin was present in supernatant. The final pellet obtained from centrifugation was lyophilized overnight.

4.3.2.3.2 Formulation Method

A GCPQ-Caspofungin formulation was prepared using an identical thin-film method utilised in the GCPQ-Curcumin formulation (outlined in 4.3.2.1) adapted from previously reported encapsulation experiments of curcumin (Bruce, 2016). 25 mg of GCPQ was weighed out and dissolved in 5 mL of Dimethyl formamide (DMF) to make a 5 mg/mL stock solution. Dimethyl formamide was the choice of solvent due to poor solubility of caspofungin in both methanol and ethanol. A 1 mg/mL solution of extracted caspofungin was created by dissolving 1 mg of lyophilized caspofungin powder in 1 mL of DMF. 0.5 mL of both GCPQ-DMF and caspofungin-DMF were pipetted into a fresh Eppendorf and centrifuged for a minute to achieve a ratio of 5:1 of GCPQ to Caspofungin in final formulation.

The Eppendorf tubes were placed in a Savant SPD131DDA vacuum evaporator (Thermo Scientific) at 45 °C under a vacuum of 2.0 Pa until a dry, thin film was formed. This took a total of two hours to achieve. The thin film was then, placed in a vacuum desiccator overnight to ensure complete evaporation of DMF then, rehydrated by adding 1 mL of deionized water. The hydrated solution was vortexed and sonicated for a total of 5 minutes in an ice water bath. Sonication was done in intervals with Eppendorf tubes cooling in ice water bath every other minute to eliminate heat until a clear solution is formed, indicating complete dissolution. Sonicated samples were then centrifuged at 4500 g for ten minutes to precipitate out any un-encapsulated caspofungin. Supernatant was removed and transferred into a clean Eppendorf tube and encapsulation as well as encapsulation efficiency was determined using Agilent HPLC.

4.3.2.4 Characterisation of Caspofungin Formulation

4.3.2.4.1 High-performance Liquid Chromatography Analysis of Caspofungin

An HPLC gradient method was developed for curcumin using an Agilent 1220 infinity chromatography system, fitted with a quaternary pump, vacuum degasser, auto sampler, column compartment, thermostat, and an ultraviolet detector (Agilent Technologies, UK). An isocratic method was developed using a mobile phase consisting of trifluoroacetic acid (0.1 %) and acetonitrile (65/30 v/v) alongside a reverse phase onyx monolithic CS18 column (100 x 4.6 mm; particle size, 5µm) (Phenomenex, UK). The column temperature was maintained at 25 ^{o}C and absorption monitored at a wavelength of 230 nm. The flow rate was 1.0 mL/min was maintained, and the total run time was 9 minutes. Retention time of curcumin was at 5.4 minutes.

For caspofungin quantification, 100 µL of prepared GCPQ-Caspofungin formulation was diluted in 200 µL methanol, vortexed and transferred to HPLC vial for injection. Ten µL of the sample was injected and curcumin concentration was determined from standard curve.

The standard curve was prepared as followed: caspofungin solution was prepared at a concentration of 2 mg/mL in methanol. Caspofungin working solutions were then prepared by serially diluting caspofungin stock solution to obtain working solutions ranging from 0.065 - 1 mg/mL.

A standard curve was created using curcumin concentrations ranging from 25 to 500 µg/mL in methanol ($y = 827.76x - 5.7716$, $R^2 = 0.9951$) (n = 3).

4.3.2.4.2 Particle Size and Zeta Potential Measurements

Particle size and size distribution of the formulations created were analysed using Dynamic light scattering measurements taken from the fixed scattering angle Zetasizer Nano-S system (Malvern Instruments Ltd, Malvern, UK).

The size distribution analysis was performed using detected at an angle of 173 ^{o} at 25 ^{o}C and collected in automatic mode. An aliquot of 100 µL was placed in a disposable cuvette and loaded into zetasizer without diluting. Particle size was reported as an intensity distribution which is the relationship between light scattering intensity and the particle hydrodynamic diameter (Stetefeld et al., 2016). Particle mean size of the individual peaks were determined and recorded as a mean ± standard deviation from three measurements.

Zeta potential is the electrokinetic potential of a colloidal system and measures the surface charge of particles in each solution (Gumustas et al., 2017). Zeta potential was measured using the electrophoretic light scattering technique. An aliquot of 700 µL was placed into a folded capillary cell (zeta cells, polycarbonate cell with gold-plated electrodes; Malvern Instruments DTS1060C) and measured at 25 ^{o}C, 40 V. Measurements were made in triplicates and results presented as mean ± SD.

Transmission Electron Microscopy (TEM) images were taken using the Philips/FEI CM120 Bio Twin (Orego, USA). Samples were imaged by a technician and prepared by drying a drop of each GCPQ formulation on a copper TEM grid (300 mesh-formvar/carbon coated) and stained with a drop of uranyl acetate (1 % w/v). Dried samples were then imaged under the microscope and used for further analysis.

4.3.2.4.3 Stability Study of GCPQ-Caspofungin Formulations

The stability of GCPQ-Caspofungin formulations was determined by measuring their physicochemical properties over one week. Formulations were stored under room temperature conditions at 25 ºC and measurements were done in triplicates.

Aliquots of 1 mL were taken from the formulation immediately after preparation and every 24 hours over 7 days of storage. The samples were analysed to investigate changes in encapsulated drug concentration, zeta potential, particle size and visible colour changes.

Two-way ANOVA statistical analysis was performed to determine significance of data.

4.4 Results and Discussion

GCPQ polymers were used in the oral formulation of both curcumin and caspofungin. These polymers varied in degrees of palmitoylation and quaternisation. It is the effect of these variations on mass of encapsulated drug which was investigated.

4.4.1 Encapsulation of Curcumin

HPLC Quantification of GCPQ – Curcumin

The HPLC chromatogram (Figure 4-2) shows curcumin has a retention time of 4.8 minutes with an injection peak at 1.5 minutes. Standard curve using area under the curve values was plotted and shows good linearity over a concentration range of 4 – 250 µg/mL with a correlation of 0.9992. The equation of the standard curve was used to calculate the concentration of encapsulated curcumin in GCPQ-curcumin formulations hence contributed to EE and DL calculations shown in Table 4-5. Equation 15 was used to determine the concentration of encapsulated curcumin in GCPQ-curcumin formulations.

Equation 15:

$$conc\ (\mu g\ /\ mL) = \frac{AUC + 84.218}{57430}$$

The measured lower limit of quantification (LLOQ) for curcumin was 4 µg/mL. The calculated limit of quantification (LOQ) and limit of detection (LOD) are listed in Table 4-3. LOQ and LOD equations according to ICH guidelines can be found below (ICH, 2006):

Equation 16:

$$LOQ = \frac{10\sigma}{S}$$

Equation 17:

$$LOD = \frac{3.3\sigma}{S}$$

Where σ is the standard deviation of the response and S is the slope of calibration curve.

Parameter	**Quantification range (µg/mL)**	**Equation of the straight line**	**R^2**	**Limit of detection (µg/mL)**	**Limit of quantification (µg/mL)**
Value	4 - 250	Y = 57430x – 84.218	0.9992	11.9	36.2

Table 4-3: HPLC assay parameters for curcumin.

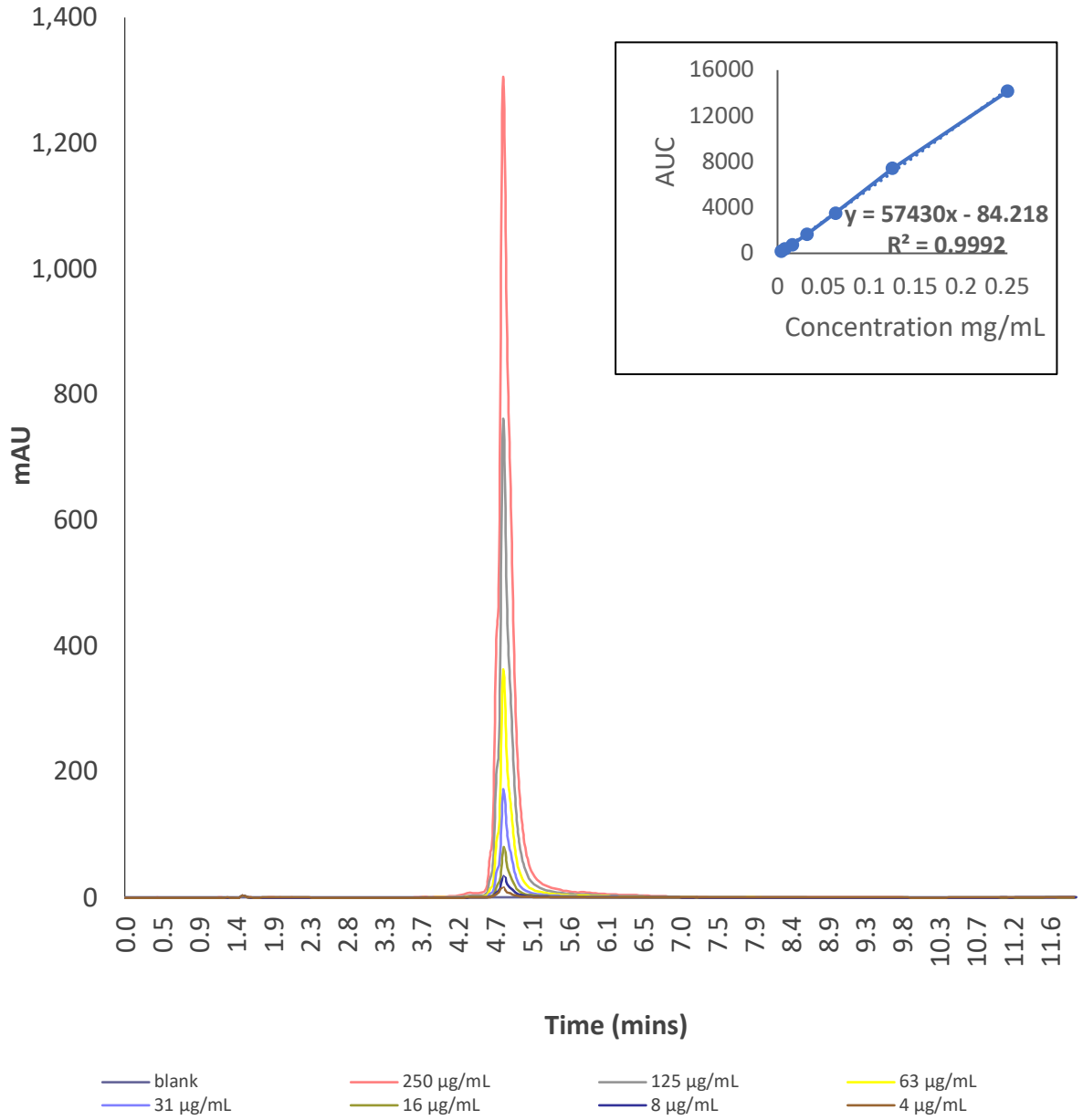

Figure 4-2: HPLC chromatogram for standard solutions of curcumin with 0.1 % phosphoric acid and acetonitrile as the mobile phase. Insert: Calibration curve plotted using AUV values obtained from chromatogram.

Formulations procedure outlined in 4.3.2.1 was performed using GCPQ polymers synthesized as described in Chapter 3 with varying degrees of palmitoylation, quaternisation and molecular weights to demonstrate how this affects encapsulation efficiency. For each formulation, GCPQ to curcumin ratio was maintained at 5:1. Encapsulation efficiency (EE %) as well as drug loading (DL %) were determined using HPLC analysis. Formula used to calculate both EE and DL are shown below:

Equation 18:

$$EE\ (\%) = \frac{colloidal\ drug\ concentration}{theoretical\ drug\ concentration} \times 100$$

Equation 19:

$$DL\ (\%) = \frac{mass\ of\ colloidal\ drug\ content}{mass\ of\ polymer + drug} \times 100$$

Effect of Solvent Selection on Encapsulation Efficiency of GCPQ– Curcumin Formulations

Encapsulation experiments were first carried out using GCP25Q19 polymer with three different processing; Rehydration, Sonication and Lyophilization, all outlined in Figure 4-3. In this experiment, the method of evaporation of solvent (methanol-water) was investigated and results represented graphically in Figure 4-4. Hypothesis was that an intricate mixture of GCPQ and drug – ideally in amorphous form would facilitate encapsulation. It was also hypothesised that lyophilisation will create a larger surface area which will in turn facilitate rehydration post-lyophilisation therefore, increasing encapsulation efficiency.

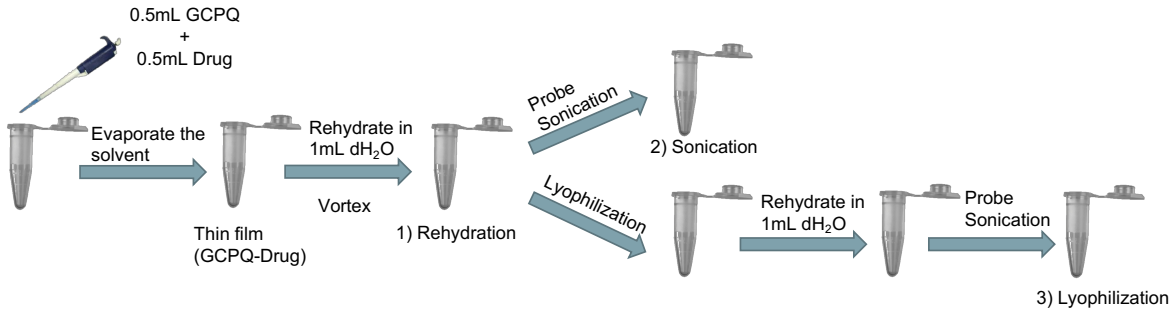

Figure 4-3: Illustration showing the steps involved in the formulation process.

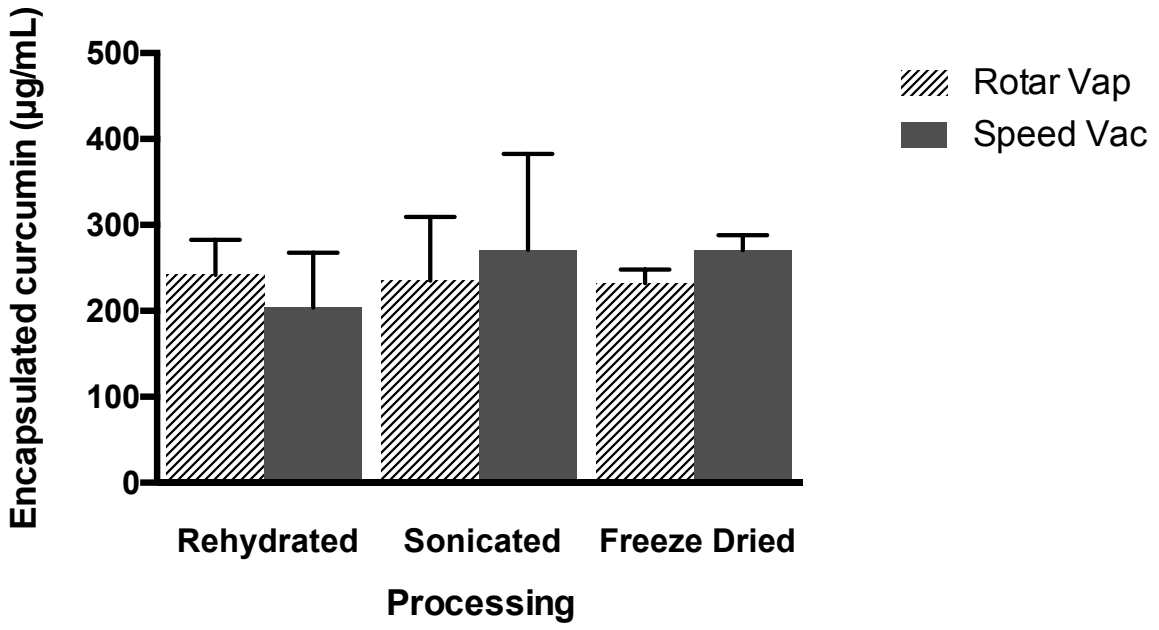

Figure 4-4: Graph showing total concentration of curcumin encapsulated in GCP25Q19 formulation (n = 3).

Thin film formulation method outlined in 4.3.2.1 was used in this investigation. A 5mg/mL solution of GCPQ25Q19 polymer was prepared using deionised water while a 1 mg/mL solution of curcumin was prepared using methanol. Following this, 0.5 µL of both GCPQ-water and curcumin-methanol were transferred into a 1.5 mL Eppendorf tube resulting in a 5:1 ratio of GCPQ polymer to curcumin and a 1:1 ratio of methanol to water. Methanol-water solvent was then evaporated to create a thin film before being rehydrated with 1mL of deionised water. Formulations were split into two groups and subjected to two typed of evaporation methods namely; speed vacuum and rotary evaporation. This was done to compare the encapsulation efficiency obtained using these two different methods of evaporation. Encapsulation efficiency values are shown in Table 4-4.

Polymer	Formulation	Processing	EE (%)	
			Rotor Vap	Speed Vac
GCP25Q19	GCP25Q19-Curcumin	Simple Rehydration	48.4 ± 40.7	40.8 ± 63.5
		Sonication	47.0 ± 74.2	54.2 ± 111.5
		Lyophilisation	46.5 ± 15.8	54.2 ± 17.4

Table 4-4: Table showing Encapsulation efficiency of GCP25Q19-Curcumin comparing method of evaporation. (n = 3)

Table 4-4 shows encapsulation efficiency values for GCP25Q19-curcumin formulations created. Data investigated effects of two main variables on the encapsulation efficiency of final formulations. These variables were method of solvent evaporation (rotary evaporation and speed vacuum evaporation) and method of processing following thin film creation (simple rehydration, sonication and lyophilisation). The data confirmed hypothesis that thin film method will facilitate encapsulation efficiency and shows similar values of encapsulation efficiency values of all formulation with high standard deviation values, indicating no significant difference between encapsulation efficiency values. Two-way ANOVA statistical calculations indicate that there is no statistical significance between encapsulation efficiency of formulations. Method of evaporation was shown to not have a significant effect on encapsulation efficiency and so, speed vacuum evaporation method was utilised in further encapsulation formulations. This is because it proves to be the most convenient and efficient method with regards to the number of Eppendorf samples which can be evaporated simultaneously. Formulations subjected to sonication had the highest standard deviation values followed by those subjected to simple rehydration, suggesting less reproducible results. Lyophilisation had the smallest standard deviation values making this method more reproducible and possibly a more

ideal formulation process. This was investigated further using a wider range of GCPQ polymers.

Overall, encapsulation efficiencies of for GCPQ-curcumin formulation was low, with an average of about 50 %. It was hypothesised that this was due to the methanol-water solvent used prior to thin film formation. Curcumin is largely insoluble in water (3.13 mg/L, Table 4-1) and so, the addition of water from the 5 mg/mL GCPQ stock solution may have reduced the amount of curcumin solubilised in the resulting 1 mL GCPQ-Curcumin mixture. Less curcumin in solution prior to solvent evaporation can explain the reduction in encapsulated curcumin. For this reason, future formulations were made using only methanol as the solvent for both GCPQ and curcumin stock solutions.

Effect of Processing on Encapsulation Efficiency

Further GCPQ-Curcumin formulations were created using only methanol as the solvent for both curcumin and GCPQ stock solutions in place of methanol and water used initially. Encapsulation efficiency was calculated after removing un-encapsulated curcumin by centrifugation. The encapsulated curcumin was then quantified using HPLC after diluting 100 µL of formulation in 200 µL of methanol within a vial in order to break open the micelles formed and free up all of the encapsulated curcumin for analysis.

Formulation	Rehydration	Sonication	Lyophilisation	Z- Average ± SD (nm)	PDI±SD	Zeta Pot. ± SD	Encapsulated Curcumin (µg/mL)	EE (%) ± SD	DL (%) ± SD
GCP8Q7+Curc	x			277.2±1.10	0.09±0.04	56.1±2.08	316.2±4.29	63±0.86	11±0.14
	x	x		2857±14.1*	0.23	58.5±1.26	85.1±19.6	17±3.91	3±0.65
	x	x	x	100.8±10.7	1	56.1±1.51	80.0±22.4	16±4.47	3±0.75
GCP25Q9+Curc	x			436.1±5.59	0.71±0.19	74.3±2.29	369.4±10.6	74±2.11	12±0.35
	x	x		9309±627.9*	1	68.2±1.43	203.7±7.57	41±1.51	7±0.25
	x	x	x	2051±133.6*	0.57±0.37	62.0±0.64	230.7±26.4	46±5.27	8±0.88
GCP25Q19+Curc	x			96.0±3.34	0.32±0.01	67.2±3.74	454.0±12.0	91±2.40	15±0.40
	x	x		20.6±7.34	0.7±0.16	70.4±1.20	228.0±12.7	46±2.54	8±0.42
	x	x	x	52.7±27.1	0.73	71.4±1.35	394.9±43.2	78±8.63	13±1.44

Table 4-5: Table showing GCPQ-curcumin formulations with encapsulated curcumin (µg/mL), encapsulation efficiency (EE%) and drug loading (DL%). (n = 4)

The GCPQ-Curcumin formulation shown in Table 4-5 were subjected to one of three different processing methods; rehydration, ‘sonication’ (rehydration + sonication), and ‘lyophilisation’ (rehydration + lyophilisation + sonication). This was done so the effects of the different processing methods on encapsulation efficiency may be compared.

The data suggests that methods which were expected to provide a more intimate mixing of drug and polymer (sonication and lyophilisation) seem to make encapsulation worse - this is most evident for low DP % polymers. Sonication is the common process shared by formulations with lower EE % values and so, a possible explanation is that curcumin drug may be subjected to degradation during sonication process. Some measured particle size data for some formulations were also unusually large (*), with values in the micrometre range. Large particle size may affect colloidal stability and sink to the bottom of the Eppendorf, resulting in less encapsulated curcumin in final formulations.

When looking at the effects of GCPQ modification on encapsulation efficiency, results suggest a correlation between DP % and encapsulation efficiency. Formulations subjected to simple rehydration show GCP8Q7 polymer achieving 63 % ± 0.86 of encapsulation efficiency compared with GCP25Q9 polymer at 74 % ± 2.11. This is expected as the degree of palmitoylation reflects how hydrophobic the GCPQ polymer is. Hence, an increase in DP % means that more hydrophobic interactions could be made between hydrophobic drug compound, curcumin and GCPQ and so, more amount of curcumin is encapsulated (316 µg/mL vs 454 µg/mL).

Interestingly, an increase in encapsulation efficiency is also observed in GCP25Q9-Curcumin and GCP25Q19-Curcumin formulations subjected to simple rehydration, with a 17% increase in encapsulation efficiency (74 % to 91 %), when DQ % is doubled. This is a higher increase in encapsulation efficiency compared to when DP % was tripled in GCP8Q7-curcumin and GCP25Q9-curcumin formulations (11 %).

Lyophilisation appears to have no significant difference on stability of the particles as zeta potential values in GCPQ-Curcumin formulations remained the same regardless of method of processing.

Initial hypothesis was that more less hydrophilic polymers (lower DQ %) such as GCP8Q7 and GCP25Q9 were unable to achieve complete dissolution when rehydrated hence, resulting in lower encapsulation efficiencies. However, this seems

less likely when considering GCPQ-Curcumin formulations made with these same polymers were also subjected to probe sonication in both the sonicated and lyophilised formulations. This was done to achieve complete dissolution after rehydration. In both processing methods, the same trend is observed where encapsulation efficiency increases with an increase in degree of palmitoylation and quaternisation. This suggests that although hydrophobic interactions between drug compound and the palmitoyl group are important for encapsulation, other factors such as degree of quaternisation have a greater influence on encapsulation. Another factor possibly influencing encapsulation is colloidal stability of the resulting nanoparticles as more unstable particles in Table 4-5 have lower encapsulation efficiencies.

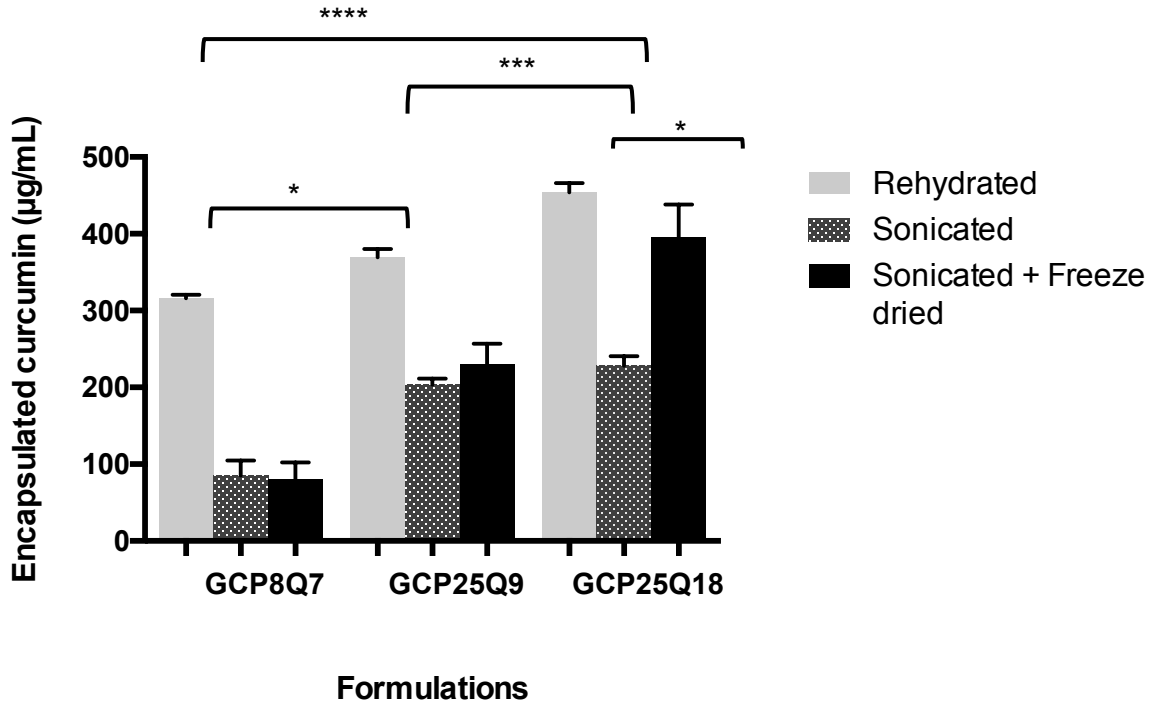

Figure 4-5: Graph shows GCPQ-Curcumin formulations and the total concentration of encapsulated curcumin when subjected different processing (simple rehydration, sonication and freeze drying)(n= 4).

Figure 4-5 allows for the easy visualisation of the effect of different processing methods on curcumin encapsulation. The general trend within each GCPQ-curcumin formulation shows simple rehydration gives rise to formulations with the highest

concentration of encapsulated curcumin followed by lyophilised processing and then sonication processing. Across all formulations and processing, there is a general increase observed with increasing degrees of palmitoylation and then, an increasing degree of quaternisation.

The differences observed in GCPQ-curcumin subjected to simple rehydration has been discussed earlier. Sonication of the GCPQ-Curcumin formulations for three minutes appears to have a negative effect on encapsulation of curcumin as observed in sonicated GCP8Q7-Curcumin, GCP25Q9-Curcumin and GCP25Q19-Curcumin formulations which have encapsulation efficiencies of 17 %, 41 % and 46 % respectively. This translates as a 46 %, 33 % and 45 % decrease in encapsulation efficiency when compared to the formulations subjected to simple rehydration..

When GCPQ-Curcumin formulations subjected to sonication is compared to those subjected to lyophilisation, a significant increase in encapsulation efficiency is observed for GCP25Q19-Curcumin. Sonicated formulations and lyophilised formulations resulting in the same encapsulation efficiency of curcumin is not surprising as lyophilised formulations were also subjected to sonication following rehydration of the white fibrous powder. This implies that a reduction in encapsulation efficiency could be attributed to the 3-minute sonication method employed in both processes. This was unexpected as sonication is believed to aid in the overall dispersion of the drug and polymer mixture within the solution and hence, encourage higher encapsulation but, the opposite was observed here. Dissolution is encouraged by reducing particle size hence, smaller particle size values are expected. However, larger particle sizes with large standard deviations were observed in sonicated formulations. A potential explanation for this could be curcumin being degraded or perhaps, falling out of solution as larger GCPQ-curcumin micelles are broken apart and reformed during sonication process.

GCP25Q19-Curcumin formulations subjected to lyophilisation increases by 32 % compared to those subjected to 3-minute sonication alone, which was interesting. Suggesting that other parameters, for example, as DP %, DQ % or stability may have influenced encapsulation. It is possible that lyophilisation of higher DP % polymers resulted in an increased stability of resulting formulation. So, possible loss of curcumin through micelles opening and reforming during sonication process is less. However, further experiments like stability studies are required to confirm this.

Effect Of Processing on Size and Zeta Potential

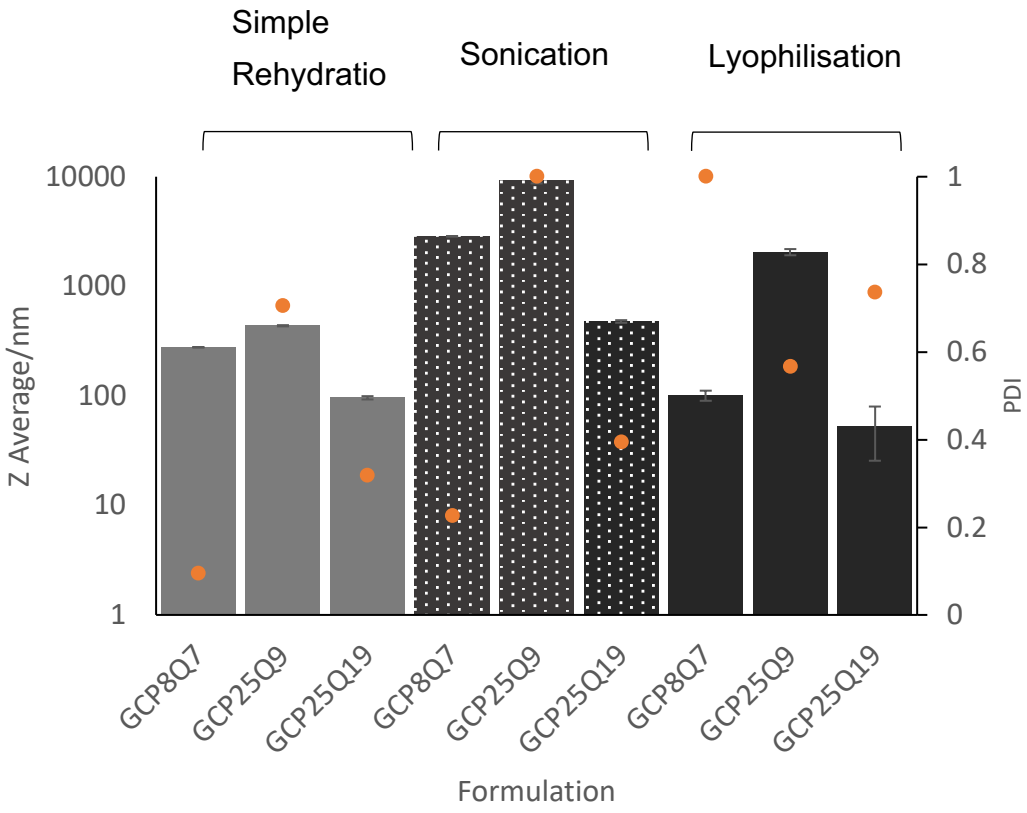

Figure 4-6: Graph showing size (Z-Average) of GCPQ-curcumin formulations obtained using DLS measurements. Second Y axis: PDI values associated with size measurements. Light grey represents simple rehydration, Patterned grey represents sonication and dark grey represents Freeze drying followed by sonication.

Figure 4-6 shows size measurements of GCP8Q7-curcumin, GCP25Q9-curcumin and GCP25Q19-curcumin formulations. The general trend shows GCP25Q19-curcumin formulations possess smallest particle size followed by GCP8Q7-curcumin and then GCP25Q9-curcumin. The particle size for GCP25Q19 may be responsible for higher encapsulation efficiencies shown in Figure 4-5 as smaller particle sized formulations are generally more stable hence, curcumin is less likely to fall out of solution. Two-way ANOVA statistical calculations show no significant difference between Z-average values of GCPQ-curcumin formulations subjected to rehydration alone even though encapsulation results show a 25 % increase in encapsulation efficiency between GCP8Q7-curcumin and GCP25Q19-curumin. This suggests that size of particles alone may not be directly correlated to the encapsulation ability of a polymer. The same observation is made when comparing size values of GCP8Q7-curcumin and

GCP25Q19-curcumin formulations subjected to rehydration and subjected to sonication. Statistical calculations show GCP8Q7-curcumin formulations subjected to sonication have Z-average values significantly higher than those subjected to rehydration alone. When comparing encapsulation efficiency, there is a 46 % decrease in encapsulation efficiency as encapsulated curcumin goes from 316.2 ± 4.29 μg/mL to 85.1 ± 19.6 μg/mL. The same 46 % decrease in encapsulation efficiency is observed when comparing GCP25Q19-curcumin formulations subjected to hydration and those subjected to sonication. However, in this case, there is no significant difference between Z-average values. This suggests once again that particle size does not appear to correlate encapsulation. Size distribution data therefore doesn't explain high encapsulation efficiencies observed as DP % and DQ % increase.

Z-average values gotten for GCP25Q9-curcumin formulations subjected to sonication and lyophilisation as well as GCP8Q7-curcumin formulations subjected to sonication are no longer within the nano range. This suggests a possible error in the centrifugation step which was used to separate the nanoparticles formed from larger aggregates created during the sonication process.

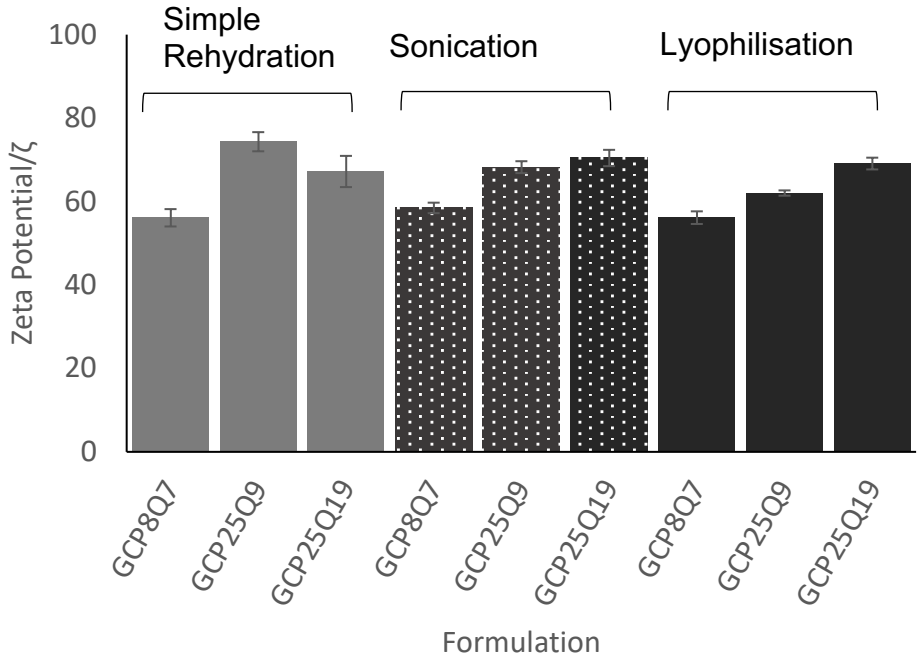

Figure 4-7: Graph showing zeta potential values for GCPQ-curcumin formulations

Zeta potential values of GCPQ-curcumin formulations created are shown in Figure 4-7. The general trend shows an increase in zeta potential as DQ % increases which could be explained by a higher proportion of quaternary ammonium groups carrying a positive charge so, the positive charge of the overall particle surface area should increase. This trend is observed in formulations subjected to sonication and those subjected to lyophilisation however, not in those subjected to simple rehydration alone. In this process, GCP25Q9-curcumin has a higher positive charge at 74.3 ± 2.29 mV than GCP25Q19-curcumin at 67.2 ± 3.74 mV. Statistical results show that this difference is significant although, unexplainable as GCP25Q9 polymer not only has a DP % value half the value of GCP25Q19 but also, has a 3:1 ratio of DP % to DQ % making it more hydrophobic than GCP25Q19 at a 1:1 ratio of DP % to DQ %. When comparing the zeta potential values of individual GCPQ-curcumin formulations subjected to different processes, there is no clear trend observed. For example, there is no significant difference in zeta potential of any of the GCP8Q7-curcumin or GCP25Q19-curcumin formulations while in GCP25Q9-curcumin, there is a significant

decrease in zeta potential between rehydrated, sonicated and lyophilised formulations. This has no clear correlation to results from encapsulation studies.

Effect of Sonication on Z-Average and Encapsulation Efficiency

Further experiments were carried out to investigate the surprising reduction of EE % in GCPQ-curcumin formulations subjected to sonication further. The working hypothesis was that sonication degrades curcumin in formulation hence resulting in smaller EE %. To investigate this, formulation process was repeated, this time, subjecting GCPQ-curcumin formulations to sonication in bursts instead. What this meant was while both formulations were still sonicated for a total of three minutes, new formulations included a break period for 1 minute after every minute of sonication. It was assumed that this may reduce the degradation effect of sonication. Table 4-6 shows the encapsulation efficiency for both GCPQ-curcumin formulations subjected to 3-minute sonication and those subjected to sonication in bursts.

Formulation	Sonication	Burst Sonication	Z- Average ± SD (nm)	PDI ± SD	EE ± SD (%)	DL ± SD (%)
GCP8Q7+Curc	x		22857±14.1	0.23	17±3.91	3±0.65
		x	340.9±7.920	0.25±0.01	22±4.07	4±0.68
GCP25Q9+Curc	x		9309±627.9	1	41±1.51	7±0.25
		x	417.9±19.35	0.38±0.07	55±2.37	9±0.39
GCP25Q19+Curc	x		477.4±13.1	0.39±0.06	46±2.54	8±0.48
		x	268.0±6.62	0.47±0.06	76±5.42	13±0.90

Table 4-6 Table showing encapsulation energy of GCPQ-Curcumin formulations subjected to different sonication methods.

Sonication in bursts resulted in smaller particle sizes all GCPQ-curcumin formulations. There is a general increase in encapsulation efficiency observed within each GCPQ-curcumin formulation when comparing those subjected to 3 minutes of sonication and those subjected to sonication in bursts. GCP8Q7-curcumin increases from 17 % to 22 %, resulting in a 5 % increase when formulation is sonicated in bursts. GCP25Q9-Curcumin however has a 14 % increase, almost 3-fold that of GCP8Q7-curcumin formulations. This is not surprising as degree of palmitoylation is 3 times more in GCP25Q9 polymer compared to that of GCP8Q7 hence, three times more encapsulation sounds ideal as the polymer is three times more hydrophobic. This is also reflective of the encapsulation results observed when comparing formulations subjected to rehydration alone in Table 4-5. GCP25Q19-Curcumin has the highest percentage increase at 30 % when sonication by burst is employed even though the polymer used in these formulations is more hydrophilic than GCP25Q9.

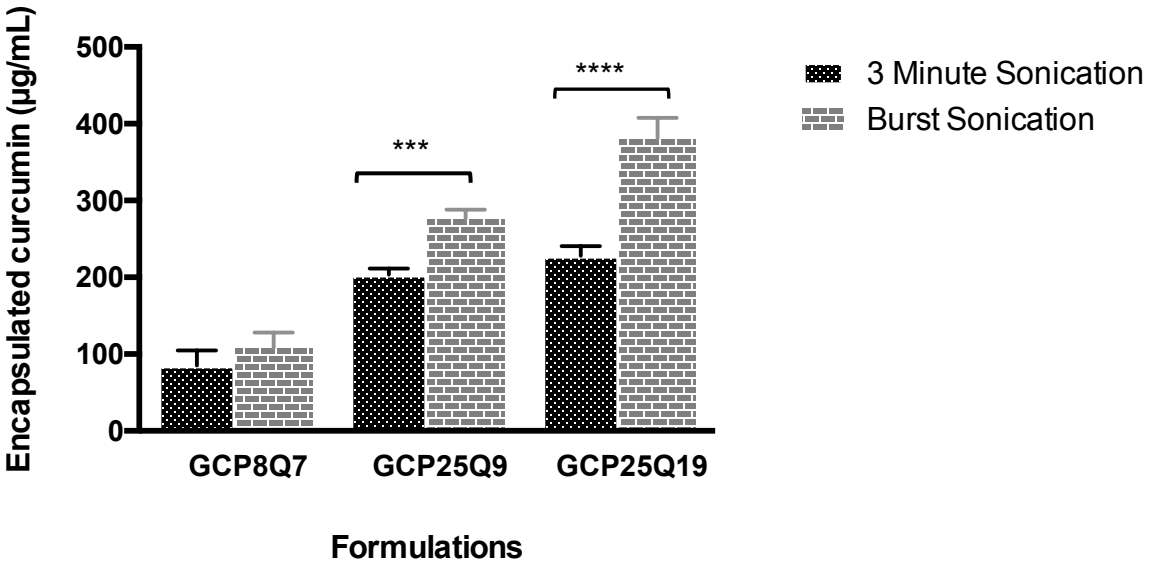

Figure 4-8: Graph showing the effect of sonicating in bursts compared to 3-minute constant sonication on GCPQ-curcumin encapsulation (n = 4).

The trend is better visualized using the graph drawn in Figure 4-8. Both GCPQ-Curcumin formulations subjected to 3 minutes of sonication and those subjected to sonication in bursts have the same trend. There is a general increase in concentration of encapsulated curcumin as DP % increases from 8 % to 25 % and, as DQ % increases from 9 % to 19 %. No significant differences were found in GCP8Q7-Curcumin formulations which suggests that regardless of the method of sonication employed in this formulation method, encapsulation efficiency is significantly less than what is achieved using simple rehydration alone. Differences found in GCP25Q9-Curcumin and GCP25Q19-Curcumin formulations subjected to sonication and sonication in bursts are calculated to be significant. So, sonication in bursts results in an increase in encapsulation of curcumin in both polymeric formulations. For all the formulations created, there is an increase in encapsulation efficiency when subjected to bursts however, this is still less than encapsulation observed from simple rehydration alone.

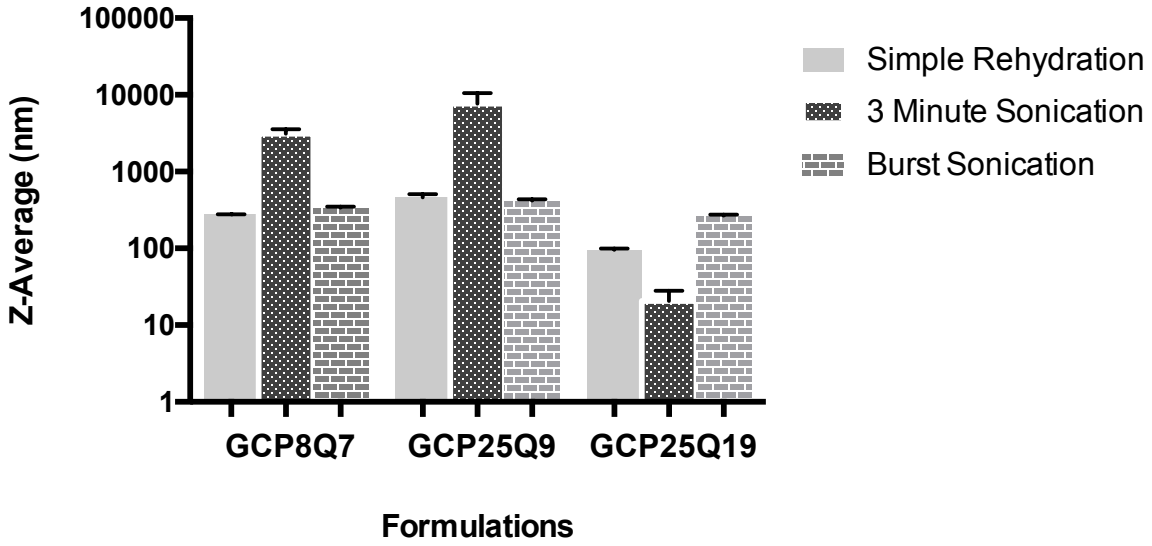

Figure 4-9: Graph comparing Z-average values of GCPQ-Curcumin formulations made subjected to either simple rehydration, 3-minute sonication or sonication in bursts (n=4).

Figure 4-9 compares Z-average values of the different GCPQ-Curcumin formulations subjected to different processes. No significant difference is observed in Z-average values comparing simple rehydration to sonication in bursts. This suggests that the micelles formed by simply rehydrating and vortexing GCPQ-Curcumin formulations are most likely the smallest and most stable confirmation of micelles as burst sonication is not able to break them down into smaller sizes. Only GCP25Q9-Curcumin formulations show significant differences in Z-average between those subjected to 3 minutes of sonication and those subjected to sonication in bursts.

DLS size measurements alone don't explain differences observed in encapsulation efficiency observed as it shows that no significant differences are observed between formulations subjected to simple rehydration and those subjected to sonication I bursts. Although, simple rehydration shows significantly higher encapsulation efficiencies of 63 %, 74 % and 91 % of rehydrated formulations compared to 22 %, 55 % and 76 % encapsulation efficiencies for GCP8Q7, GCP25Q9 and GCP25Q19-Curcumin formulations respectively.

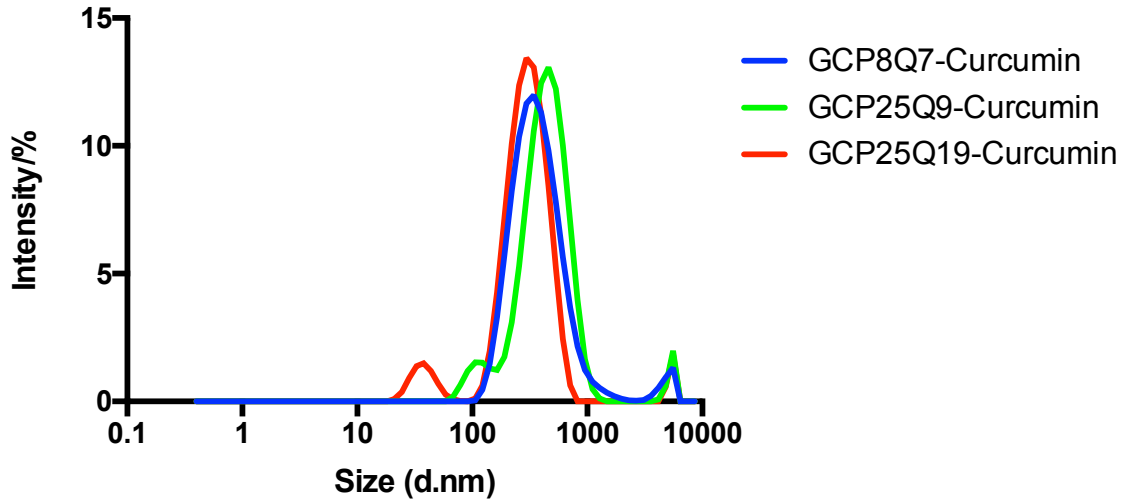

Figure 4-10: Size distribution graph of GCPQ-Curcumin formulations subjected to sonication in bursts measured using Dynamic Light Scattering.

GCPQ-Curcumin formulations for GCP8Q7 and GCP25Q9 show similar distribution with larger aggregates present in aqueous solution (Figure 4-10). This may account for higher Z-average sizes in these micelle formulations of 340.9 ± 7.9 nm and 417.9 ± 19.4 nm respectively. Distribution graphs appear to overlap with no clear size differences. This is confirmed by statistical calculations of raw size values of formulations subjected to sonication in bursts.

Short Term Stability

Short term stability experiments were carried out on GCPQ-Curcumin formulations to investigate stability of particles formed in formulations subjected to sonication in bursts. All samples were stored in the fridge at (5 ± 3 ^{o}C) in aqueous solution to mimic accelerated stability studies. Table 4-7 shows a decrease in size for GCP8Q7-Curcumin formulations, from 340.9 ± 7.9 nm to 324.9 ± 3.2 nm. While for both GCP25Q9 and GCP25Q19-Curcumin formulations, Z-average goes from 417.9 ± 19.3 nm to 534.6 ± 23.6 nm and 268 ± 6.6 nm to 295.8 ± 0.68 nm showing a general increase in Z average between days 1 and 5.

Formulation	Day 1			Day 5		
	Z-average ± SD	Zeta P. ± SD	PDI ± SD	Z-average ± SD	Zeta P. ± SD	PDI ± SD
GCP8Q7-Curcumin	340.9±7.9	57.6±1.53	0.25±0.01	324.9±3.2	57.3±2.8	0.22±0.006
GCP25Q9-Curcumin	417.9±19.3	66.3±0.78	0.38±0.07	534.6±23.6	67.1±2.34	0.43±0.05
GCP25Q19-Curcumin	268±6.6	63.7±0.67	0.47±0.06	295.8±0.68	63.9±0.5	0.21±0.03

Table 4-7: Changes in size distribution of GCPQ-Curcumin formulations subjected to sonication in bursts over 5 days.

When comparing zeta potential values (Figure 4-11), there is no significant difference observed between day 1 and Day 5 in any of the GCPQ-Curcumin formulations. Zeta potential values measured on day one are high, with 57.6 mV being the lowest. This suggests high colloidal stability which should be observed in short term stability studies. Although interestingly, there are changes in GCP25Q9 Z-Average sizes.

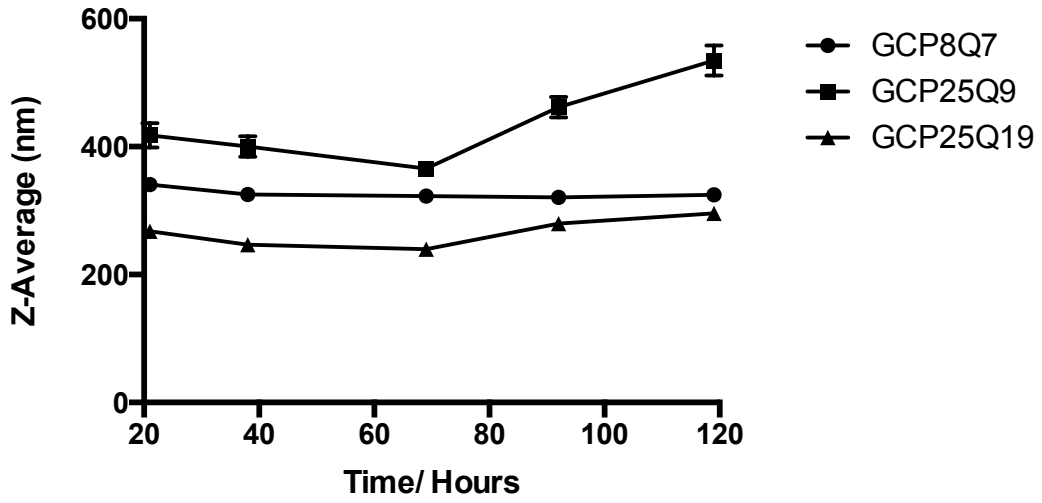

Figure 4-11: Stability test for GCPQ-Curcumin formulations created using sonication in bursts over a period of 120 hours (5 days).

Statistical two-way ANOVA analysis showed no significant differences in Z-average values between days 1 and 5 for GCP8Q7-Curcumin formulations suggesting it is the formulation with the highest colloidal stability. Significant differences were seen between GCP25Q19-Curcumin Z-average of day 1 and day three (*) suggesting less stability in aqueous solution. Although, zeta potential values remained unchanged at 57 mV in Table 4-7, suggesting maintained stability. The same trend is seen in both GCP25Q9-curcumin and GCP25Q19-curcumin formulations. GCP25Q9-Curcumin shows a 28 % increase in particle size, also with zeta potential remaining relatively unchanged and again with GCP25Q19.

TEM Images

TEM images of GCPQ-Curcumin formulations subjected to rehydration and sonication in bursts were investigated to analyse the effect of processing on particle morphology.

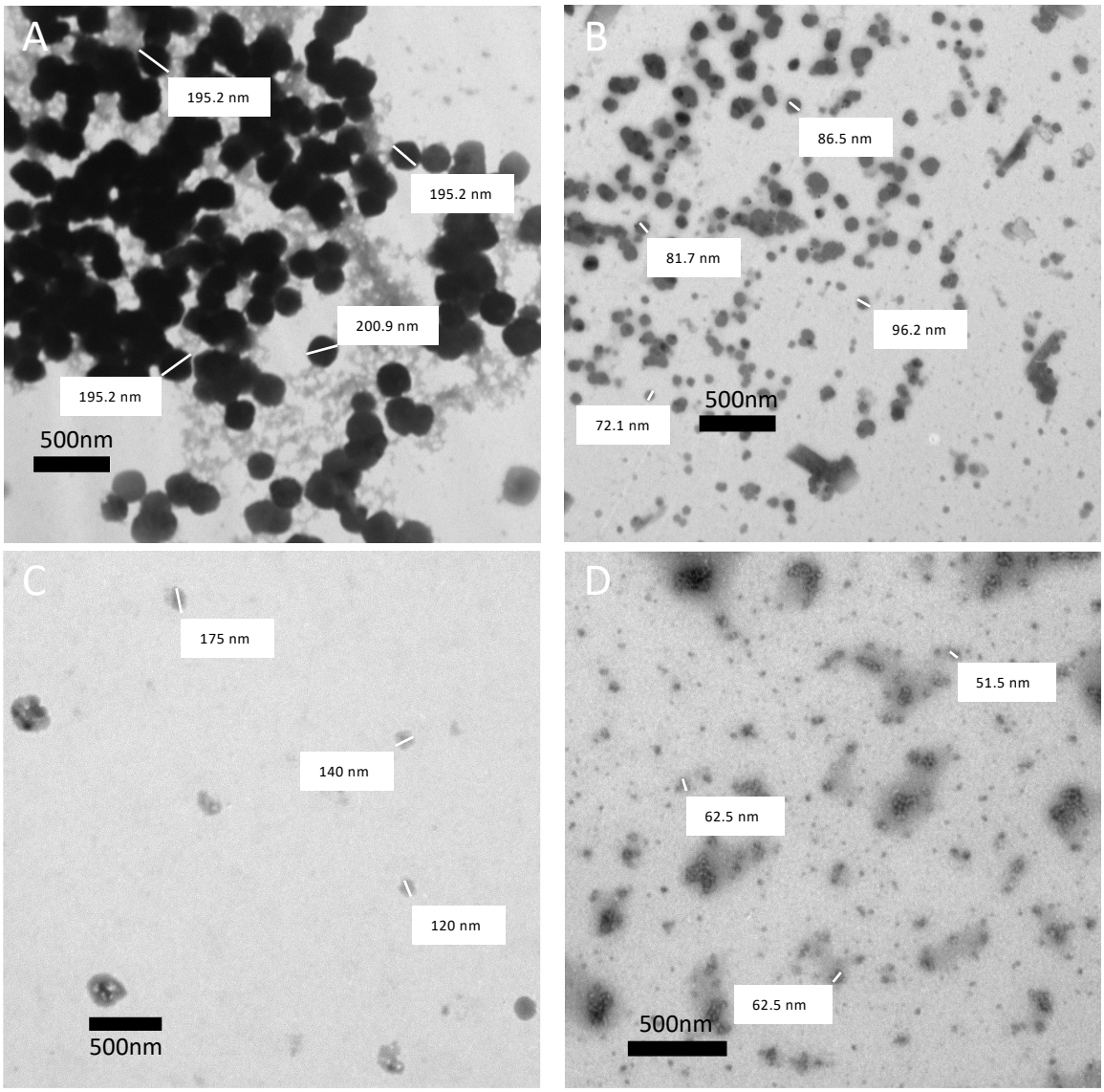

Figure 4-12: Transmission Electron Microscopy (TEM) images of GCPQ-Curcumin formulations showing A. GCP8Q7-curcumin micelles rehydrated B. GCP8Q7-Curcumin micelles sonicated in bursts C. GCP25Q9-Curcumin micelles rehydrated D. GCP25Q9-Curcumin micelles sonicated in bursts.

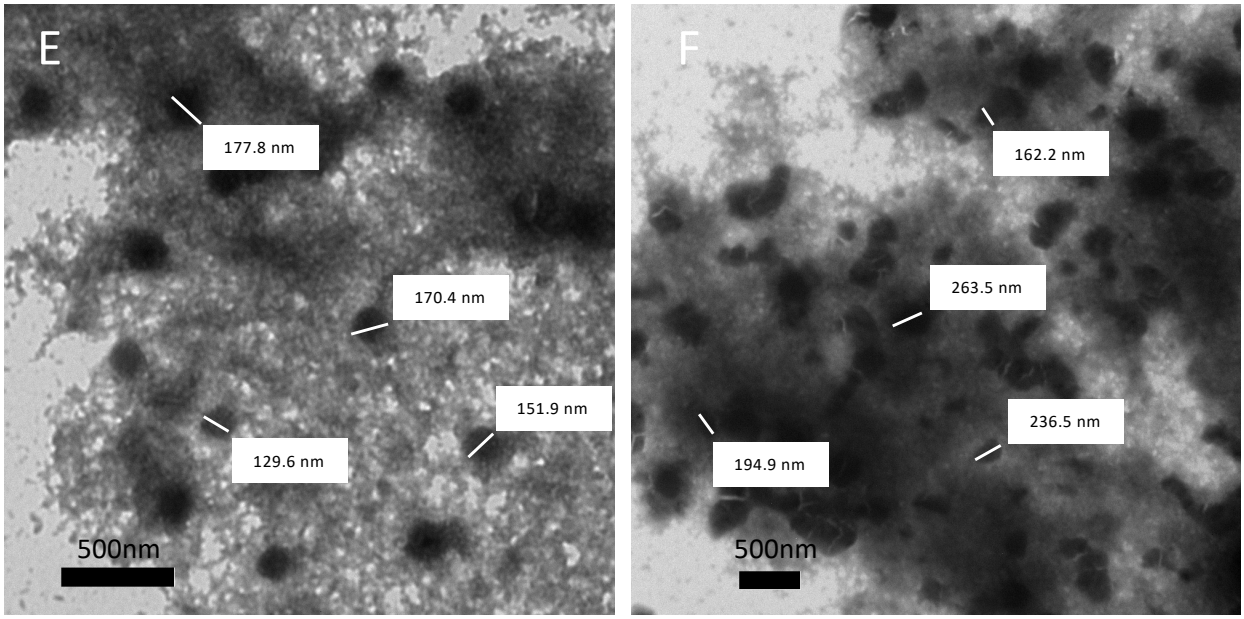

Figure 4-13: Transmission Electron Microscopy (TEM) images of GCPQ-Curcumin formulations showing E. GCP25Q19-curcumin micelles rehydrated and D. GCP25Q19-Curcumin micelles sonicated in bursts.

Figure 4-12 and Figure 4-13 show morphology of GCPQ-Curcumin formulations. Most of these exist as spherical shaped particles with the exception of GCP25Q9-Curcumin subjected to sonication in bursts which are identical to irregular clusters. When comparing TEM size values with Z-average values determined by dynamic light scattering, there are very clear differences. One of which is the average size of particles measured using TEM and DLS. For example, GCP25Q9-curcumin formulations subjected to rehydration processing is shown to have an average size of 145 ± 27.8 nm while DLS measurements determined its average size to be 436.1 ± 5.59 nm, an increase of 67 %. This appears to be a trend in all the aqueous formulations as GCP8Q7-curcumin subjected to rehydration increases from 196.6 ± 2.85 nm to 277.2 ± 1.10 nm, an increase of 29 % when comparing TEM sizes to DLS sizes. While GCP25Q19-curcumin subjected to sonication in bursts also has a similar percentage increase of 20 %. This can be explained as DLS measures the hydrodynamic size of the particles which is larger than the actual size. Size distribution graph in Figure 4-10 shows two different populations in GCP25Q19-Curcumin formulation which is also reflected visually in TEM images Figure 4-13 and in the large standard deviation value.

In reference to the general trend, DLS measurements show larger particle sizes are formed when GCP8Q7-Curcumin and GCP25Q19-Curcumin are subjected to sonication in bursts and a decrease in average particle size with GCP25Q9-Curcumin when compared to those subjected to rehydration alone. The opposite is observed in TEM images where the average size of GCP8Q7-Curcumin reduces from 196.6 ± 2.85 nm to 84.1 ± 10.03 nm and although both GCP25Q9-Curcumin and GCP25Q19-Curcumin values still have a general decrease in particle size as shown in DLS measurements, the percentage decrease varies.

With GCP8Q7 and GCP25Q19-Curcumin formulations subjected to rehydration alone and sonication in bursts, more spherical micelles are being formed. As they both are hydrophilic molecules with a 1:1 ratio of DQ:DP, it is possible that morphology of micelles formed is influenced by structural modifications made on GCPQ polymers. In all formulations, sonication in bursts appeared to produce smaller micelles when simply visualised.

Curcumin Degradation Hypothesis

Data from sonication in bursts supports the loss of curcumin from micelle theory as EE % is higher than EE % of 3-minute sonication. However, this does not address the hypothesis of curcumin degradation or curcumin loss through micelle reformation as a result of sonication. To test this out, GCPQ-curcumin formulations were quantified before and after centrifugation step. In this experiment, GCP25Q19-Curcumin formulations were subjected to both 3-minute sonication and sonication in burst then quantified for curcumin content before and after centrifugation step. Centrifugation at 3000 g for 10 minutes was used during formulation process in order to eliminate un-encapsulated curcumin. So, this was a measure of total concentration of curcumin in solution compared to concentration of encapsulated curcumin in sonicated formulations.

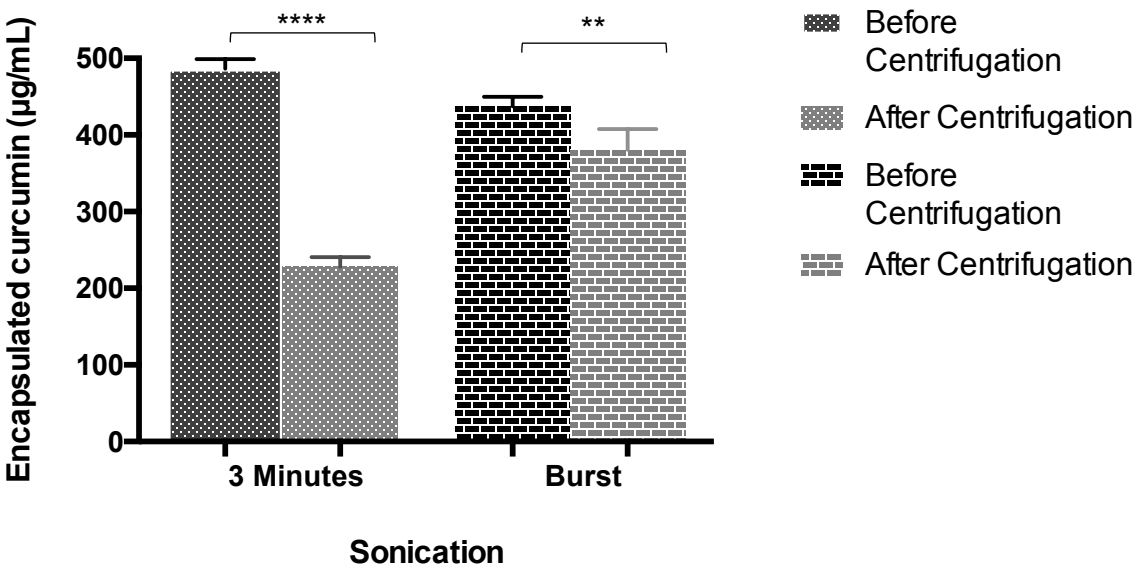

Figure 4-14: Graph showing encapsulation efficiency of GCP25Q19-Curcumin formulations subjected to 3-minute sonication and sonication in burst. Encapsulation was measured before and after centrifugation (n=4).

GCP25Q19-Curcumin formulations were investigated further as they gave rise to micelles with the highest encapsulation efficiencies and short-term stability. Figure 4-14 aims to show the difference in encapsulated curcumin present in supernatant before and after centrifugation. This is to represent the concentration of curcumin which is being forced out of GCPQ micelles during sonication process. When considering the 3-minute sonication process, sonicated formulation before centrifugation was seen to have a total encapsulation of 486.3 ± 12.49 µg/mL. After centrifugation, concentration quantified reduced 228 ± 12.7 µg/mL, showing a 53 % loss in curcumin concentration. This accounts for the reduction in encapsulation efficiency observed between rehydrated samples and sonicated samples in Figure 4-5. Data confirms hypothesis of curcumin being forced out of GCPQ micelles.

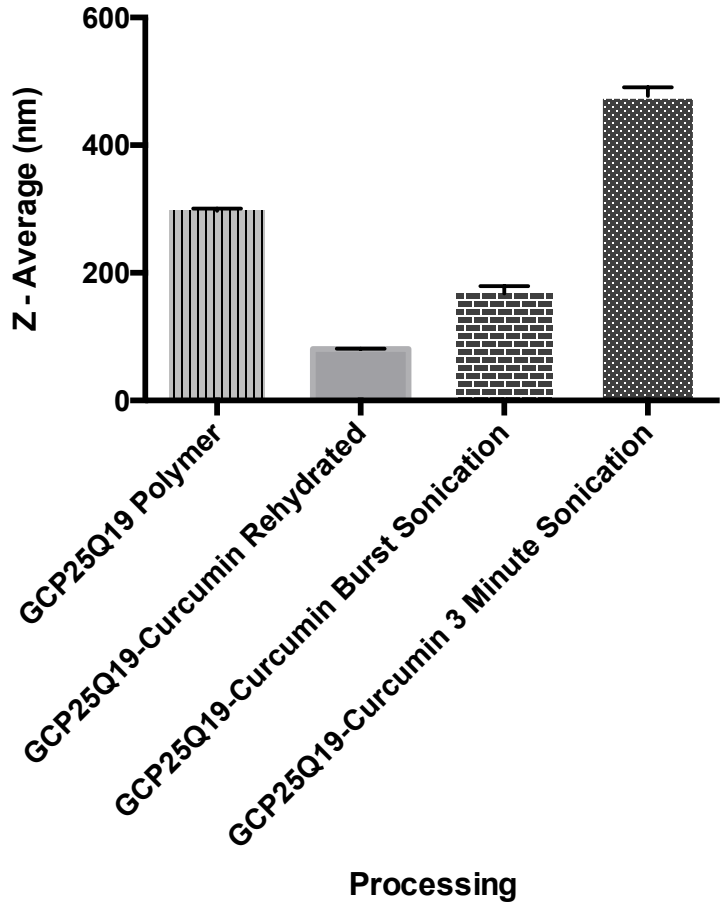

Figure 4-15: Graph comparing size measurements of GCPQ03 formulations subjected to different processes.

With respect to sonication in bursts, a similar trend is observed as there is a 13 % reduction in total concentration of encapsulated curcumin as values decrease from 437.2 ± 12.7 µg/mL to 380.7 ± 27.1 µg/mL. There is no significant difference observed between 3-minute sonication and burst sonication followed by centrifugation.

Z-average values of GCP25Q19 formulations measured using DLS are shown in Figure 4-15. GCP25Q19 polymer is seen to have an average size of 297.3 ± 3.4 nm which decreased drastically in GCP25Q19-Curcumin formations subjected to simple rehydration and sonication in bursts as they have z-average values of 80.9 ± 0.57 nm and 167.5 ± 11.8 nm respectively. However, when GCP25Q19-Curcumin formulations are sonicated for three minutes, they form larger particle sizes at 477.4 ± 13.1 nm which is possibly due to aggregation.

4.4.2 Encapsulation of Caspofungin

Caspofungin Extraction

Caspofungin is sold as its base salt formulation, caspofungin acetate. This is in order to increase the general solubility of the drug but most importantly, its solubility at pH 7 as it is administered by intravenous infusion. To carry out encapsulation experiments, caspofungin was extracted as its free base. Hypothesis was that a hydrophobic drug (caspofungin) will have maximum interactions with the hydrophobic moieties of GCPQ.

Extraction pH	Recovery of Lyophilised Powder (%)	Yield of Caspofungin in Lyophilised Powder (%)
8	5.2	39.2
9	63.7	79.6
10	82.9	47.9

Table 4-8: Table showing recovery and yield of caspofungin extracted at pH 8, 9 and 10.

The caspofungin extraction process was outlined in 4.3.2.3. Recovery was calculated as a percentage of final mass of powder obtained after lyophilisation. A 0.25 mg/mL solution in methanol of extracted caspofungin powder at pH 8, 9 and 10 of was then analysed using HPLC. Actual concentration of CFG was measured and converted into a percentage to give the final yield of CFG for each of the pH. While extraction at pH 10 initially gave the highest recovery of lyophilised powder, HPLC quantification showed that only 47.9 % of this was caspofungin. It is possible that majority of the powder was salt produced from extraction process hence, a wash step was introduced.

HPLC Quantification of GCPQ – Caspofungin

The HPLC chromatogram (Figure 4-16) shows caspofungin has a retention time of 5.4 minutes with an injection peak at 1.5 – 2.0 minutes. Standard curve using area under

the curve values was plotted and shows good linearity over a concentration range of 4 – 250 µg/mL with a correlation of 0.9992. The equation of the standard curve was used to calculate the concentration of encapsulated curcumin in GCPQ-curcumin formulations hence contributed to EE and DL calculations shown in Table 4-5. Equation 15 was used to determine the concentration of encapsulated curcumin in GCPQ-curcumin formulations.

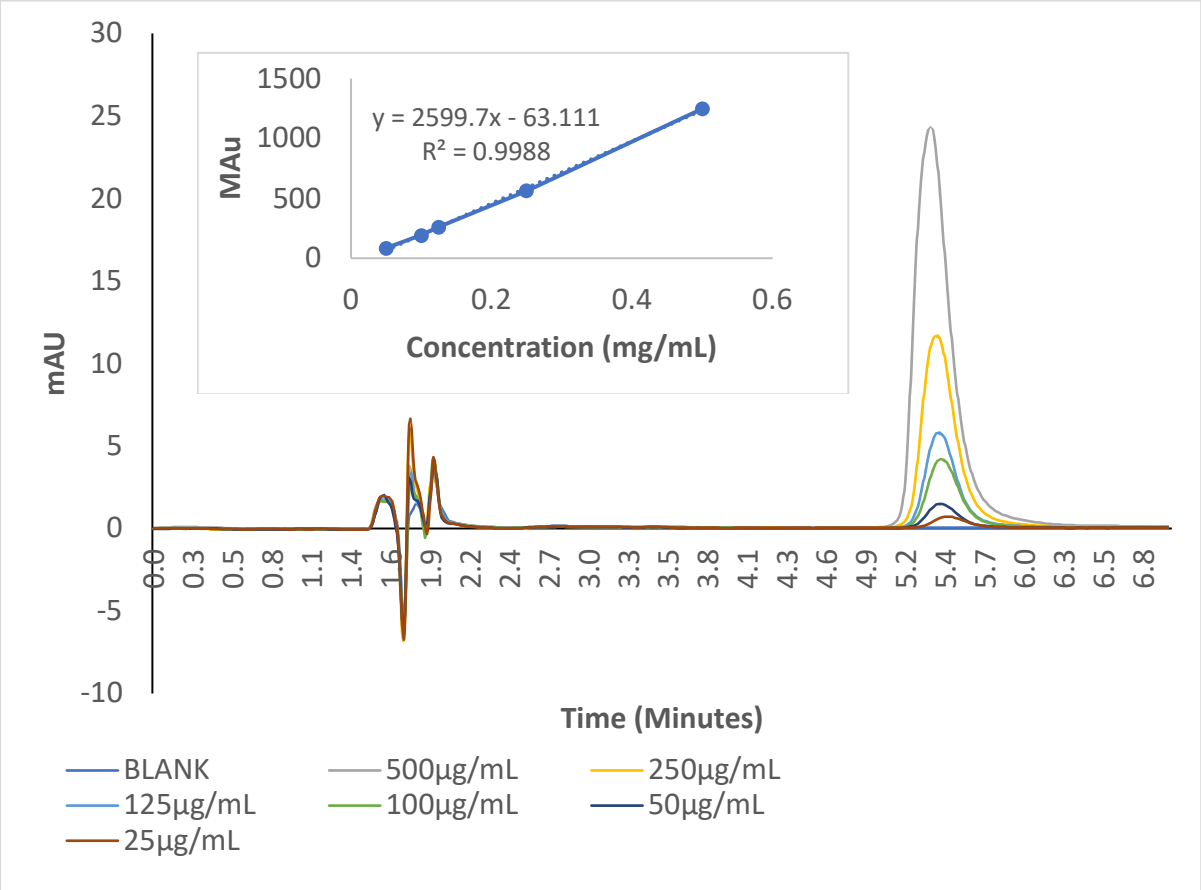

Figure 4-16: HPLC chromatogram for standard solutions of Caspofungin with 0.1% Trifluoroacetic acid : acetonitrile (65:35) as the mobile phase. Insert: Calibration curve plotted using AUV values obtained from chromatogram.

The HPLC chromatogram shows caspofungin has a retention time of 5.4 minutes and the standard curve plotted shows a correlation coefficient of 0.9988. The equation of the standard curve was used to calculate final concentrations of encapsulated caspofungin in the GCPQ-caspofungin formulations created. This in turn was used to determine both EE % and DL % which are displayed in Table 4-10.

Equation 20 was used to determine concentration of caspofungin in GCPQ-caspofungin formulations.

Equation 20

$$conc\ (\mu g\ /\ mL) = \frac{AUC + 63.111}{2599.7}$$

The calculated limit of quantification (LOQ) and limit of detection (LOD) are listed in Table 4-3. LOQ and LOD equations according to ICH guidelines can be found in Equation 16 and Equation 17 (ICH, 2006)

Parameter	**Quantification range (µg/mL)**	**Equation of the straight line**	**R^2**	**Limit of detection (µg/mL)**	**Limit of quantification (µg/mL)**
Value	50 - 500	Y = 2599.7x – 63.111	0.9988	38.8	117.7

Table 4-9: HPLC assay parameters for caspofungin.

GCPQ-CFG Formulations

GCPQ-CFG formulations were created as outlined in 4.3.2.3. Below is the HPLC chromatogram observed in the first round of GCP24Q11-CFG formulations.

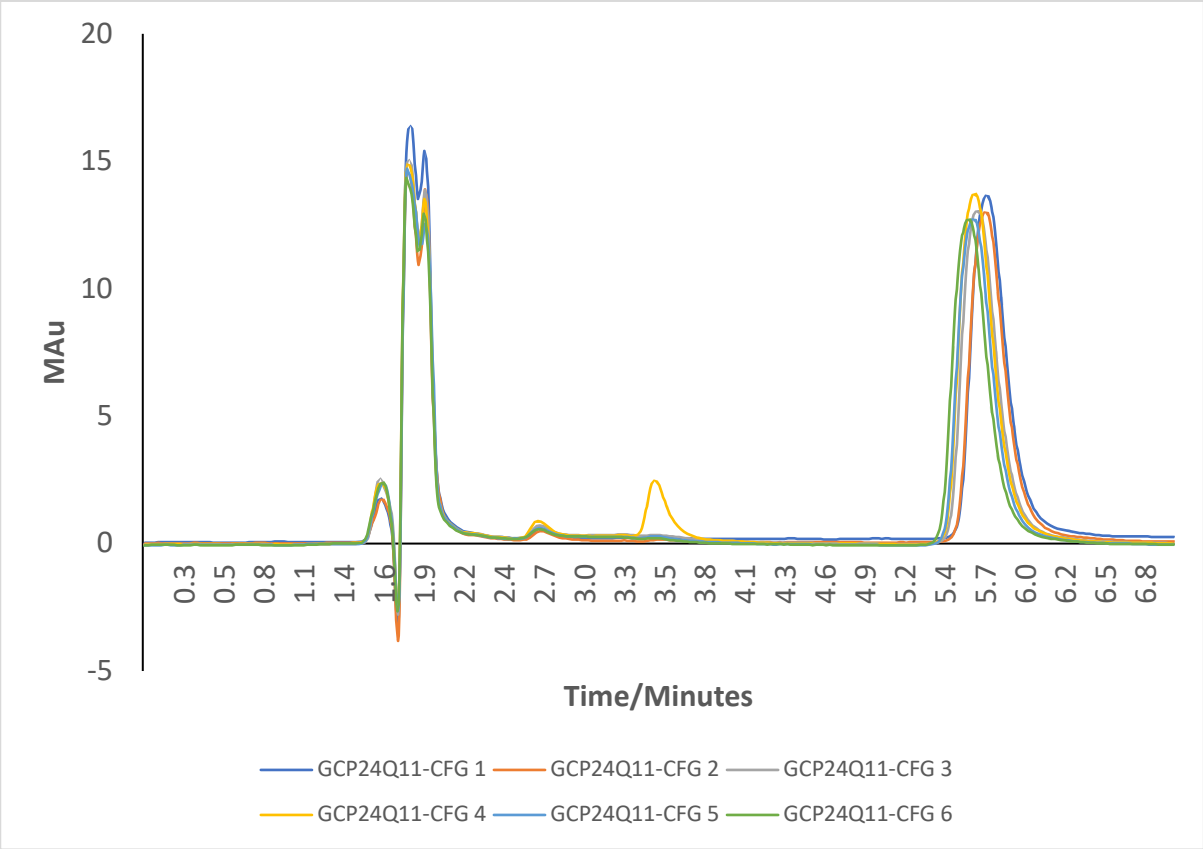

Figure 4-17: HPLC chromatogram of first set of GCP24Q11-CFG formulations created (n=6).

In Figure 4-17, a large peak was observed between 1.9 and 2.0 minutes on the chromatogram. This peak was present in all GCP24Q11-CFG repeats which were formulated on the day and at 15 MAu, absorbance values were too high to attribute peak to injection peak. GCP24Q11-CFG4 also displayed a smaller peak eluting at 3.5 minutes which wasn't accounted for. Also, it is important to note that the elution time for caspofungin moved slightly downstream at 5.8 minutes possibly due to the presence of residual salt from the extraction process.

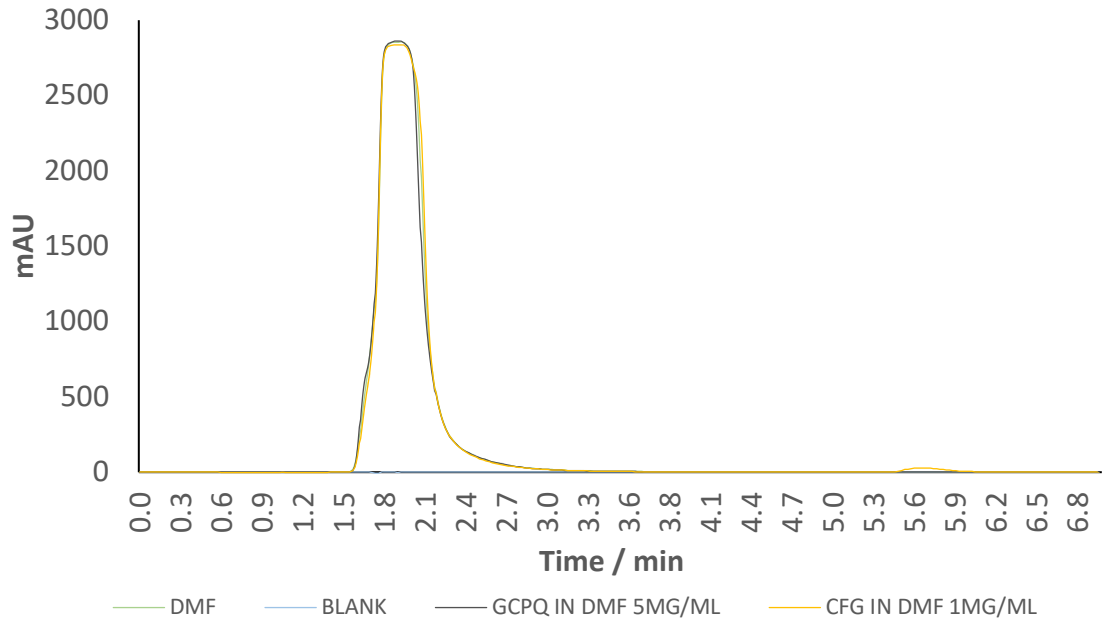

Figure 4-18: HPLC Chromatogram showing elution time of DMF solvent.

In order to investigate the peak eluting at 1.9 to 2.0 minutes, DMF, the solvent used to make stock solutions of both GCP24Q11 and CFG was run using the same method as used to quantify encapsulation of CFG on the HPLC machine. To further confirm, actual stock solutions of GCP24Q11 and CFG dissolved in DMF were also run on the HPLC machine to not only ensure that DMF eluted at the same time as the strange peak observed in Figure 4-17 but also, to confirm that DMF peak also overlaps with GCPQ dissolved in DMF and CFG dissolved in DMF.

The conclusion from investigating Figure 4-17 and Figure 4-18 was DMF is still present in formulation even after being subjected to 2 hours of speed vacuum evaporation method. This is understandable as DMF has a high boiling point of 153 ^{o}C, more than twice that of methanol (64.7 ^{o}C) which was used in GCPQ-curcumin formulations. So, it is possible that incomplete evaporation of the solvent may occur. To address this setback, thin-film formulations obtained after speed vacuum evaporation were subjected to overnight drying in a vacuum desiccator in attempt to remove leftover DMF.

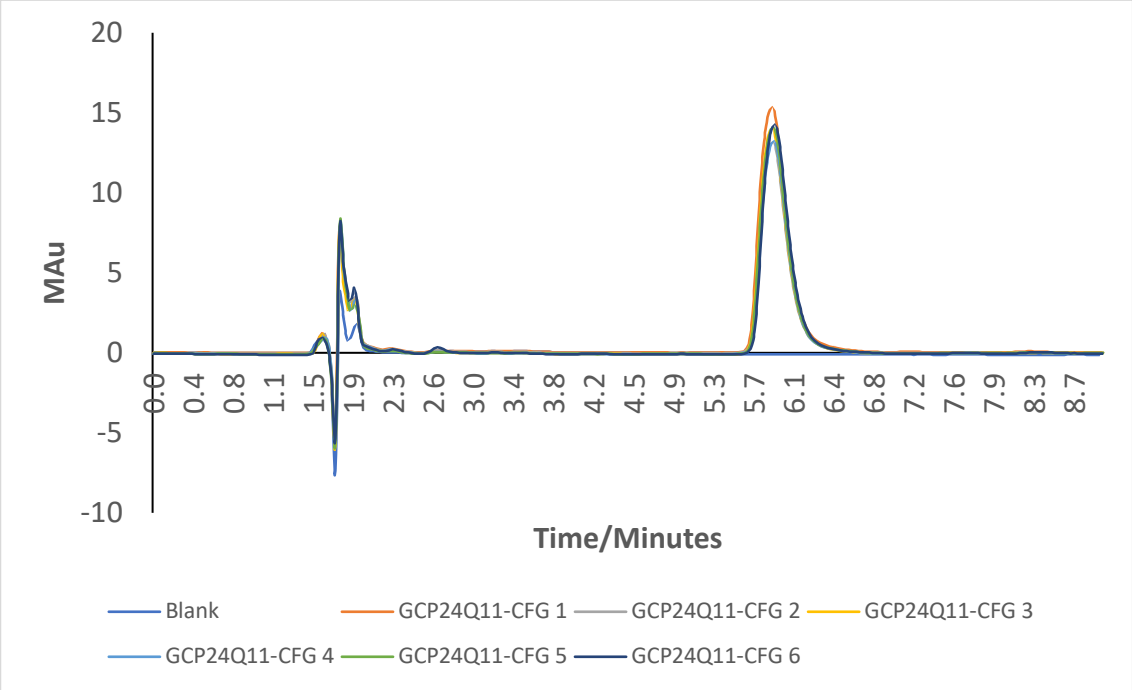

Figure 4-19: HPLC chromatogram comparing evaporation using speed vacuum only with a combination of speed vacuum and vacuum dececator.n=6

Chromatogram obtained in Figure 4-19 shows the absence of DMF peak in second set of formulations created. Also, the extra peak at 3.5 minutes, previously observed in GCP24Q11-CFG4 is not present in any of the formulations and may have been due to carry over from previous run.

Effect of Degree of Modification on GCPQ-CFG Encapsulation Efficiency

Formulations procedure outlined in 4.2.2 was performed using GCPQ polymers synthesized as described in Chapter 3 with varying degrees of palmitoylation, quaternisation and molecular weights to demonstrate how this affects encapsulation efficiency. For each formulation, GCPQ to caspofungin ratio was maintained at 5:1. Encapsulation efficiency (EE %) as well as drug loading (DL %) were determined Equation 18 and Equation 19. In curcumin encapsulation, all polymers were subjected to sonication as there was no significant difference in encapsulation efficiency between rehydrated formulation and sonicated formulations. Ind addition to that, sonicated formulations had smaller particle size. Overall, GCPQ-CFG experimental methods were guided by data observed in GCPQ-curcumin encapsulation studies.

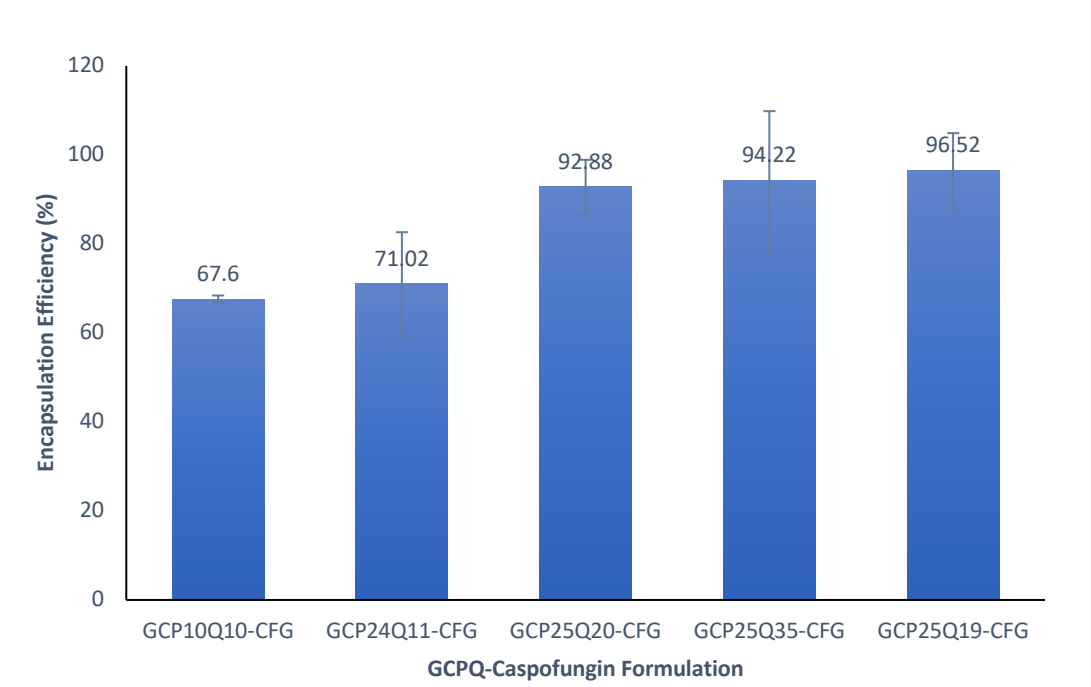

Figure 4-20: Graph showing encapsulation efficiency of GCPQ-Caspofungin formulations created. (n=3)

Figure 4-20 shows the effect of DP % and DQ % of polymer on the encapsulation efficiency of GCPQ-CFG formulations. From the graph, we observe a similar trend to that of GCPQ-Curcumin formulations, where polymers with lower DP % values possess lower encapsulation efficiency values. For example, GCP10Q10-CFG has an

EE % of 68 % compared to GCP24Q11 has an EE % of 71 %. Another similarity is observed with GCP25Q19 being the best performing polymer in encapsulating hydrophobic caspofungin, at 97 % EE %.

Further investigations were carried out to understand if a further increase in DQ % beyond 19 % will promote even more encapsulation of caspofungin. The data however shows a 2 % reduction in encapsulation efficiency as DQ % of GCPQ polymer is increased by 2 % (from 19 % to 35%). This suggests that while increasing DQ % and hence hydrophilicity of the polymer increases encapsulation efficiency of hydrophobic drugs, perhaps there is a limit of about 19 % molar equivalence.

Higher DP % GCPQ polymers were synthesised to also investigate the possible limit at which DP % no longer improves EE %. Although GCPQ30Q40 and GCP45Q50 polymers created had low solubility in DMF solvent at 5 mg/mL. Solution formed was visibly cloudy, showing colloidal instability and so excluded from investigation. Also, due to their high lipophilic nature (high DP %), it can be assumed that rehydration in water following solvent evaporation will prove difficult.

Effect of Degree of Modification on GCPQ-CFG Particle Size

Formulation	Z-average ± SD (nm)	PDI±SD	Encapsulated Caspofungin ±SD (µg/mL)	EE (%)±SD	DL (%)±SD
GCP25Q19-CFG	45.1±3.10	0.49±0.05	482.6±8.36	96.5±1.67	16.1±0.28
GCP24Q11-CFG	167.9±5.80	0.55±0.09	355.1±11.6	72.2±4.07	11.8±0.40
GCP25Q20-CFG	84.9±1.95	0.48±0.03	464.4±6.01	92.9±1.22	15.5±0.20
GCP25Q35-CFG	104.7±5.08	0.65±0.05	471.1±15.6	94.2±3.03	15.7±0.51
GCP10Q10-CFG	154.7±5.08	0.30±0.01	282.8±2.6	67.6±0.81	11.3±0.14

Table 4-10: Table showing concentration of encapsulated curcumin, encapsulation efficiency (EE%) and drug loading (DL%) of GCPQ-Caspofungin formulations (n=6).

Table 4-10 shows the encapsulation efficiency of caspofungin using various polymers, concentration of encapsulated caspofungin, % drug loading as well as particle size determined by dynamic light scattering experiments.

All GCPQ-CFG formulations measured were in the nanometre range (<200 nm) with no obvious trends observed between particle size and degree of GCPQ modulation. All formulations had low standard deviation values, showing good reproducibility. PDI values for most formulations were similar, with the exception of GCP25Q35 which had a high PDI of 0.65. This suggests a broad distribution of particles within the formulation. Overall, GCP25Q19 proved to be the best polymer with small particle size of 45 nm and high encapsulation efficiency of 97 %.

An intensity (%) size distribution profile for GCP24Q11 was obtained using measurements taken from dynamic light scattering and displayed in Figure 4-21. This was to observe the effect of encapsulation on size distribution graph.

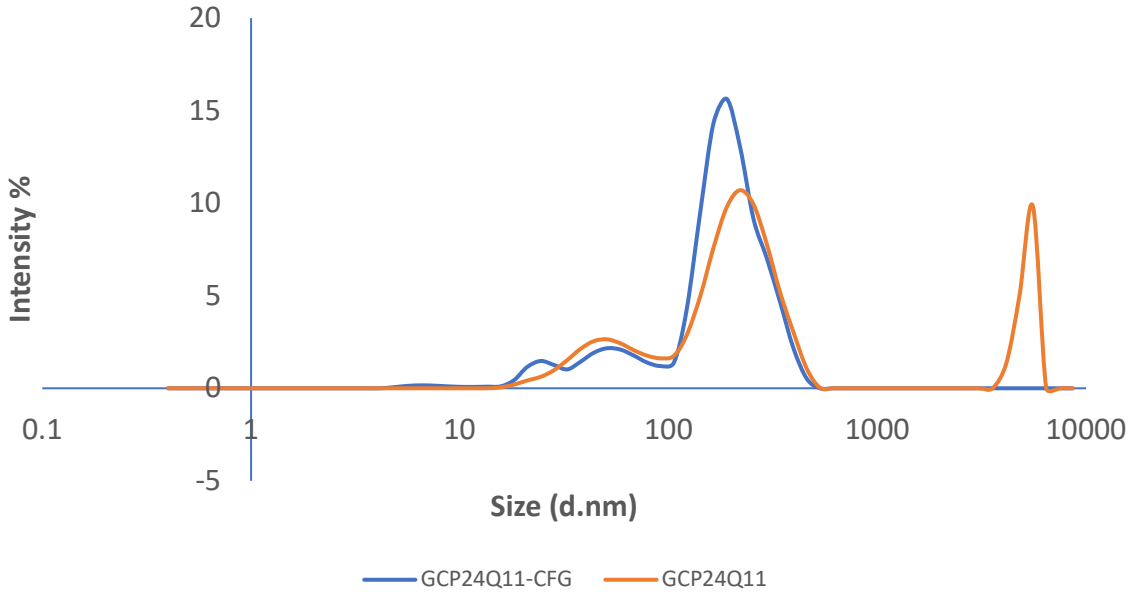

Figure 4-21: Size distribution of GCP24Q11-Caspofungin formulation and GCP24Q11 polymer alone measured using Dynamic Light Scattering (DLS).

GCP24Q11 polymer and GCP24Q11-CFG size distribution graphs mirror each other. A major difference is observed in GCP24Q11-CFG alone (orange) which is seen to contain larger aggregates in aqueous solution. However, once caspofungin is encapsulated within polymeric micelles (blue), large aggregate peak disappears. Although, solution is still not considered to have a monomodal distribution as there are peak shoulders representing the presence of micelles with lower particle size between 10 and 100 nm. A rational explanation for this could be due to GCPQ polymer chains forming reversible clusters in solution. When a drug molecule is introduced and micelle formation occurs, it may be more thermodynamically favourable for these clusters to instead solubilise drug. Causing clusters peak to disappear.

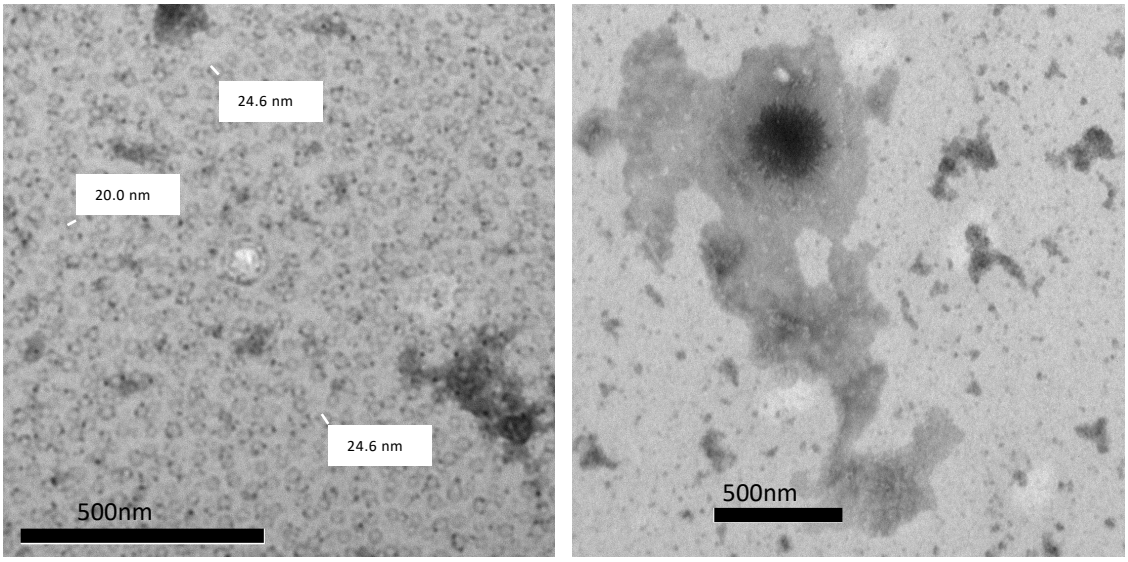

Figure 4-22: Transmission Electron Microscopy (TEM) images of GCPQ-Caspofungin formulations showing GCP24Q11-Caspofungin formulation (Left) and GCP24Q11 micelles in aqueous solution at a concentration of 1mg/mL (Right).

To test this theory, TEM images of GCP24Q11 polymers and GCP24Q11-CFG formulations were analysed in Figure 4-22. GCP24Q11 in deionised water solution presents as irregular clusters and so average sizes of individual particles were unable to be determined. Irregularity in GCP24Q11 particles support theory of cluster peaks suggested above. While well-rounded spherical shaped particles with homogenous distribution are observed in GCP24Q11-CFG formulations. This suggests that upon introduction of caspofungin drug, GCPQ particles are encouraged to form more regular micelles encapsulating caspofungin. GCP24Q11-CFG formulations are shown to have an average size of 23.1 $\pm$ 2.66nm compared to 167.9 $\pm$ 5.80 nm recorded by DLS measurements. Once again, because DLS measures hydrodynamic radius of a particle in solution.

Short Term Stability Studies on GCPQ-CFG Formulations

Short term stability experiments were carried out on GCPQ-Curcumin formulations to investigate the stability of formulations over seven days in aqueous solution at room temperature (25 ± 2 ºC / 60 ± 5 % RH). Data was represented in Table 4-11.

	Day 1			**Day 7**		
Formulation	**Encapsulated Caspofungin (µg/mL) ±SD**	**Z-Average ±SD (nm)**	**PDI ± SD**	**Encapsulated Caspofungin (µg/mL) ±SD**	**Z-Average ±SD (nm)**	**PDI ±SD**
GCP24Q11-CFG	355.1±11.6	167.9±5.80	0.56±0.04	213.3±8.16	197.4±70.9	0.45±0.10
GCP25Q19-CFG	482.6±8.36	45.1±3.10	0.49±0.05	417.3±12.2	70.6±3.50	0.83±0.04
GCP25Q20-CFG	464.4±6.01	84.9±1.95	0.48±0.03	422.5±34.1	207.4±13.9	0.55±0.06
GCP25Q35CFG	471.1±15.6	104.7±5.08	0.65±0.05	418.9±16.2	156.2±9.05	0.64±0.18

Table 4-11: Graph comparing drug content and Z-average values of GCPQ-CFG formulations over a 1-week time period.

Changes in encapsulated caspofungin of GCPQ-CFG formulations were observed in aqueous solution over 7 days. As GCPQ-CFG intended formulation is as a dry, lyophilised powder, it was hypothesised that degradation in aqueous solution will occur at an accelerated rate hence, formulations were observed over 7 days. Also at room temperature. The general trend observed in Table 4-11 is a reduction in encapsulated caspofungin and an increase in Z-average of formulations between day 1 and day 7.

This is an indication of degradation occurring particularly in GCP24Q11-CFG formulations where there is a 40% decrease in caspofungin content. Statistical calculations showed significant reductions in encapsulated caspofungin in both GCP24Q11-CFG and GCP25Q19-CFG formulations by 40 % and 14 % respectively. It is important to note that formulations were stored at room temperature and so, stability at 4 ^{o}C would vary. Also, while GCP25Q19-CFG formulations experience a loss in drug content, concentration of caspofungin after 7 days is not significantly different from that of GCP25Q20-CFG and GCP25Q35-CFG. Although, GCP25Q19-CFG also has very high PDI value at (0.83) suggesting broad particle distribution. GCP25Q19 remains the best polymer for caspofungin encapsulation due to its small particle size and high encapsulation efficiency. While formulation performs poorly in short term stability studies, it is important to note that final GCPQ-caspofungin formulation will not be stored as aqueous solution.

4.5 Discussion

4.5.1 Curcumin

Curcumin formulations created using GCPQ polymers were shown to give rise to particles with different physical properties based on the ratios of polymer's DP% to DQ% (QPR) (Figure 4-9 and Figure 4-10). GCP8Q7 and GCP25Q19 polymers both have similar QPR (0.87 and 0.76) and formed spherical shaped nanostructures with a homogeneous distribution when encapsulated with curcumin. On the other hand, GCP25Q9-curcumin formulations using a polymer with a QPR of 0.36 formed irregular clusters. This was previously observed by Qu et al. that where GCPQ nanoparticles formed micellar clusters in solution which was proposed enhanced carrying capacity for hydrophobic drug compounds and enhance their bioavailability by facilitating transport of drugs across biological barriers (Qu et al., 2006b).

Curcumin, a class IV drug with a log P of about 3.62 is poorly soluble in aqueous solutions under alkaline and neutral conditions, with a solubility of 3.12 mg/L due to its chemical composition. Although, it is soluble in dimethylsulfoxide (DMSO), acetone and ethanol. Solubilisation of curcumin has been attempted by covalently binding

sugar to curcumin (Arezzini et al., 2004) however, a majority of the formulations in the literature employ the use of nano formulations to increase solubility of curcumin. (Young et al., 2014; Zhongfa et al., 2012; Sahu et al., 2011).

One of such formulations involves the use of PEGylated PLGA in curcumin formulation and was shown to yield a high encapsulation efficiency of 90.88 ± 0.14 % with particle size distribution ranging from 35 nm to 100 nm, and mean particle size being 45 nm (Mukerjee and Vishwanatha, 2009). The results presented here achieved a similar encapsulation efficiency with the use of GCP25Q19 polymers where encapsulation efficiency was 91 % ± 2.40 and total curcumin encapsulated was 454.0 ± 12.0 µg/mL out of 500 µg/mL. Similar encapsulation efficiencies were observed in the use of pluronic micelles to encapsulate curcumin, where encapsulation efficiencies as high as 95.5 % with a 1:50 drug : polymer ratio was achieved (Sahu et al., 2011).

Effect of DP% and DQ% on Encapsulation Efficiency

The results of the encapsulation studies show the correlation between GCPQ polymer modification and enhanced encapsulation of curcumin within the polymer. In general, an increase in both DQ % and DP % resulted in more curcumin encapsulated in the formulation. This can be seen, when comparing GCP8Q7-curcumin and GCP25Q9-curcumin formulations in Table 4-5. DP % is increased by three folds in GCP25Q9 polymer and the resulting effect is an 11 % increase in encapsulation efficiency. In this comparison, not only does GCP25Q9 possess a more hydrophobic moiety due to an increase in DP but also, when comparing ratio of DP % to DQ %, there is a 3:1 ratio. This suggests that the molecule contains three times more hydrophobic moieties than GCP8Q7 and is also three times more hydrophobic than it is hydrophilic. Due to curcumin being a hydrophobic molecule, it is expected that encapsulation would increase as hydrophobicity increases as there are more interactions between the hydrophobic moieties of GCPQ micelles formed in solution and curcumin compound. This is observed when comparing the concentration of curcumin encapsulated using GCP8Q7 and GCP25Q9 polymers. Regardless of the processing they were subjected to, GCP25Q9-curcumin formulations results show higher encapsulated curcumin than GCP8Q7-curcumin formulations.

However, in GCP25Q19-curcumin formulations, the polymer used possesses the same DP % value as in GCP25Q9 but, also, a higher DQ %. In these formulations, concentration of encapsulated curcumin was 454.0 ± 12.0, 228.0 ± 12.7 and 394.9 ±

43.2 µg/mL for simple rehydration, sonication and lyophilisation processing. This translated to a 17 %, 5 % and 32 % increase in encapsulation efficiency which was unexpected. With a DP% of 25 % and a DQ% of 19%, DP% to DQ% ratio is about 1:1 which is similar to that of GCP8Q7. It was expected that encapsulation would either remain the same as there is no increase in DP % between GCP25Q9 and GCP25Q19 or reduce due to a total reduction in the degree of hydrophobicity of the GCP25Q19 polymer however, the opposite was observed. Results in Table 4-5 initially show a positive correlation between an increase in hydrophobic moieties (increase in DP%) of a polymer and encapsulation efficiency. The results show that when DQ % is doubled at an optimum DP% value of 25 %, encapsulation efficiency increases more than when DP % is tripled except for formulations subjected to sonication.

The reason for higher encapsulation when DQ % may be explained based on findings from Ahmad et al (Ahmad et al., 2010). Research using MARTINI modelling showed hydrophobic propofol was located in an interphase between the hydrophobic and hydrophilic moieties of GCPQ micelles (Ahmad et al., 2010). With this rationale, it can be assumed that an increase in DQ % contributes to drug interactions occurring at interphase hence, higher drug encapsulation.

Effect of Encapsulation Method

Analysis of encapsulation experiments showed that the yield of encapsulated curcumin is not only dependent on the modifications made in GCPQ synthesis such as degree of palmitoylation and quaternization. The different processes each formulation was subjected to following thin-film formation also influenced encapsulation efficiency. The general trend in Figure 4-5 shows rehydrated formulations the highest encapsulation efficiency followed by those subjected to lyophilisation and then, sonicated formulations have the least amount of encapsulated curcumin. This suggests that curcumin readily interacts with palmitoyl groups located within the micelles formed in aqueous solution to avoid interactions with the surrounding water molecules. However, a decrease in encapsulation after sonication poses an important question about what sonication does to already encapsulated curcumin. It was initially thought that curcumin was somehow being degraded during the sonication stage due to exposure to high energies and temperatures from probe sonicator. Figure 4-14 shows instead, it is being forced out of solution as the total

curcumin (%) in GCP25Q19-curcumin formulations subjected to sonication in bursts is similar to those in GCP25Q19-curcumin formulations subjected to rehydration alone (shown in Figure 4-5). However, when centrifuged at 3000 g to remove un-encapsulated curcumin, the apparent reduction in curcumin present in supernatant is observed. Therefore, the concentration of un-encapsulated curcumin increases because of sonication. This is also observed when formulation is subjected to burst sonication although, to a lesser degree. Regardless, it is impossible to completely rule out degradation of curcumin as a contributing factor to lower encapsulation efficiencies until the pellet formed from centrifugation is isolated, rehydrated and quantified.

Particle sizes from TEM images varied significantly from those obtained from dynamic light scattering (DLS). It is proposed that this is due to the presence of larger aggregates in aqueous solution as majority of the formulations in Table 4-5 have a high polydispersity index (PDI). Sonication or sonication in bursts should eliminate this factor as it is seemingly expected to give rise to smaller particle sizes. However, a closer look at Figure 4-9 shows formulations subjected to 3-minute sonication have the largest particle size and no significant difference is observed between those subjected to simple rehydration and those subjected to sonication in bursts. This is also supported by Figure 4-10 which shows peaks at higher Z-average values for formulations sonicated in bursts, confirming the presence of larger particle sizes believed to be aggregates, possibly un-encapsulated curcumin.

Colloidal Stability

Short term stability tests in Table 4-7 show that GCP25Q9-Curcumin formulations form larger particles after a 5-day period. These were believed to be attributed to large aggregates and often correlated with colloidal instability in formulation. Making GCP25Q9-curcumin the least stable formulations and possibly the least ideal even though it has encapsulation efficiencies of 74 % ± 2.29. This was unexpected as zeta potential values are usually used as an indicator of colloidal stability. A colloidal system with a sufficiently high charge density causes repulsion of the individual particles hence, maintaining stability for a longer period (Particle Sciences, 2012). GCP25Q9-curcumin formulations subjected to sonication have a zeta potential of 68.2 ± 1.43 mV which was significantly higher than GCP8Q7-curcumin formulations which was 58.5 ±

1.26 mV so, it was expected that GCP25Q9 formulations would be more stable. Although, it is important to note that stability tests only involved the measurement of Z-average and a better indicator of stability would have been a combination of changes in Zeta Potential and curcumin content within the formulation and in the pellet, all in addition to Z-average values over the 5-day period.

In summary, the data suggests that modifications performed on GCPQ polymer such as changed in DP % and DQ % influence encapsulation efficiency. The general trend shows the best polymer property is an optimum DP % of 25 % and a DQ % value of at least 18 %. As GCPQ polymers with higher DQ values were not investigated in GCPQ-Curcumin encapsulation studies. Although sonication has been employed in pharmaceutical formulations to encourage encapsulation as well as reduce particle size, none of these were observed in GCPQ-Curcumin formulations. In some instances, 3-minute sonication and burst sonication processing gave rise to formulations with Z-average values significantly larger than those subjected to simple rehydration alone. While in other instances, encapsulation efficiency was significantly reduced when formulations were sonicated. So, for all GCPQ-Curcumin formulations investigated, simple rehydration and vortexing following the thin-film method proved to be the most efficient formulation technique when comparing Z-average, Encapsulation efficiency and Drug loading.

4.5.2 Caspofungin

GCPQ-Caspofungin formulations were created using GCPQ polymers with a range of different DP % and DQ % modifications. These were shown to influence physical properties of resulting formulations. Aim for these studies was to understand the effect of GCPQ modulation on enhanced encapsulation ability of hydrophobic caspofungin. Evidence supporting this has been reported in the literature (Qu et al., 2006b).

Caspofungin is poorly soluble in aqueous solutions, with a solubility of 28 mg/L at 25 ^{o}C. Due to caspofungin's poor solubility as well as poor permeability, it is currently formulated as an acetate base salt, addressing solubility issues. There are currently no data on oral formulations of caspofungin in the literature due to its poor

bioavailability of 0.2 % following a 50 mg/kg dose in rats (European Medicines Agency, 2005).

Effect of GCPQ modification on Encapsulation Efficiency

To test initial encapsulation efficiency, GCP24Q11 polymer was utilised. GCP24Q11-CFG formulations were shown to have an average encapsulation efficiency of 72.2 % ± 4.1 with a total encapsulation of 355.1 ± 11.6 µg/mL out of 500 µg/mL of caspofungin. This was compared to GCP10Q10-CFG formulations to observe the effect of DP % on encapsulation as encapsulation studies in Table 4-5 showed increasing DP % improved encapsulation efficiency of curcumin. Table 4-10 shows the concentration of encapsulated caspofungin in GP10Q10 formulations was 282.8 ± 2.6 µg/mL which was significantly less than that of GCP24Q11, a trend also observed in GCPQ-Curcumin formulations.

The effect of DQ on encapsulation was then investigated. From the data in Table 4-10, an increase in encapsulation efficiency is observed when DQ % is increased from 11 % to 19 % in GCP25Q19-CFG formulations. These attained an encapsulation efficiency of 96.5 % ± 1.67 with total caspofungin concentration of 482.6 ± 8.36 µg/mL out of 500 µg/mL. GCP25Q20-CFG and GCP25Q35-CFG formulations were also created in attempt to further increase total encapsulated drug in formulation however, there was no significant difference in encapsulation efficiency of total drug content between GCP25Q19-CFG, GCP25Q20-CFG and GCP25Q35-CFG formulations. This suggests that the optimum parameters for efficient encapsulation of caspofungin was a polymer with DP % of 25 % and DQ % of 19 %. Although, further encapsulation studies using GCPQ polymers with higher degrees of palmitoylation would be required to confirm this.

No general trend was observed when comparing Z-average values to encapsulation efficiency or degree of modification of GCPQ particles.

Colloidal Stability

Short term stability tests in Table 4-11 show a significant increase in particle size of GCPQ-CFG formulations after one week. Although, they are still within the typical nanoparticle size of about 200 nm. PDI values remained similar after 7 days meaning

there was no significant difference in particle dispersity within formulation so, changes in particle size may not be due to formation of large aggregates.

When comparing encapsulated caspofungin between Day 1 and Day 7, significant differences are only observed in GCP25Q19-CFG and GCP25Q11-CFG formulations. HPLC analysis showed significantly less caspofungin was present in the formulation after 7 days. It is possible that some of the caspofungin fell out of solution however, this was not visually observed as there was no obvious pellet in the Eppendorf.

As Z-Average values proved to be inadequate in predicting colloidal stability of GCPQ-Curcumin formulations in Table 4-7, Zeta Potential values of GCPQ-CFG formulations would have been an ideal indicator of colloidal stability in this study.

Trends Observed In GCPQ-CFG and GCPQ-Curcumin

Overall, GCPQ polymer was able to encapsulate both curcumin and caspofungin drug compounds despite high RED values, high difference of HSP parameters and Hansen sphere plots shown in Chapter 2. HSP data showed low possibility of interactions between GCPQ constituent and drug compounds, suggesting no encapsulation will occur. Contrary to theoretic data, GCPQ can encapsulate both class IV drugs with increasing encapsulation efficiencies as both degrees of palmitoylation and quaternisation increased.

There are no significant differences between GCP24Q11-CFG formulations and GCP25Q9-curcumin formulations subjected to simple rehydration alone. Results from comparison of both encapsulation efficiencies seem reasonable as the polymers utilised have similar degrees of modifications with GCP25Q9 and GCP24Q11 polymers having DP % values of 25 % and 24 % and DQ % values of 9 % and 11 %.

When comparing Z-average sizes of both polymers made, there is no clear correlation between the two. GCP25Q9 has an average particle size of 973 nm while Z-average of GCP24Q11 was 33.4 nm. When formulation sizes were compared, GCP25Q9-curcumin was seen to have an average size of 436 nm compared to 167.9 nm of GCP24Q11-CFG formulations. TEM measurements show particle size of 26.6 nm in GCP24Q11-CFG formulations compared to 143 nm in GCP25Q9-curcumin.

The GCP25Q19 polymer yielded the highest encapsulation efficiencies in both caspofungin (97 %) and curcumin (91 %).

It is interesting to observe similar trends in both formulations as caspofungin and curcumin possess different physiochemical properties. Attaining the same level of encapsulation efficiency in both drugs from using GCPQ polymers with similar degrees of modification suggests that degree of modification greatly influences encapsulation. If that is true then, a single set of encapsulation experiments using a varied library of GCPQ polymers with different modifications could act as a predictive measure for encapsulation of all hydrophobic drug compounds regardless of their physiochemical properties. Although, a more extensive set of encapsulation experiments are required to confirm this.

4.6 Conclusions

Despite HSPiP simulations suggesting low probability of interaction between GCPQ constituents and class IV drugs curcumin and caspofungin, Data showed modified GCPQ polymers can form strong enough interactions and solubilise these hydrophobic class IV drug compounds by encapsulating them within stable nanoparticles. This highlights the limitations in HSPiP predictions. Disparity may be attributed to the added level of complexity which may not accounted for in thermodynamic calculations. Therefore, supporting the notion that data from predictive tools alone may not be sufficient in making decisions in pharmaceutical formulations. For the encapsulation of curcumin, having a high DP % of about 25 % coupled with a DQ % greater than 19 % is essential for achieving high encapsulation efficiencies greater than 90 %. Lower DQ values resulted in a 20 % decrease in EE %. QPR ratios appear to have no effect on EE % of curcumin as there is a 30 % difference in EE % of GCP8Q9-Curc and GCP25Q19-Curc.

For the encapsulation of caspofungin, another BCS Class IV drug, a similar trend is observed where having a DP % of 25 % coupled with a DQ % of about 19 % is essential for achieving high encapsulation efficiencies greater than 95 %. DQ % values higher than 19 % showed no further increase in encapsulation of caspofungin. QPR ratios appear to influence EE % where QPR ratios less than 1 result in EE % values lower than 70 %.

The different processing methods usually employed to improve encapsulation efficiency did not have the same effect on GCPQ-CFG and GCPQ-Curcumin

formulations. Lyophilisation of curcumin formulations did not improve encapsulation efficiency. Also, stability of formulations was not improved with lyophilisation as there was no significant difference between zeta potential values of formulations subjected to lyophilisation and those which were sonicated or rehydrated. Sonication was also not ideal in the curcumin formulations due to larger particle sizes and less encapsulation efficiencies. However, sonication of GCPQ-CFG formulations achieved an encapsulation efficiency of 96 %. Both formulations were very stable for one week in aqueous solution without stabiliser at 5 ^{o}C and 25 ^{o}C. While caspofungin and curcumin can be encapsulated in GCPQ, the question of efficacy arises. *In vivo* experiments will be required to determine if encapsulation studies are merely a proof of concept or if encapsulated drugs have high enough oral bioavailability to have therapeutic effect.

5 *In vivo* Bioavailability Pilot Study

5.1 Introduction

In vitro models can aid in the selection of suitable drug compounds and the rationalisation of formulation design for these drug candidates (Porter and Charman, 2001; Zangenberg et al., 2001). Although, there remains a significant challenge in translating results gotten from *in vitro* models to clinical applications. This is due to several factors; the most significant of which is the inability to fully reproduce physiological conditions *in vitro*, hence, making it difficult to effectively predict *in vivo* outcome (Lin, 1998). A solution to this is to utilise animal models as the complexity of the drug interactions in a living organisms can in many cases only be captured using *in vivo* models (Katt et al., 2016) .

Previous chapters showed the effect of structural modifications of GCPQ polymers and their resulting effects on encapsulation efficiency of different classes of drugs. It was observed that increasing the degrees of palmitoylation (DP) resulted in an increase in encapsulation efficiency. A similar effect as observed when degree of quaternisation (DQ) was increased. A maximum encapsulation efficiency (96%) of caspofungin and curcumin (91 %) was observed with GCP25Q19 polymer (QPR = 0.76). Both formulations were stable in aqueous solution at 5 ^{o}C and 25 ^{o}C for 7 days, with the most stable formulations being those with degrees of quaternisation above 15 % and palmitoylation above 25 %.

In this chapter, *in vivo* PK experiments were carried out using the optimum GCPQ-Caspofungin formulation for two reasons. First, to determine if GCPQ-Caspofungin formulations result in better oral bioavailability of caspofungin compared to the existing caspofungin acetate. This is important as it gives insight to the effects of GCPQ micelle's ability to protect encapsulated drugs and influence their release profile. Secondly, to explore the uptake of caspofungin in the GCPQ-Caspofungin formulations into tissues. This will test GCPQ's ability to traverse tissue membrane.

5.1.1 Mechanism of GCPQ oral uptake

GCPQ has been shown to form stable micellar nanoparticles which drug compounds can be encapsulated (Uchegbu et al., 2001). These micellar systems are able to enhance oral uptake of drug molecule through three main mechanisms; protection, proximity and transport across cellular membranes (Figure 5-1) (Qu et al., 2006; Siew et al., 2011; Lalatsa et al., 2012; Serrano et al., 2015). Protection is established as within the stable nano-system, there is lesser chance for drug carriers to disaggregate upon interaction with biological fluids *in vivo*. This means that nano-carriers would be able to get their encapsulated drug to the site of action efficiently (Siew et al., 2011). Following that, GCPQ's mucoadhesive properties allow for micellar nanoparticles to adhere and penetrate the mucus layer. This extends the contact time between drug molecule and absorptive cells located on the intestine and increases proximity to absorption site, therefore facilitating transcytosis of hydrophobic drugs (Siew et al., 2011). Finally, there is evidence to prove augmented oral delivery via paracellular transport with the help of GCPQ (Odunze, 2018).

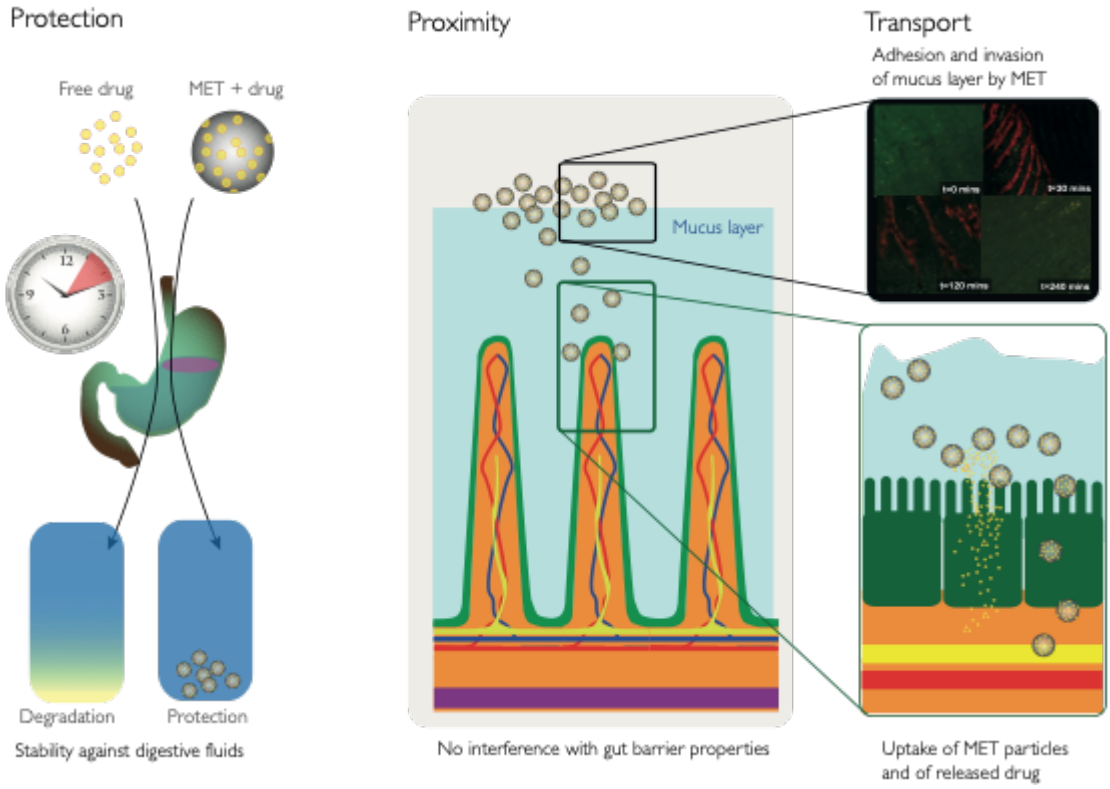

Figure 5-1: Schematic diagram of GCPQ method of enhancing oral uptake

GCPQ's ability to increase the solubility and dissolution rate of hydrophobic drugs in the BCS Class IV drugs and therefore increase bioavailability of drugs was investigated in GCPQ-based formulations of amphotericin B. Results showed an enhancement in the oral bioavailability of amphotericin B from 1.5% to 24.7%. Translocation of drug to tissues in organs such as the liver, brain and lungs were also increased compared to other lipid based oral formulations of amphotericin B (Serrano et al., 2015a). Its ability to increase oral bioavailability of hydrophobic drug compounds makes GCPQ an interesting polymeric nanoparticle to study as a possible oral drug delivery system and one that will be explored using caspofungin.

5.1.2 Caspofungin Anti-fungal Therapy

Fungal diseases are becoming an increasingly greater threat, particularly to patients with immunocompromised systems. In the last decade, the number of available antifungal treatments have been limited to the conventional polyenes (nystatin, amphotericin B) and first generation triazoles (ketoconazole, itraconazole and fluconazole). Both classes present unique challenges. For example, while polyenes are effective against a broad spectrum of fungal pathogens, their limitations are present in the toxicities that they possess. In the instance of first generation triazoles, limitations are observed in the range of fungal infections which fluconazole is effective against and itraconazole's drug to drug interactions *in vivo*. In addition to that, an acquired resistance to triazoles also pose a potential threat to the use of is class of antifungals hence, demand for a new class of antifungals is important (Patterson, 2000; Walsh et al., 2000; Chiou et al., 2000; Arikan and Rex, 2000).

Caspofungin, developed by Merck Research Laboratories is a semisynthetic lipopeptide derivative of pneumocandin B0 – A product gotten through fermentation of the Glarea lozoyensis fungus (Chen et al., 2015; Balkovec et al., 2014b). It is the first approved antifungal compound from a new class of antifungal agents called echinocandins. This class of antifungal drugs inhibit the synthesis of β-1, 3-D-glucan which is an essential component of pathogenic fungal cell wall (Sawistowska-Schröder et al., 1984). In theory, this new mechanism of action eliminates the possibility of cross resistance to existing antifungal agents hence, making them effective against strains of yeast which have developed a resistance to azoles (Pfaller et al., 2003; Diekema et al., 2003). Also, as mammalian cells do not contain cell walls, it allows for specific targeting of fungal cells hence, a more favourable safety profile. Thus, addressing the two main limitations observed in Polyenes and first generation triazoles. (Patterson, 2000; Walsh et al., 2000; Chiou et al., 2000; Arikan and Rex, 2000). An additional benefit to caspofungin is that it is neither a substrate for nor an inhibitor of the cytochrome p450 or P-glycoprotein transporter. Hence, resulting in a gradual metabolism of caspofungin *in vivo*. This is beneficial because caspofungin metabolites have no antifungal activity (Balani SK et al., 2000) so, there is little potential for drug–drug interactions.

Caspofungin has been shown to have *in vitro* activity against pathogens of Candida and Aspergillus species which are commonly encountered in clinics (Espinel-Ingroff, 1998) and preclinical efficacy of caspofungin has been established in a range of animal models of fungal infection (Abruzzo et al., 1997, 2000; Graybill et al., 1997b, 1997a). So far, animal models of mice with C.albicans or A.famigatus infections have been characterised for caspofungin. End points were defined by an improvement in survival or reduction in fungal load in target organs. These models mimicked different immune systems present in human patients allowing for a better representation of clinical applications (Abruzzo et al., 1997; Graybill et al., 1997b). Results showed efficacies of caspofungin were equivalent to that of amphotericin B (Abruzzo et al., 1997).

In another study, a 28-day murine model of immunosuppressed animals infected with C.albicans showed fungicidal activity and a significant reduction in fungal load present in the tissues of animals following a 7-day Caspofungin therapy. In contrast, those treated with fluconazole experienced few deaths and significant mortality rates within the 28-day study (Abruzzo et al., 2000). Further confirming the efficacy of caspofungin.

However, Caspofungin is not without its own limitations. Its' extremely poor oral bioavailability, unfavourable log p value and high molecular weight all contribute to its limitations in development of an oral formulation (Stone et al., 2002). The current formulation in clinical use is Caspofungin Acetate and has improved solubility but, it administered through intravenous infusions. A method which presents its own challenge such as the need for train medical staff, observation of patients for an extended duration post IV, daily hospital visits and difficulties in needle insertion (Zhou et al., 2015; McDonald et al., 2010).

It is therefore necessary to develop more optimal caspofungin formulations which can be administered orally with biodistribution profiles better than or comparable to those observed in clinically available formulations. One approach is with the use of nano systems as they have been shown to be biocompatible, protect drugs from *in vivo* degradation by preventing premature release. Also, these systems can resolve uptake challenges associated with large molecular size compounds (Blanco et al., 2015). In this chapter, we administered one group of rats with GCPQ-Caspofungin formulation and another with caspofungin acetate formulation, these were referred to as the treated and control groups. The objective was to assess the pharmacokinetics and biodistribution of caspofungin following oral administration in a novel GCPQ-

Caspofungin formulation and to compare results with oral administrations using commercial caspofungin-acetate formulations.

5.2 Materials and Methods

5.2.1 Materials

Caspofungin acetate powder was purchased from Glentham Life Sciences (Glentham, UK), Roxithromycin was purchased from Sigma Aldrich (Sigma, UK), LC-MS Grade solvents were purchased from Fischer Scientific (Leicestershire, UK). All other chemicals and reagents used were of analytical grade.

5.2.2 Animals

Male Sprague Dawley rats 450 – 650 g were acclimatised for at least seven days before being used for the study. The animals were housed in groups of 3 in plastic cages under controlled laboratory conditions. Ambient temperature was maintained at 22 ^{o}C and humidity kept at 60 %. A 12 hour-light and dark cycle was maintained with food and water ad libitum. All experiments were carried out under a UK Home Office Licence.

5.2.3 Methods

Bioanalytical LC-MS/MS Assay

Preparation of stock solutions:

Caspofungin stock solution (STK) was prepared at a concentration of 100 µg/mL in LC-MS grade methanol. Caspofungin is reported to dissolve in organic solvents such as DMSO, ethanol and MeOH (20 mg/mL) (Cayman Chemical 2022). Caspofungin working stock solutions were prepared by making serial dilutions of caspofungin stock solutions into MeOH to obtain stock solutions in Table 5-2, ranging from 17 – 33,400 ng/mL.

Caspofungin working standards (WS) were prepared by serially diluting caspofungin working stock solutions (STKS) into MeOH to obtain working standards in Table 5-1

ranging from 0.5 – 1000 ng/mL. A stock solution of the roxithromycin internal standard was freshly prepared at a concentration of 100 ng/mL in methanol.

Stock (STK) is 100 µg/mL (CFG in MeOH)					
Code	**Take from**	**µL**	**Add MeOH (µL)**	**Final volume (µL)**	**Final concentration CFG (ng/mL)**
STK 10	**STK**	668	1332	2000	33,400
Stks 9	**Stks 10**	1125	375	1500	25,050
Stks 8	**Stks 9**	1000	500	1500	16,700
Stks 7	**Stks 8**	750	750	1500	8,350
Stks 6	**Stks 7**	600	900	1500	3,340
Stks 5	**Stks 6**	750	750	1500	1,670
Stks 4	**Stks 5**	750	750	1500	835
Stks 3	**Stks 4**	600	900	1500	334
Stks 2	**Stks 3**	150	1350	1500	33
Stks 1	**Stks 2**	750	750	1500	17

Table 5-1: Preparation of CFG stock solutions

Code	CFG stock concentration (ng/mL)	CFG/MeOH (µL)	ROX/MeOH (µL)*	Final volume (µL)	Final concentration CFG (ng/mL)
WS 10	33,400	50	60	1670	1000
WS 9	25,050	50	60	1670	750
WS 8	16,700	50	60	1670	500
WS 7	8,350	50	60	1670	250
WS 6	3,340	50	60	1670	100
WS 5	1,670	50	60	1670	50
WS 4	835	50	60	1670	25
WS 3	334	50	60	1670	10
WS 2	33	50	60	1670	1
WS 1	17	50	60	1670	0.5

Table 5-2: Preparation of CFG working standard solutions.

**Roxithromycin concentration in MeOH (100 ng/mL)*

Plasma standard preparation:

Ten (10) series dilutions of caspofungin were made in the mobile phase. This ranged from 1000 ng/mL to 0.5 ng/mL. 100 µL of blank plasma was collected and transferred into 2 mL Eppendorf tubes corresponding with each standard dilution. 100 µL of each standard dilution was transferred into corresponding Eppendorf tubes containing blank plasma and vortexed for 1 minute. 100 µL of a 100 ng/mL concentration of the internal standard was added to the sample tubes and vortexed another minute. 700 mL of methanol was added to each Eppendorf tube, vortexed for 10 minutes and centrifuged at 4000 g for 10 minutes. 800 mL of supernatant was collected and placed in fresh Eppendorf tubes. This was then placed in a speed vacuum for 2 hours at 45 ^{0}C and 1Pa to evaporate the solvent. Thin film was then reconstituted with 80 µL of the mobile phase, vortexed, centrifuged at 1000 g for 10 minutes and supernatant transferred into amber HPLC vials for LC-MS/MS analysis. Quality control standard curves were generated to evaluate the recovery rate and matrix effect on drug extraction process Table 5-3.

Sample No	Plasma (µL)	Spike with CFG/MeOH (µL)	From	Spike with IS ROX/MeOH* (µL)	In final volume MeOH (µL)	Final conc after reconstituting (µg/mL)
STD10	100	100	**WS10**	100	700	2000
STD9	100	100	**WS9**	100	700	1000
STD8	100	100	**WS8**	100	700	750
STD7	100	100	**WS7**	100	700	500
STD6	100	100	**WS6**	100	700	250
STD5	100	100	**WS5**	100	700	100
STD4	100	100	**WS4**	100	700	50
STD3	100	100	**WS3**	100	700	10
STD2	100	100	**WS2**	100	700	1
STD1	100	100	**WS1**	100	700	0.5

Table 5-3: Preparation of quality control (blank) standard curves of CFG in plasma.

**Roxithromycin concentration in MeOH (100 ng/mL)*

Preparation of standard and quality control solutions:

Working standard solutions of caspofungin were prepared to create a standard calibration curve in plasma and each individual organ blank tissues: the brain, lungs, heart, liver, kidneys, pancreas and spleen. Tissues were homogenised according to the following protocol.

Tissue standard preparation:

Tissues were homogenised according to the following protocol. The absolute mass of tissue mass was weighed and tissue was placed in freezer at -80 ^{o}C to freeze. Solid frozen tissues were cut into smaller pieces using a pair of scissors and then ground into a fine powder using a mortar and pestle in dry ice. Tissue samples were then homogenized with deionised water at 4 mL/g of tissue. Homogenised mixture was vortexed-mixed for 5 minutes and 1 mL of homogenate transferred into a 5 mL cuvette. 2 mL of methanol was added into 1 mL of homogenate to precipitate the protein and sample bath sonicated for 10 minutes. Following this, samples were placed in centrifuge at 7000 g for 5 minutes. 100 µL of supernatant was collected and spiked with 100 µL of internal standard and 100 µL of CFG working standard (0.5 – 1000 ng/mL) to generate standard curves. The solvents from samples were evaporated using a speed vacuum evaporator for 2 hours at 45 ^{o}C and 1 Pa and reconstituted with 100 µL of mobile phase. Reconstituted samples were vortexed for 5 minutes and placed in a centrifuge at 1000 g for 5 minutes. 80 µL of supernatant was transferred into HPLC vial for LC-MS analysis. 20 µL of reconstituted samples were injected into the LC-MC/MS system. Quality control standard curves were generated to evaluate the recovery rate and matrix effect on drug extraction process.

Liquid Chromatography Tandem Mass Spectrometry (LC-MS/MS) Method:
Instrumentation:

Samples were analysed using an Agilent 6400 Series Triple Quadrupole LC/MS system (Agilent technologies, Berkshire, UK) comprising a degasser (HiP Degasser 1260/G4225A), a binary pump (HiP 1260 binary pump/G1312B), an auto sampler (HiP sampler 1260/G1367E), a column oven (G1316A) and a triple-quadrupole mass spectrometer (G6460A). Agilent MassHunter Workstation Software was used for system control, data acquisition and data processing.

Chromatographic Conditions:

A sensitive LC-MS/MS method was used to determine the concentration of caspofungin in the blood plasma and tissue samples as well as blank samples. Samples (20 µL injection volume) were chromatographed over an XSelect HSS T3 2.1 x 50 mm XP C-18 column, pore size 2.5 µm, particle size 100 Å, equipped with a

cartridge XSelect HSS T3 2.1 X 5 mm XP guard column and at a temperature of 30 ^{o}C with the mobile flow rate of 0.200 mL/min. The mobile phase was water-formic acid (A; 100:0.1 [vol/vol]) and methanol-formic acid (B; 100:0.1 [vol/vol]). The gradient elution program was as follows: 0.0 to 0.5 min from 40 % B to 100 % B, 0.5 to 4.5 min from 100 % B was maintained, 4.5 to 6.0 min from 100 % B to 40 % B (Table 5-4). The total run time was 7.0 min, including a 1-minute post run time.

Time (min)	**0.1 % FA in H_2O**	**0.1% FA in MeOH**
	Solvent A (%)	**Solvent B (%)**
0.00	60	40
0.5	60	40
1.00	0	100
4.00	0	100
4.50	60	40
6.00	60	40

Table 5-4: LC conditions of caspofungin and internal standard in LC-MS/MS analysis

Mass Spectrometer Conditions:

Caspofungin and Roxithromycin were monitored by positive electrospray ionisation (ESI) on an Agilent Jet Stream (AJS) ion source with ionization source parameters shown in Table 5-5.. Samples were scanned using multiple reaction monitoring (MRM) mode for transitions of m/z 547.3 → 137.0 and m/z 837.7 → 158.0 for caspofungin and roxithromycin respectively.

Parameter	Caspofungin (Analyte)	Roxithromycin (Internal Standard)
Capillary voltage (V)	3500	3500
Gas temperature (°C)	300	300
Gas flow (L/min)	5	5
Sheath gas heater (°C)	250	250
Sheath gas flow (L/min)	11	11
Nebuliser (psi)	45	45
Fragmentor (V)	245	245
Collision energy (V)	25	19
Precursor ion (m/z)	547.3	837.7
Product ion (m/z)	137.0	158.0

Table 5-5: LC-MS/MS source parameters for caspofungin and roxithromycin

Plasma Pharmacokinetics of Caspofungin:

Rats were allocated into two groups for the study: A treated group receiving oral gavage of caspofungin encapsulated in GCPQ micelles (GCP24Q19-CFG) and control group receiving oral gavage of caspofungin acetate. In both groups, rats were dosed at 5mg/kg of allocated formulation. Multiple tissue samples: Brain, lungs, heart, kidney, liver, spleen and pancreas were harvested, washed twice with deionised water and dried on filter paper. Dried tissue samples were immediately put on ice before eventually being stored at -80 ^{o}C. Blood samples were collected by cardiac puncture using a 25-gauge needle attached to a 2 mL syringe at the end of each time point. This was to ensure sufficient volume of blood plasma sample to analyse. Blood samples were transferred into EDTA coated plasma collection tubes and immediately stored at -80 ^{o}C until ready for processing. The concentration of caspofungin in plasma and tissues were determined by means of LC-MS/MS. Rat tissues and plasma were analysed at six time points: 30 minutes, 1 hour, 2 hours, 4 hours, 12 hours, and 24 hours, with four rats allocated per time point. At each timepoint, rats from each treatment group were culled by CO_2 asphyxiation.

Blood Plasma Sample preparation:

Plasma samples were collected from blood samples by centrifuging EDF blood collection tubes at $1x10^3$ rpm for 10 minutes. 100 µL of each plasma sample was collected and transferred into 2 mL Eppendorf tubes. 100µL of 100 ng/mL concentration of internal standard was added to each sample and vortexed for 1 minute. 800 µL of methanol was added to each tube and vortexed for 10 minutes. The tubes were centrifuged at 4000 g for 10 minutes and 800 µL of supernatant was collected and placed in fresh Eppendorf tube. This was then placed in a speed vacuum for 2 hours at 45 ^{0}C and 1 Pa to evaporate the solvent. The thin film was then reconstituted with 80 µL of mobile phase, vortexed, centrifuged at 1000 g for 10 minutes and supernatant was transferred into amber HPLC vials for LC-MS/MS analysis.

Tissue Sample preparation:

Tissues were homogenised according to the following protocol. The absolute mass of tissue mass was weighed and tissue was placed in freezer at -80 ^{o}C to freeze. Solid frozen tissues were cut into smaller pieces using a pair of scissors and then ground into a fine powder using a mortar and pestle in dry ice. Tissue samples were then homogenized with deionised water at 4 mL/g of tissue. Homogenised mixture was vortexed-mixed for 5 minutes and 1 mL of homogenate transferred into a 5 mL cuvette. 2 mL of methanol was added into 1 mL of homogenate to precipitate the protein and sample bath sonicated for 10 minutes. Following this, samples were placed in centrifuge at 7000 g for 5 minutes. 100 µL of supernatant was collected and spiked with 100 µL of internal standard and placed in new Eppendorf tubes. The solvents from samples were evaporated using a speed vacuum evaporator for 2 hours at 45 ^{o}C and 1 Pa and reconstituted with 100 µL of mobile phase. Reconstituted samples were vortexed for 5 minutes and placed in a centrifuge at 1000 g for 5 minutes. 80 µL of supernatant was transferred into HPLC vial for LC-MS analysis. 20 µL of reconstituted samples were injected into the LC-MC/MS system.

5.3 Results and Discussion

5.3.1 LCMS Method Development and Validation

The LC-MS/MS chromatogram for caspofungin and roxithromycin is shown in Figure 5-2. Both caspofungin and roxithromycin were ionised using the positive electrospray ionisation (ESI^+) for quantification of the analyte as there are hydroxyl groups present in both compounds.

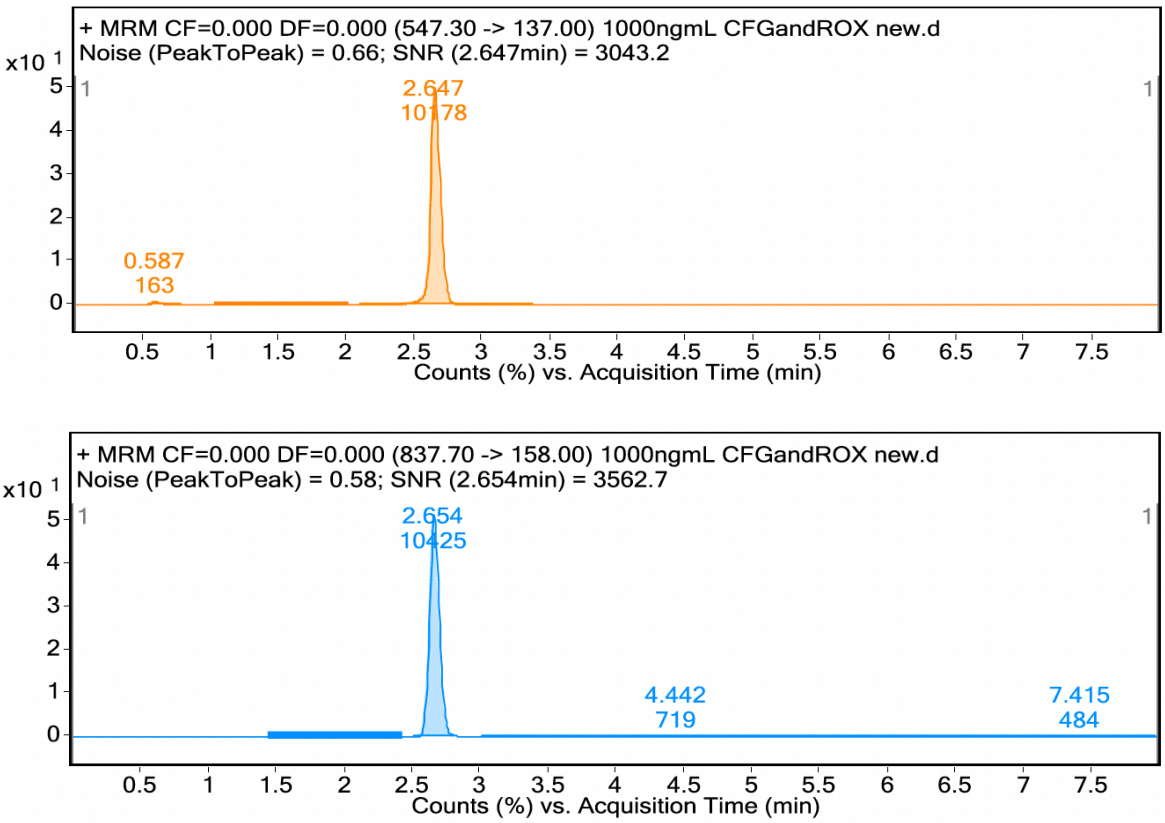

Figure 5-2: LC Chromatogram for caspofungin (1µg/mL) with retention time at 2.65 minutes (top) and roxithromycin (1µg/mL) with retention time at 2.65 minutes (bottom) in Methanol (0.1% FA) and Water (0.1 FA)

Multiple reactions monitoring mode was used to detect caspofungin and roxithromycin. The precursor ions to product ions transitions of m/z 547.3 → 137.1 and m/z 836 → 158.0 were chosen for caspofungin and roxithromycin respectively, based on the most abundant product ions shown in Figure 5-3. The assay conditions had an adequate specificity for caspofungin and roxithromycin with no interfering peaks being observed

at its retention time. Retention time was 2.65 minutes for both caspofungin and roxithromycin (Figure 5-2). The mrm transition for caspofungin was adapted from a reported study (Rochat et al. 2007). Roxithromycin was used as the internal standard due to its similar structural similarity to caspofungin as well as similar fragmentation pattern and elution time.

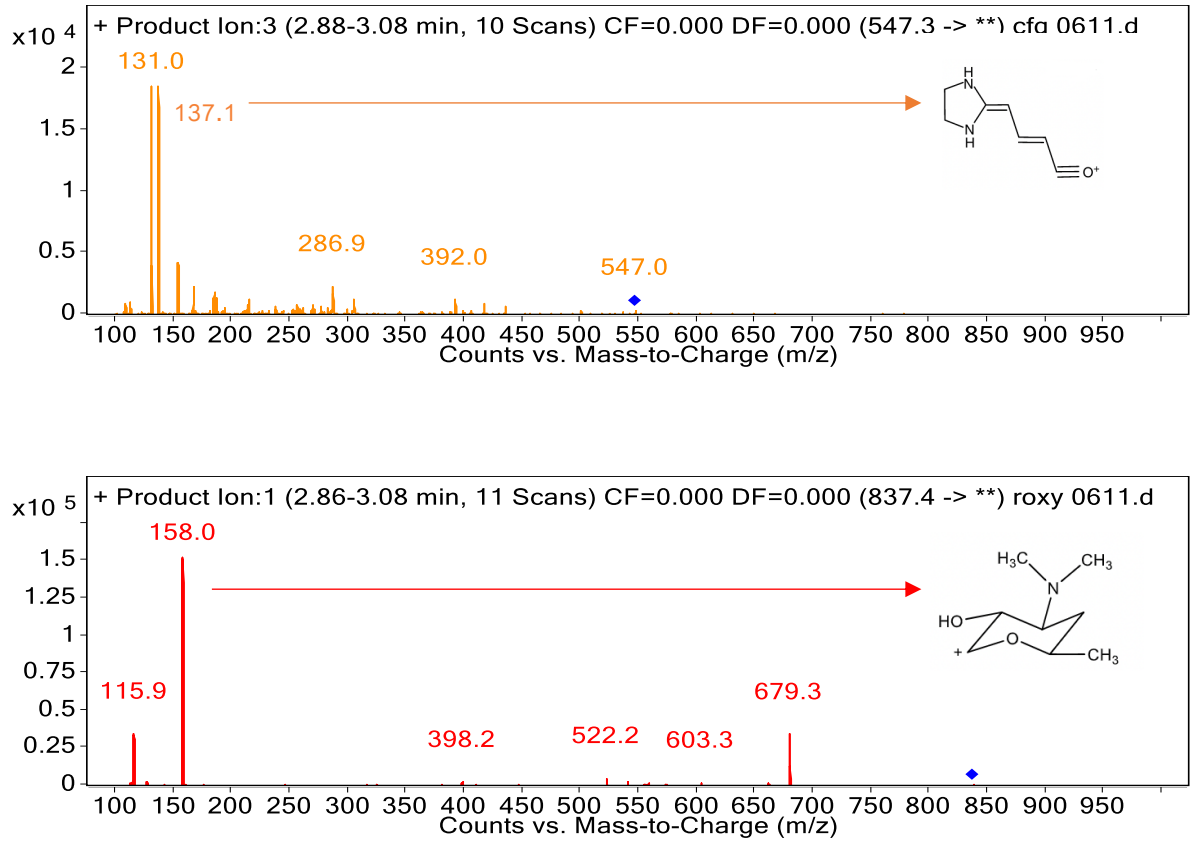

Figure 5-3: Mass spectrometry spectra for caspofungin (2 µg/mL) (top) and roxithromycin (2 µg/mL) (bottom) in methanol by ESI $^{+}$ mode.

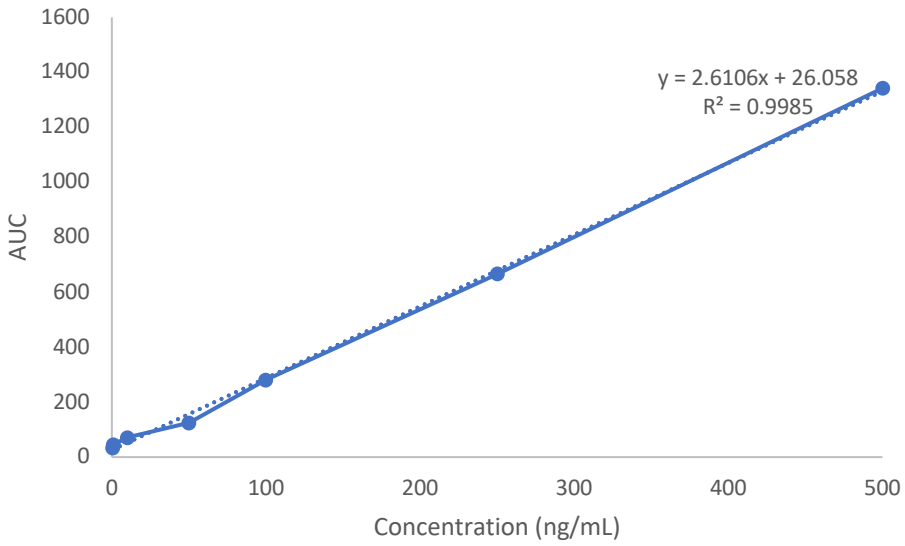

Figure 5-4: Calibration curve for caspofungin in rat plasma samples run in 60:40 methanol (+0.1% v/v Formic acid).

Figure 5-4 shows the calibration curve for caspofungin obtained by plotting the peak area ratios (CFG/Internal standard) versus the analyte concentration. Linearity was observed between 0.5 ng/mL and 500 ng/mL of caspofungin following in rat plasma extraction protocol. The coefficient calculated was greater than 0.99 hence, calibration curve produces acceptable results within the concentration range of 0.5ng/mL to 500ng/mL.

Caspofungin and Roxithromycin were efficiently extracted and separated from the blank matrices. Measured LLOQ for caspofungin was 0.5 nm/mL for the blank with SNR ≥ 10 at the lower limit of quantification.

5.3.2 Plasma pharmacokinetics

GCP25Q19-CFG was used for *in vivo* pharmacokinetics studies for three reasons. Firstly, due to its ability to an encapsulation efficiency of approximately 96 % and drug loading of 16 %. Secondly, GCP25Q19-CFG was shown to maintain its micellar stability at 25 ^{o}C for 7 days. Finally, due to its small particle size of approximately 45 nm.

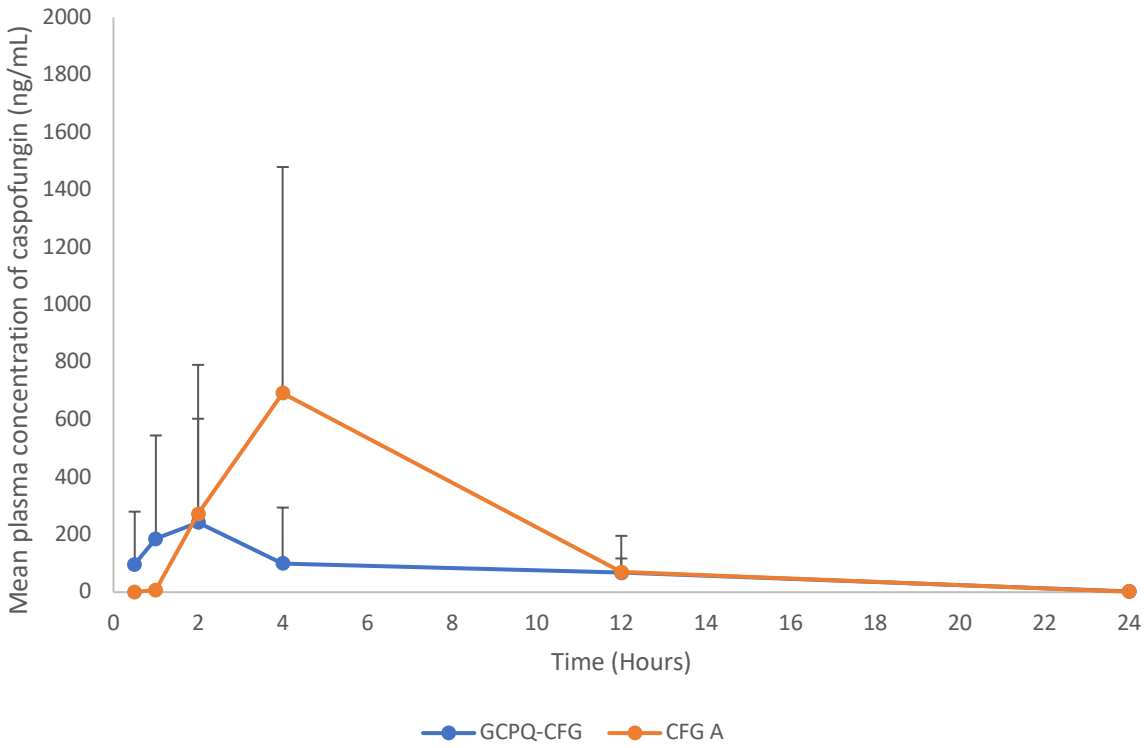

Time Point	Mean Plasma Concentration ± SD (ng/mL)	
	GCP25Q19-CFG	CFG A
0.5	96.2±183.9	0.2±3.1
1	185.4±359.8	7.9±7.8
2	242.1±361.3	273.1+517.8
4	100.3±194.1	692.3±787.1
12	67.3±49.9	69.7±126.1
24	2.5±4.8	1.6±3.0

Figure 5-5: (Top) Blood plasma concentration of GCPQ-Caspofungin formulations (green) over time administration to male Sprague Dawley rats by oral gavage at a dose of 5mg/kg and Caspofungin-acetate (orange) at the same dose. (Bottom) Numerical data used to plot mean plasma concentration graph n = 4.

Figure 5-5 shows the blood plasma concentration of caspofungin following the oral administration of GCP25Q19-CFG formulation and the control, Caspofungin-acetate formulation with the former having higher plasma levels. However, the numerical data shows a large spread around the mean, supported by two-way anova statistical analysis which shows no significant difference between caspofungin levels in treated and control group.

An increase in caspofungin plasma concentration is observed between 30 mins and 2 hours post-dose in GCPQ-caspofungin formulation. Plasma levels for caspofungin acetate formulations were seen to increase between 1 hour and two hours post dose where concentrations were similar to that of GCPQ-caspofungin. However, between 2 hours and 12 hours, caspofungin acetate was shown to have higher plasma levels than that of GCPQ-caspofungin before levels are seen to level out again with GCPQ-caspofungin from 12- 24 hours as caspofungin concentration approaches 0 ng/mL.

Formulation	Dose ($mgKg^{-1}$)	AUC_{0-4h} ($ng/h/mL^{-1}$)	C_{max} ($ngmL^{-1}$)	T_{max} (h)
GCP25Q19-CFG	5	1297	242±361	2
CFG-A	5	4156	692±2031	4

Table 5-6: Bioavailability of GCP25Q19-CFG and Caspofungin Acetate formulations administered through oral gavage at a dose of 5mg/mL to male Sprague Dawley rats.

Table 5-6 shows the pharmacokinetic characteristics of both GCP25Q19-CFG and caspofungin-acetate formulations following oral administration. A high dose of 5 mg/mL of caspofungin in each formulation was chosen which is five times the current clinical dose (1 $mgkg^{-1}$) (Merck, n.d.). This was done in attempt to circumvent possible loss of caspofungin through first pass metabolism as the current clinical dose is administered through I.V rather than oral administration. Oral bioavailability for caspofungin has been said to be very low (Rybowicz and Gurk-Turner, 2002).

Both caspofungin acetate and lipid based GCPQ formulations were shown to have a later T_{max} values (2-4 hours) possibly due lymphatic absorption. The lipid-based formulation however had a T_{max} value of 2 hours compared to 4 hours which was observed in the caspofungin-acetate control group. This was interesting as GCPQ micelles have been shown to slow down release rates (Serrano and Lalatsa, 2017)

due to its cmc value hence, the reverse trend would have predicted. Although further research would be required to investigate effects of GCPQ with varied degrees of palmitoylation and quaternisation on release profile of caspofungin. Alternatively, an earlier T_{max} may suggest faster uptake of caspofungin due to GCPQ's permeation enhancement effect.

The peak concentration (C_{max}) values observed in GCP25Q19-CFG formulation was 3 times less than that of caspofungin acetate formulation at 242±361 $ngmL^{-1}$ and 692±2031 $ngml^{-1}$ respectively. This suggests better drug bioavailability for the control formulation. However, larger error bars were also observed in this group meaning there is a large variation in individual plasma concentration values compared to the mean plasma concentration value. Statistical data also showed no significant difference between control and treated group. A larger sample size may be required to determine if differences observed in GCP25Q19-CFG and caspofungin acetate formulations are significant. C_{max} values for oral caspofungin formulations haven't been reported in the literature however, reported MIC values for caspofungin range from ≤0.19 to 0.78 µg/ml (Barchiesi et al., 1999) with C albicans, C. glabrata and C. tropicalis, the most common candida strains responsible for candidiasis, MIC values are well within the C_{max} of GCPQ-Caspofungin at ≤0.19 µg/mL. When compared to C_{max} values for GCPQ-Amphotericin B, another GCPQ-antifungal oral formulation, drug plasma concentrations are similar. With GCPQ-Amphotericin B at 308 $ngmL^{-1}$ and GCPQ-CFG at 242 $ngmL^{-1}$ (Serrano et al., 2015b). Similarly, $AUC_{0\text{-}4h}$ of GCP25Q19-CFG (1297 $ng/h/mL^{-1}$) follows a similar pattern as C_{max} with its value three times less than that of Caspofungin Acetate (4156 $ng/h/mL^{-1}$).

5.3.3 Biodistribution of Caspofungin

In addition to blood plasma analysis, seven tissues – brain, lungs, heart, liver, pancreas, spleen and kidney from each rat was analysed to gain an understanding of biodistribution in both the control and treated group. This analysis showed caspofungin present in only the liver and heart tissues.

Oral gavage of 5 mg/kg GCP25Q19-CFG resulted in detectable and quantifiable caspofungin levels in only liver (LLOQ = 5 ng/mL) and heart (LLOQ = 5 ng/mL) tissues (Figure 5-6).

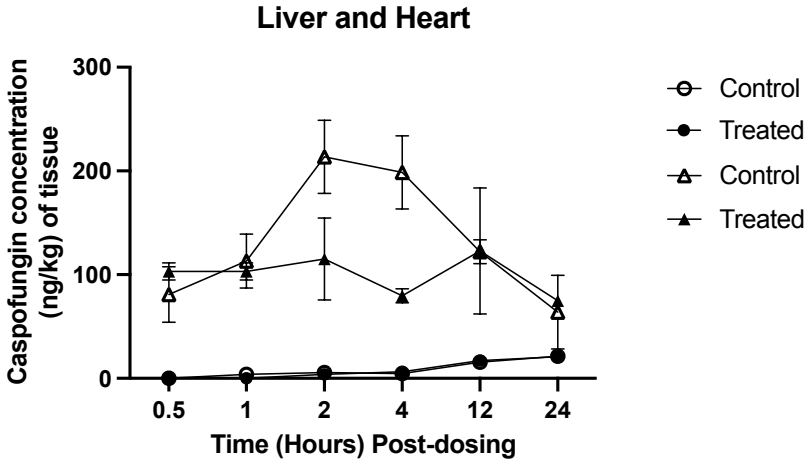

Figure 5-6: Graph showing In vivo CFG drug distribution in rat liver and heart tissues following the oral administration of 5mg/kg of CFG acetate (Control) and GCPQ-CFG (Treated).

Transcellular and paracellular are possible pathways for drug to gain access to tissues and GCPQ has been shown to aid in these with, high QPR polymers having higher apparent permeability coefficient (Siew et al., 2011; Odunze, 2018) Blood plasma data showed low caspofungin concentrations and it was therefore hypothesised that majority of caspofungin may be sequestered in rat tissues due to GCPQ transcellular and paracellular ability.

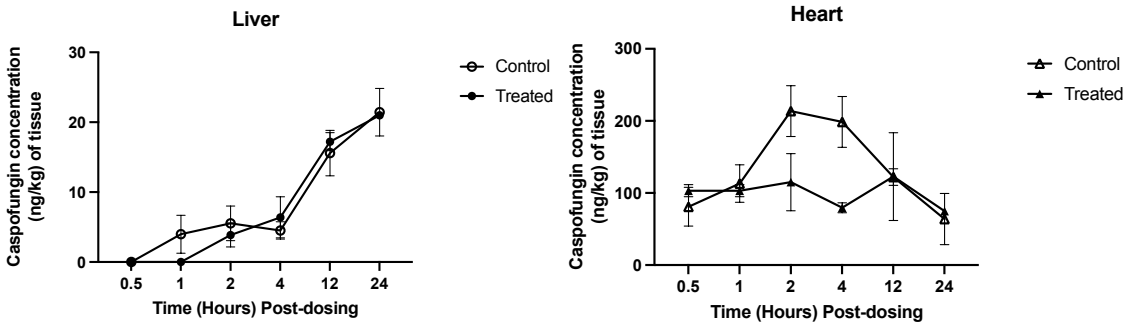

Figure 5-7: Graphs showing In vivo CFG drug distribution in rat Liver and Heart tissues following the oral

Figure 5-7 shows the distribution profile of caspofungin in rat liver and heart tissues at 6 time points post oral administration. In the liver tissues, both the control and treated group show a general increase in caspofungin concentration between 0.5 and 24 hours post dosing. In the control group, caspofungin concentrations increase significantly from 0 ng/kg of tissue to 4.52±1.2 ng/kg of tissue between 0.5hours and 4 hours post-dosing. With a C_{max} concentration of 5.54±2.5 ng/kg at 2 hours post-dosing. This was different to blood plasma data, where a C_{max} was at 4 hours post-dosing. At 24 hours post dosing, caspofungin concentration was 21.4± 3.4 ng/kg, 4 times more than what was observed at 2 hours post dosing.

Rats dosed with GCPQ-CFG nanoparticle formulations presented a slightly different release profile in the first four hours post-dosing compared to those in the control group. Here, caspofungin concentrations remain at 0ng/kg of liver tissue between 0.5 and 2 hours before reaching a similar C_{max} of 6.34±2.9 ng/kg 4 hours post-dosing. This was also different to what was observed in plasma data where C_{max} was observed at 2 hours post-dosing. Between 4 and 24 hours, measured caspofungin concentrations follow a similar trend to that of the control group, with a C_{max} of 21.0±0.4 ng/kg. There is no significant difference between caspofungin concentration values measured in the control group and the treated group at each post-dose timepoint.

Higher caspofungin concentration per gram of tissue was quantified in the heart with a C_{max} value of 213.6±35.2 ng/kg for control group and 122.8±60.9 ng/kg for treated group compared to a C_{max} of 20 ng/kg for liver tissues of both control and treated

group. A possible explanation could be that C_{max} values are due to a blood pool in the heart. Hence, caspofungin concentration values represent caspofungin present in blood plasma rather than caspofungin sequestered in heart tissues.

When comparing heart distribution curves in the control and treated groups, a different trend is observed. Statistical analysis shows no significant difference in caspofungin concentration per gram of heart tissue at all 6 timepoints in the treated group. This means that an average of 100 ng/kg was maintained in the heart tissues of rats dosed with GCPQ-Caspofungin formulations.

In contrast to that, the control group mimics a more conventional trend, with lower caspofungin concentration values of 81.0±26.9 ng/kg observed 30 minutes post oral dosing. This then increases until a peak of 213.6±35.2 ng/kg at 2 hours post dosing which is maintained for 2 more hours. Beyond 4 hours post oral dosing, caspofungin concentration per gram of tissue reduced until a final value of 63.8±35.5 ng/kg at 24 hours post-dose. This was similar to the concentration observed at 30 minutes post dose.

5.4 Discussion

Oral bioavailability of caspofungin has been reported to be less than 0.2% post oral dose of 50 mg/kg in rats (European Medicines Agency 2005). Results from current study shows oral availability as C_{max} to be 0.05 %, 0.03 % higher than what is expected if bioavailability and drug dose concentration had a linear relationship. This may be attributed to the oral enhancing effect of GCPQ nanoparticles used in formulation. Other studies have shown similar effect of GCPQ on oral drug bioavailability (Marimuthu, 2017; Serrano and Lalatsa, 2017; Serrano et al., 2015b; Siew et al., 2011) however, exact mechanism of enhancement is unknown. A possible explanation for such effects results from the permanent positive charge that GCPQ possesses due to the presence of quaternary ammonium groups (Uchegbu et al., 2001; Kanwal et al., 2019; Siew et al., 2011). It is then hypothesised that GCPQ will attach electrostatically to the negatively charged mucin in the GIT (Bansil and Turner, 2006), hence prolonging contact between drug loaded GCPQ particle and absorptive enterocytes of the GI tract, resulting in more efficient diffusion of caspofungin from GIT to blood

stream (Lalatsa et al., 2012b). Caspofungin acetate data was not considered as results were too varied to be significant.

Plasma concentrations comparison of GCPQ-caspofungin and GCPQ-paclitaxel post oral administration was made as both drug compounds belong to the BCS Class IV and have similar HSP predictions with GCPQ. In both instances, HSP predictions high RED values as well as high HSP distances between drug and GCPQ, suggesting interaction was thermodynamically unfavourable. Previous chapters have discussed similarities in encapsulation efficiencies for paclitaxel (Odunze, 2018) and caspofungin. Similarities are also seen in *in vivo* plasma data for both drugs.

GCPQ-paclitaxel formulations had $AUC_{0\text{-}4h}$ values twice that of GCP25Q19-CFG. With GCP20Q22-paclitaxel at 2048 ng/h/mL^{-1} and GCP37Q23-paclitaxel at 2417 ng/h/mL^{-1}, twice the recovered amount of GCP25Q19-CFG (Odunze, 2018). Polymers used in both formulations had different degrees of modification from polymer used in GCPQ-CFG however, the most similar polymer was GCP20Q23. GCPQ-paclitaxel formulations appear to perform better than that GCPQ-CFG although, it is important to consider the drug concentration of administered drug. Paclitaxel was dosed at a concentration of 20 mg/kg (Odunze, 2018) while caspofungin was dosed at a concentration of 5 mg/kg. Assuming oral bioavailability is directly proportional to administered drug dose, then GCPQ-CFG may be considered to have a higher drug bioavailability, as its $AUC_{0\text{-}4h}$ is greater than 600 ng/h/mL^{-1}, which is four times less than that of and GCPQ-Paclitaxel best performing formulation (Odunze, 2018). Experimental date will be needed to confirm this assumption.

Similarities are also observed when comparing C_{max} values of GCPQ-paclitaxel and GCPQ-CFG as a percentage of administered drug dose. With GCPQ-paclitaxel formulations having values of 0.03% and 0.04 % (Odunze, 2018) and GCPQ-CFG being slightly higher, at 0.05%. In both formulations, GCPQ is shown to perform similarly despite unfavourable HSP predictions. It will be interesting to observe experimental data for GCPQ-CFG at a dosing concentration of 20 mg/mL and compare C_{max}/dose (%) to that of 5 mg/mL. This will aid in understanding if perhaps HSP predictions sets a limit to C_{max}/dose (%) values.

Overall, plasma results demonstrate the presence of caspofungin in blood following oral delivery, which is preferable in a systemic disease such as invasive candidiasis.

Observed biodistribution assay was different to what was expected for two major reasons. Firstly, results showed an increase in caspofungin concentration beyond 4 hours post oral dosing. The final and most significant difference was the amount of caspofungin present in rat tissues was unexpected. It was expected that majority of caspofungin will be recovered in tissue samples due to GCPQ's ability to enhance cellular uptake (Siew et al., 2011; Odunze, 2018). Previous *in vitro* data showed GCPQ's ability to significantly enhance paracellular transport of FITC-dextran across both monolayers of MDCK cells (Odunze, 2018).

Disparity in expected and realised results could be due to three possible reasons. Firstly, it may be possible that while encapsulation efficiency data contradicts HSP predictions, *in vivo* data may be more dependent on thermodynamic data. For example, according to HSP, interaction between caspofungin and GCPQ is thermodynamically unstable. Instability of this interaction may not be observed in encapsulated formulation as aqueous nature of formulation strongly encourages encapsulation of hydrophobic caspofungin into hydrophobic GCPQ core. This however is not the situation *in vivo* as formulation is exposed to conditions less favourable to encapsulation for example, pH, enzymatic juices and temperature. This may result in premature release of caspofungin *in vivo*, encouraging drug degradation. Although, GCPQ-amphotericin B formulations have been shown to have good biodistribution data compared to rival oral formulation (Serrano et al., 2015).

As both amphotericin B and caspofungin have unfavourable HSP predictions with GCPQ, it is possible that disparity in expected and realised results may be due to permeative ability of GCPQ used. This has been shown to be determined by the degree of modification of GCPQ used. Significant enhancement of FITC-dextran paracellular transport was achieved using GCPQ polymer properties of 20% DP and 22% DQ (Odunze, 2018). Polymer used in this study has a QPR of 1.31 compared to 0.9 of the paracellular transport enhancing polymer. Further research using polymer with more similar parameters may yield more favourable results however, oral bioavailability data using GCPQ-amphotericin B showed enhanced drug delivery of

amphotericin B by 2-fold to liver, lung and spleen compared to its deoxycholate-amphotericin B rival formulation (Serrano et al., 2015). Polymer used in this formulation had a DP% of 16.9 and DQ of 16.5%, resulting in QPR of 1.02 (Serrano et al., 2015), more similar to 0.9 belonging to the paracellular transport enhancing polymer.

The final hypothesis relies on the assumption that drug molecule may be released from nanoparticle at the site of absorption rather than nanoparticle-drug micelle permeating drug tissue before drug release within the tissues. This way, drug absorption is solely dependent on drug physicochemical properties. Caspofungin has a high molecular weight of 1093.33 Daltons and poor log P value, contributing to its poor solubility and permeability properties, both of which discourage absorption into tissues (Lipinski et al., 2001). We see evidence to support this in the liver tissue data where GCPQ-CFG and caspofungin acetate graphs mimic each other. In both instances, free caspofungin *in vivo* could be the reason for low caspofungin concentration. Although, with GCPQ-amphotericin B oral formulations, good biodistribution was achieved with amphotericin B concentrations of 1 µg/g, 1.1 µg/g and 1.3 µg/g in the liver, kidney and spleen tissues respectively (Serrano et al., 2015). Same loading dose and polymer:drug ration was used in amphotericin B and caspofungin experiments however, a major difference was in the properties of polymer used as mentioned above. As exact mechanism by which GCPQ delivers caspofungin to tissues is not clear, repeat experiment using GCPQ properties similar to one used in both GCPQ-amphotericin B and GCPQ-paclitaxel formulations may give insight into effect of paracellular transport in.

5.5 Conclusion

We have been able to show that encapsulation of a hydrophobic BCS class IV drug within structurally modified GCPQ micelles results in similar oral drug bioavailability as the control formulation. *In vivo* data suggests a better release profile is obtained using GCPQ formulations with blood plasma concentrations within Cancidas MIC range. Caspofungin uptake in tissues appears to be unaffected by GCPQ modifications as both caspofungin and caspofungin acetate have similar oral bioavailability. In essence,

GCPQ formulation appears to work just as efficiently as acetate base formulation of caspofungin. It is possible that poor performance of GCPQ-CFG formulation may be due to negative HSP predictions being realised *in vivo*.

6 Conclusion and future work

6.1 Conclusion

While oral drug delivery is the preferred route of administration, it is associated with its own challenges. These include biological barriers such as bile acids, digestive enzymes and mucus as well as physicochemical properties of the drug compound. These unfavourable physicochemical properties are observed in BCS Class IV drugs, where low permeability and low solubility make them poor candidates for oral drug delivery. Alternative routes of delivery are through intravenous injections however, this is associated with drawbacks such as discomfort to patients, particularly infants and elderly patients. Also, additional resources such as labour and equipment costs associated with IV administration. These limitations may be overcome utilising novel drug delivery systems such as polymeric nanoparticles in oral drug formulations.

GCPQ is a glycol chitosan-based polymeric nanoparticle which possesses a permanent positive charge due to the presence of quaternary ammonium groups in its structure. This has been stipulated to provide GCPQ with mucoadhesive properties, as electrostatic interactions can be formed between the polymer and negatively charged sialic acid residues of mucin in the gastrointestinal tract. Interactions are presumed to promote gut absorption through prolonged contact time with GI membrane hence, increasing proximity to absorption site and facilitating transcytosis of hydrophobic drugs. Tissue concentration data has confirmed GCPQ's ability to enhance and significantly increase permeative ability of hydrophobic drugs following oral administration.

GCPQ's glycol chitosan backbone is a water-soluble chitosan derivative made up of hydrophilic ethylene glycol branches and reactive functional groups which allow easy chemical modifications. It is through these modifications that amphiphilic properties can be added to glycol chitosan base hence, allowing for the encapsulation of hydrophobic drug compounds. One of such modifications is observed when variations in molecular weight, degree of mole % of palmitoylation (DP %) and quaternisation (DQ %) are made. These were successfully synthesised and characterised in this

study. Synthesised amphiphilic GCPQ polymers were then used to create aqueous-based curcumin and caspofungin oral formulations.

Prior to experimental data, this study employed Hansen solubility parameters as a predictive approach to determine optimal GCPQ polymer parameters needed to encapsulate two class IV drug compounds (curcumin and caspofungin). These predictions were based on extent of variability between calculated Hansen solubility parameters (δ_D, δ_P and δ_H) of GCPQ constituents (chitosan, glycol chitosan, palmitic acid) and drug compounds. Results from these predictions showed unfavourable HSP data as a result of high RED values (above 1) and large distances from the centre of Hansen spheres, all of which suggests unsuitable thermodynamic conditions for GCPQ-drug encapsulation. Interestingly, similar results were observed with paclitaxel and amphotericin B. These are both hydrophobic class IV drug compounds which have previously been formulated using GCPQ nano carriers with encapsulation efficiencies about 90% and maintained stability for at least 28 days. This gives rise to questions surrounding accuracy of HSP predictive tool in polymer-drug interactions.

Experimental encapsulation studies were carried out for curcumin and caspofungin to investigate accuracy of HSP predictions. Study showed encapsulations efficiencies for curcumin and caspofungin mirrored that of paclitaxel and amphotericin B, with encapsulation efficiencies above 95% being achieved despite unfavourable HSP predictions. The best performing polymers were those with DP% ≥ 25% and DQ% ≥ 19%. Beyond this, further increase in DP% and DQ% had little effect on encapsulation efficiency. Formulations with this polymer were within the nanometre range (<300 nm) and remained stable in aqueous solution at RT and 5 ^{o}C for one week.

The disparity in HSP data and encapsulation efficiency data may be explained by considering the possibility that there are other interactions within the GCPQ nanocarrier system that influence drug interactions. Some of which may not be accounted for by HSP simulations, resulting in a huge discrepancy between theoretical and experimental data. This is significant as HSP simulation only took modification of DP% into account due to hydrophobic interactions between palmitic groups and hydrophobic drug compounds. It is possible that the influence of DP% on polymer-drug interaction is only significant until a DP% of about 25%. Beyond this, degree of quaternisation may have greater impact on encapsulation efficiency, leading to discrepancy in HSP predictions. Reported data from MARTINI force field simulations

showed lipopholic molecules present in the interphase between hydrophobic and hydrophilic moieties of GCPQ micelle. This couls also explain reason for DQ % influence on encapsulation efficiency.

Further *in vivo* studies of a 5mg/kg GCPQ-caspofungin formulation demonstrated GCPQ's ability to solubilise and increase oral bioavailability of caspofungin. Here we showed maximum blood plasma concentration of caspofungin (0.24 µg/mL) within the MIC range (≤0.19 to 0.78 µg/ml) for three most prevalent candida species; C albicans, C. glabrata and C. tropicalis. The lack of significant difference between GCPQ-caspofungin and caspofungin acetate C_{max} values acts as a proof of concept, confirming GCPQ's ability to solubilise caspofungin as it now performed on a similar level as its soluble formulation. A major difference was observed in release profiles, where GCPQ formulation had a better release profile with less variation, and a T_{max} of 2 hours compared to 4 hours in caspofungin acetate formulations. Similar to blood plasma data, GCPQ-caspofungin and caspofungin acetate biodistribution data mirrored each other. Trace amounts of caspofungin was found in the liver compared to blood plasma concentrations which was an interesting observation however, not concerning as candida is a systemic infection and focus is placed on blood plasma concentration of caspofungin.

Overall, GCPQ-caspofungin formulation has shown a degree of oral bioavailability. This lays the foundation to allow opportunity for further development on formulation which will increase oral bioavailability. Further development of formulation may offer patients the opportunity to conveniently self-dose using GCPQ-caspofungin oral tablets as an alternative to intravenous injections. This is particularly beneficial for patients who suffer from immunocompromised systems due to organ transplant procedures or, diseases such as AIDS as they overcome the possibility of side effects resulting from invasive measures. Also, the healthcare industry is set to benefit from cost and labour savings.

6.2 Future work

We observed from the project that HSP predictive models postulate unfavourable thermodynamic interactions between GCPS constituents and BCS class IV drugs:

curcumin and caspofungin. Experimental encapsulation data however proves otherwise for these drugs. Due to HSP only taking into account the palmitic acid modulation of GCPQ polymer, it will be interesting to factor in quaternary ammonium groups in future HSP analysis. Although, the limitation of looking at individual GCPQ constituents and their interactions with drug remains. As we do not know the effects of interactions between GCPQ constituents on drug encapsulation, it will be interesting to model this. Perhaps an alternative predictive model which can factor in effect of intermolecular interactions within the GCPQ polymer, alongside GCPQ-drug interactions may give rise to a more accurate prediction. Or GCPQ polymer components can be investigated in pairs. This allows for better understanding of the relationship between the glycol chitosan backbone and palmitic acid chain for example, and their influence on interaction with drug compound. Here, a combination of glycol chitosan and palmitic acid as well as glycol chitosan and quaternary ammonium salts can be investigated.

We have established GCPQ's ability to efficiently encapsulate hydrophobic drugs in the literature and in this project, despite HSP predictions. Increase in encapsulation efficiency was observed as DP % and DQ % increased, suggesting this to be the optimal polymer modification for encapsulation of Class IV drugs studied. It will be interesting to take a closer look at the resulting effect of structural modulation on particle-drug morphology and stability. Furthermore, to understand if the same polymer modulations have similar effects on encapsulation of hydrophilic drugs and possibly, oral bioavailability.

Finally, from *in vivo* pharmacokinetic study, GCPQ-CFG proved promising as blood plasma concentrations for caspofungin were within reported MIC range for most prevalent candida species. We hypothesised that GCPQ will enhance both solubility and permeability parameters of caspofungin drug. Data supported hypothesis as plasma concentrations were not significantly different to that of solubilised caspofungin acetate formulation. Similarities in biodistribution data between GCPQ-caspofungin and caspofungin acetate also supported hypothesis. It will be interesting to construct a repeat experiment, this time comparing two GCPQ-CFG formulations with using polymers with different degrees of modification and particle morphology. We know from the literature that GCPQ polymers with specific modulations have the ability to

enhance paracellular transport hence, effect of these GCPQ polymers on caspofungin oral pharmacokinetic profile may be investigated.

References

Abbott, S. et al. (2008). *Hansen Solubility Parameters in Practice*.

Abruzzo, G. K. et al. (1997). Evaluation of the echinocandin antifungal MK-0991 (L-743,872): Efficacies in mouse models of disseminated aspergillosis, candidiasis, and cryptococcosis. *Antimicrobial Agents and Chemotherapy*, 41 (11), pp.2333–2338. [Online]. Available at: doi:10.1128/aac.41.11.2333.

Abruzzo, G. K. et al. (2000). Efficacy of the echinocandin caspofungin against disseminated aspergillosis and candidiasis in cyclophosphamide-induced immunosuppressed mice. *Antimicrobial Agents and Chemotherapy*, 44 (9), pp.2310–2318. [Online]. Available at: doi:10.1128/AAC.44.9.2310-2318.2000.

Aggarwal, B. B. and Harikumar, K. B. (2009). Potential therapeutic effects of curcumin, the anti-inflammatory agent, against neurodegenerative, cardiovascular, pulmonary, metabolic, autoimmune and neoplastic diseases. *The International Journal of Biochemistry & Cell Biology*, 41 (1), pp.40–59. [Online]. Available at: doi:10.1016/j.biocel.2008.06.010.

Aguiar, A. J. et al. (1967). Effect of polymorphism on the absorption of chloramphenicol from chloramphenicol palmitate. *Journal of Pharmaceutical Sciences*, 56 (7), pp.847–853. [Online]. Available at: doi:10.1002/jps.2600560712.

Ahmad, I., Aqil, F. and Owais, M. (2006). *Modern Phytomedicine: Turning Medicinal Plants into Drugs*. [Online]. Available at: doi:10.1002/9783527609987.

Ahmad, S. et al. (2010). In silico modelling of drug-polymer interactions for pharmaceutical formulations. *Journal of the Royal Society Interface*, 7 (4). [Online]. Available at: doi:10.1098/rsif.2010.0190.focus.

Al-Hilal, T. A., Alam, Farzana. and Byun, Youngro. (2013). Oral drug delivery systems using chemical conjugates or physical complexes. *Advanced Drug Delivery Reviews*, 65 (6), pp.845–864. [Online]. Available at: doi:10.1016/j.addr.2012.11.002.

Alqahtani, M. S. et al. (2021). Advances in Oral Drug Delivery. *Frontiers in Pharmacology*, 12, pp.1–21. [Online]. Available at: doi:10.3389/fphar.2021.618411.

Amidon, G. L. et al. (1995). A theoretical basis for a biopharmaceutic drug classification: the correlation of in vitro drug product dissolution and in vivo

bioavailability. *Pharmaceutical research*, 12 (3), pp.413–420. [Online]. Available at: doi:10.1023/a:1016212804288.

Anand, P. et al. (2007). Bioavailability of Curcumin: Problems and Promises. *Molecular Pharmaceutics*, 4 (6), pp.807–818. [Online]. Available at: doi:10.1021/mp700113r.

Anaya, P. et al. (2013). Chitosan gel film bandages: Correlating structure, composition, and antimicrobial properties. *Journal of Applied Polymer Science*, 128 (6), pp.3939–3948. [Online]. Available at: doi:doi:10.1002/app.38621.

Anderson, J. M. and van Itallie, C. M. (2009). Physiology and function of the tight junction. *Cold Spring Harbor perspectives in biology*, 1 (2), pp.2584–2584. [Online]. Available at: doi:10.1101/cshperspect.a002584.

Arbiser, J. L. et al. (1998). Curcumin is an in vivo inhibitor of angiogenesis. *Molecular medicine*, 4 (6), pp.376–383.

Arezzini, B. et al. (2004). Glycosyl-Curcuminoids as Potential New Chelating Agents in Iron Overload Chelation Therapy. *European Journal of Inorganic Chemistry*, 2004 (3), pp.646–652. [Online]. Available at: doi:doi:10.1002/ejic.200300463.

Arikan, S. and Rex, J. H. (2000). New agents for treatment of systemic fungal infections. *Expert Opinion on Emerging Drugs*, 5 (2), pp.135–160. [Online]. Available at: doi:10.1517/14728214.5.2.135.

Arya, G., Das, M. and Sahoo, S. K. (2018). Evaluation of curcumin loaded chitosan/PEG blended PLGA nanoparticles for effective treatment of pancreatic cancer. *Biomedicine and Pharmacotherapy*, 102, pp.555–566. [Online]. Available at: doi:10.1016/j.biopha.2018.03.101.

de Assis, D. N. et al. (2008). Release profiles and morphological characterization by atomic force microscopy and photon correlation spectroscopy of 99mTechnetium-fluconazole nanocapsules. *International Journal of Pharmaceutics*, 349 (1–2), pp.152–160. [Online]. Available at: doi:10.1016/j.ijpharm.2007.08.002.

Auras, R. et al. (2010). *Poly(lactic acid): Synthesis, Structures, Properties, Processing, and Applications*. Auras, R. et al. (Eds). John Wiley & Sons, Inc.

Auras, R., Harte, B. and Selke, S. (2006). Sorption of ethyl acetate and d-limonene in poly(lactide) polymers. *Journal of the Science of Food and Agriculture*, 86 (4), pp.648–656. [Online]. Available at: doi:10.1002/jsfa.2391.

Authimoolam, S. P. and Dziubla, T. D. (2016). Biopolymeric mucin and synthetic polymer analogs: Their structure, function and role in biomedical applications. *Polymers*, 8 (3). [Online]. Available at: doi:10.3390/polym8030071.

Balani SK et al. (2000). Metabolites of Caspofungin Acetate, a Potent Antifungal Agent, in Human Plasma and Urine. *Pharmacology*, 28 (11), pp.1274–1278.

Balkovec, J. M. et al. (2014a). Discovery and development of first in class antifungal caspofungin (CANCIDAS®) - A case study. *Natural Product Reports*, 31 (1), pp.15–34. [Online]. Available at: doi:10.1039/c3np70070d.

Balkovec, J. M. et al. (2014b). Discovery and development of first in class antifungal caspofungin (CANCIDAS®) - A case study. *Natural Product Reports*, 31 (1), pp.15–34. [Online]. Available at: doi:10.1039/c3np70070d.

Bansil, R. and Turner, B. S. (2006). Mucin structure, aggregation, physiological functions and biomedical applications. *Current Opinion in Colloid and Interface Science*, 11 (2–3), pp.164–170. [Online]. Available at: doi:10.1016/j.cocis.2005.11.001.

Barchiesi, F. et al. (1999). In vitro activity of the New Echinocandin Antifungal, MK-0991, against common and uncommon clinical isolates of Candida species. *European Journal of Clinical Microbiology and Infectious Diseases*, 18 (4), pp.302–304. [Online]. Available at: doi:10.1007/s100960050283.

Barton, A. F. M. (1983). *CRC handbook of solubility parameters and other cohesion parameters*. Boca Raton, Fla: CRC Press.

Behrens, S. H., Borkovec, M. and Schurtenberger, P. (1998). Aggregation in Charge-Stabilized Colloidal Suspensions Revisited. *American Chemical Society* , 14, pp.1951–1954. [Online]. Available at: https://pubs.acs.org/sharingguidelines.

Beloqui, A., des Rieux, A. and Préat, V. (2016). Mechanisms of transport of polymeric and lipidic nanoparticles across the intestinal barrier. *Advanced Drug Delivery Reviews*, 106, pp.242–255. [Online]. Available at: doi:10.1016/j.addr.2016.04.014.

Bhagwat, R. R. and Vaidhya, I. S. (2013). Novel drug delivery systems: An overview. *Int J Pharm Sci Res*, 4 (3), pp.970–982.

Biswas, A. K. et al. (2014). Nanotechnology based approaches in cancer therapeutics. *Advances in Natural Sciences: Nanoscience and Nanotechnology*, 5 (4). [Online]. Available at: doi:10.1088/2043-6262/5/4/043001.

Blagden, N. et al. (2007). Crystal engineering of active pharmaceutical ingredients to improve solubility and dissolution rates. *Advanced Drug Delivery Reviews*, 59 (7), pp.617–630. [Online]. Available at: doi:10.1016/j.addr.2007.05.011.

Blanco, E., Shen, H. and Ferrari, M. (2015). HHS Public Access. *Nature biotechnology*, 33 (9), pp.941–951. [Online]. Available at: doi:10.1038/nbt.3121.ChIP-nexus.

Blanks, R. F. and Prausnitz, J. M. (1964). Thermodynamics of polymer solubility in polar and nonpolar systems. *I & EC Fundamentals*, 3 (1), p.9. [Online]. Available at: https://pubs.acs.org/sharingguidelines.

Blyth, C. et al. (2007). Antifungal therapy in infants and children with proven, probable or suspected invasive fungal infections. *Cochrane Database of Systematic Reviews*, (1). [Online]. Available at: doi:10.1002/14651858.CD006343.

Boddupalli, B. et al. (2010). Mucoadhesive drug delivery system: An overview. *Journal of Advanced Pharmaceutical Technology & Research*, 1 (4), p.381. [Online]. Available at: doi:10.4103/0110-5558.76436.

Boyd, B. J. et al. (2019). Successful oral delivery of poorly water-soluble drugs both depends on the intraluminal behavior of drugs and of appropriate advanced drug delivery systems. *European Journal of Pharmaceutical Sciences*, 137, pp.104–967. [Online]. Available at: doi:10.1016/j.ejps.2019.104967.

Bromberg, L. (2008). Polymeric micelles in oral chemotherapy. *Journal of Controlled Release*, 128 (2), pp.99–112. [Online]. Available at: doi:10.1016/J.JCONREL.2008.01.018 [Accessed 19 April 2019].

Bruce, G. (2016). *Development of an Orally Administered Curcumin Nanomedicine*. University College London.

Bruschi, M. L. and de Freitas, O. (2005). Oral bioadhesive drug delivery systems. *Drug Development and Industrial Pharmacy*, 31 (3), pp.293–310. [Online]. Available at: doi:10.1081/DDC-52073.

Cayman Chemical. (2022). *Product Specification Caspofungin (acetate)*.

Chan, M. M. et al. (1998). In vivo inhibition of nitric oxide synthase gene expression by curcumin, a cancer preventive natural product with anti-inflammatory properties. *Biochemical pharmacology*, 55 (12), pp.1955–1962.

Chavda, H., Patel, C. and Anand, I. S. (2010). Biopharmaceutics Classification System. *Systematic reviews in pharmacy*, 1 (1), pp.62–69. [Online]. Available at: doi:10.4103/0975-8453.59514.

Cheba, B. (2011). Chitin and chitosan: marine biopolymers with unique properties and versatile applications. *Global Journal of Biotechnology & Biochemistry*, 6 (3), pp.149–153.

Chen, L. et al. (2015). Engineering of Glarea lozoyensis for exclusive production of the pneumocandin B0 precursor of the antifungal drug caspofungin acetate. *Applied and Environmental Microbiology*, 81 (5), pp.1550–1558. [Online]. Available at: doi:10.1128/AEM.03256-14.

Chen, M.-C. et al. (2013). Recent advances in chitosan-based nanoparticles for oral delivery of macromolecules. *Advanced Drug Delivery Reviews*, 65 (6), pp.865–879. [Online]. Available at: doi:10.1016/j.addr.2012.10.010.

Chen, S. C.-A., Slavin, M. A. and Sorrell, T. C. (2011). Echinocandin antifungal drugs in fungal infections: a comparison. *Drugs*, 71 (1), pp.11–41. [Online]. Available at: doi:10.2165/11585270-000000000-00000.

Chiou, C. C., Groll, A. H. and Walsh, T. J. (2000). New Drugs and Novel Targets for Treatment of Invasive Fungal Infections in Patients with Cancer. *The Oncologist*, 5 (2), pp.120–135. [Online]. Available at: doi:10.1634/theoncologist.5-2-120.

Cho, E. C. et al. (2009). Understanding the role of surface charges in cellular adsorption versus internalization by selectively removing gold nanoparticles on the cell surface with a I 2/KI etchant. *Nano Letters*, 9 (3), pp.1080–1084. [Online]. Available at: doi:10.1021/nl803487r.

Cho, K. et al. (2008). Therapeutic nanoparticles for drug delivery in cancer. *Clinical Cancer Research*, 14 (5), pp.1310–1316. [Online]. Available at: doi:10.1158/1078-0432.CCR-07-1441.

Chooi, K. W. et al. (2014). Physical Characterisation and Long-Term Stability Studies on Quaternary Ammonium Palmitoyl Glycol Chitosan (GCPQ)—A New Drug Delivery

Polymer. *Journal of Pharmaceutical Sciences*, 103 (8), pp.2296–2306. [Online]. Available at: doi:10.1002/JPS.24026 [Accessed 21 April 2019].

Chung, T.-H. et al. (2007). The effect of surface charge on the uptake and biological function of mesoporous silica nanoparticles in 3T3-L1 cells and human mesenchymal stem cells. *Biomaterials*, 28 (19), pp.2959–2966. [Online]. Available at: doi:10.1016/j.biomaterials.2007.03.006.

Clogston, J. and Patri, A. (2011). Zeta Potential Measurement. In: McNeil, S. (Ed). *Characterization of Nanoparticles Intended for Drug Delivery*. New York: Hamana Press. pp.63–70. [Online]. Available at: www.springer.com/series/7651.

Clogston J.D. and Patri A.K. (2011). Zeta Potential Measurement. In: McNeil, S. (Ed). *Characterization of Nanoparticles Intended for Drug Delivery*. New York: Hamana Press. pp.63–70.

Coaker, H. (2014). Development and in vitro evaluation of slippery nanoparticles for enhanced diffusion through native mucus. *Nanomedicine UK*, 9, pp.382–383.

Cochin, D., Hendlinger, P. and Laschewsky, A. (1995). Polysoaps with fluorocarbon hydrophobic chains. *Colloid and Polymer Science*, 273, pp.1138–1143. [Online]. Available at: doi:10.1007/BF00653081.

Conner, S. D. and Schmid, S. L. (2003). Regulated portals of entry into the cell. *Nature*, 422 (6927), pp.37–44. [Online]. Available at: doi:10.1038/nature01451.

Cornell, B. (2016). *Lipid Digestion*. [Online]. Available at: https://ib.bioninja.com.au/standard-level/topic-6-human-physiology/61-digestion-and-absorption/lipid-digestion.html [Accessed 19 September 2019].

Crowther, R. S. and Marriott, C. (2011). Counter-ion binding to mucus glycoproteins. *Journal of Pharmacy and Pharmacology*, 36 (1), pp.21–26. [Online]. Available at: doi:10.1111/j.2042-7158.1984.tb02980.x.

Cyriac, J. and James, E. (2014). Switch over from intravenous to oral therapy: A concise overview. *Journal of Pharmacology and Pharmacotherapeutics*, 5 (2), p.83. [Online]. Available at: doi:10.4103/0976-500x.130042.

Delgado, A. V. et al. (2007). Measurement and interpretation of electrokinetic phenomena. *Journal of Colloid and Interface Science*, 309 (2), pp.194–224. [Online]. Available at: doi:10.1016/j.jcis.2006.12.075.

Deli, M. A. (2009). Potential use of tight junction modulators to reversibly open membranous barriers and improve drug delivery. *Biochimica et Biophysica Acta (BBA) - Biomembranes*, 1788 (4), pp.892–910. [Online]. Available at: doi:10.1016/j.bbamem.2008.09.016.

Desai, M. P. et al. (1996). Gastrointestinal uptake of biodegradable microparticles: effect of particle size. *Pharmaceutical research*, 13 (12), pp.1838–1845.

Descamps, M. and Willart, J. F. (2016). Perspectives on the amorphisation/milling relationship in pharmaceutical materials. *Advanced Drug Delivery Reviews*, 100, pp.51–66. [Online]. Available at: doi:10.1016/j.addr.2016.01.011.

Díaz de los Ríos, M. and Hernández Ramos, E. (2020). Determination of the Hansen solubility parameters and the Hansen sphere radius with the aid of the solver add-in of Microsoft Excel. *SN Applied Sciences*, 2 (4). [Online]. Available at: doi:10.1007/s42452-020-2512-y.

Diekema, D. J. et al. (2003). Activities of caspofungin, itraconazole, posaconazole, ravuconazole, voriconazole, and amphotericin B against 448 recent clinical isolates of filamentous fungi. *Journal of Clinical Microbiology*, 41 (8), pp.3623–3626. [Online]. Available at: doi:10.1097/01.idc.0000121033.62151.b2.

Dodane, V. and Vilivalam, V. D. (1998). Pharmaceutical Applications of Chitosan. *Pharmaceutical Science Technology Today*, 1, pp.246–253.

Domard, A. and Domard, M. (2001). Chitosan: Structure–Properties Relationship and Biomedical. In: *Polymeric Biomaterials, Revised and Expanded*. (1). Boca Raton, FL, USA. pp.187–212. [Online]. Available at: doi:10.1002/bip.21334.

Drewe, J. et al. (1993). Enteral absorption of octreotide: absorption enhancement by polyoxyethylene-24-cholesterol ether. *British journal of pharmacology*, 108 (2), pp.298–303.

Duan, Y. et al. (2016). Evaluation in vitro and in vivo of curcumin-loaded mPEG-PLA/TPGS mixed micelles for oral administration. *Colloids and surfaces. B, Biointerfaces*, 141, pp.345–354. [Online]. Available at: doi:10.1016/j.colsurfb.2016.01.017.

Dutta, P. K., Duta, J. and Tripathi, V. S. (2004). Chitin and Chitosan: Chemistry, properties and applications. *Journal of Scientific and Industrial Research*, 63 (1), pp.20–31.

Elder, D. P., Holm, R. and Diego, H. L. de. (2013). Use of pharmaceutical salts and cocrystals to address the issue of poor solubility. *International Journal of Pharmaceutics*, 453 (1), pp.88–100. [Online]. Available at: doi:10.1016/j.ijpharm.2012.11.028.

Ernst, E. J. et al. (1999). In Vitro Pharmacodynamic Properties of MK-0991 Determined by Time-kill Methods. *Diag Microbiol Infect Dis*, 33, pp.75–80.

Espinel-Ingroff, A. (1998). Comparison of in vitro activities of the new triazole SCH56592 and the echinocandins MK-0991 (L-743,872) and LY303366 against opportunistic filamentous and dimorphic fungi and yeasts. *Journal of Clinical Microbiology*, 36 (10), pp.2950–2956. [Online]. Available at: doi:10.1128/jcm.36.10.2950-2956.1998.

Ettmayer, P. et al. (2004). Lessons Learned from Marketed and Investigational Prodrugs. *Journal of Medicinal Chemistry*, 47 (10), pp.2393–2404. [Online]. Available at: doi:10.1021/jm0303812.

European Medicines Agency. (2005). *Cancidas, EPAR: Scientific Discussion*. [Online]. Available at: https://www.ema.europa.eu/en/documents/scientific-discussion/cancidas-epar-scientific-discussion_en.pdf [Accessed 31 July 2022].

Fardi, T. et al. (2014). Artwork conservation materials and Hansen solubility parameters: A novel methodology towards critical solvent selection. *Journal of Cultural Heritage*, 15 (6), pp.583–594. [Online]. Available at: doi:10.1016/j.culher.2013.11.006.

Farokhzad, O. C. and Langer, R. (2009). Impact of Nanotechnology on Drug Delivery. *ACS Nano*, 3 (1), pp.16–20. [Online]. Available at: doi:10.1021/nn900002m.

Florence, A. T. and Hussain, N. (2001). Transcytosis of nanoparticle and dendrimer delivery systems: evolving vistas. *Advanced drug delivery reviews*, 50 Suppl 1, pp.S69-89.

Forstner, G., Sherman, P. and Forstner, J. (1984). Mucus: function and structure. In: E, B. (Ed). *Attachment of organisms to the gut mucosa*. Fla: CRC Press. pp.13–21.

Fricker, G. et al. (1992). Enteral absorption of octreotide. *British journal of pharmacology*, 105 (4), pp.783–786.

Fricker, G. and Drewe, J. (1996). Current Concepts in Intestinal Peptide Absorption. *Journal of Peptide Science*, 2 (4), pp.195–211. [Online]. Available at: doi:10.1002/psc.66.

Fujiwara, N., Imai, S. and Yamamoto, H. (2019). Evaluation of the influence of fine particle surface modification with the Hansen solubility parameters. *Materials Chemistry and Physics*, 229, pp.139–148. [Online]. Available at: doi:10.1016/j.matchemphys.2019.02.091.

Fujiwara, N., Nishida, T. and Yamamoto, H. (2019). Adaptation of Hansen solubility parameter in evaluating transparency of composite materials. *Heliyon*, 5 (12), pp.1–10. [Online]. Available at: doi:10.1016/j.heliyon.2019.e02833.

Galandrin, S., Oligny-Longpré, G. and Bouvier, M. (2007). The evasive nature of drug efficacy: implications for drug discovery. *Trends in Pharmacological Sciences*, 28 (8), pp.423–430. [Online]. Available at: doi:10.1016/J.TIPS.2007.06.005 [Accessed 19 April 2019].

Galindo-Rodriguez, S. A. et al. (2005). Polymeric nanoparticles for oral delivery of drugs and vaccines: a critical evaluation of in vivo studies. *Critical reviews in therapeutic drug carrier systems*, 22 (5), pp.419–464.

Gao, X. et al. (2008). Quantum dots for tracking cellular transport of lectin-functionalized nanoparticles. *Biochemical and biophysical research communications*, 377 (1), pp.35–40. [Online]. Available at: doi:10.1016/j.bbrc.2008.09.077.

Gaucher, G. et al. (2005). Block copolymer micelles: preparation, characterization and application in drug delivery. *Journal of Controlled Release*, 109 (1–3), pp.169–188. [Online]. Available at: doi:10.1016/j.jconrel.2005.09.034.

Gaucher, G. et al. (2010). Polymeric micelles for oral drug delivery. *European Journal of Pharmaceutics and Biopharmaceutics*, 76 (2), pp.147–158. [Online]. Available at: doi:10.1016/J.EJPB.2010.06.007 [Accessed 19 April 2019].

Gautier, S., Boustta, M. and Vert, M. (1999). Alkylated poly(L-lysine citramide) as models to investigate the ability of amphiphilic macromolecular drug carriers to

physically entrap lipophilic compounds in aqueous media. *Journal of controlled release : official journal of the Controlled Release Society*, 60 (2–3), pp.235–247.

Goldberg, M. and Gomez-Orellana, I. (2003). Challenges for the oral delivery of macromolecules. *Nature reviews. Drug discovery*, 2 (4), pp.289–295. [Online]. Available at: doi:10.1038/nrd1067.

van de Graff, K. (1986). Anatomy and physiology of the gastrointestinal tract. *Pediatric Infectious Disease*, 5 (1), pp.11–16.

Graybill, J. R. et al. (1997a). Treatment of murine Candida krusei or Candida glabrata infection with L- 743,872. *Antimicrobial Agents and Chemotherapy*, 41 (9), pp.1937–1939. [Online]. Available at: doi:10.1128/aac.41.9.1937.

Graybill, J. R. et al. (1997b). Treatment of murine disseminated candidiasis with L-743,872. *Antimicrobial Agents and Chemotherapy*, 41 (8), pp.1775–1777. [Online]. Available at: doi:10.1128/aac.41.8.1775.

Grcev, S., Schoenmakers, P. and Iedema, P. (2004). Determination of molecular weight and size Exclusion, distribution and branching characteristics of PVAc by means of size chromatography/multi-angle laser light scattering (SEC/MALLS). *Polymer*, 45, pp.39–48.

Guggi, D. and Bernkop-Schnürch, A. (2003). In vitro evaluation of polymeric excipients protecting calcitonin against degradation by intestinal serine proteases. *International journal of pharmaceutics*, 252 (1–2), p.187—196. [Online]. Available at: doi:10.1016/s0378-5173(02)00631-2.

Gumustas, M. et al. (2017). Effect of Polymer-Based Nanoparticles on the Assay of Antimicrobial Drug Delivery Systems. In: *Multifunctional Systems for Combined Delivery, Biosensing and Diagnostics*. Elsevier. pp.67–108. [Online]. Available at: doi:10.1016/B978-0-323-52725-5.00005-8.

Gupta, S. V. et al. (2011). Enhancing the intestinal membrane permeability of zanamivir: a carrier mediated prodrug approach. *Molecular pharmaceutics*, 8 (6), pp.2358–2367. [Online]. Available at: doi:10.1021/mp200291x.

Gusterson, R. J. et al. (2003). The transcriptional co-activators CREB-binding protein (CBP) and p300 play a critical role in cardiac hypertrophy that is dependent on their

histone acetyltransferase activity. *The Journal of biological chemistry*, 278 (9), pp.6838–6847. [Online]. Available at: doi:10.1074/jbc.M211762200.

Ha, P. T. et al. (2012). Preparation and anti-cancer activity of polymer-encapsulated curcumin nanoparticles. *Advances in Natural Sciences: Nanoscience and Nanotechnology*, 3 (3), p.035002. [Online]. Available at: doi:10.1088/2043-6262/3/3/035002.

Hamed, I., Özogul, F. and Regenstein, J. M. (2016). Industrial applications of crustacean by-products (chitin, chitosan, and chitooligosaccharides): A review. *Trends in Food Science and Technology*, 48, pp.40–50. [Online]. Available at: doi:10.1016/j.tifs.2015.11.007.

Hanai, H. and Sugimoto, K. (2009). Curcumin has bright prospects for the treatment of inflammatory bowel disease. *Current pharmaceutical design*, 15 (18), pp.2087–2094.

Hancock, B. C., York, P. and Rowe, R. C. (1997). The use of solubility parameters in pharmaceutical dosage form design. *International Journal of Pharmaceutics*, 148, p.21.

Hansen, C. (1967). *THE THREE DIMENSIONAL SOLUBILITY PARAMETER*.

Hansen, C. M. and Smith, A. L. (2004). Using Hansen solubility parameters to correlate solubility of C 60 fullerene in organic solvents and in polymers. *Carbon*, 42, pp.1591–1597. [Online]. Available at: doi:10.1016/j.carbon.2004.02.011.

Hatcher, H. et al. (2008). Curcumin: from ancient medicine to current clinical trials. *Cellular and molecular life sciences : CMLS*, 65 (11), pp.1631–1652. [Online]. Available at: doi:10.1007/s00018-008-7452-4.

Haugstad, K. E. et al. (2015). Direct determination of chitosan-mucin interactions using a single-molecule strategy: Comparison to alginate-mucin interactions. *Polymers*, 7 (2), pp.161–185. [Online]. Available at: doi:10.3390/polym7020161.

Hauss, D. J. (2007). Oral lipid-based formulations. *Advanced Drug Delivery Reviews*, 59 (7), pp.667–676. [Online]. Available at: doi:10.1016/j.addr.2007.05.006.

Heading, R. C. et al. (1973). The dependence of paracetamol absorption on the rate of gastric emptying. *British Journal of Pharmacology*, 47 (2), pp.415–421. [Online]. Available at: doi:10.1111/j.1476-5381.1973.tb08339.x.

Hildebrand, J. H. (1951). *The solubility of nonelectrolytes*. 3rd ed. Scott, R. L. (Ed).

Hildebrand, J. H. (1962). *Regular solutions*. Scott, R. Lane. (Ed). Prentice-Hall.

Hillaireau, H. and Couvreur, P. (2009). Nanocarriers' entry into the cell: relevance to drug delivery. *Cellular and molecular life sciences : CMLS*, 66 (17), pp.2873–2896. [Online]. Available at: doi:10.1007/s00018-009-0053-z.

Hofmann, A. (1989). The Gastrointestinal System. Salivary, Gastric, Pancreatic, and Hepatobiliary Secretion. *Handbook of Physiology*, 3, pp.567–596.

Hofmann, A. and Eckmann, L. (2006). The Gastrointestinal System. Salivary, Gastric, Pancreatic, and Hepatobiliary Secretion. *Proc Natl Acad Sci U S A*, 103 (10), pp.4333–4334.

Hoo, C. M. et al. (2008). A comparison of atomic force microscopy (AFM) and dynamic light scattering (DLS) methods to characterize nanoparticle size distributions. *Journal of Nanoparticle Research*, 10 (SUPPL. 1), pp.89–96. [Online]. Available at: doi:10.1007/s11051-008-9435-7.

Hörter, D. and Dressman, J. B. (2001). Influence of physicochemical properties on dissolution of drugs q in the gastrointestinal tract. *Advanced Drug Delivery Reviews*, 46, pp.75–87. [Online]. Available at: www.elsevier.com/locate/drugdeliv.

Hwang, D., Ramsey, J. D. and Kabanov, A. v. (2020). Polymeric micelles for the delivery of poorly soluble drugs: From nanoformulation to clinical approval. *Advanced Drug Delivery Reviews*, 156, pp.80–118. [Online]. Available at: doi:10.1016/j.addr.2020.09.009.

ICH. (2006). *Validation of Analytical Procedures: Text and Methodology*.

Illum, Lisbeth; Farraj, Nidal F.; Davis, S. S. (1994). *Chitosan as a Novel Nasal Delivery System for Peptide Drugs; Pharmaceutical Research, Vol. 11, No. 8*.

Inano, H. (1999). Chemoprevention by curcumin during the promotion stage of tumorigenesis of mammary gland in rats irradiated with gamma-rays. *Carcinogenesis*, 20 (6), pp.1011–1018. [Online]. Available at: doi:10.1093/carcin/20.6.1011.

Instruments, M. (2000). *MRK654-01 An Introduction to Zeta Potential v3*. 2, pp.1–6.

Jäger, A. et al. (2007). Physico-chemical characterization of nanocapsule polymeric wall using fluorescent benzazole probes. *International Journal of Pharmaceutics*, 338 (1–2), pp.297–305. [Online]. Available at: doi:10.1016/j.ijpharm.2007.01.051.

James, T. L. (1998). *Fundamentals of NMR. Online Textbook*. San Francisco,: Department of Pharmaceutical Chemistry, University of California.

Jani, P. et al. (1990). Nanoparticle Uptake by the Rat Gastrointestinal Mucosa: Quantitation and Particle Size Dependency. *Journal of Pharmacy and Pharmacology*, 42 (12), pp.821–826. [Online]. Available at: doi:10.1111/j.2042-7158.1990.tb07033.x.

Jannin, V. et al. (2014). Rectal route in the 21st Century to treat children. *Advanced Drug Delivery Reviews*, 73, pp.34–49. [Online]. Available at: doi:10.1016/j.addr.2014.05.012.

Jayakumar, R. et al. (2007). Sulfated chitin and chitosan as novel biomaterials. *International journal of biological macromolecules*, 40 (3), pp.175–181. [Online]. Available at: doi:10.1016/j.ijbiomac.2006.06.021.

Jiang, M. C. et al. (1996). Differential regulation of p53, c-Myc, Bcl-2 and Bax protein expression during apoptosis induced by widely divergent stimuli in human hepatoblastoma cells. *Oncogene*, 13 (3), pp.609–616.

Jothi, N. and Nachiyar, R. K. (2012). Identification and isolation of chitin and chitosan from cuttle bone of Sepla prashadi Winckworth, 1936. *Current Biotica*, 6, pp.304–313.

Juère, E. et al. (2017). In Vitro Dissolution, Cellular Membrane Permeability, and Anti-Inflammatory Response of Resveratrol-Encapsulated Mesoporous Silica Nanoparticles. *Molecular Pharmaceutics*, 14 (12), pp.4431–4441. [Online]. Available at: doi:10.1021/acs.molpharmaceut.7b00529.

Kakde, D. et al. (2016). Amphiphilic block copolymers from a renewable Ɛ-decalactone monomer : prediction and characterization of micellar core effects on drug encapsulation and release. *Journal of Materials Chemistry B,* 4, pp.7119–7129. [Online]. Available at: doi:10.1039/x0xx00000x.

Kanwal, U. et al. (2019). Doxorubicin-loaded quaternary ammonium palmitoyl glycol chitosan polymeric nanoformulation: Uptake by cells and organs. *International Journal of Nanomedicine*, 14, pp.1–15. [Online]. Available at: doi:10.2147/IJN.S176868.

Katt, M. E. et al. (2016). In vitro tumor models: Advantages, disadvantages, variables, and selecting the right platform. *Frontiers in Bioengineering and Biotechnology*, 4 (FEB). [Online]. Available at: doi:10.3389/fbioe.2016.00012.

Kaur, S. and Dhillon, G. S. (2015). Recent trends in biological extraction of chitin from marine shell wastes: a review. *Critical reviews in biotechnology*, 35 (1), pp.44–61. [Online]. Available at: doi:10.3109/07388551.2013.798256.

Kazunori, K. et al. (1993). Block copolymer micelles as vehicles for drug delivery. *Journal of Controlled Release*, 24 (1–3), pp.119–132. [Online]. Available at: doi:10.1016/0168-3659(93)90172-2.

Kean, T. and Thanou, M. (2010). Biodegradation, biodistribution and toxicity of chitosan. *Advanced drug delivery reviews*, 62 (1), pp.3–11. [Online]. Available at: doi:10.1016/j.addr.2009.09.004.

Keihanian, F. et al. (2018). Curcumin, hemostasis, thrombosis, and coagulation. *Journal of Cellular Physiology*, 233 (6), pp.4497–4511. [Online]. Available at: doi:10.1002/jcp.26249.

Keskin, D. and Tezcaner, A. (2018). Micelles As Delivery System for Cancer Treatment. *Current Pharmaceutical Design*, 23 (35). [Online]. Available at: doi:10.2174/1381612823666170526102757.

Khadka, P. et al. (2014). Pharmaceutical particle technologies: An approach to improve drug solubility, dissolution and bioavailability. *Asian Journal of Pharmaceutical Sciences*, 9 (6), pp.304–316. [Online]. Available at: doi:10.1016/J.AJPS.2014.05.005.

Khayet, M. and Fernández, V. (2012). Estimation of the solubility parameters of model plant surfaces and agrochemicals: A valuable tool for understanding plant surface interactions. *Theoretical Biology and Medical Modelling*, 9 (1). [Online]. Available at: doi:10.1186/1742-4682-9-45.

Kim, J. H. et al. (2006). Hydrophobically modified glycol chitosan nanoparticles as carriers for paclitaxel. In: *Journal of Controlled Release*. 111 (1–2). 10 March 2006. pp.228–234. [Online]. Available at: doi:10.1016/j.jconrel.2005.12.013.

Kiptoo, P., Calcango, A. and Siahaan, T. (2016). Physiological, Biochemical, And Chemical Barriers To Oral Drug Delivery. In: Wang, B., Hu, L. and Siahaan, T. (Eds).

Drug Delivery: Principles And Applications. Second. John Wiley & Sons, Inc. p.632. [Online]. Available at: doi:10.1201/9781315382579.

Kirkpatrick, P. (2003). Pressures in the pipeline. *Nature Reviews Drug Discovery*, 2 (5), p.337. [Online]. Available at: doi:10.1038/nrd1095.

Knopp, M. M. et al. (2018). Effect of amorphous phase separation and crystallization on the in vitro and in vivo performance of an amorphous solid dispersion. *European Journal of Pharmaceutics and Biopharmaceutics*, 130, pp.290–295. [Online]. Available at: doi:10.1016/j.ejpb.2018.07.005.

Kofla, G. and Ruhnke, M. (2011). Pharmacology and metabolism of anidulafungin, caspofungin and micafungin in the treatment of invasive candidiosis - Review of the literature. *European Journal of Medical Research*, 16, pp.159–166.

Koo, H. et al. (2013). Enhanced drug-loading and therapeutic efficacy of hydrotropic oligomer-conjugated glycol chitosan nanoparticles for tumor-targeted paclitaxel delivery. *Journal of Controlled Release*, 172 (3), pp.823–831. [Online]. Available at: doi:10.1016/j.jconrel.2013.08.297.

Kothamasu, P. et al. (2012). Nanocapsules: The weapons for novel drug delivery systems. *BioImpacts*, 2 (2), pp.71–81. [Online]. Available at: doi:10.5681/bi.2012.011.

van Krevelen, D. W. and te Nijenhuis, K. (2009). Cohesive Properties and Solubility. In: *Properties of polymers: their correlation with chemical structure; their numerical estimation and prediction from additive group contributions*. Oxford: Elsevier Science & Technology. pp.189–227.

Kumari, A., Yadav, S. K. and Yadav, S. C. (2010). Biodegradable polymeric nanoparticles based drug delivery systems. *Colloids and Surfaces B: Biointerfaces*, 75 (1), pp.1–18. [Online]. Available at: doi:10.1016/J.COLSURFB.2009.09.001.

Kuper, K. M. (2008). *Text Book of Competence Assessment Tools for Health-System Pharmacies. 4th ed. ASHP Intravenous to oral therapy conversion*.

Kurtz, M. B. et al. (1994). Morphological Effects of Lipopeptides against Aspergillus fumigatus Correlate with Activities against (1,3)-1-D-Glucan Synthase. *Antimicrobial Agents And Chemotherapy*, 38 (7), pp.1480–1489.

Lai, S. K., Wang, Y. Y. and Hanes, J. (2009). Mucus-penetrating nanoparticles for drug and gene delivery to mucosal tissues. *Advanced Drug Delivery Reviews*, 61 (2), pp.158–171. [Online]. Available at: doi:10.1016/j.addr.2008.11.002.

Laksitorini, M. et al. (2014). Pathways and progress in improving drug delivery through the intestinal mucosa and blood-brain barriers. *Therapeutic delivery*, 5 (10), p.1143—1163. [Online]. Available at: doi:10.4155/tde.14.67.

Lalatsa, A. et al. (2012a). A prodrug nanoparticle approach for the oral delivery of a hydrophilic peptide, leucine5-enkephalin, to the brain. *Molecular Pharmaceutics*, 9 (6), pp.1665–1680. [Online]. Available at: doi:10.1021/mp300009u.

Lalatsa, A. et al. (2012b). Delivery of peptides to the blood and brain after oral uptake of quaternary ammonium palmitoyl glycol chitosan nanoparticles. *Molecular Pharmaceutics*, 9 (6), pp.1764–1774.

Laschewsky, A. and Zerbe, I. (1991). Polymerizable and polymeric zwitterionic surfactants: 2. Surface activity and aggregation behaviour in aqueous systems. *Polymer*, 32, pp.2081–2086. [Online]. Available at: doi:10.1016/0032-3861(91)90176-J.

Lavelle, E. C. et al. (2000). Mucosal immunogenicity of plant lectins in mice. *Immunology*, 99 (1), pp.30–37. [Online]. Available at: doi:10.1046/j.1365-2567.2000.00932.x.

Lecchi, P. and Abramson, F. P. (1999). Size exclusion chromatography-chemical reaction interface mass spectrometry: ‘A perfect match’. *Analytical Chemistry*, 71 (14), pp.2951–2955. [Online]. Available at: doi:10.1021/ac981098r.

Lee, M.-K. (2020). Liposomes for Enhanced Bioavailability of Water-Insoluble Drugs: In Vivo Evidence and Recent Approaches. *Pharmaceutics*, 12 (3), p.264. [Online]. Available at: doi:10.3390/pharmaceutics12030264.

Lee, V. M. et al. (1991). A68: a major subunit of paired helical filaments and derivatized forms of normal Tau. *Science*, 251 (4994), pp.675 LP – 678. [Online]. Available at: doi:10.1126/science.1899488.

Lefkowitz, R. J. (2004). Historical review: A brief history and personal retrospective of seven-transmembrane receptors. *Trends in Pharmacological Sciences*, 25 (8), pp.413–422. [Online]. Available at: doi:10.1016/j.tips.2004.06.006.

Lehr, C. M. et al. (1992). In vitro evaluation of mucoadhesive properties of chitosan and some other natural polymers. *International Journal of Pharmaceutics*, 78 (1–3), pp.43–48. [Online]. Available at: doi:10.1016/0378-5173(92)90353-4.

Letscher-bru, V. and Herbrecht, R. (2003a). Caspofungin : the first representative of a new antifungal class. *Journal of Antimicrobial Chemotherapy*, 51, pp.513–521. [Online]. Available at: doi:10.1093/jac/dkg117.

Letscher-bru, V. and Herbrecht, R. (2003b). Caspofungin : the first representative of a new antifungal class. *Journal of Antimicrobial Chemotherapy*, 51, pp.513–521. [Online]. Available at: doi:10.1093/jac/dkg117.

Li, L., Braiteh, F. S. and Kurzrock, R. (2005). Liposome-encapsulated curcumin: in vitro and in vivo effects on proliferation, apoptosis, signaling, and angiogenesis. *Cancer*, 104 (6), pp.1322–1331. [Online]. Available at: doi:10.1002/cncr.21300.

Liang, N. et al. (2018). Polymeric micelles based on modified glycol chitosan for paclitaxel delivery: Preparation, characterization and evaluation. *International Journal of Molecular Sciences*, 19 (6). [Online]. Available at: doi:10.3390/ijms19061550.

Lin, J. H. (1998). Applications and limitations of interspecies scaling and in vitro extrapolation in pharmacokinetics. *Drug Metabolism and Disposition*, 26 (12), pp.1202–1212.

Lipinski, C. A. et al. (2001). Experimental and computational approaches to estimate solubility and permeability in drug discovery and development settings. *Advanced drug delivery reviews*, 46 (1–3), pp.3–26.

Lipka, E., Crison, J. and Amidon, G. L. (1996). Transmembrane transport of peptide type compounds: Prospects for oral delivery. *Journal of Controlled Release*, 39, pp.121–129.

Liu, H., Taylor, L. S. and Edgar, K. J. (2015). The role of polymers in oral bioavailability enhancement; a review. *Polymer*, 77, pp.399–415. [Online]. Available at: doi:10.1016/j.polymer.2015.09.026.

Liu, Z. and Liu, K. (2013). The transporters of intestinal tract and techniques applied to evaluate interactions between drugs and transporters. *Asian Journal of Pharmaceutical Sciences*, 8 (3), pp.151–158. [Online]. Available at: doi:10.1016/j.ajps.2013.07.020.

López-Lázaro, M. (2008). Anticancer and carcinogenic properties of curcumin: Considerations for its clinical development as a cancer chemopreventive and chemotherapeutic agent. *Molecular Nutrition and Food Research*, 52 (SUPPL. 1). [Online]. Available at: doi:10.1002/mnfr.200700238.

Lu, F. et al. (2009). Size effect on cell uptake in well-suspended, uniform mesoporous silica nanoparticles. *Small*, 5 (12), pp.1408–1413. [Online]. Available at: doi:10.1002/smll.200900005.

van der Lubben, I. M. et al. (2001). Chitosan for mucosal vaccination. *Advanced Drug Delivery Reviews*, 52, pp.139–144. [Online]. Available at: www.elsevier.com/locate/drugdeliv.

Luo, Y. Y. et al. (2016). A review of biodegradable polymeric systems for oral insulin delivery. *Drug delivery*, 23 (6), pp.1882–1891. [Online]. Available at: doi:10.3109/10717544.2015.1052863.

M. Jensen, K. and A. Paladino, J. (1997). *Cost-Effectiveness of Abbreviating the Duration of Intravenous Antibacterial Therapy with Oral Fluoroquinolones*. [Online]. Available at: doi:10.2165/00019053-199711010-00008.

MacIerzanka, A. et al. (2011). Adsorption of bile salts to particles allows penetration of intestinal mucus. *Soft Matter*, 7 (18), pp.8077–8084. [Online]. Available at: doi:10.1039/c1sm05888f.

Marimuthu, P. (2017). Oral Delivery of Therapeutic Peptides Using GCPQ Nanoparticles Preethi Marimuthu. *PhD Thesis*.

Martinez, M. et al. (2002). Applying the biopharmaceutics classification system to veterinary pharmaceutical products. Part II. Physiological considerations. *Advanced drug delivery reviews*, 54 (6), pp.825–850.

Maurya, V. K. et al. (2020). Structure-based drug designing for potential antiviral activity of selected natural products from Ayurveda against SARS-CoV-2 spike glycoprotein and its cellular receptor. *VirusDisease*, 31 (2), pp.179–193. [Online]. Available at: doi:10.1007/s13337-020-00598-8.

McDonald, T. A. et al. (2010). Subcutaneous administration of biotherapeutics: Current experience in animal models. *Current Opinion in Molecular Therapeutics*, 12 (4), pp.461–470.

Mehrizi, T. Z. et al. (2018). Novel nano-sized chitosan amphotericin B formulation with considerable improvement against Leishmania major. *Nanomedicine*, 13 (24), pp.3129–3147. [Online]. Available at: doi:10.2217/nnm-2018-0063.

Mei, L. et al. (2013). Pharmaceutical nanotechnology for oral delivery of anticancer drugs. *Advanced Drug Delivery Reviews*, 65 (6), pp.880–890. [Online]. Available at: doi:10.1016/j.addr.2012.11.005.

de Mello, C. G. C. et al. (2016). Efficacy of lychnopholide polymeric nanocapsules after oral and intravenous administration in murine experimental Chagas disease. *Antimicrobial Agents and Chemotherapy*, 60 (9), pp.5215–5222. [Online]. Available at: doi:10.1128/AAC.00178-16.

Merck Sharp Dohme. (2021). *Caspofungin MSD: summary of product characteristics*. [Online]. Available at: https://www.medicines.org.uk/emc/medicine/12843# [Accessed 30 September 2021].

Merzendorfer, H. (2006). Insect chitin synthases: a review. *Journal of Comparative Physiology B*, 176 (1), pp.1–15. [Online]. Available at: doi:10.1007/s00360-005-0005-3.

Mitra, A. and Kesisoglou, F. (2013). Impaired drug absorption due to high stomach pH: a review of strategies for mitigation of such effect to enable pharmaceutical product development. *Molecular pharmaceutics*, 10 (11), pp.3970–3979. [Online]. Available at: doi:10.1021/mp400256h.

Mohanraj, V. J. and Chen, Y. (2006). Nanoparticles-A Review. *Tropical Journal of Pharmaceutical Research*, 5 (1), pp.561–573. [Online]. Available at: http://www.tjpr.freehosting.net.

Mohanty, C. et al. (2010). Curcumin-encapsulated MePEG/PCL diblock copolymeric micelles: a novel controlled delivery vehicle for cancer therapy. *Nanomedicine (London, England)*, 5 (3), pp.433–449. [Online]. Available at: doi:10.2217/nnm.10.9.

Mollaei, S. et al. (2016). Improvement of curcumin solubility by polyethylene glycol/chitosan-gelatin nanoparticles (CUR-PEG/CS-G-nps). *Biomedical Research*, 27 (3), pp.659–665. [Online]. Available at: www.biomedres.info.

Moore, J. C. (1964). Gel permeation chromatography. I. A new method for molecular weight distribution of high polymers. *Journal of Polymer Science Part A: Polymer Chemistry*, 34 (10), pp.1833–1841. [Online]. Available at: doi:10.1002/pola.1996.842.

van den Mooter, G. (2012). The use of amorphous solid dispersions: A formulation strategy to overcome poor solubility and dissolution rate. *Drug Discovery Today: Technologies*, 9 (2), pp.e79–e85. [Online]. Available at: doi:10.1016/j.ddtec.2011.10.002.

Mora-Huertas, C. E., Fessi, H. and Elaissari, A. (2010). Polymer-based nanocapsules for drug delivery. *International Journal of Pharmaceutics*, 385 (1–2), Elsevier B.V., pp.113–142. [Online]. Available at: doi:10.1016/j.ijpharm.2009.10.018.

Morimoto, T. et al. (2008). The dietary compound curcumin inhibits p300 histone acetyltransferase activity and prevents heart failure in rats. *The Journal of clinical investigation*, 118 (3), pp.868–878. [Online]. Available at: doi:10.1172/JCI33160.

Mourya, V. K. and Inamdar, N. (2008). Chitosan—Modifications and applications: Opportunities galore. *Reactive & Functional Polymers*, 68, pp.1013–1051. [Online]. Available at: doi:10.1016/j.reactfunctpolym.2008.03.002.

Mukerjee, A. and Vishwanatha, J. K. (2009). Formulation, characterization and evaluation of curcumin-loaded PLGA nanospheres for cancer therapy. *Anticancer research*, 29 (10), pp.3867–3875.

Müller, C. E. (2009). Prodrug Approaches for Enhancing the Bioavailability of Drugs with Low Solubility. *Chemistry and Biodiversity*, 6, pp.2071–2083. [Online]. Available at: http://en.wikipe-.

Nagavarma, B. V. N. et al. (2012). Different techniques for preparation of polymeric nanoparticles- A review. *Asian Journal of Pharmaceutical and Clinical Research*, 5 (3), pp.16–23.

Narang, N. and Sharma, J. (2011). Sublingual mucosa as a route for systemic drug delivery. *International Journal of Pharmacy and Pharmaceutical Sciences*, 3, pp.18–22.

Negi, P. S. et al. (1999). Antibacterial Activity of Turmeric Oil: A Byproduct from Curcumin Manufacture. *Journal of Agricultural and Food Chemistry*, 47 (10), pp.4297–4300. [Online]. Available at: doi:10.1021/jf990308d.

Nobbmann, U. et al. (2007). Dynamic light scattering as a relative tool for assessing the molecular integrity and stability of monoclonal antibodies. *Biotechnology and Genetic Engineering Reviews*, 24 (1), pp.117–128. [Online]. Available at: doi:10.1080/02648725.2007.10648095.

Norris, D. A. and Sinko, P. J. (1997). Effect of Size, Surface Charge, and Hydrophobicity on the Translocation of Polystyrene Microspheres Through Gastrointestinal Mucin. *J Appl Polym Sci*, 63, pp.1481–1492.

Odds, F. C., Brown, A. J. P. and Gow, N. A. R. (2003). Antifungal agents: mechanisms of action. *Trends in microbiology*, 11 (6), pp.272–279.

O'Driscoll, C. M. (2002). Lipid-based formulations for intestinal lymphatic delivery. *European Journal of Pharmaceutical Sciences*, 15 (5), pp.405–415. [Online]. Available at: doi:10.1016/S0928-0987(02)00051-9.

Odunze, U. (2018). *Engineering of Polymeric Nanoparticles Based on Structure-Activity Relationships (SARs) for Oral Drug Delivery*. (July), Doctor of Philosophy, UCL School of Pharmacy.

Odunze, U. et al. (2019). Unusual Enthalpy Driven Self Assembly at Room Temperature with Chitosan Amphiphiles. *Pharmaceutical Nanotechnology*, 7 (1), pp.57–71. [Online]. Available at: doi:10.2174/2211738507666190311123401.

Oppenheimer, A. (1937). Turmeric (Curcumin) in Biliary Diseases. *The Lancet*, 229 (5924), pp.619–621. [Online]. Available at: doi:10.1016/S0140-6736(00)98193-5.

Panyam, J. and Labhasetwar, V. (2003). Biodegradable nanoparticles for drug and gene delivery to cells and tissue. *Advanced Drug Delivery Reviews*, 55 (3), pp.329–347. [Online]. Available at: doi:10.1016/S0169-409X(02)00228-4.

Park, K. and Robinson, J. R. (1984). Bioadhesive polymers as platforms for oral-controlled drug delivery: method to study bioadhesion. *International journal of Pharmaceutics*, 19, pp.107–127.

Park, M. J., Balakrishnan, P. and Yang, S. G. (2013). Polymeric nanocapsules with SEDDS oil-core for the controlled and enhanced oral absorption of cyclosporine. *International Journal of Pharmaceutics*, 441 (1–2), pp.757–764. [Online]. Available at: doi:10.1016/j.ijpharm.2012.10.018.

Particle Sciences. (2012). An Overview of the Zeta Potential. *Particle Sciences*, 2, pp.1–4. [Online]. Available at: doi:10.1016/0021-9797(82)90296-X.

Parvez, S. et al. (2020). Recuperating Biopharmaceutical Aspects of Amphotericin B and Paromomycin Using a Chitosan Functionalized Nanocarrier via Oral Route for Enhanced Anti-leishmanial Activity. *Frontiers in Cellular and Infection Microbiology*, 10. [Online]. Available at: doi:10.3389/fcimb.2020.570573.

Patterson, T. F. (2000). Current and future approaches to antifungal therapy. *Current Opinion in Infectious Diseases*, 13 (6), pp.579–581. [Online]. Available at: doi:10.1097/00001432-200012000-00001.

Paulekuhn, G. S., Dressman, J. B. and Saal, C. (2007). Trends in Active Pharmaceutical Ingredient Salt Selection based on Analysis of the Orange Book Database. *Journal of Medicinal Chemistry*, 50 (26), pp.6665–6672. [Online]. Available at: doi:10.1021/jm701032y.

Pawar, K. S. et al. (2021). Oral Curcumin With Piperine as Adjuvant Therapy for the Treatment of COVID-19: A Randomized Clinical Trial. *Frontiers in Pharmacology*, 12. [Online]. Available at: doi:10.3389/fphar.2021.669362.

Peterson, D., Jones, J. and Petit II, R. (2007). Randomized, placebo-controlled trial of Saforis for prevention and treatment of oral mucositis in breast cancer patients receiving anthracycline-based chemotherapy. *Cancer*, 109 (2), pp.322–331. [Online]. Available at: doi:doi:10.1002/cncr.22384.

Pfaller, M. A. et al. (2003). In vitro activities of caspofungin compared with those of fluconazole and itraconazole against 3,959 clinical isolates of Candida spp., including 157 fluconazole-resistant isolates. *Antimicrobial Agents and Chemotherapy*, 47 (3), pp.1068–1071. [Online]. Available at: doi:10.1128/AAC.47.3.1068-1071.2003.

Phan, S. et al. (2014). Self-assembled structures formed during lipid digestion: characterization and implications for oral lipid-based drug delivery systems. *Drug Delivery and Translational Research*, 4 (3), pp.275–294. [Online]. Available at: doi:10.1007/s13346-013-0168-5.

Plapied, L. et al. (2011). Fate of polymeric nanocarriers for oral drug delivery. *Current Opinion in Colloid and Interface Science*, 16 (3), pp.228–237. [Online]. Available at: doi:10.1016/j.cocis.2010.12.005.

Podzimek, S. (1994). The use of GPC coupled with a multiangle laser light scattering photometer for the characterization of polymers. On the determination of molecular weight, size and branching. *Journal of Applied Polymer Science*, 54 (1), pp.91–103. [Online]. Available at: doi:doi:10.1002/app.1994.070540110.

Pohlmann, A. R. et al. (2008). Determining the simultaneous presence of drug nanocrystals in drug-loaded polymeric nanocapsule aqueous suspensions: A relation between light scattering and drug content. *International Journal of Pharmaceutics*, 359 (1–2), pp.288–293. [Online]. Available at: doi:10.1016/j.ijpharm.2008.04.007.

Porter, C. J. H. and Charman, W. N. (2001). In vitro assessment of oral lipid based formulations. *Advanced Drug Delivery Reviews*, 50, pp.127–147. [Online]. Available at: doi:10.1016/S0169-409X(01)00182-X.

Pouton, C. W. (2000). Lipid formulations for oral administration of drugs: non-emulsifying, self-emulsifying and 'self-microemulsifying' drug delivery systems. *European Journal of Pharmaceutical Sciences*, 11, pp.S93–S98. [Online]. Available at: doi:10.1016/S0928-0987(00)00167-6.

Powell, D. W. (1981). Barrier Function of Epithelia. *American Journal of Physiology*, 241 (4), pp.275–288.

Prabaharan, M. (2008). Review paper: Chitosan derivatives as promising materials for controlled drug delivery. *Journal of Biomaterials Applications*, 23 (1), pp.5–36. [Online]. Available at: doi:10.1177/0885328208091562.

Qu, X. et al. (2006a). Carbohydrate-based micelle clusters which enhance hydrophobic drug bioavailability by up to 1 order of magnitude. *Biomacromolecules*, 7 (12), pp.3452–3459. [Online]. Available at: doi:10.1021/bm0604000.

Qu, X. et al. (2006b). Carbohydrate-based micelle clusters which enhance hydrophobic drug bioavailability by up to 1 order of magnitute. *Biomacromolecules*, 7 (12), pp.3452–3459. [Online]. Available at: doi:10.1021/bm0604000.

Radhika, P. R. and Sivakumar, T. (2011). Nanocapsules: A new approach in drug delivery. *International Journal of Pharmaceutical Science and Research*, 2 (6), pp.1426–1429. [Online]. Available at: www.ijpsr.com.

Ramírez Arrebato, M. et al. (2010). Chitin and its derivatives as biopolymers with potential agricultural applications. *Biotecnología Aplicada*, 27, pp.270–276.

Rautio, J. et al. (2008). Prodrugs: design and clinical applications. *Nature Reviews Drug Discovery*, 7 (3), pp.255–270. [Online]. Available at: doi:10.1038/nrd2468.

Raymond, J. and Aujard, Y. (2000). Nosocomial infections in pediatric patients: a European, multicenter prospective study. European Study Group. *Infection control and hospital epidemiology*, 21 (4), pp.260–263. [Online]. Available at: doi:10.1086/501755.

des Rieux, A. et al. (2006). Nanoparticles as potential oral delivery systems of proteins and vaccines: a mechanistic approach. *Journal of controlled release : official journal of the Controlled Release Society*, 116 (1), pp.1–27. [Online]. Available at: doi:10.1016/j.jconrel.2006.08.013.

Ritika, H. and Aggarwal, G. (2012). Formulation Tactics for the Delivery of Poorly Soluble Drugs. *International Journal of PharmTech Research CODEN (USA): IJPRIF ISSN*, 4 (3), pp.914–923.

Rochat, B. et al. (2007). Liquid chromatography-mass spectrometry method for quantification of caspofungin in clinical plasma samples. *Journal of Mass Spectrometry*, 42 (4), pp.440–449. [Online]. Available at: doi:10.1002/jms.1171.

Roemer, T. and Krysan, D. J. (2014). Antifungal Drug Development: Challenges, Unmet Clinical Needs, and New Approaches. *Cold Spring Harbor Perspectives in Medicine* , 4 (5). [Online]. Available at: doi:10.1101/cshperspect.a019703.

Rybowicz, J. and Gurk-Turner, C. (2002). Caspofungin: The First Agent Available in the Echinocandin Class of Antifungals. *Baylor University Medical Center Proceedings*, 15 (1), pp.97–99. [Online]. Available at: doi:10.1080/08998280.2002.11927822.

Sachs-Barrable, K. et al. (2007). Lipid Excipients Peceol and Gelucire 44/14 decrease P-glycoprotein mediated efflux of Rhodamine 123 partially due to modifying P-glycoprotein protein expression within Caco-2 Cells. *J Pharm Pharmaceut Sci (www. cspsCanada.org)*, 10 (3), pp.319–331.

Sahay, G., Alakhova, D. Y. and Kabanov, A. V. (2010). Endocytosis of nanomedicines. *Journal of controlled release : official journal of the Controlled Release Society*, 145 (3), pp.182–195. [Online]. Available at: doi:10.1016/j.jconrel.2010.01.036.

Sahu, A. et al. (2011). Encapsulation of Curcumin in Pluronic Block Copolymer Micelles for Drug Delivery Applications. *Journal of Biomaterials Applications*, 25 (6), pp.619–639. [Online]. Available at: doi:10.1177/0885328209357110.

Salamat-Miller, N. and Johnston, T. P. (2005). Current strategies used to enhance the paracellular transport of therapeutic polypeptides across the intestinal epithelium. *International Journal of Pharmaceutics*, 294 (1–2), pp.201–216. [Online]. Available at: doi:10.1016/j.ijpharm.2005.01.022.

Sanches, B. M. A. and Ferreira, E. I. (2019). Is prodrug design an approach to increase water solubility? *International Journal of Pharmaceutics*, 568, p.118498. [Online]. Available at: doi:10.1016/j.ijpharm.2019.118498.

Sant, V. P., Smith, D. and Leroux, J.-C. (2005). Enhancement of oral bioavailability of poorly water-soluble drugs by poly(ethylene glycol)-block-poly(alkyl acrylate-co-methacrylic acid) self-assemblies. *Journal of Controlled Release*, 104 (2), pp.289–300. [Online]. Available at: doi:10.1016/j.jconrel.2005.02.010.

Sarode, A. L. et al. (2013). Hot melt extrusion (HME) for amorphous solid dispersions: Predictive tools for processing and impact of drug–polymer interactions on supersaturation. *European Journal of Pharmaceutical Sciences*, 48 (3), pp.371–384. [Online]. Available at: doi:10.1016/j.ejps.2012.12.012.

Sato, H. et al. (1998). Determination of the Degree of Acetylation of Chitin/Chitosan by Pyrolysis-Gas Chromatography in the Presence of Oxalic Acid. *Analytical Chemistry*, 70 (1), pp.7–12. [Online]. Available at: doi:10.1021/ac9706685.

Savjani, K. T., Gajjar, A. K. and Savjani, J. K. (2012). Drug Solubility: Importance and Enhancement Techniques. *ISRN Pharmaceutics*, 2012, pp.1–10. [Online]. Available at: doi:10.5402/2012/195727.

Savla, R. et al. (2017). Review and analysis of FDA approved drugs using lipid-based formulations. *Drug Development and Industrial Pharmacy*, 43 (11), pp.1743–1758. [Online]. Available at: doi:10.1080/03639045.2017.1342654.

Sawistowska-Schröder, E. T., Kerridge, D. and Perry, H. (1984). Echinocandin inhibition of 1,3-B-D-glucan synthase from Candida albicans. *Federation of European Biochemical Societies*, 173 (1), pp.134–138.

Schatz, C. et al. (2003). Typical physicochemical behaviors of chitosan in aqueous solution. *Biomacromolecules*, 4 (3), pp.641–648. [Online]. Available at: doi:10.1021/bm025724c.

Serajuddin, A. T. (2018). Development of solid dispersion for poorly water-soluble drugs. . In: *Water-insoluble drug formulation*. CRC Press. pp.541–573.

Serajuddin, A. T. M. (2007). Salt formation to improve drug solubility. *Advanced Drug Delivery Reviews*, 59 (7), pp.603–616. [Online]. Available at: doi:10.1016/j.addr.2007.05.010.

Serralheiro, A. et al. (2015). Direct nose-to-brain delivery of lamotrigine following intranasal administration to mice. *International Journal of Pharmaceutics*, 490 (1–2), pp.39–46. [Online]. Available at: doi:10.1016/j.ijpharm.2015.05.021.

Serrano, D. et al. (2015a). Oral particle uptake and organ targeting drives the activity of amphotericin B nanoparticles. *Molecular pharmaceutics*, 12 (2), pp.420–431. [Online]. Available at: doi:10.1021/mp500527x.

Serrano, D. R. et al. (2015b). Oral particle uptake and organ targeting drives the activity of amphotericin B nanoparticles. *Molecular Pharmaceutics*, 12 (2), pp.420–431. [Online]. Available at: doi:10.1021/mp500527x.

Serrano, D. R. and Lalatsa, A. (2017). Oral amphotericin B: The journey from bench to market. *Journal of Drug Delivery Science and Technology*, 42, pp.75–83. [Online]. Available at: doi:10.1016/j.jddst.2017.04.017.

Sharp, R. (2013). A Review of the Applications of Chitin and Its Derivatives in Agriculture to Modify Plant-Microbial Interactions and Improve Crop Yields. *Agronomy*, 3 (4), pp.757–793. [Online]. Available at: doi:10.3390/agronomy3040757.

Shishodia, S., Sethi, G. and Aggarwal, B. B. (2005). Curcumin: getting back to the roots. *Annals of the New York Academy of Sciences*, 1056, pp.206–217. [Online]. Available at: doi:10.1196/annals.1352.010.

Sievänen, E. (2007). Exploitation of Bile Acid Transport Systems in Prodrug Design. *Molecules (Basel, Switzerland)*, 12, pp.1859–1889. [Online]. Available at: doi:10.3390/12081859.

Siew, A. et al. (2011). Enhanced oral absorption of hydrophobic and hydrophilic drugs using quaternary ammonium palmitoyl glycol chitosan nanoparticles. *Molecular Pharmaceutics*, 9 (1), pp.14–28. [Online]. Available at: doi:10.1021/mp200469a.

Simões, S. M. N. et al. (2015). Polymeric micelles for oral drug administration enabling locoregional and systemic treatments. *Expert Opinion on Drug Delivery*, 12 (2), pp.297–318. [Online]. Available at: doi:10.1517/17425247.2015.960841.

Singh, A. and van den Mooter, G. (2016). Spray drying formulation of amorphous solid dispersions. *Advanced Drug Delivery Reviews*, 100, pp.27–50. [Online]. Available at: doi:10.1016/j.addr.2015.12.010.

Singh, R. and Lillard, J. W. J. (2009). Nanoparticle-based targeted drug delivery. *Experimental and molecular pathology*, 86 (3), pp.215–223. [Online]. Available at: doi:10.1016/j.yexmp.2008.12.004.

Skoog, D. A., Holler, F. J. and Crouch, S. R. (2007). *Principles of Instrumental Analysis*, International student edition. Thomson Brooks/Cole. [Online]. Available at: https://books.google.co.uk/books?id=GrOsQgAACAAJ.

Sogias, I. A., Williams, A. C. and Khutoryanskiy, V. v. (2008). Why is chitosan mucoadhesive? *Biomacromolecules*, 9 (7), pp.1837–1842. [Online]. Available at: doi:10.1021/bm800276d.

Sohail, A. et al. (2021). Comparative efficacy of amphotericin B-loaded chitosan nanoparticles and free amphotericin B drug against Leishmania tropica. *Bulletin of the National Research Centre*, 45 (1). [Online]. Available at: doi:10.1186/s42269-021-00644-5.

Song, L. et al. (2011). Polymeric micelles for parenteral delivery of curcumin: Preparation, characterization and in vitro evaluation. *Colloids and Surfaces A: Physicochemical and Engineering Aspects*, 390 (1), pp.25–32. [Online]. Available at: doi:https://doi.org/10.1016/j.colsurfa.2011.08.031.

Stetefeld, J., McKenna, S. A. and Patel, T. R. (2016). Dynamic light scattering: a practical guide and applications in biomedical sciences. *Biophysical Reviews*, 8 (4), pp.409–427. [Online]. Available at: doi:10.1007/s12551-016-0218-6.

Stone, J. A. et al. (2002). Single- and Multiple-Dose Pharmacokinetics of Caspofungin in Healthy Men. *Antimicrobial Agents and Chemotherapy*, 46 (3), pp.739–745. [Online]. Available at: doi:10.1128/AAC.46.3.739.

Subramanian, S. and Zaworotko, M. J. (1995). Manifestations of noncovalent bonding in the solid state. 6.' [H4(cyclam)]4+ (cyclam = 1,4,8,11 -tetraazacyclotetra- decane) as a template for crystal engineering of network hydrogen- bonded solids. *J. Chem.* , 73 (4), pp.414–424.

Suh, J. K. and Matthew, H. W. (2000). Application of chitosan-based polysaccharide biomaterials in cartilage tissue engineering: a review. *Biomaterials*, 21 (24), pp.2589–2598. [Online]. Available at: doi:10.1016/s0142-9612(00)00126-5.

Suresh, D. and Srinivasan, K. (2007). Studies on the in vitro absorption of spice principles – Curcumin, capsaicin and piperine in rat intestines. *Food and Chemical Toxicology*, 45 (8), pp.1437–1442. [Online]. Available at: doi:10.1016/j.fct.2007.02.002.

Synowiecki, J. and Al-Khateeb, N. A. (2003). Production, Properties, and Some New Applications of Chitin and Its Derivatives. *Critical Reviews in Food Science and Nutrition*, 43 (2), pp.145–171. [Online]. Available at: doi:10.1080/10408690390826473.

Tang, B. C. et al. (2009). Biodegradable polymer nanoparticles that rapidly penetrate the human mucus barrier. *Proceedings of the National Academy of Sciences of the United States of America*, 106 (46), pp.19268–19273. [Online]. Available at: doi:10.1073/pnas.0905998106.

Tate, P., Stephens T and Seeley, R. (2003). *Anatomy and Physiology, Sixth Edition 6th Edition*.

Teng, D. (2011). *From chitin to chitosan*. In K. Yao, J. Li, F.Yao, & Y. Y. (Ed). Florida: CRC Press.

Terada, T. et al. (2004). Genetic variant Arg57His in human H+/peptide cotransporter 2 causes a complete loss of transport function. *Biochemical and biophysical research communications*, 316 (2), pp.416–420. [Online]. Available at: doi:10.1016/j.bbrc.2004.02.063.

Thangapazham, R. L. et al. (2008). Evaluation of a nanotechnology-based carrier for delivery of curcumin in prostate cancer cells. *International journal of oncology*, 32 (5), pp.1119–1123.

Thanou, M., Verhoef, J. C. and Junginger, H. E. (2001). Oral drug absorption enhancement by chitosan and its derivatives. *Advanced drug delivery reviews*, 52 (2), pp.117–126.

Thong, P. Q. et al. (2014). *Impact of PLA / PEG ratios on Curcumin solubility and encapsulation efficiency , size and release behavior of Curcumin loaded poly (lactide) -poly (ethylenglycol) polymeric micelles*. 6, pp.279–285.

Toden, S. and Goel, A. (2017). The Holy Grail of Curcumin and its Efficacy in Various Diseases: Is Bioavailability Truly a Big Concern? *Journal of Restorative Medicine*, 6 (1), pp.27–36. [Online]. Available at: doi:10.14200/jrm.2017.6.0101.

Tournier, N. et al. (2011). Opioid transport by ATP-binding cassette transporters at the blood-brain barrier: implications for neuropsychopharmacology. *Current pharmaceutical design*, 17 (26), pp.2829–2842.

Ubbink, J. (2016). Structural and thermodynamic aspects of plasticization and antiplasticization in glassy encapsulation and biostabilization matrices. *Advanced Drug Delivery Reviews*, 100, pp.10–26. [Online]. Available at: doi:10.1016/j.addr.2015.12.019.

Uchegbu, I. F. et al. (2001). Quaternary ammonium palmitoyl glycol chitosan - A new polysoap for drug delivery. *International Journal of Pharmaceutics*, 224 (1–2), pp.185–199. [Online]. Available at: doi:10.1016/S0378-5173(01)00763-3.

Uchegbu, I. F. et al. (2014). Chitosan amphiphiles provide new drug delivery opportunities. *Polymer International*, 63 (7), pp.1145–1153. [Online]. Available at: doi:10.1002/pi.4721.

Uchegbu, I. and Siew, A. (2013). Nanomedicines and Nanodiagnostics Come of Age. *Journal of Pharmaceutical Sciences*, 102 (2), pp.305–310. [Online]. Available at: doi:10.1002/JPS.23377.

Varshosaz, J., Ghassami, E. and Ahmadipour, S. (2018). Crystal Engineering for Enhanced Solubility and Bioavailability of Poorly Soluble Drugs. *Current*

Pharmaceutical Design, 24 (21), pp.2473–2496. [Online]. Available at: doi:10.2174/1381612824666180712104447.

Vasconcelos, T. et al. (2016). Amorphous solid dispersions: Rational selection of a manufacturing process. *Advanced Drug Delivery Reviews*, 100, pp.85–101. [Online]. Available at: doi:10.1016/j.addr.2016.01.012.

Vásquez Marcano, R. G. del J. et al. (2018). Chitosan functionalized poly (ε-caprolactone) nanoparticles for amphotericin B delivery. *Carbohydrate Polymers*, 202, pp.345–354. [Online]. Available at: doi:10.1016/j.carbpol.2018.08.142.

Vemula, V. R., Lagishetty, V. and Lingala, S. (2010). Solubility Enhancement Techniques. *International Journal of Pharmaceutical Sciences Review and Research*, 5 (1), pp.41–51.

Verma, P. et al. (2010). Routes of Drug Administration. *International Journal of Pharmaceutical Studies and Research*, 1 (1), pp.54–59. [Online]. Available at: doi:10.1016/B978-008055232-3.60070-4.

Veronese, F. M. and Pasut, G. (2005). PEGylation, successful approach to drug delivery. *Drug Discovery Today*, 10 (21), pp.1451–1458. [Online]. Available at: doi:10.1016/S1359-6446(05)03575-0.

Vierling, P. and Greiner, J. (2003). Prodrugs of HIV Protease Inhibitors. *Current Pharmaceutical Design*, 9 (22), pp.1755–1770. [Online]. Available at: doi:10.2174/1381612033454441.

Vllasaliu, D. et al. (2010). Tight junction modulation by chitosan nanoparticles: Comparison with chitosan solution. *International Journal of Pharmaceutics*, 400 (1–2), pp.183–193. [Online]. Available at: doi:10.1016/j.ijpharm.2010.08.020.

Wagner, D. et al. (2001). Intestinal drug efflux: formulation and food effects. *Advanced drug delivery reviews*, 50 Suppl 1, pp.S13-31.

Walsh, T. J. et al. (2000). New targets and delivery systems for antifungal therapy. *Medical mycology*, 38 Suppl 1, pp.335–347.

Wang, J., Ma, W. and Tu, P. (2015). The mechanism of self-assembled mixed micelles in improving curcumin oral absorption: In vitro and in vivo. *Colloids and surfaces. B, Biointerfaces*, 133, pp.108–119. [Online]. Available at: doi:10.1016/j.colsurfb.2015.05.056.

Wang, Y. et al. (2014). Shape-Controlled Paclitaxel Nanoparticles with Multiple Morphologies: Rod-Shaped, Worm-Like, Spherical, and Fingerprint-Like. *Molecular Pharmaceutics*, 11 (10), pp.3766–3771. [Online]. Available at: doi:10.1021/mp500436p.

Waring, M. J. (2010). Lipophilicity in drug discovery. *Expert opinion on drug discovery*, 5 (3), pp.235–248. [Online]. Available at: doi:10.1517/17460441003605098.

Weng, M. (2016). Determination of the Hansen solubility parameters with a novel optimization method. *Journal of Applied Polymer Science*, 133 (16). [Online]. Available at: doi:10.1002/app.43328.

Wiederhold, N. P. and Lewis, R. E. (2003). The echinocandin antifungals: an overview of the pharmacology, spectrum and clinical efficacy. *Expert opinion on investigational drugs*, 12 (8), pp.1313–1333. [Online]. Available at: doi:10.1517/13543784.12.8.1313.

Williams, H. D. et al. (2014). Ionic liquids provide unique opportunities for oral drug delivery: structure optimization and in vivo evidence of utility. *Chem. Commun.*, 50 (14), pp.1688–1690. [Online]. Available at: doi:10.1039/C3CC48650H.

Wilson, O. C. and Omokanwaye, T. (2013). Biomimetic lessons for processing chitin-based composites. *Biopolymer nanocomposites: Processing, properties, and applications*, pp.53–83.

Wisplinghoff, H. et al. (2003). Current trends in the epidemiology of nosocomial bloodstream infections in patients with hematological malignancies and solid neoplasms in hospitals in the United States. *Clinical infectious diseases : an official publication of the Infectious Diseases Society of America*, 36 (9), pp.1103–1110. [Online]. Available at: doi:10.1086/374339.

Wisplinghoff, H. et al. (2004). *Nosocomial Bloodstream Infections in US Hospitals : Analysis of 24 , 179 Cases from a Prospective Nationwide Surveillance Study*. 0019 (April 2003), pp.309–317.

Wu, C.-Y. and Benet, L. Z. (2005). Predicting Drug Disposition via Application of BCS: Transport/Absorption/Elimination Interplay and Development of a Biopharmaceutics DrugDisposition Classification System. *Pharmaceutical Research*, 22 (1), pp.11–23. [Online]. Available at: doi:10.1007/s11095-004-9004-4.

Xavier-Junior, F. H. et al. (2016). Match of Solubility Parameters Between Oil and Surfactants as a Rational Approach for the Formulation of Microemulsion with a High Dispersed Volume of Copaiba Oil and Low Surfactant Content. *Pharmaceutical Research*, 33 (12), pp.3031–3043. [Online]. Available at: doi:10.1007/s11095-016-2025-y.

Xu, R. (2008). Progress in nanoparticles characterization: Sizing and zeta potential measurement. *Particuology*, 6 (2), pp.112–115. [Online]. Available at: doi:10.1016/j.partic.2007.12.002.

Yoshioka, H. et al. (1995). Chitosan-derived Polymer-surfactants and Their Micellar Properties. *Bioscience, Biotechnology, and Biochemistry*, 59 (10), pp.1901–1904. [Online]. Available at: doi:10.1271/bbb.59.1901.

Young, N. A. et al. (2014). Oral administration of nano-emulsion curcumin in mice suppresses inflammatory-induced NFkB signaling and macrophage migration. *PLoS ONE*, 9 (11). [Online]. Available at: doi:10.1371/journal.pone.0111559.

Yu, H. and Huang, Q. (2012). Improving the oral bioavailability of curcumin using novel organogel-based nanoemulsions. *Journal of Agricultural and Food Chemistry*, 60 (21), pp.5373–5379. [Online]. Available at: doi:10.1021/jf300609p.

Yu, L. X. et al. (2002). Biopharmaceutics classification system: the scientific basis for biowaiver extensions. *Pharmaceutical Research*, 19 (7), pp.921–925. [Online]. Available at: doi:10.1023/A:1016473601633.

Yuan, Y. et al. (2011). Deacetylation of Chitosan: Material Characterization and in vitro Evaluation via Albumin Adsorption and Pre-Osteoblastic Cell Cultures. *Materials*, 4 (8), pp.1399–1416. [Online]. Available at: doi:10.3390/ma4081399.

Zangenberg, N. H. et al. (2001). A dynamic in vitro lipolysis model. I. Controlling the rate of lipolysis by continuous addition of calcium. *European Journal of Pharmaceutical Sciences*, 14 (2), pp.115–122. [Online]. Available at: doi:10.1016/S0928-0987(01)00169-5.

Zhang, J. et al. (2010). Chitosan Modification and Pharmaceutical/Biomedical Applications. *Marine Drugs*, 8 (7), pp.1962–1987. [Online]. Available at: doi:10.3390/md8071962.

Zhang, T. et al. (2017). Novel oral administrated paclitaxel micelles with enhanced bioavailability and antitumor efficacy for resistant breast cancer. *Colloids and Surfaces B: Biointerfaces*, 150, pp.89–97. [Online]. Available at: doi:10.1016/j.colsurfb.2016.11.024.

Zhang, Y. et al. (2016). Investigation into Efficiency of a Novel Glycol Chitosan-Bestatin Conjugate to Protect Thymopoietin Oligopeptides from Enzymatic Degradation. *Journal of Pharmaceutical Sciences*, 105 (2), pp.828–837. [Online]. Available at: doi:10.1002/jps.24567.

Zhongfa, L. et al. (2012). Enhancement of curcumin oral absorption and pharmacokinetics of curcuminoids and curcumin metabolites in mice. *Cancer Chemotherapy and Pharmacology*, 69 (3), pp.679–689. [Online]. Available at: doi:10.1007/s00280-011-1749-y.

Zhou, Q. et al. (2015). The optimal choice of medication administration route regarding intravenous, intramuscular, and subcutaneous injection. *Patient Preference and Adherence*, 9, p.923. [Online]. Available at: doi:10.2147/PPA.S87271.